DOCTORAL THESIS

Improvements in Image Compression and RF Transmission for Wireless Capsule Endoscopy

A Thesis submitted to Brunel University London

in accordance with the requirements

for award of the degree of Doctor of Philosophy

in

the department of Electronic and Computer Engineering

Ioannis G. Intzes

December 3, 2020

Declaration of Authorship

Ioannis G. Intzes, declare that the work in this research thesis was carried out in accordance with the requirements of the University's Regulations and Code of Practice for Research Degree Programmes and that it has not been submitted for any other academic award. Except where indicated by specific reference in the text, the work is the candidate's own work. Work done in collaboration with, or with the assistance of, others, is indicated as such. Any views expressed in the dissertation are those of the author.

SIGNED: ..... DATE: .....

(Signature of student)

Abstract

Endoscopes and colonoscopes are used by many doctors and physicians for diagnoses of pathologies of the gastrointestinal (GI) track. These methods are painful and dangerous for the life of the patients, due to these drawbacks: a wireless capsule endoscopy (WCE) is used. The reason is that diagnosing the small intestine is impossible those the WCE improves the overall performance of endoscopy and colonoscopy. The use of these systems provide benefits in the diagnosis of pathologies of the GI such us, cancer, blooding, lymphoma or Cronh's diseases. WCE has an image sensor that captures images. The amount of data produced by the image sensor is huge. Also, there is the need of wireless transmission of this data. In order to power these systems by a single battery, the system should use compression of this data and an extra low power transmitter with high data rate transmission. The energy of this battery is currently not sufficient to keep the system working for more than 8 hours continuously with conventional compression algorithms and wireless transmitters. For these reasons, mainly, the use of a novel design that can compress and send efficiently this data is needed.

In this research, an entirely improved WCE system is proposed. From the perspective of camera lenses that can be used, through camera sensor and compression algorithm, to wireless transmission system. Hundreds of WCE images were used to identify the unique characteristics of them. Statistical analysis was made and finally achieved the best of the performance for the compression algorithm. Additionally, camera lenses where selected to provide a new perspective of view. Traditionally, WCE uses simple lenses to capture the GI track. A 360° degree lenses is proposed to be used. The reason is the fact that the use of them gives the advantage to map the entire GI track and make a virtual reconstruction of the GI outside human body. With this method, the physician/doctor could be able to walk-through in the entire GI track to make a diagnosis.

A compression algorithm designed and implemented. Firstly, evaluation of proposed schemes, of the realized by the help of Matlab software. The compression algorithm that was suitable for a medical application like WCE, were implemented in hardware. The implementation in hardware is made with help of an FPGA development board using Hardware Description Language (HDL). Finally, the proposed compression algorithm was designed in Cadence tool-set software in 16nm FinFet technology. The proposed compression algorithm is designed to be able to connect directly to most common commercially available camera sensors. Furthermore, the output of the compression algorithm is not parallel, but the output data is in serial mode. This feature, makes the proposed system to be connected directly to any RF transmitter that is available now. The proposed system except from the compression performance, offers a compact system that can work as it is, without any modifications with most common used camera sensors and RF transmitters.

Apart from the compression algorithm, the design and simulation of a low energy wireless transmitter was made. Digital modulation, On-Off Keying (OOK) was used. The selection of the modulation and the

working carrier frequency was based in the body characteristics and the performance in the manner of bit-error-rate (BER) and low energy usage. A low power design of a specially implemented OOK transmitter is designed and simulated. The wireless transmitter is designed and surface optimized by using fewer internal and external parts, so it can fit inside the capsule. The design and simulation of the proposed wireless transmitter was done with the Cadence tool-set in 16nm FinFet technology.

Furthermore, there is another field of research in WCE. Until now, the research in WCE was focused on the internal part of the WCE, the pill. In our research project, the main effort was focused not only on the internal part of the WCE but also in the external part. The external part consists of a receiver, and a recorder, both of them placed in a jacket that the patient wears. In this research work a multi-receiver system is proposed. Existed systems use only one receiver and this introduces the possibility to receive false or corrupted data. For this reason, existing systems use bi-directional RF transmission link. While using bi-directional RF transmission link in the capsule, both transmitter and receiver should be placed. This needs more space and consumes more energy for operation. The proposed multi-receiver system eliminates the need of bi-directional link. Less space and power inside the capsule needed because there is no receiver inside the capsule to operate. Multi-receiver system is used also to increase the BER performance of the wireless link. While using multi-receivers, weak or corrupted reception of RF signal is eliminated because always there will be receivers with good reception that can capture the correct data. Furthermore, error correction algorithm is used that compares the received data of all the receivers which improves the decision making method for the transmitted data.

Finally, the entire WCE with a set of special lenses with a 360° degree angle of view is proposed. High resolution images can be captured and transmitted wirelessly. The set of special lens, low complexity and low energy compression algorithm, along with the use of the high data rate, low power transmitter, pushes the WCE technology to the next level.

Acknowledgements

During the preparation of this thesis, I was fortunate to have the guidance and support of many remarkable people, each of whom in his own way contributed to its completion. From this position, I feel, as a minimum indebtedness, the need to thank them warmly.

I would like to first and foremost thank my supervisor Professor Hongying Meng, whose guidance has always been essential and necessary. I thank him for our discussions in the field of scientific research and personal reflection. Thank him for our cooperation and his practical help over the last 7 years, for his patience, his friendship and his love. Without him, this thesis would never have been completed, and for that I express my gratitude. He is a model of academic teacher and human.

I would like to thank Professor John Cosmas for his continuous interest in the preparation of my dissertation and his well-intentioned criticism, for his constant encouragement and interest, his moral support, the knowledge he imparted to me, and our excellent cooperation over the years.

I also thank my life partner Margarita Patsia for giving me the opportunity to start, continue and complete this doctoral thesis and provided me with selfless and incalculable support during difficult times of moments.

In an act of recognition of their contribution to the completion of my Ph.D. dissertation, I express my gratitude to my colleague, friend and teacher Dr. Vasileios Vassios, Professor at ATEI of Thessaloniki in the Department of Electronics for the scientific help and valuable guidance he provided me.

In an act of gratitude, I would like to express my warmest thanks to my parents Georgios Intzes and Paraskevi Pasatsiflikiwti and my brother Stelios for the support, understanding, trust, love, moral and material support they have shown all these years. Without them, nothing would be possible. I hope to justify their expectations in the years to come.

In conclusion, I would like to thank my 2-years-old twins daughters, Anastasia and Georgia, for their daily "spiritual energy" kisses that, so richly, gave me every morning. They are dedicated to this thesis and I believe that their generation will achieve what they dream of.

With Appreciation

Ioannis G. Intzes

Contents

List of Figures

List of Tables

List of Algorithms

List of Abbreviations

AC	Alternating Current
AM	Amplitude Modulation
ASIC	Application Specific Integrated Circuit
ASK	Amplitude-shift Keying
BER	Bit Error Rate
CCD	Charge-Coupled Device
CE	Capsule Endoscope
CLE	Confocal Laser Endomicroscopy
CMOS	Complementary-symmetry Metal Oxide Semiconductor
CPU	Central Processing Unit
CR	Compression Ratio
DC	Direct Current
DCT	Discrete Cosine Transform
DPCM	Differential Pulse Code Modulation
DVP	Digital Video Port
DWT	Discrete Wavelet Transform
FEC	Forward Error Correction
FHD	Full High Definition
FICE	Flexible Spectral imaging Color Enhancement
FIFO	First In First Out
FOV	Field Of View
FPGA	Field Programmable Gate Array
FPS	Frames per Second
FSK	Frequency-shift keying
GI	Gastrointestinal
HD	High Definition
HDL	High Description Language
IMD	Inter-Modulation Distortion
JPEG	Joint Photographic Expert Group
JPEG-LS	Joint Photographic Experts Group - Lossless
KLT	Karhunen-Loeve Transform

LBI	Lifting Based Implementation
LUT	Lookup Table
LZ	Lempel-Ziv
MHT	Modified Hermiter Transform
MSE	Mean Square Error
NBI	Narrow Band Imaging
NMSE	Normalize Mean Square Error
OOK	On-off keying
PA	Power Amplifier
PE	Power Element
PSNR	Peak Signal to Noise Ratio
PTM	Predictive Technology Model
PVT	Process Voltage Temperature
QFSK	Quadrature Frequency-shift keying
QPSK	Quadrature Phase-shift keying
QVGA	Quarter Video Graphics Array
RICE	Radial Imaging Capsule Endoscope
RF	Radio Frequency
RGB	Red Green Blue
RLE	Run Length Encoding
RMSE	Root Mean Square error
SAR	Specific absorption rate
SCLA	Spatial Combinative Lifting Algorithm
SQ	Scalar Quantization
SNR	Signal to Noise Ratio
SRAM	Static Random Access Memory
SXGA	Super Extended Graphics Array
UHD	Ultra High Definition
UHF	Ultra High Frequency
USB	Universal Serial Bus
UWB	Ultra Wide Band
VCO	Voltage Controlled Oscillator

VGA	Video Graphics Array
VHDL	VHSIC hardware description language
VLSI	Very-large-scale integration
VQ	Vector Quantization
WCE	Wireless Capsule Endoscopy
WVGA	Wide Video Graphic Array
XGA	Extended Graphics Array
ZCS	Zero Current Switching
ZVS	Zero Voltage Switching

Chapter 1

Introduction

In this chapter, a small introduction about internal examination of human body and its role in the diagnostic procedures, will be reported. There are many medical test/diagnostic procedures for human body. Most of them are performed outside the human body, like blood analysis, toxicology tests, urinalysis, brain scanning, magnetic resonance imaging, etc.

There are many more that are performed outside the human body. However, there are few parts of the human body that cannot be examined externally. Nowadays, there no available diagnostic tests that can be performed outside the human body. The digestive system is one of them. The GI track which consists of many organs that play a major role in human health. The organs of GI track in order are, esophagus in the beginning, stomach, small intestine, cecum, colon and rectum at the end. [35] An overview of how these organs are placed in human body is shown in Figure 1.1. As mentioned a health issue in these organs if it's left untreated can lead potentially to life threaten situations.

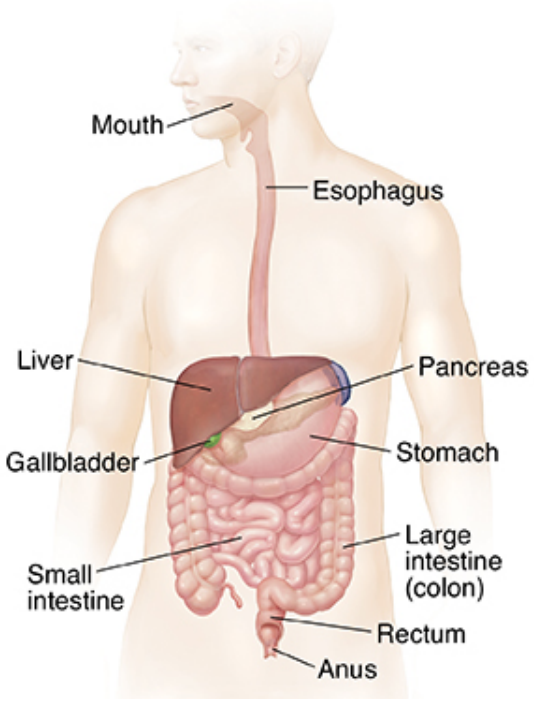

Figure 1.1: Human body diagram showing the main parts of the GI track. [1]

1.1 Background

Nowadays, the doctors use technology and, in this way try to minimize the feeling of pain in their patients. At the same time, they want a less pain-full examination with better diagnostic results. A classical endoscope is used by doctors in order to examine the gastrointestinal (GI) track. Endoscope is a tool made by fiber optics and is inserted into human body to capture a photo/video or extract tissue for biopsy. A typical endoscope tool can be seen in Figure 1.2. These tools help doctors to examine the large intestine (colon) and esophagus.

Figure 1.2: Commercial endoscope product, produced by Olympus. [2]

It is necessary to emphasize the disadvantages of the endoscopy procedure. First of all, endoscopy procedure is painful. Secondly, this procedure puts the patients under some risks such as bleeding, fever and pain in the area of the endoscopy, etc. [36] For these reasons some patients don't like or don't want to perform this procedure and the doctor doesn't have any other diagnostic tool to use. Another disadvantage that should be referred is that the endoscope cannot reach the small intestine. The next step in endoscopy is the wireless capsule endoscopy (WCE). A small pill consists of integrated electronic circuits, like RF transmitter, CPU, sensors, camera, etc. The pill captures and transmits useful data to the doctors. Also, such type of pills are used to collect tissue for biopsy. Such a procedure in the small intestine will not be able to be done without performing a surgical operation. So, the use of WCE provides advantages for both doctors and patients. Doctors can acquire precise clinical data of the patient and the patient can perform the examination without pain. A typical WCE procedure is the use of laxative that helps to clean the digestive track from "dirties". After this, the WCE is swallowed, a special belt with an integrated wireless receiver is used to receive the captured data (from sensors or camera). Then the received data is stored in a memory which is available later to the doctor to perform the diagnosis. This procedure takes from 8 to 12 hours and during this time, the patient, can go to work or do any other daily tasks. However, the patient should avoid any physical activity like running during WCE procedure. After 8-12 hours the battery life of the WCE runs out and stops the data transmission. [37] The capsule comes out of the human body by the natural way. It is a huge bottleneck that can lead to wrong diagnosis. Furthermore, existed systems lack from special lens that can lead to capture of more area. Also, the existing systems can miss-rate about 20%-30% of the human intestine. [38]

1.2 Motivation

This research project is focused on the design and implementation of a lossless-multiplierless image compressor with a suitable low power, high data-rate wireless transmitter. WCEs are tiny pills that are powered by tiny batteries. The design of a low hardware complexity compressor is needed, such a design will consume less energy. Also, by reducing the amount of data for transmission, the wireless transmitter will need less time of operation to transmit all of them. Moreover, the design of a wireless transmitter that can send faster and have a low power design will reduce the overall power, needed for the capsule to operate. As a result, from all of them is the increase of battery life. The increase of battery life will prevent the incomplete examination.

1.3 Aim and objectives

As noted in previous paragraph, the drawbacks of WCEs is the lack of energy. Capsule stops working before the end of its travel. The challenges in WCE is to increase the resolution of the captured images and the same time to keep the power consumption in low levels. In this research, the main aim is to design and implement a low-complexity, low power consumption, loss-less compressor and to design and implement a wireless transmitter that consumes low energy and is capable to achieve high data-rates. Based on literature review, the drawbacks and the areas that need improvement pointed out and the research objectives are set:

- A new image compressor will be designed and implemented with satisfied image compression performance with the conditions of easy implementation in hardware, lower computation complexity, lower requirements on hardware resources. A image database will be generated and image compressor will be design and evaluated in simulation, hardware implementation will be done and evaluated on FPGA and ASIC platforms.

- Low energy use and high data-rate wireless transmitter will be design and implemented for specific WCE applications. The suitable RF carrier frequency band and suitable wireless communication protocol will be investigated and selected. It will be implemented and evaluated using ASIC design tools in comparison with all the existing state-of-the-art designs in the world in term of data rate as well as power consumption.

- For the WCE receiver, a new robust multi-receiver system will be designed in order to reduce the communication errors and receive data from the proposed transmitter in previous work. In this work, human body model will be built and RF communication protocol will be used in the simulation. The performance will be then evaluated.

- In order to capture more information by the camera, the camera inside of WCE will be investigated and 360° degree lens will be used. The associated problem such as image distortion will be studied and associate algorithm will be developed and evaluated.

1.4 Thesis contribution

This work which is presented in this thesis gathers an amount of results that will improve the point of view of physicians/doctors in diagnoses using capsule endoscopy. There are 4 main contributions presented.

1.4.1 Lossless image compressor and its multiplierless implementation

The first contribution is the design and the hardware implementation of a lossless-multiplierless image compression scheme. The compressor is based in the statistical analysis of about 200 WCE images where statistics for each color plane are extracted. Red color plane was compressed using huffman encoder. It is the best way to compress red color without increasing the circuit complexity and the power requirements. Green and blue color planes were compressed using DPCM and huffman encoders. The use of DPCM was based in the analysis of WCE images. It was observed that the consecutive pixels of green and blue planes in WCE images were too close in value. So, a DPCM encoder was applied, and the results were passed into a huffman encoder. The results were acceptable, and complexity kept low due to the use of simple logic operations without multiplications. The proposed compression algorithm can be attached/connected in any commercial camera sensor that outputs the data in raster scan mode. The proposed design can process the incoming pixels directly and output the compressed data without need to store them. This provides another advantage in this implementation which is the need of memory buffer that is not used. In summary a loss-less, multiplier-less, memory-less compression algorithm with low circuit complexity is designed and implemented.

1.4.2 Design of FinFet On-Off Keying transmitter for wireless capsule endoscopy

The second contribution is the design and implementation of a high data rate wireless transmitter. The methodology used to create the proposed transmitter, was by creating the performance profile of the wireless transmitter needed.

There were some assumptions taken under consideration. The main assumption was that the system should work inside the human body. The second was the low power consumption and the third was the high data rate wireless link that is needed for transmission of the high resolution-images.

Because the pill is working inside the human body, the selection of the carrier frequency was set to 144MHz. So, there is less absorption of the RF signal from human body. The use of 16nm FinFet technology that was selected for the implementation, improves further the power performance of the transmitter and also to decreases the operating power supply in the level of 0.85V. Except from these, FinFet technology allows the integration of the matching network with the power amplifier of the transmitter.

Finally, an OOK wireless transmitter is designed and simulated using Cadence Virtuoso software suite. The performance of this design is up-to 33Mbps of data rate and an average power consumption as low as 1.04mW.

1.4.3 Intelligent system of wireless multi-receiver system

The third contribution is the design of a multi-receiver system for capsule endoscopy which increases the BER performance of these systems. Also, there is no need for a bi-direction wireless communication. So, there is an overall increase of performance in the power consumption domain. Furthermore, the BER performance can be improved.

This system was designed and simulated, and the algorithm was applied in the digital output of each receiver. A more intelligent system could apply the algorithm in the base-band signal of each transmitter. The proposed system applies the algorithm in the output of each receiver. Where the "decision" of demodulation for each receiver output is already made. Every analogue receiver has a threshold value for the output result. This is constant, so the performance of the system is only relied in the performance of proposed algorithm. For future work the design of a system without the use of hardware design RF receivers is proposed. The new system will consist of multiple A/D (Analog-to-Digital) converters that can work for RF signals and the new algorithm will be applied to this data.

1.4.4 Omnidirectional lens for use in wireless capsule endoscopy systems

In the fourth and last contribution the use of a special designed lens is proposed. This type of lens can capture with one image a frame of 360° degrees of view. Using this type of lens, the entire intestine could be captured. The main advantage only one frame is needed to capture a "ring" of intestine and transmit it outside the human body. Outside the human body a computer is used to deploy the ring image and stitch the multiple images and so the intestine map could be created. Existing systems are able to capture as many images as possible, but with the disadvantage of the power consumption. By this technique high resolution images can be acquired, and the output result is improved.

1.5 Thesis organization

This thesis deals about the state-of-art technology that supports wireless capsule endoscopy systems. Improvements for every part of the WCE is shown. Furthermore, the increase of the performance of the entire system is demonstrated. This thesis consists of six main chapters. The organization of this thesis is as follows.

In Chapter 2 a literature review of the entire WCE system is discussed. Existing works from universities and companies are presented and compared. This review helps the investigation methods in order to improve further the technologies of the WCE systems.

In Chapter 3, the proposed image compression algorithm is proposed. Firstly, a dedicated review of existing systems is shown. Also, several image compressors have been described and tested. Methods that were used are discussed and finally the proposed image compression algorithm is selected. In the end of this

chapter there is a comparison of the software and hardware implementation. The algorithm was evaluated in Matlab software and then it was implemented in hardware in an FPGA development board. Finally, the ASIC designed. Simulation is shown and a compablack with other existing systems is presented.

In Chapter 4 a dedicated review in wireless transmission systems for capsule endoscopy is discussed. The motivation of existed methods and the new technologies that arrive gave as the opportunity to design and evaluate the proposed system design and improve the performance of such type of systems. In this chapter the design was simulated and evaluated with existed systems.

In Chapter 5 an innovative design of a multi-receiver system is proposed. A literature review of existing systems in WCE was held. An explanation about our inspiration is written and then the proposed system is designed. A model of the proposed system is designed, and it is tested under various RF reception scenarios. In the end of this chapter the performance of this robust system is discussed. Also, further applications that this system can be used is discussed.

In Chapter 6 an ingenious camera lens is shown. In the beginning of this chapter a literature review of existing lens is made. Then existing systems in wireless capsule endoscopy systems is discussed. A comparative analysis of existing systems with the new approach was held. Implementation and results are shown at the end of this chapter.

The last Chapter 7 is a summary of the overall work made in this thesis. Discussion of future work is made.

1.6 Publication list

Parts of this research work have been published in journals and conference proceeding. “Design of wireless swallowable capsule with minimum power consumption and high resolution-images” presented in a research conference at the conference center of the University of Giannena in Greece at 8-9 May of 2015, the conference name was PAnhellenic Conference on Electronics & Telecommunications (PACET) 2015. “Intelligent system of Wireless multi-receiver system for Wireless Capsule Endoscopy” was presented at Electronic and Computer Engineering Brunel PhD Symposium (ECEBPS 2019) via Skype.

- I. Intzes, H. Meng and J. Cosmas, “An ingenious design of a high performance-low complexity image compressor for WCE”, MDPI Sensors 2020, Vol. 20, Issue 6, 2020
  https://doi.org/10.3390/s20061617 This article contains content which contributed to Chapters 3.

- I. Intzes, H. Meng and J. Cosmas, “Intelligent system of Wireless multi-receiver system for Wireless Capsule Endoscopy”, Electronic and Computer Engineering Brunel PhD Symposium (ECEBPS 2019), 2 pages, 2019.
  This article contains content which contributed to Chapters 5.

- I. Intzes, H. Meng and J. Cosmas, "High Data Rate FinFET On-Off Keying Transmitter for Wireless Capsule Endoscopy," VLSI Design, vol. 2018, Article ID 1757903, 7 pages, 2018. https://doi.org/10.1155/2018/1757903/.
  This article contains content which contributed to Chapters 4.

- I. Intzes, H. Meng and J. Cosmas, "Design of wireless swallowable capsule with minimum power consumption and high resolution images", Journal of Engineering Science and Technology Review Vol. 9, Issue 6, 2016, pp 39 − 42.
  This article contains content which contributed to Chapters 2.

- I. Intzes, H. Meng and J. Cosmas "Technology of Swallowable capsule for medical applications" International Journal of Biomedical Engineering and Technology, Vol. 14, No. 4, April 2014.
  This article contains content which contributed to Chapters 2, 3, 4 and 5.

Chapter 2

Literature review

In this chapter, an overview of the current technology and existed research, will be introduced. The results of this overview will identify the areas where further investigation and improvements needed. This review will cover historic data of WCEs, and other key technologies used during the years until today.

2.1 Wireless capsule endoscopy

Wireless capsule endoscopy (WCE) is a state-of-art technology for medical diagnosis of gastrointestinal diseases and illnesses [39, 40, 41, 42]. This idea was originally conceived in 1950 [43, 44].

The idea of WCE has it's origins in 1950's when a lot of research effort had been done to improve the diagnosis abilities using new technologies. Through the years, WCE has been named by different names like, smartpill, wireless endoscopy, video capsule, etc. The very first attempts of WCEs, used transmitters with low frequency carrier and the diagnosis was based only from the sensor's data like temperature, pH, and pressure [45, 46]. Later, WCEs were equipped with small cameras [47]. The most common diseases that WCEs can diagnose are

Figure 2.1: PillCam horizontal placement of the camera. [3]

some types of cancer [48], Crohn's disease [49] and obscure gastrointestinal bleeding [50]. Due to the technology evolution, WCEs were used for the diagnosis by small cameras with low resolution, combining sensors' data. The final diagnosis was more accurate.

For medical practice, capsule endoscopy was introduced commercially by the Israeli company GivenImaging, Inc. [47] at 2009. The first capsules were designed for investigating the small bowel because it was hard to examine with the traditional techniques. These commercial products were able to provide low resolution images at low frame rate. Nowadays there are capsules dedicated for specific investigation areas, such as esophagus (PillCam ESO) [47] and colon (PillCam COLON) [47]. Apart from GivenImaging, there are other companies offering similar products. The most recent product of GivenImaging, contains two cameras, (PillCam COLON) [47] horizontally placed in the pill, one in the front of the pill and one in the back, and it can support up to 30 frames per second. The academic/scientific community has also taken part in the evolution of this technology and has come up with interesting products and ideas.

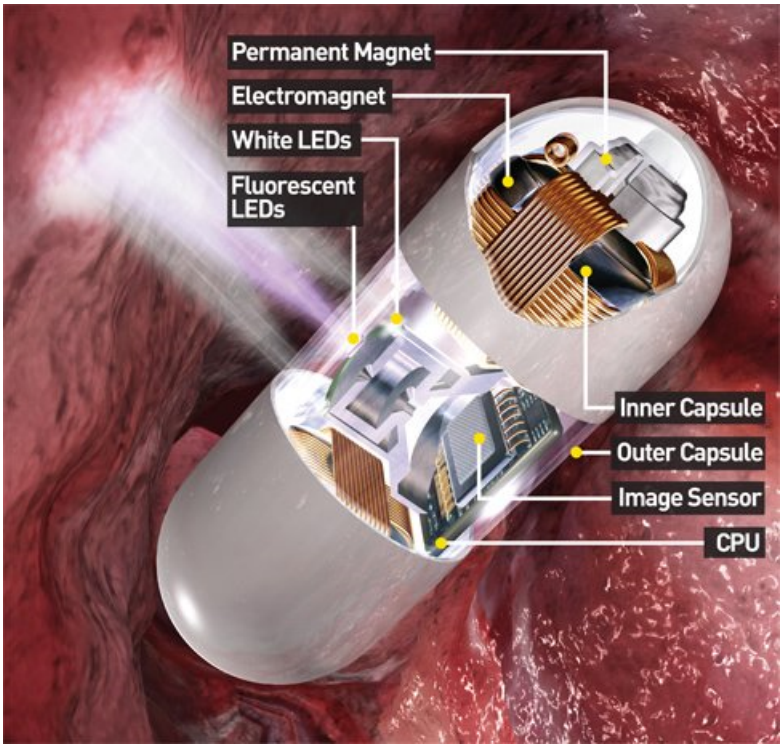

Figure 2.2: SAYAKA pill vertical placement of the camera. [4]

There is a plethora of WCE products, so categorization is needed. The pills can be categorized by their function as drug delivery capsule, sensor capsule, camera capsule and the most hardware complicated category, robotic capsule which has parts for locomotion and electro-mechanical actuators for biopsy. Usually it is difficult to categorize a capsule into only one category such as the drug delivery category. In this category the pill is composed with a "drug delivery" mechanism and a number of sensors. The pill is programmed in such a way that it can deliver the drug based on the sensors' data in the GI. In the category of sensor capsule, the pill uses sensors and a wireless system to transmit the measurements to a host computer for further processing. The most common sensors are temperature, pH, pressure and dissolved oxygen. The camera capsule category, as the title suggests, contains one or more cameras and with the use of wireless communications schemes, transmits the images/video to a host computer. Most of them have the ability for real time image/video representation. The last category is the most complex one that combines a lot of parts from the other three categories and has moving mechanical parts. One of the most interesting category is the camera capsule.

The evolution of technology and the decreasing size of cameras and microprocessors gain the interests of the scientific community to design and improve the existing systems to the next level. In this category, two different ways of camera placement are observed, vertically to the pill and horizontally. In Figure 2.1, is an example of horizontal placement from GivenImagine, Inc. In Figure 2.2, an example of a vertical placement of the camera in the SAYAKA pill from RF System Lab [4]. Due to the camera's placement and an electro-mechanical system, that can rotate the camera, SAYAKA pill can take 3600 photos. The camera module has a resolution of 2 mega pixels and a frame rate of 30 fps, a full rotation of the camera takes about 12 seconds. The drawback of this system is the unstable speed of the capsule. Due to this problem, approximately the 70% of the GI can be captured. Pills like this, with vertical placement of the camera, are used in the mapping of the entire GI with high resolution images. To accommodate different functional requirements, the pills have different resolutions and frame rates. For example the Olympus [16] pill has an HD camera module with a resolution of 1920×1080 pixels which is horizontally placed in the capsule and takes 2 frames per second. On the other hand, GivenImagin's pill takes lower resolution images but at a higher frame rate.

Capsule/Pill	Size mm	Weight g	Vision	Resolution	Field of view	Company/University
PillCam SB2	27×11	2.8	CMOS	256×256	156	Given Imaging
PillCam SB2EX	27×11	2.8	CMOS	256×256	156	Given Imaging
PillCam ESO2	26×11	<4	CMOS	256×256	169	Given Imaging
Norika	23×9		CCD	320×320		RF System Lab, JP
Endoscope	30×11		CMOS			Uni Kyungpook, KR
Endocapsule	26×11	3.5	CCD	512×512	145	Olympus
IVP	23×11		CMOS			IMS, DE
SAYAKA	NA		CMOS	2Mpixel		RF System Lab, JP
MiRoCAM	24×11	3.3	CMOS	320×320	170	Intromedic Co Ltd

Table 2.1: Table of existing WCE with camera and their characteristics.

Table 2.1 is the summary of the most known WCEs from companies and universities. At Table 2.2 shows a summary of wireless capsules without the use of camera as sensor. These types of capsules are only measuring pH, temperature, pressure or are used for drug delivery.

Capsule/Pill	Freq MHz	Size mm	Localization	Power	Company/University	Type
Enterion	1.8	32×2	Scintigraphy	external	Phaeton, UK	Drug delivery
Tohoku pH	N/A	2×2	N/A.	battery	Uni Tohoku, JP	Sensor
InteliSite	6.78	35×10	Scintigraphy	external	Glaxo, US	Drug delivery
IDEAS	38	36×12	NO	battery	Uni Glasglow, UK	Sensor
Radio pill	0.35	22×9	NO	battery	Mackay, US	Sensor
Telemetric	108	39×11	Cogwheel	battery	Strasbourg, FR	Drug delivery
HF capsule	4	28×12	X-ray	external	Battelle, DE	Drug delivery
Temperature pill	1	35×9	NO	battery	NASA, US	Sensor

Table 2.2: Table of existing wireless capsules that use sensor or are drug delivery pills and their characteristics.

Except from wireless capsules based on camera sensors there are wireless capsules that are using sensors like temperature, pressure, pH or are used for drug delivery. These are shown in Table 2.2. As it can be seen, there are using low carrier frequency for data transmission and their size is varying. Until now localization

of capsules is used only in sensor or drug delivery capsules. Radio Pill in Table 2.2 is the first ever pill implemented and used back in 1957. This pill was used for pH measurements, in Figure 2.3 a disassembly of the pill is shown.

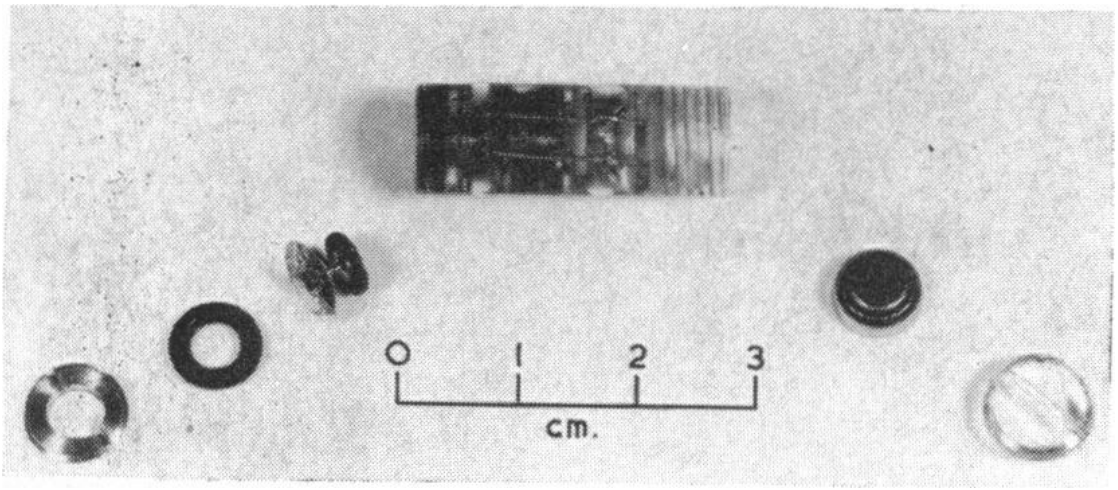

Figure 2.3: First capsule ever used back in 1957, for pH measurements. [5]

2.2 Diseases of the gastrointestinal (GI) tract

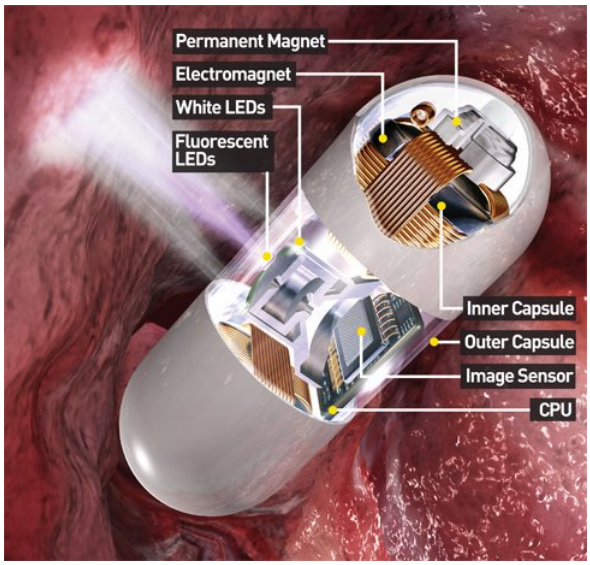

Figure 2.4: SAYAKA pill vertical placement of the camera. [4]

As mentioned in previous paragraph the most common diseases that WCEs can diagnose, are some types of cancer, Crohn's disease and obscure gastrointestinal bleeding, celiac disease, polyps and tumors of small intestine.

Crohn's disease is an inflammatory disease that can affect any part of the GI, from mouth to anus. Capsule endoscopy is very useful for the diagnosis of the small intestine where there is no other diagnostic tool for this area. In Figure 2.6 images of Crohn's disease is shown. Gastrointestinal bleeding means any bleeding of the GI track from esophagus to anus.

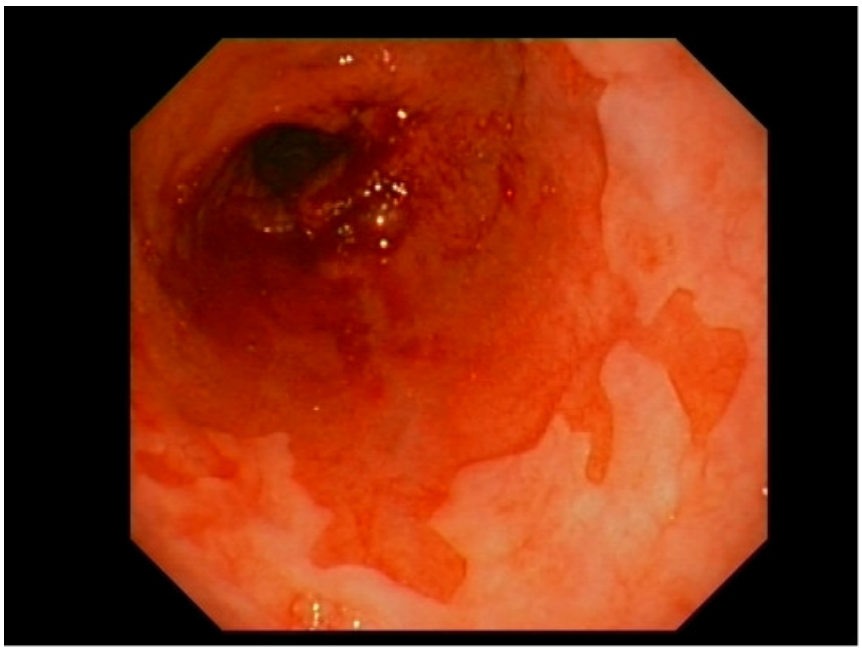

Figure 2.5: Wireless capsule images of bleeding. [6]

To diagnose it the most common methods are endoscopy and colonoscopy. These methods are painful for the patient. In Figure 2.5 a capsule's captured image of obscure gastrointestinal bleeding is shown. Both diseases can be diagnosed by the use a wireless capsule camera which is less painful.

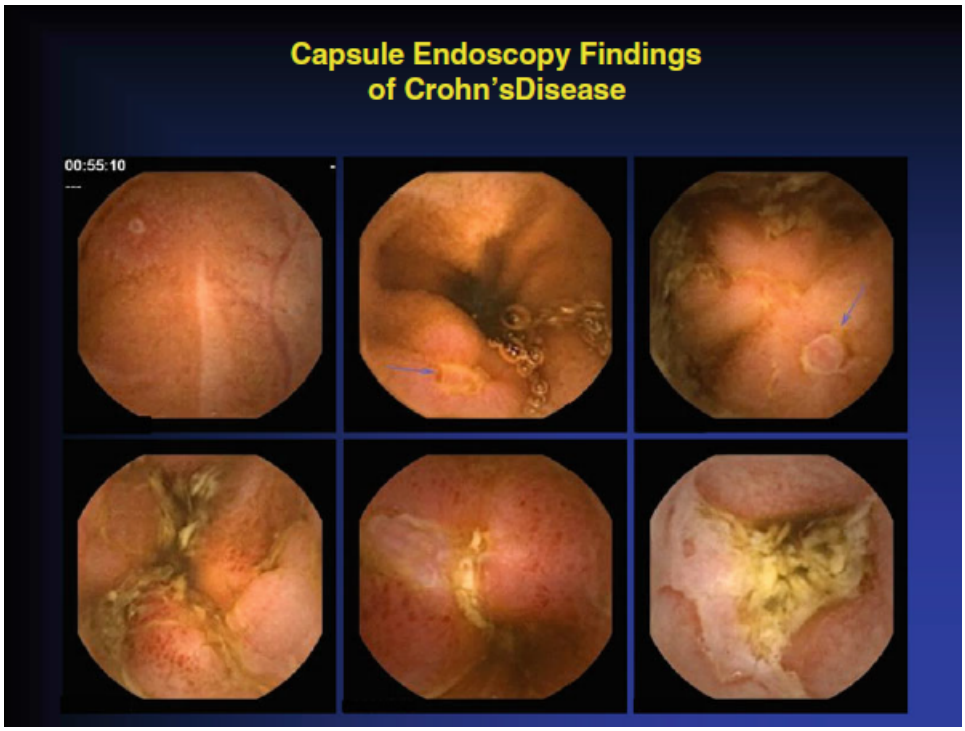

Figure 2.6: Wireless capsule images of Crohn's disease. [6]

By using WCE, some types of cancer can be diagnosed, and tissue can be taken from specific areas for biopsy. That is so important because wireless capsule can take tissue from the beginning of the colon

without the need of a surgical operation. The tissue then is coming out from human body with the capsule and it used for biopsy.

2.3 Key technologies in WCEs

The endoscopic capsules play a major role in the diagnosis of the GI. The traditional methods are painful for patients and is not possible to examine the entire GI.

It is obvious that to achieve the high demands and accuracy of medical diagnosis of the entire gastrointestinal track, state-of-art technology must be used.

A wireless capsule, despite its size, consist of a lot of electronic parts. There are sensors, the processing unit, the wireless transmission unit and the power management unit, which is usually integrated within the processing unit.

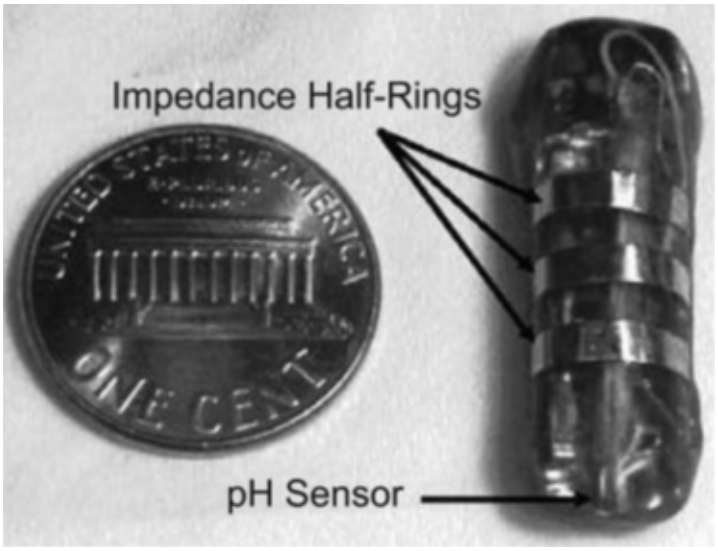

Figure 2.7: Prototype of the pH-sensing capsule, the pH sensor and the half-rings for impedance sensing can observed. [7]

In the part of the sensors, as previously mentioned, various types are used like, pressure sensor, temperature sensor, inertial sensor, pH sensor, conductivity sensor and oxygenation sensor. For example, with a pH sensor the detection of acidic reflux can be diagnosed, or with the electrical conductivity sensor the detection of non-acidic reflux can be diagnosed. [7] Both of these measurements can provide more information, for the final diagnoses, to the physicians.

2.4 Sensors and vision equipment

Normally every capsule contains one kind of sensor and can take measurements for up to 24 hours, like VitalSense ingestible telemetric physiological monitoring system, which is a pill that uses thermistor to measure the temperature. Another way to measure the temperature is the way that CorTemppill system utilizes. It uses the frequency oscillation of a crystal to sense the temperature [8]. However, there are capsules that contain more than one type of sensor. The Lab-on-a-Pill capsule [51] is a capsule that can sense pH, conductivity, and oxygen levels. The abilities of these biosensors can provide useful information to the physicians. Apart from these sensors new techniques are researched for specific uses, like biopsy.

Using light, the WCE can perform an optical biopsy without the need of extraction of tissue samples, which in some cases, may be impossible.

Figure 2.8: VitalSense pill system. [8]

In the section of sensor, camera modules are included. The pills that uses camera to diagnose are using state-of-art technology for capture, compression and transmission circuits. Just like the previous sensor, the camera's characteristics are dependent on the investigating area, such as esophagus (PillCam ESO) and colon (PillCam COLON). These two pills can be seen in the Figure 2.1. Two types of camera sensor are used, namely: CCD and CMOS. Most of the existing systems of camera pills are using CMOS technology camera sensor, except of Olympus EndoCapsule, that uses CCD.

The resolution of the camera is not the only criterion for obtaining the best images/video. In the part of a camera module the optic lenses can have a serious advantage in the final quality of the image/video. All the commercial products mentioned before have lenses with static angle of view. There is research in liquid lens and their electric control so the adjustment of the focal length can be obtained via electronics. [52]

In summary, there are a lot of challenges in the sensors inside. In the sensors of temp, pH, oxygen, conductivity, etc. the challenges are in the domain of the size mostly and in the accuracy. These types of sensors do not need high sampling rate because the pill is moving too slow. But in a vision sensor, or cameras, there are a lot more challenges that researchers need to provide a solution. For example, in these systems the need of clear and sharp images is obvious. So, a small camera with great characteristics (resolution, FPS, etc.) and optics is the area that needs to be improved. With high quality images, better diagnosis can be achieved.

Figure 2.9: Miniaturized prototype. [9]

2.5 Processing unit

All these sensors need control, so a processing unit is used. It is the heart of the capsule that can handle all the data from the sensors. It converts the analog signals of the sensors to digital for further processing, also takes huge amount of data from camera and compresses them so it can be possible to be transmitted outside human body with a low data rate wireless link.

A state-of-the-art development system of capsule endoscopy [9] has been created and can achieve QVGA resolution images at 19.53fps, the power consumption of this system is only 26mA@1.8V. At Figure 2.9 a prototype of this system is shown. It is obvious that the need of a high performance and low power consumption system is needed. The processing unit must have low power consumption but at the same time it must handle all these data in a short time. A novel design of a processing unit, as mentioned, has been made and has interesting characteristics. A VLSI design architecture of a three-stage clock management is applied, so a power saving of up-to 46% is achieved, compared to designs without this low-power technique. The main characteristics of this capsule design are the image resolution of 320 $\times$ 288 pixels at 8fps and transmitted via a wireless link of 2Mbps bandwidth. The process unit has been implemented in 0.18- m CMOS process and it consumes only 6.2mW (only the process unit). [53]

In the next paragraphs the compression algorithm techniques that are used in WCEs will be introduced.

2.6 Image compression

2.6.1 Background

When an image is captured by a camera sensor the raw data must be stored in a memory or transmitted. Due to the evolution of camera sensors, images that can be captured have high resolution. This produces the need of image compression to effectively store and/or transmit image data. For example, a low resolution RGB image of $512 \times 512 \times 8$ bit/pixel $\times$ 3 is about 786,4Kbyte of data without compression. If a compression scheme is applied the memory needed to store is less and if this data needs to be transmitted the time will be less and the energy needed for transmission will be less.

The last decades the amount of the data to be transmitted or stored is increased. This creates the need of fast transmission channels and a huge amount of storage. For these reasons data compression is needed. Data compression is the process used to reduce the amount of data to be transmitted or stored. This research investigates the implementation of an image compression method with low power consumption, low complexity and with the loss-less characteristic for images captured inside human body.

For endoscopic camera capsule, to work efficiently means mainly to perform the image compression more efficient. It was shown in [54] that about the 63% of the total consumed power, was used by the RF wireless transmission system. This was because the image compression did not compress enough the original image and for this reason the wireless transmitter need to operate more time. If a more efficient image compressor is used, the total energy consumed by the wireless transmitter could be reduced by 50%. Image compression and a low complexity circuit can contribute to the overall energy consumption performance of the entire capsule. The power consumption in these systems is a limitation factor due to the limited power capacity of existing batteries.

An image is defined by several pixels. These elements represent a value which can be 8-bit or 16-bit depth. This data values without compression will be hard to be transmitted or stored. The purpose of image compression is to reduce the data to be transmitted and at the same time to keep the information contained in the original image. Multimedia applications which contain video/image and audio data need high bandwidth channels to be transmitted or huge storage. Data compression has a significant role in the evolution of data streams, while compression techniques achieve higher compression ratio (CR), data streamed are in better quality with increased image/video resolution and higher audio quality. In real word the data are analog and are converted to digital. This conversion provides the ability of transmission and storage. Compression techniques are studied for years and will be improved further over the next years. In image/video data, compressors and de-compressors, are named CODECS and are implemented in software. However, in applications which need low complexity and low power consumption CODECS can be implemented directly to hardware. The hardware implementation improves the speed, the power consumption and the complexity. There are two categories of image compression techniques, the lossy and the lossless compression techniques.

In lossy compression techniques the original and the reconstructed image are not identical. Depending on the requirements of the application, the selection of the image compression technique is made. In capsule

endoscopy the requirements need a lossless technique, so the reconstructed image will be the same, with the original and will provide useful information to the physician/doctor without any loss. In data compression to design a compressor it is important to recognize the redundancies in data. There are three types of redundancies. The coding redundancy, the inter-pixel redundancy and the psycho-visual redundancy. In image compression when one or more of these redundancies is reduced then the total amount of data is reduced. By removing all this unnecessary data, the compression is achieved without the loss of important information. Psycho-visual redundancy means the redundancies where the human vision is sensitive. In compression based on these redundancies the reconstructed image is not identical with the original. However, the results are acceptable. Inter-pixel redundancy based on the statistical analysis along the pixels of an image and especially between neighbor pixels. The last type of redundancy is the coding redundancy. In this technique of compression, the fixed length of the uncompressed pixels are represented by variable length. By this way, the original image size is reduced, and compression is achieved.

$$CR = \frac{N}{N'} \tag{2.1}$$

In Equation 2.1 N represents the amount of data of the original image and N' is the data of the compressed image.

2.6.2 Compression methods

The compression methods can be classified in two main categories, lossy and lossless methods. In lossy compression methods the reconstructed image is not the same with the original. This degradation of the image can give a CR of 50:1 or higher. However, in lossless compression methods the reconstructed image is identical with the original. The main disadvantage of lossless methods is that CR can be about 2-3:1. The method to use is selected based on the application. In medical applications, loss-less methods are a requirement. The reason is that there is no degradation in the reconstructed image and the physicians/doctors could perform a more accurate diagnosis.

2.6.3 Lossy compression methods

Lossy compression methods, as its name implies, are methods where high compression ratios but with a reconstructed image which differs from the original. In most lossy methods there are three stages of the compressor.

2.6.3.1 Transform coding

As seen in Figure 2.10 the first stage of a lossy image compressor is the transform coding. There are various transformation techniques like Karhunen-Loeve Transform (KLT), Modified Hermite Transform (MHT) Discrete Cosine Transform (DCT), and Discrete Wavelet Transform (DWT). The result of transform coding is the separation of coefficients that contain the most energy of the picture and the coefficients with

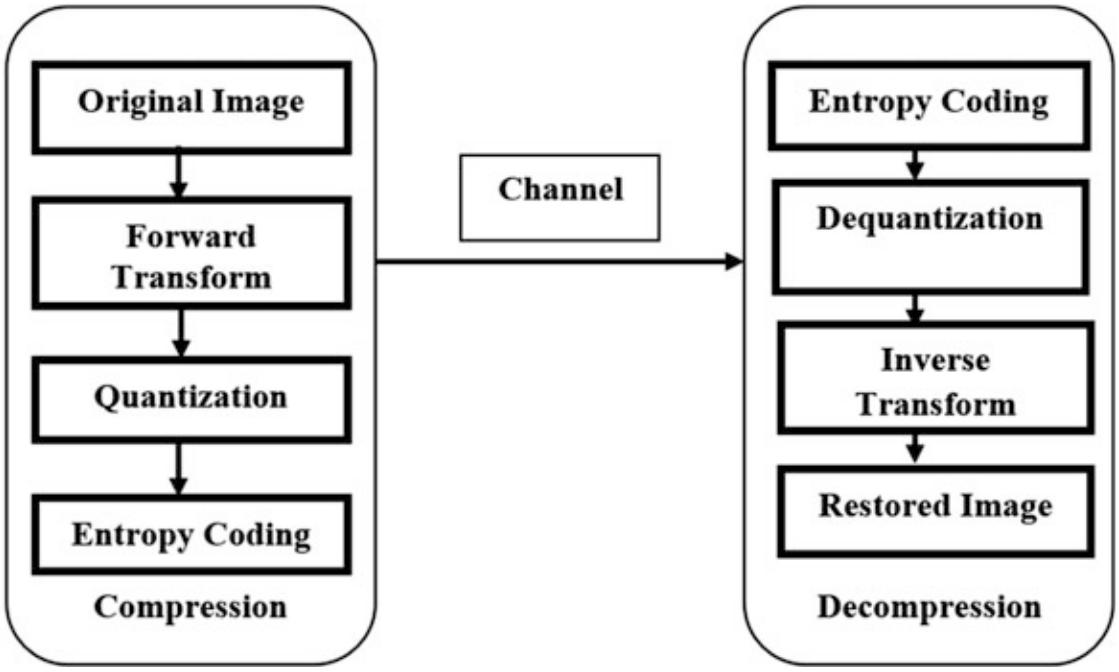

Figure 2.10: Block diagram of a typical procedure of lossy compression. [10]

low energy. Coefficients with low energy can be quantized or deleted with low visible damage in the reconstructed image. Thus the compression is lossy. Karhunen-Loeve transform is a statistically based transform method. It can be applied in one image or sequential images. However, it will not have the best performance if the input image is not in the statistical basis set. Discrete Fourier Transform has also good performance in transform coding. It is not based in statistical models like KLT. Its disadvantage is when dealing with large images it requires high accuracy coefficient numbers, which is hard to implement in hardware. Like DFT, Discrete Cosine Transform performs better than KLT and in practice DCT is used by most of the transformations due to the need by the half of storage compared with DFT. The most used transformation is DWT. Like the other types of transformation it can be applied in blocks. There are many different wavelet functions applied to different applications. The first wavelet transform was invented by a Hungarian mathematician named Fred Haar. Is one of the simplest transforms that can be applied. One of the most widely used in image compression/processing is Daubechies and it was invented by the Belgian Mathematician Ingrid Daubechies in 1988.

2.6.3.2 Quantization

Next block after transform is the quantization block. There are two types of quantization, the Scalar Quantization (SQ) and Vector Quantization (VQ). In SQ a many-to-one mapping of each pixel is performed and in VQ the input is replaced by a close to the input value. Shannon [55] showed that VQ can reduce the bit rate than SQ. An example of use is after DCT transform when DCT is applied the output of this block produces fractions. The quantization block rounds the fraction to the nearest integer. It is obvious that by rounding, a part of the image is lost. The reconstructed image will not be identical with the original.

2.6.3.3 Entropy coding

The last block is the entropy coder. In this block further compression is made. The basic and widely used entropy coders are huffman encoder and Arithmetic coder. In huffman coding a table of probabilities of each pixel value which occurs frequently is replaced with a value with less bits.
Arithmetic coding works like huffman coding, the value which occurs frequently is represented with less bits. The main difference is that arithmetic coding encodes the entire message. Huffman encoder replaces each input symbol separated from the other.

2.6.4 Lossless methods

In previous paragraphs fundamental facts of Lossy compression methods is described. As mentioned in lossy compression methods a three-stage compressor is used, in loss-less methods a two-stage compressor is used. In Figure 2.11 a block diagram of a typical loss-less Compressor is shown.

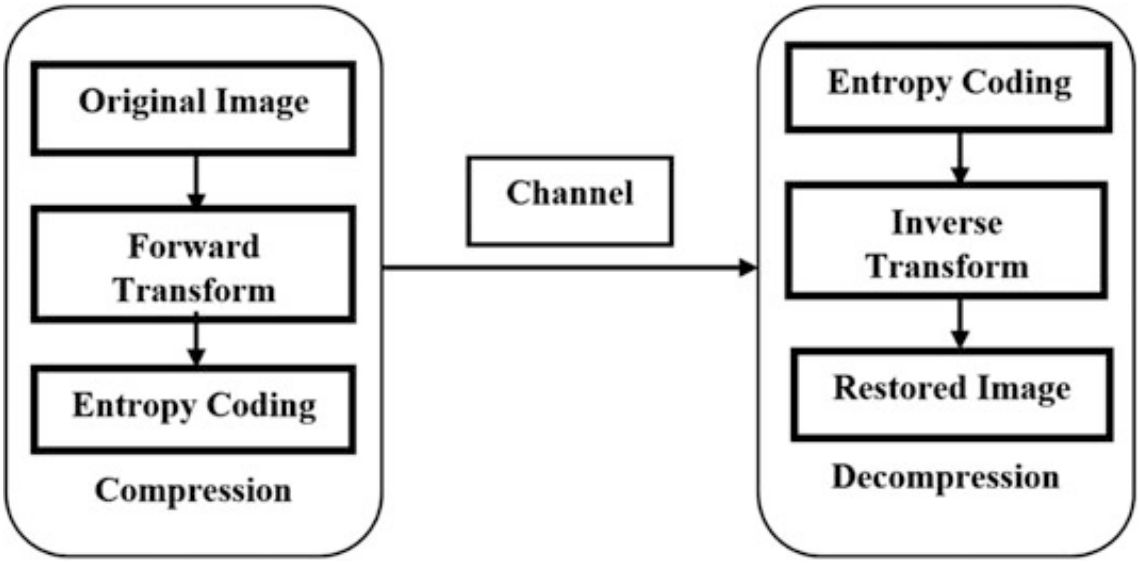

Figure 2.11: Block diagram of a typical procedure of loss-less compression. [10]

As seen in Figure 2.11 the original image goes first to the transform block where the image pixels are transformed to another format to reduce inter-pixel redundancy. Next stage is the Entropy Coder. In this block the coding redundancy is removed, and image compression is achieved. There are four categories of loss-less methods, that will be described in the next paragraph. These four categories are Run Length Coding, Predicting Coding, Entropy Coding and Multi-Resolution Coding.

2.6.4.1 Predictive coding

Predictive coding is used in loss-less compression schemes. It is working by predicting the difference between neighboring pixel values. So, in the place of the original value of the pixel the encoded value is the difference between two successive pixels. Normally the difference/error between two successive pixels has lower value than the pixel itself, so less bits required to store or transmit them. The most Known Predictive

coding method is Differential Pulse Code modulation (DPCM). In this predictive coder the JPEG loss-less compression is based. This encoder is based in the fact that successive pixels have significant correlation. So, the difference between successive pixels will have a lower value than the pixels value and can produce an output with lower bits. In Figure 2.12 a histogram of Lena's gray-scale image is shown.

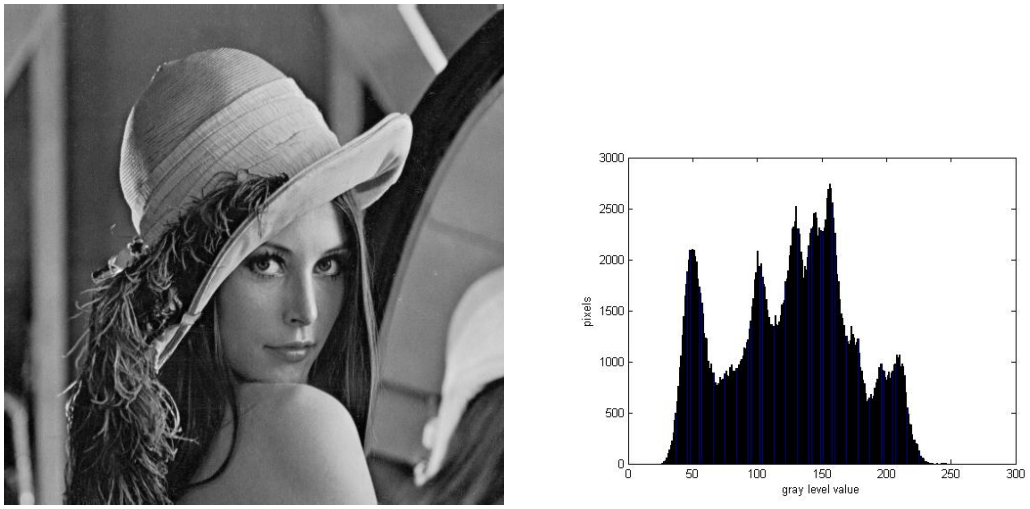

(a) Grayscale image of Lena.

(b) Histogram of Lena's gray-scale image.

Figure 2.12: Lena gray-scale image with its histogram.

.

It is obvious that in the right histogram where DPCM encoding is applied, that the compression is easier to compress due to the fact that the most frequently pixels are in the center of the histogram. Can be compressed with a value with fewer bits and higher compression ratio could be achieved.

2.6.4.2 Entropy coding

Entropy coding, are the algorithms used to decrease the entropy of the system. Entropy by itself means how random a system is. In image compression an original image with low entropy means that it needs less bits to compress and represent the original image without any loss of information. According to Shannon entropy theorem, to find the entropy of source S the equation is:

$$H(S) = -\sum_{i=1}^{m} p_i log_2 p_i \tag{2.2}$$

In Equation 2.2 S is the input source, i is the input symbol and p_i is the probability of occurrence of each symbol. The measurement output of Shannon entropy is the information in unit of bits/symbol. There are a few entropy coding techniques that are used in image compression. The most known are huffman coding [56], arithmetic coding [57], run-length coding [58], etc. All these coding techniques can compress without any loss of the input image. In the next paragraphs a small introduction of these techniques will be made.

2.6.4.3 Huffman coding

Back on 1951 David A. Huffman [56] was assigned to solve the problem of finding the most efficient binary code, by his Professor Robert M. Fano. In the end of this term paper he concludes with the known huffman coding. Huffman coding compresses data by assigning small code-words to most frequent values and wider words in values that are less frequent. A simple example to understand the way it works is, if a symbol has 16-bit width, the most frequent the huffman coder will represent it with a prefix code that has less bits. By this way huffman coding reduces the size of original data/image. In huffman coding when saying prefix codes, it means that no other code of another symbol could be the same. Huffman coding is based on occurrence probabilities. First thing is to build the huffman tree, which is used to assign the new prefix codes to each input symbol. To create the huffman tree there is a specific methodology. In Table 2.3 a simple example of input symbols and there fixed-size codes is shown.

Table 2.3: Input symbols and their fixed length is shown

Symbol	Fixed-length code	Occurrences
A	000	4
B	001	2
C	010	16
D	011	6
E	100	8
F	101	12

Assuming the next message must be compressed.

$$ACBCFFCDEF \tag{2.3}$$

Then the total uncompressed data will be 30 bits. While applying huffman coding to this message the results are shown in the next table.
The final compressed message will have only 25 bits. The compression rate of this example can be computed by the Equation 2.1. The result is 1.2.

2.6.4.4 Arithmetic coding

Arithmetic coding is a method that can compress data without any loss in reconstruction. It is used both for photo and video compression. It is an entropy coding and it is like huffman coding. Like huffman coding, for Arithmetic coding to work, it needs to produce a data table of the symbols and their probabilities of occurrences. The main advantage of Arithmetic coding over huffman coding is that it encodes the inputs as in single data and not like huffman which treat them symbol-by-symbol. As a result, is to produce better compression than huffman coding. A simple example is described below. In this example there is a total of four separate symbols and their probabilities:

- **Probability 60% of symbol A**

- **Probability 20% of symbol B**
- **Probability 10% of symbol C**
- **Probability 10% of symbol END**

So, for this example the table is converted:

- **A [0 , 0,6)**
- **B [0,6 , 0,8)**
- **C [0,8 , 0,9)**
- **END [0,9 , 1)**

If the result of the compressed data is the number 0.538. The decoding will start for the first character in this way. We firstly try to find in which range it belongs. Number 0.536 belongs to the range of 0 to 0,6. So the first character should be A. For the next step, the table is transformed. The results are below:

- **A [0 , 0,36) - 60%**
- **B [0,66 , 0,48) - 20%**
- **C [0,48 , 0,54) - 10%**
- **END [0,54 , 0.6) - 10%**

Now we need to find where the number 0.538 belongs to. As we can see the next symbol should be C. The next step is to transform the table with the new values.

- **A [0,48 , 0,516) - 60%**
- **B [0,516 , 0,528) - 20%**
- **C [0,528 , 0,534) - 10%**
- **END [0,534 , 0.54) - 10%**

This table shows that the value 0.538 belongs to symbol END. Because by using this symbol as the termination symbol of the message, we know that this is the end of the transmission packet. Decimal numbers are used in this example for convenience. Converting the compressed signal into binary, 8 bits of accuracy (10001010) are needed. This was a simple example of how an arithmetic coder works. A major disadvantage of the Arithmetic coding is that a simple error in the transmission of the compressed signal could cause a decoder fault and the transmission packet to be corrupted. One-bit error could cause many symbol losses because arithmetic coder processes many symbols in one packet. In the other hand in huffman coding a one-bit error could make the decoder lose only the symbol where the error bit occurred.

2.6.4.5 Run length coding

Run Length coding is a loss-less compression method where the encoder replaces the input data to length and value in the output. Where value is the data, in the input, repeated and length the time this value occurred. This method of compression is more effective when the image is separated in bit-planes. A simple example and the RLE output is shown in the next Figure 2.13.

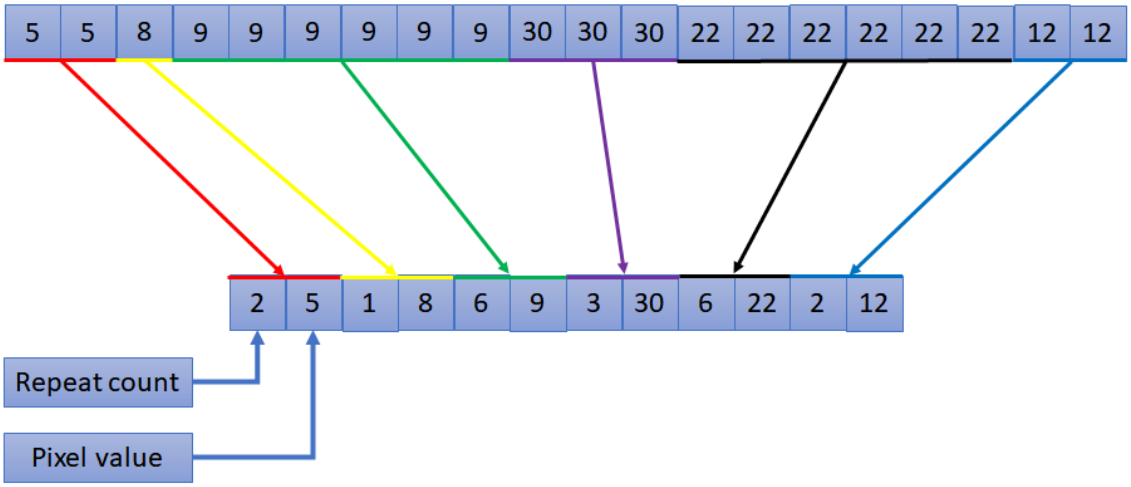

Figure 2.13: Block diagram of RLE system and how it works.

2.6.5 Measurements for compression methods

As mentioned, there are two main categories of compression methods, lossy and loss-less. In both categories there are some measurements we can use to characterize the performance of each method. In lossy compression methods due to the distortion of the reconstructed image there are three measurements that can be applied: Normalize Mean Square Error (NMSE), Root Mean Square Error (RMSE) and Peak signal-to-noise Ratio (PSNR).

$$NMSE = \frac{\sum_{x=1}^{N}\sum_{y=1}^{M}(\bar{D_{xy}} - D_{xy})^2}{\sum_{x=1}^{N}\sum_{y=1}^{M}D_{xy}^2} \tag{2.4}$$

$$PSNR = 10log\frac{255^2}{\frac{1}{NM}\sum_{x=1}^{N}\sum_{y=1}^{M}(\bar{D_{xy}} - D_{xy})^2} \tag{2.5}$$

$$RMSE = \sqrt{\frac{1}{NM}\sum_{x=1}^{N}\sum_{y=1}^{M}(\overline{D_{xy}} - D_{xy})^2} \tag{2.6}$$

where N and M are the numbers of pixel that compose the image. We assure the size of its pixel is 8-bits. D_{xy} represents the original image and $\overline{D_{xy}}$ the reconstructed for quality measurements, of lossy reconstructed images, only NMSE and PSNR are preferred. These measurements are effective for comparison only between lossy compression methods. In loss-less compression methods is useless to use the above measurements. The reason is because there is no distortion or information loss in loss-less compression. A

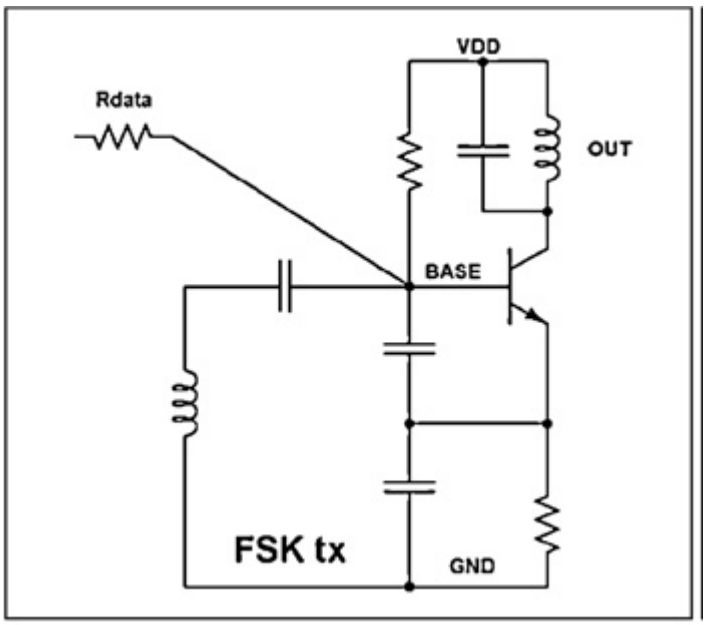

Figure 2.14: Wireless transmitter of 2 Mbps data rate and 2mW power consumption. [11]

good measurement for loss-less methods comparison is the bit rate. Bit rate measures the average number of bits needed to represent a single pixel of the original image. The bit rate is measured at bpp (bit-per-pixel), it is obvious that lower this number is the better compression is achieved.Finally, the most important measurement, that can be applied for both lossy and loss-less methods, is the Compression Ratio (CR).

$$CR = \frac{N1}{N2} \tag{2.7}$$

where N1 is the original size of the image and N2 the compressed sized. The higher CR means lower amount of data to be stored or transmitted.

2.7 Wireless transmission

The ability of the capsule to achieve high quality diagnostic results mostly relies on the wireless communication link and its characteristics.

Endoscopic capsules have some characteristics which are unchangeable, like its size. It is obvious that with this small size the energy that can be stored, is too low. So, the power consumption is an important criterion for the design of the whole system and especially of the wireless link. The circuit for wireless transmission can be made by commercially available chips but in most cases the utilization of a custom solution is used due to the small size needed. The wireless link used in wireless pills can be categorized into two categories, the bidirectional and unidirectional. In most cases the use of a unidirectional link is implemented, since the reason is that the capsules are only transmitting the compressed data of the sensor/camera to the external device for further processing. A unidirectional wireless link is proposed in this paper [11]. Is a design of a simple topology FSK modulation transmitter that can achieve up to 2Mbps of data rate and power

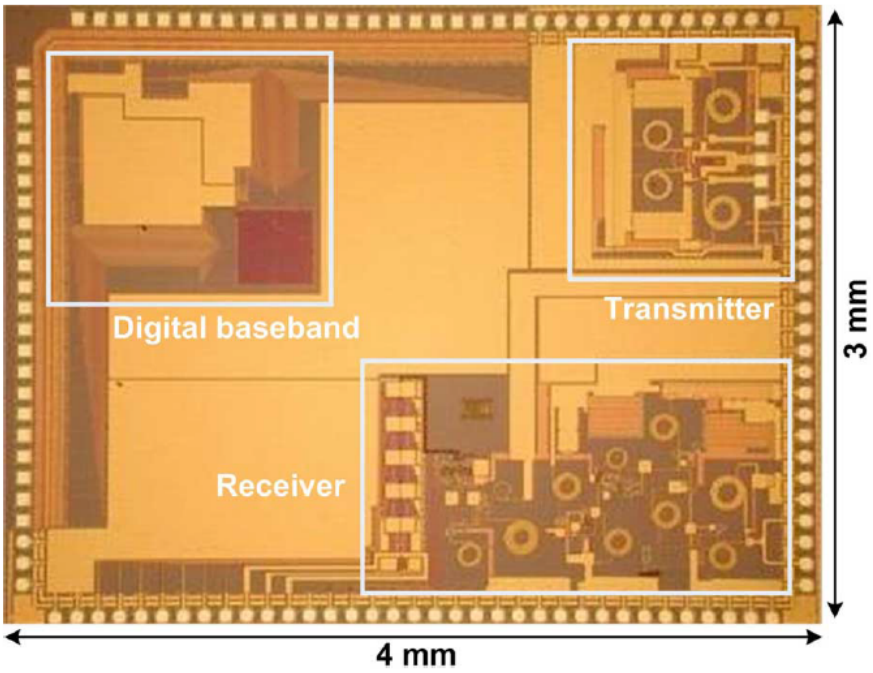

Figure 2.15: Die photo of the transceiver system. [12]

consumption to as low as 2mW at 1.8V. This was an example of a wireless unidirectional circuit used on the other hand there are also system with bidirectional links. The reason for using a bidirectional link is that there are some robot capsules that need to receive commands from outside the patient's body.

A design of a uni-directional wireless link has been made [12] and has great characteristics. It has an up-link up to 10Mbps and a down-link of 10Mbps. Down-link and up-link are both configurable from 1Mbps to 10Mbps. It works in Ultra-Wide Band (UWB) frequency area at 3-5GHz. Both transmitter and receiver consume only 10mW with a work cycle of 80-100% and 1-80% respectively. Due to the small data rates that the existing systems have, the resolution of the images is not high, and they operate at a low frame rate 2-4fps. So, the design of a wireless link with high data rates and with low power consumption can improve the performance of the whole system. In the next table a few high-performance designs are presented.

	Power requirements [mW]	Freq. [MHz]	Data rate [Mbps]
Shen (2005)	4mW@1.85V	416	2
Chi (2007)	7.9mW@2.5V	2400	1
Itoh (2006)	1.4mW@2V	20	2.5
Liu (2007)	19.5mW@1.5V	400	1.5
Hancock (2007)	9.7mW@1.8V	1.35-1.75GHz	2
Turis (2007)	6 mW@1.7V	120	1
2Mbps-2mW TX (2008)	2mW@1.9V	144	2
UHF Transmitter(2010)	3.9mW@2.5-3.3V	400	3
A Low-Power 13.56 MHz(2012)	0.594mW@1.8V	13.56	-
2 Mbps FSK near-field transmitter (2009)	2mW@1.8V	144	2
Wireless power and data transmission (2011)	5mW	333	2
Low-Power Ultra wideband Wireless Telemetry (2011)	0.35mW	3-5GHz	10
A Low-Power, High Data-Rate CMOS ASK (2012)	7.2mW@1.8V	902-928	15

Table 2.5: Comparison table of existing wireless systems for capsule endoscopy.

2.8 Power stage

The power stage of an endoscopy capsule is the most important part. Especially for the robotic capsules this part is critical. Generally, the power stage has two different types, the battery powered capsules and the capsule that uses wireless energy transmission. It is obvious that the second type has the advantage of the uninterrupted power of the capsule. It is known that there are commercial batteries with high capacity and an extra small size, but it is certain that these commercial batteries cannot be used in case of a medical capsule because the material used in the battery must conform to International safety standards. Endoscopic capsules use for power silver-oxide batteries like the one's watches use. This type of battery are approved for clinical use. [59] It is impossible to power a robotic capsule using this kind of batteries, since they can only be used for sensor-based capsules.

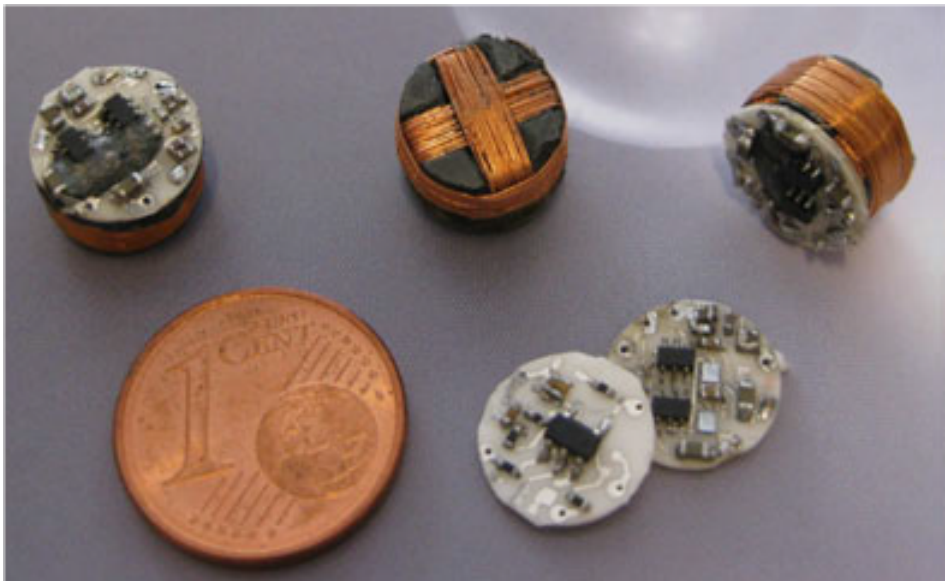

Figure 2.16: 3D coils of an energy harvesting system compared with the size of 1-cent coin. [13]

The category without battery can provide the capsule with much more energy but the system for energy harvesting is bigger than a battery. Figure 2.16 shows such systems and comparison with the size of 1-cent coin. A system with high energy consumption is a 12-legged robotic capsule [60] and consumes up to 300mW of energy. It is obvious that in such a system, it is not possible to use only batteries to power it.
In system with low energy consumption, battery is the best solution. But in robotic capsules system, the use of wireless energy transfer is more suitable. An inductive power transmission has been developed [13] and can deliver up to 150mW. This system is designed to work at 1MHz and has an efficiency of about 90%. The selection of this frequency was due to the restriction of the SAR, so with this frequency, the absorption rate is kept down to 0.4W/Kg. The whole system can fit in 10mm ø and 13mm length.
In previous paragraphs sensors/cameras, process unit, wireless and power system are discussed. These parts are frequently used in the endoscopic capsules. There are also some types of capsules that use three different systems, localization, locomotion and intervention and tissue manipulation systems. [61] All of them are used in robotic capsules except of the localization system that some sensor capsules are using.

2.9 Localization

To determine where the images/video is taken or where the robotic capsule must operate, localization systems has been researched and developed. These systems give the ability to the physician to have a clear view of the problem when they are looking at an image which is captured from the capsule. It helps to know the distance travelled so an intersection or the diagnosis can have better results. There are a few ways to locate the capsule in the GI. The most known and used is the RF localization. It uses the triangulation of the radio frequency that the capsule transmits to compute the capsule's position. RF localization is used by the commercial product of Israel Company GivenImaging M2A capsule. [62]

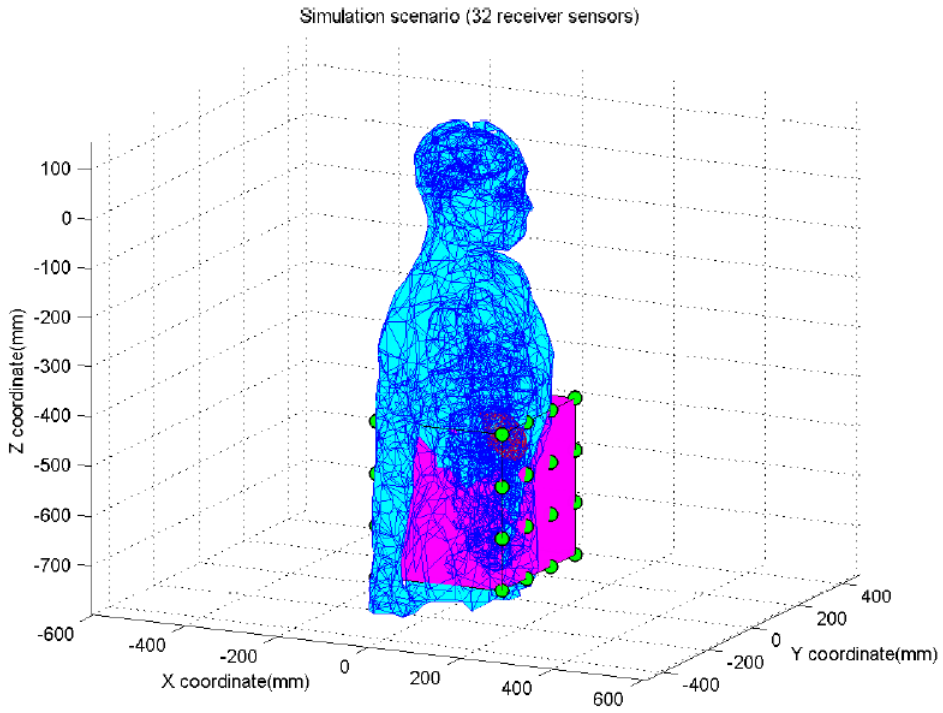

Figure 2.17: Simulation of 32 sensor localization system. [14]

This technique is commonly used because it needs only external sensors to find the location of the capsule and is not expensive. A work in localization systems reported in [14], found that by the use of 32 external sensors, 16 in front of the patient and 16 in the back of the patient great accuracy can be achieved. The system is working at 402-405MHz.

Human gastrointestinal track is a challenging environment for investigation. It has the ability to move into the abdominal cavity and this means that is difficult to know where the pill is located. This problem can reduce the opportunity of a physician to make a diagnosis. This system, by providing the location of the pill, may make the captured image more understandable. As mentioned, the GI is moving into the abdominal cavity so there are many curves and fewer straights surfaces and some images are not clear enough, so without the location of the pill it is too hard to understand a possible disease. It is obvious that the localization system can take a major role into the diagnosis.

2.10 Locomotion

The movement of the capsule is made by the movement of the GI, named peristalsis. There are typically two main categories of locomotion, the active and the passive. Peristalsis is a passive way which does not need any electronic circuits or special mechanical design of the capsule. The active category has obtained a lot of interest. In passive locomotion, a physician is not able to control the movement of the capsule. Due to this problem, critical images will not be captured, and the diagnosis will be incomplete. Using of active locomotion, the physician can “drive” the capsule and take more images, which are probably clearer, at the areas of interest. There are two categories of active propulsion methods, internal and external. The internal

method uses micro mechanisms to move the capsule and the external uses external forces like magnetic field.

2.10.1 Internal

Internal method of locomotion uses state of the art electrical and mechanical design to work. Capsule with internal locomotion uses "legs" for locomotion. The main advantage of this technique is the physical contact and the movement can be more precise.

There is a lot of research effort in internal locomotion techniques. Another technique of locomotion is proposed [15] and it uses special alloys that have shape memory. This means that they use this special function of these alloys to make movement. There are various ways to create movement. Another approach is the propelled capsule, which is using a propeller to give a boost in the movement of the capsule.

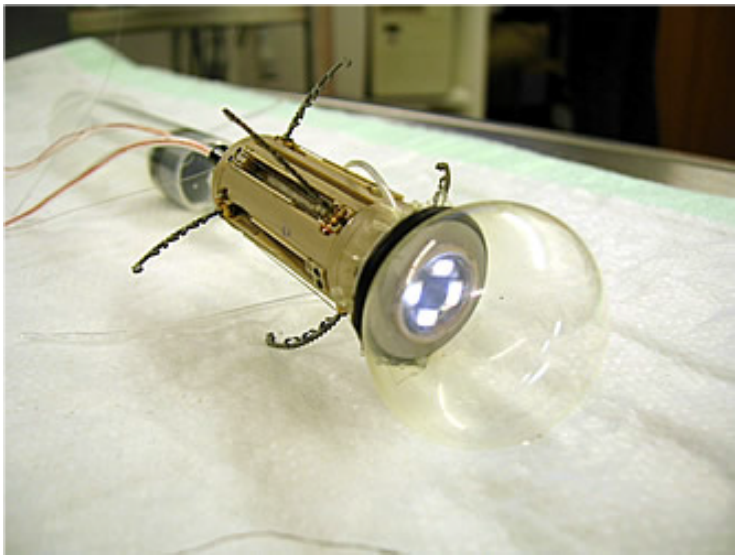

Figure 2.18: Capsule with legged locomotion. [15]

2.10.2 External

In the previous section, a description of internal locomotion systems has been presented. There are also commercial products and capsules under research with an external locomotion system.

The method used for external locomotion of capsule is by using of magnetic fields. Such systems have been introduced previously for use inside humans' eye. [63]

Magnetic locomotion systems have a lot of advantages. The most useful and critical advantage of that the system, unlike internal locomotion system, does not need a lot of components, just coils or permanent magnets. This means less space is needed. Such a system does not need actuation mechanisms and extra batteries for locomotion. In the design of an external locomotion system the use of magnetic coils or a permanent magnet are taken under consideration. The use of magnetic coils can provide better control of the capsule, but permanent magnets can provide a stronger magnetic field in a more compact system and without the use of a power source.

It is obvious that the external locomotion technology has a lot of benefits and has started the research for a commercial product. In their design for the external magnetic coil they used a handheld magnet to generate

the magnetic field for the capsule's locomotion.

In summary, the use of external locomotion in capsule endoscopy is a state-of-the-art technology. There are also some drawbacks that should be solved. The equipment required for control of the capsule's locomotion is expensive and in some cases the patient must stay to the hospital to do the diagnosis. Furthermore, the cost of such systems may be prohibited for use in small clinics or in doctors' offices. However, the advantages of these systems can provide accurate diagnosis and can perform better biopsy for patients. A hybrid system that can combine the advantages of both external and internal locomotion can achieve better results and solve the problem of locomotion.

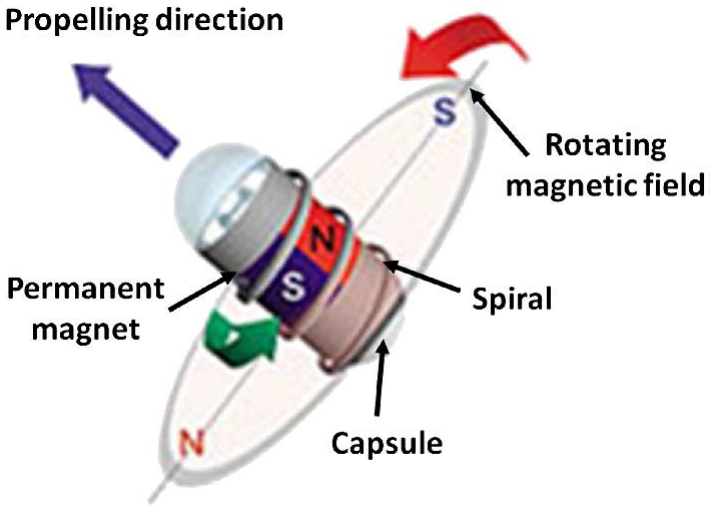

Figure 2.19: Olympus Inc. magnetic locomotion capsule concept. [16]

2.11 Summary

In previous paragraphs, the main parts of different capsule endoscopy pills was presented. Improvements for all of the parts has been attracting a lot of research effort. However, improvements need to be held in compression algorithm and wireless transmission sub-systems. It is shown that there are not high resolution capsule that can provide better images and help doctors to perform better diagnosis. Furthermore, in the wireless part of the pill there is not something new that can provide more data rate without effects in the power performance or the data rate performance of the pill. A better compression algorithm combined with a different type of lens could improve further the "view" of the doctor to the intestine of the patient. Also, until now, in the wireless part, the main contribution was based in the enhancement of the wireless transmitter which is placed inside the pill. A better implementation that enhances not only the internal wireless part, but also, the external, could improve the performance of the pill in the domains of power, data rate and area that is used inside the pill. Focusing in these two sub-systems of the pill, could start a new era in the capsule endoscopy field.

Chapter 3

Lossless image compressor and its multiplier-less implementation

3.1 Introduction

In this chapter, an overview of image compression techniques is presented. Especially, a walk-through the investigation of the most suitable algorithms for capsule endoscopy. Different types of image compression will be discussed, and the methodology used to create a new compression algorithm for capsule endoscopy images. Finally, the proposed algorithm will be presented and its evaluation. Comparison with existed system will be made.

For many years, doctors, in order to investigate diseases of the colon, have used classical colonoscopy tools. Such tools are painful for the patients and the investigation area is limited only to the area of the colon. Wireless capsule endoscopy (WCE) is a state-of-the-art technology for medical diagnoses of gastrointestinal diseases and illnesses [43]. The patient just swallows the capsule and the capsule does the rest of the work. A block diagram of a simple wireless endoscopic capsule is shown in Figure 3.1. The idea was originally conceived in 1950 [43, 44], and since then a plethora of research effort has been done to improve the diagnostic procedures using new technologies. Through the years, WCE has been referred to using different names, like smart-pill, wireless endoscopy, video capsule, etc.

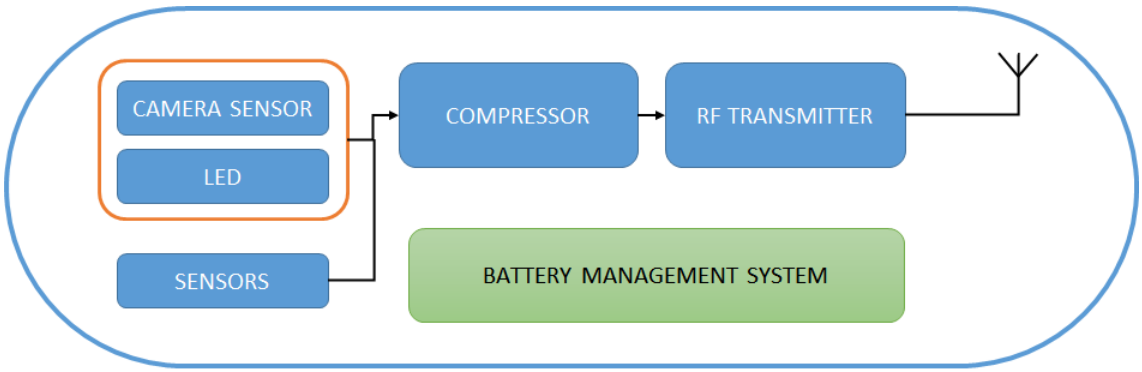

Figure 3.1: Simple block diagram of an entire endoscopic capsule system.

Current commercial wireless capsules utilize a resolution of up to 512 × 512 pixels and can capture and transmit up to 2 images per second. [64] In this work, a lossless image compression algorithm for WCE application is proposed. The aim is to design a low complexity, low power consumption and high compression ratio algorithm, that can improve the capsule endoscopy diagnosis. The factors taken under consideration are the power consumption, the size of the system in die and the compression ratio.

WCE are state-of-the-art electronic devices that consist of a camera sensor, lens, power unit, compression controller and wireless transmitter. Camera sensors are getting higher resolution and smaller size. A huge amount of data needs to be processed and transmitted. Low complexity and high compression schemes must be used to increase the efficiency of such systems. Until now, a low-resolution system exists which poses a problem for the doctors/physicians to extract valuable information from these images. There have been a lot of works reported in image compression for WCE. Khan et al. [65], presented a lossless compression algorithm based in predictive coding. Color conversion is used, and the error produced from the conversion is encoded by Golomb-rice encoder and Unary coding. This system can compress 2 frames per second with a resolution of 320 × 240 × 24 bits. The maximum operating frequency of the system is 42MHz and the resources used are 618 cells and 2k logic gates. Peak signal-to-noise ratio (PSNR) of the reconstructed image is ∞ because it is lossless. The average compression ratio (CR) obtained is 2.2:1. However, this system can compress at maximum a resolution of 320 × 240 pixels. The proposed system can compress up to 512 × 512 pixels. Chen et al. [21], have designed a low power compressor based on the JPEG-LS. This implementation is complex and hard to implement. The result of this system is a compressor which can process VGA resolution images. The working frequency of this system is 40MHz and the average CR is 2.5:1. The PSNR of the reconstructed image is ∞. This implementation needs 110 k logic gates, which are too many resources in total. Despite the use of such many resources the maximum resolution that can compress is up-to VGA. The drawback in this implementation is the huge amount of hardware resources needed to work. Liu et al. [66], have implemented an image compression module for WCE that can compress at resolution of up-to 400 × 400 pixel and can have a compression ratio of 3.69. However, the disadvantage of this implementation is that the reconstructed image is not identical with the original. The PSNR of this implementation is 46.2dB. Furthermore, this implementation needs a buffer a size of 100Kb to operate. Memory implementation needs area and consumes energy to operate. That is a huge bottleneck in such

type of applications. Lin et al. [67] has designed and implemented an image compression scheme based on 2D-DCT. His application is oriented in WCE usage. However, his implementation has some disadvantages. The usage of 2D-DCT means that there is some computational cost for his implementation. Performing multiplications, divisions, data synchronization, buffering, etc., results in more area occupation and higher power consumption than systems that are not so complicated. Moreover, this implementation is not lossless, but is near-lossless and has an image quality of 32.51dB. These implementations are not preferable due to their complexity and the loss of data. The only advantage in these techniques is the higher CR than the lossless techniques.

In the next paragraphs a state-of-art compression algorithms will presented. In Figure 3.2 the proposed algorithm is shown in diagram.

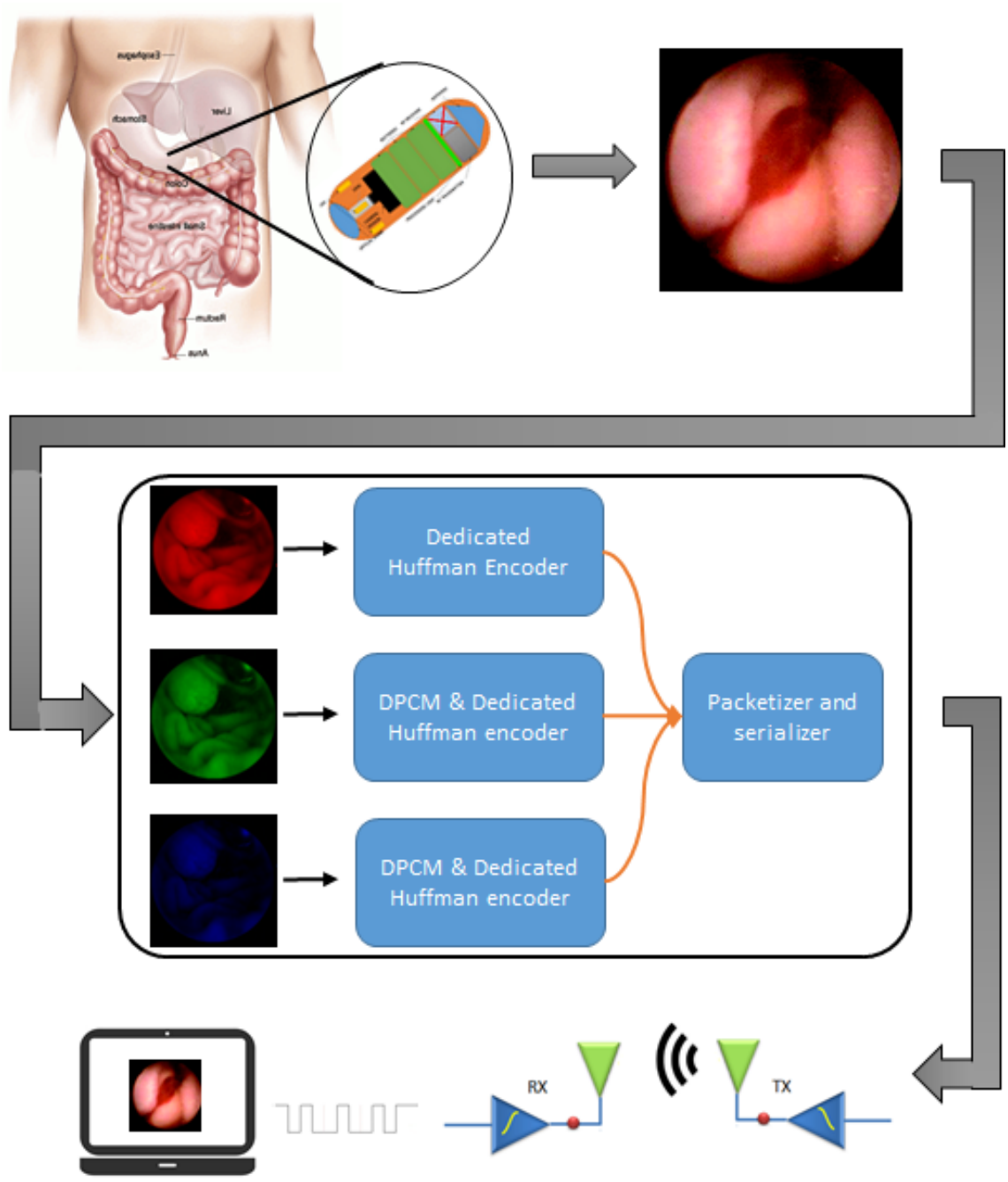

Figure 3.2: Simplified block diagram of image compression system.

3.2 Image compression

In this research the development of a compression algorithm is investigated. In the beginning was the literature review of the previous research works. This review made evident that there is a lot of research effort in this area but also there is a lot of improvements needed. These are capsule endoscopy images of various sizes. The resolution of these images varies from 150 × 150 × 24 bits, 250 × 250 × 24 bits, 512 × 512 × 24 bits, up to 1280 × 1080 × 24 bits. These endoscopic images were not only from capsule endoscopy systems but there are also from traditional endoscopy systems. That is the reason why there

are some images with resolution up to 1280 $\times$ 1080 pixels. These images were used for the evaluation of the proposed compression algorithm. Other systems [68, 17, 65] and [69] used these images in their experiments. So, the results could be able to be compared. For this comparison 200 endoscopic images were selected from [6, 70, 71]. These images were also used in other systems [68, 17, 65] and [69] in their experiments/evaluations. As mentioned these images were from the beginning of the capsule's travel, mouth, until the end of the colon. The half of them were from healthy persons and the rest from patients with the most common diseases found with capsule endoscopic systems, like some types of cancer [48], blooding [50], colitis, Crohn's disease [49], etc.

3.2.1 Requirements

Wireless camera capsules are a state-of-art diagnosis tool. The literature review provides useful information about the design criterion of the overall system.

- WCE is used inside human body. Patient should be able to swallow it. Size matters. In a compression system that uses memory/storage for its operations, the overall size of the system consists of the memory. Memory part requires more silicon area than logic elements. A compression scheme without memory is preferred.
- For an accurate diagnosis, not only the resolution should be high, but the compression algorithm should be loss-less. A lossy algorithm could provide false or noise corrupted information to physicians/doctors and the diagnosis will not be accurate. Medical applications use loss-less techniques than lossy. So, for a wireless capsule endoscopic camera loss-less technique is preferred [72].
- Another criterion in such application is the power required to complete the overall procedure. A WCE will travel inside human body from 8 to 12 hours. A power source should be able to provide energy for all the time the capsule is inside the body. A compression algorithm with low computation effort and with low or without the need of memory will require less power to complete the compression task. Increasing the power life of an WCE an in-completed examination will be prevented. Also, a reduction in power requirements will provide more power resources and it will be possible to increase the camera resolution. In this way a better and more accurate diagnosis could be provided by the physician/doctors.
- The design of the compressor should be able to work with commercial CMOS camera sensors. This type of sensors provides pixels one by one in a raster mode scheme.

3.2.2 Near-lossless compression schemes

In WCE applications except from loss-less compression techniques, near-lossless techniques are proposed. These techniques are based, mainly, in Discrete Cosine Transform (DCT), Discrete Wavelet Transform (DWT) and other insufficient, in computational power, techniques. Mostafa et al. [17] presents an image

compressor based on DCT. The input of the compressor is in Bayer format, though there is no need for color-space conversion.

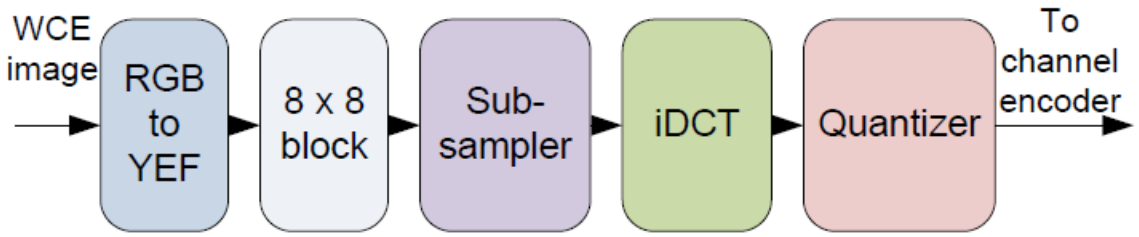

Figure 3.3: Block diagram Mostafa's proposed DCT near-loss-less implementation. [17]

Then 2-D DCT was applied. The output of DCT goes throughout modified JPEG quantization tables. This system runs at 150MHz with an image resolution of 256 x 256 pixels. The average CR of this system is almost 10:1 with a PSNR of 32.95dB.

Image compression systems based on DCT are presented in many works [73], [67], [74]. There are many disadvantages in compression schemes based on DCT. CMOS camera sensors output's pixels one-by-one, row-by-row. The output of a commercial CMOS camera sensor can be seen in Figure 3.4.

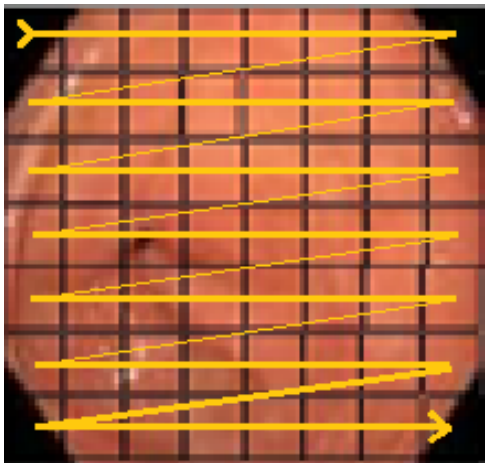

Figure 3.4: Yellow lines indicate the sequence of pixels from a commercial CMOS sensor

To apply DCT memory/storage is needed. For example, in a 512 $\times$ 512 image size picture, to apply 8 $\times$ 8 block DCT the system needs to wait until the CMOS sensor has send 512 pixels $\times$ 7 rows + 8 pixels = 3592 pixels. Assuming that pixels are in RGB format and every color is represented by 8-bits, then the memory needed is 3592 $\times$ 3 $\times$ 8 = 86.2kbits. This memory is needed just to store the incoming data. To process this data another memory of the same size is needed to store the processed data. It is clear that compression techniques based on DCT need memory which is a part that consumes power to store the data. Also, DCT needs more computation power because the need of multiplication/divisions exists. The implementation in hardware of multiplications/divisions consumes more hardware resources than simple addition/subtraction. Hu et al. [75], proposes a wavelet-based compression algorithm. Haar transform is used, the average compression ratio achieved was up to 42.07:1, with a quantization level of 32 and a PSNR of 20.95dB. Like in DCT based systems, wavelet transform uses multiplication, also memory is needed because DWT works in

block like DCT.

Xie et al. [53], proposes a low complexity near-lossless image compressor. The system is based on JPEG-LS engine. The maximum resolution that can be processed is $640 \times 480 \times 8bits$ at 40MHz system clock. The size of the compressor is 2.7K logic gates plus 10k for the design of the SRAM. The performance of this design is 3.5:1 average CR and 45dB PSNR in average. The main advantage of such systems is the high CR.

3.2.3 Image compression based on wavelet transform and combinative lifting algorithm

The first attempt was based on the design of a compression algorithm based on DWT and huffman encoding. For DWT, a spatial combinative lifting algorithm (SCLA) [76] was used. DWT uses a 5/3 filter. The use if SCLA scheme reduced the multiplication needed by 50%. By this way the computational effort is also reduced compared to conventional lifting-based implementations (LBI).

In Figure 3.5 the working diagram of the SCLA algorithm is shown.

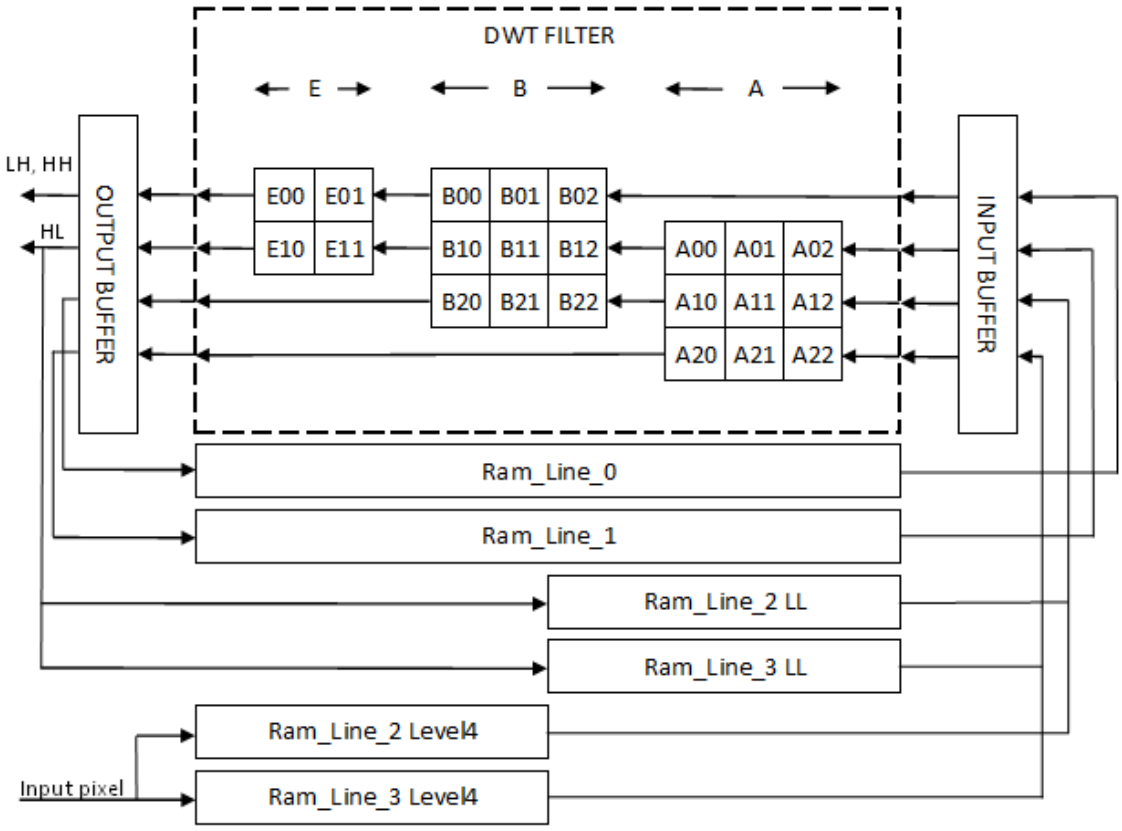

Figure 3.5: SCLA algorithm block diagram of DWT core with the memories used.

This algorithm is identical to work with real-time pixel data. It receives the pixel data produced from the camera through serial communication and outputs the processed image. The proposed algorithm reads the image data stream and produces the HL, LH, HH wavelet coefficients directly of each decomposition

level. Simultaneously, the LL coefficients are prepared for the next decomposition level. A 5-level DWT decomposition was implemented in this design.

SCLA algorithm is based on the LBI architecture. Due to this feature the memory organization is almost the same. The access to a memory organization like LBI is not sufficient and needs sophisticated computations. The memory organization of the SCLA algorithm consists of four-line buffers memories in total. Two line buffers named Line0-Line1 for storage of intermediate data of the level decomposition and two buffer memories split in four buffers (half line capacity each), Line2_Level4, Line3_Level4 and Line2_LL, Line3_LL. Line2_Level4, Line3_Level4 are used for buffering the raw image data and the last two buffer memories are used to store the LL output of the previous decomposition level. So, for an image size of 512 $\times$ 512 $\times$ 8bit, the required memory is 4 $\times$ 512 = 2048 8-bit memory locations. A and B PE (Process Element) has a 3 $\times$ 3 working area and C PE has a 2 $\times$ 2 working area.

The computations needed for wavelet transform are the above:

$$s_i^{(0)} = x_{2i} \tag{3.1}$$

$$d_i^{(0)} = x_{2i+1} \tag{3.2}$$

$$d_i^{(1)} = d_i^{(0)} + a * (s_i^{(0)} + s_{i+1}^{(0)}) \tag{3.3}$$

$$s_i^{(1)} = s_i^{(0)} + b * (d_i^{(1)} + d_{i-1}^{(1)}) \tag{3.4}$$

$$s_i = c * s_i^{(1)} \tag{3.5}$$

$$d_i = c\_inv * d_i^{(1)} \tag{3.6}$$

The wavelet parameters used are:

$$a = -\frac{1}{2} \tag{3.7}$$

$$b = \frac{1}{4} \tag{3.8}$$

$$c = \sqrt{2} \tag{3.9}$$

$$c_{inv} = \frac{\sqrt{2}}{2} \tag{3.10}$$

In the previous paragraph we demonstrated how the SCLA algorithm is working and how it uses less memory. The next step is to describe the computation needed to produce the wavelet coefficients.
Figure 3.5 shows the three processing elements (PE) inside the DWT filter.

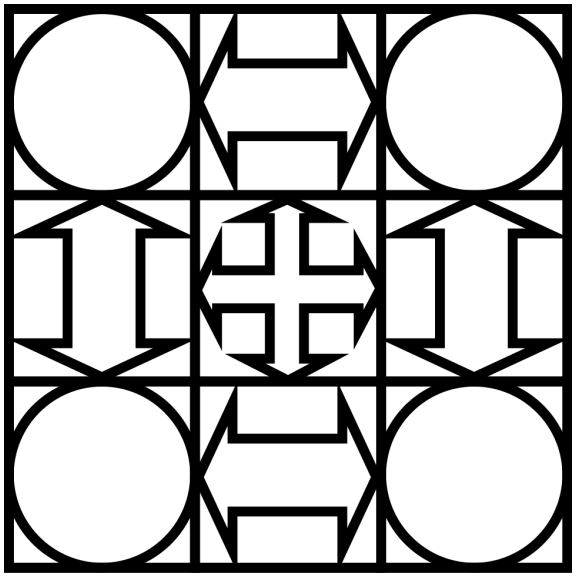

Figure 3.6: A and B PE showing element computations.

In Figure 3.6 there is the PE forboth A and B elements. The operation that takes part is described in this figure.
The circles in the four corners means that these elements don't change. The center pixel, of this 3 x 3 PE, after the operation will have the same value plus the sums of the four pixels, pointed by the arrows, multiplied by the wavelet parameter. If the PE is for A the parameter will be 'a' and for B PE will be 'b'. The last PE is C and it can be seen in Figure 3.7.

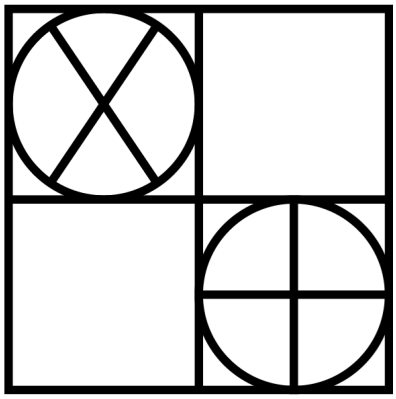

Figure 3.7: C PE element computations.

In this PE, it is easier to compute the result. In the upper right box, the operation made is to multiply the current value with the constant c and leave it in place. In the downright element is the same operation, the only change is that the constant parameter is c_{inv}.
In conclusion, it is clear that with the use of the SCLA algorithm memory and computation reduction can be achieved. As expected, this algorithm is suitable for systems that need to use less memory and reduce

the energy consumption like cameras in capsule endoscopy.

The use of this algorithm leads to the decrease of the multiplications needed. In Table 3.1 a summary is shown.

Table 3.1: Number of multiplications required by MALLAT, LBI and SCLA algorithm with 5/3 filter.

Algorithm	Level = 1	Level = j
Typical Mallat [77]	$(N/2\times5+N/2\times3)\times2N=8N\times N$	$8/3\times(4-4^{j+1})$
Symmetrical Mallat [77]	$(N/2\times3+N/2\times2)\times2N=5N\times N$	$5/3\times(4-4^{j+1})\times N\times N$
LBI	$(N/2\times2+N)\times2N=4N\times N$	$4/3\times(4-4^{j+1})\times N\times N$
SCLA [76]	$3/2N\times N+N\times N/2=2N\times N$	$2/3\times(4-4^{j+1})\times N\times N$

For the verification and implementation of the algorithm Matlab R2014a and Xilinx ISE Version 14.3 was used respectively.

By the use of the integrated tools of Xilinx's software the Table 3.2 was composed, with details of the proposed algorithm in hardware.

Table 3.2: Number of resources used by the DWT algorithm.

	Nr. of Slice registers	**Nr. of LUTs**	**Nr. of LUT-FF pairs**
DWT_core[a]	759	1077	417
Memory	24576	42642	24576
Total:	25335	43719	24993

[a] DWT_core uses also three DSP48A1 DSP modules

When finished with the implementation of the SCLA DWT, the implementation of the huffman encoder should be done. Gathering the output of the SCLA algorithm, the huffman tree was about to be generated. Many images were used to export the probabilities. The use of these statistical data will lead to the generation of the huffman codebook.

The output of the SCLA DWT was not integer numbers. The input of the SCLA algorithm was 8-bit wide unsigned values for each color. The output of the algorithm can be selected to be 20-bit wide or 17-bit wide for each color. By this way, the data were increased than decreased. Entropy coders are used to decrease the redundancies of the SCLA output.

The tests are performed with an 8-bit gray-scale value with a resolution of 512 $\times$ 512 pixels. While selected to export 20-bit output, the processed output image is more accurate, while the fraction part of each number is represented by more bits. In 17-bit mode selection the output uses less bits to represent the fraction part of the output. This means less accuracy and probably some data loss. For both output resolutions, entropy coders applied to reduce the amount of generated data. The SCLA output is separated in 20- or 17-bit planes. In every bit plane a bit-wise X-OR operation is applied to normalize the output. This output is processed by run length encoder (RLE). A typical RLE, counts the repetition of the input and exports two numbers, the input number and the number of times it occurs. In Figure 3.8 a diagram of a typical RLE system and how it works is presented.

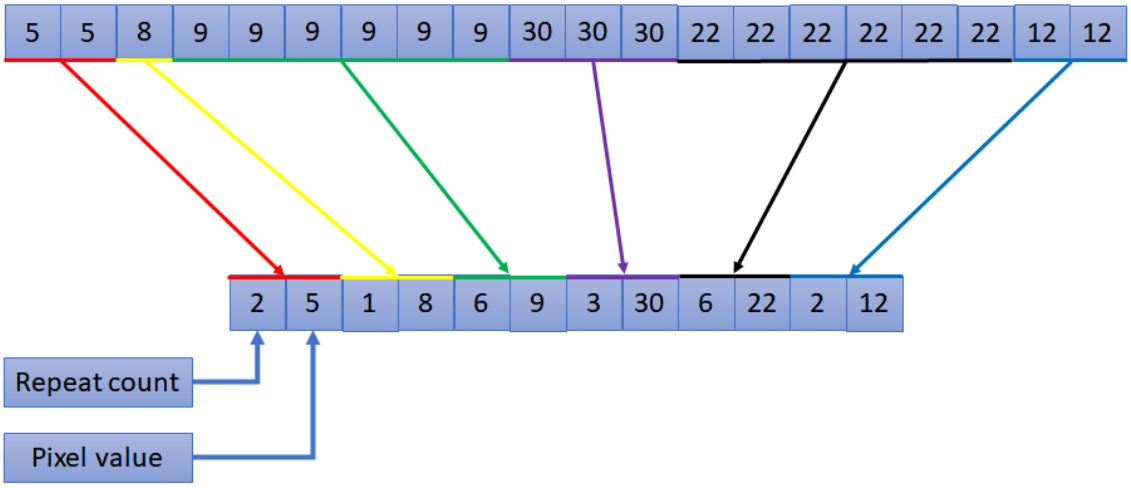

Figure 3.8: How a typical RLE system works.

For this design to further reduce the length of the output, only the RLE counts are exported. In this design RLE is applied in every bit-plane. There are 20 or 17 bit planes, depending on the selection. The When the RLE algorithm starts, it sends, only for the first, time the start value, which can be '0' or '1'. Then the count follows. In Figure 3.9 an example is presented.

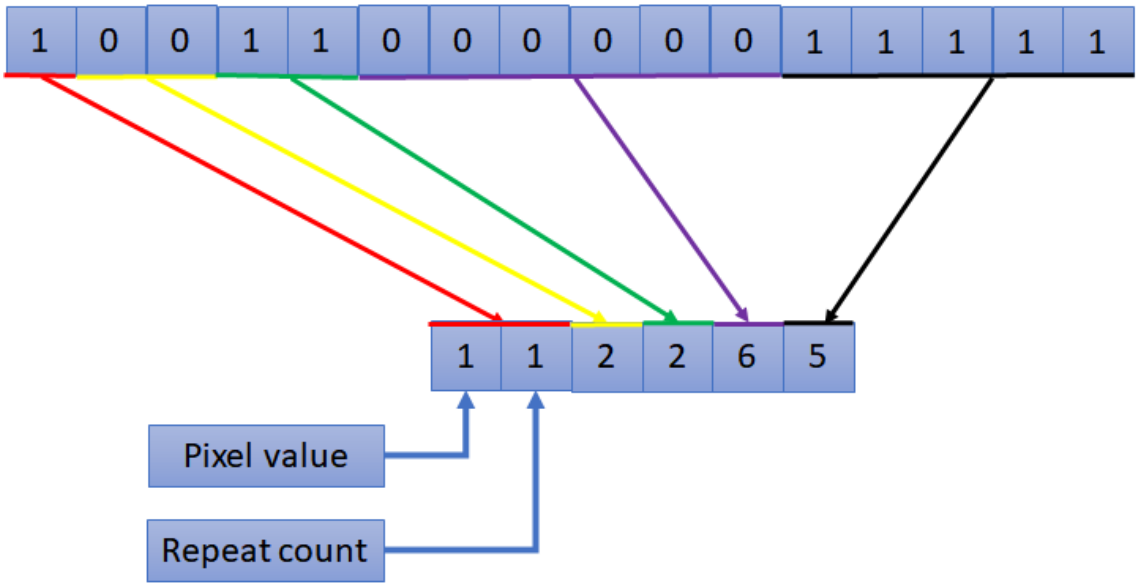

Figure 3.9: Modified RLE system.

The RLE encoder usually is used with an 8-bit word input. In this design the input is 1-bit. Because the bit planes produced by the output of the SCLA algorithmare are 1-bit wide, the repetition produced sometimes are over 255 counts. The count output is 8-bit wide; this means that the maximum value it can show is 255. Because of these two reasons the RLE algorithm is modified more so it can work for this application. The RLE encoding algorithm has an overflow function. The set-point of the overflow is set at 250 count. When the counts are over this limit, then the RLE algorithm outputs the value 255 for two times and starts from the beginning. By this way, the RLE encoder can recognize that there was an overflow and can perform the decoding process. In Figure 3.10 is a flow diagram of the modified RLE encoder.

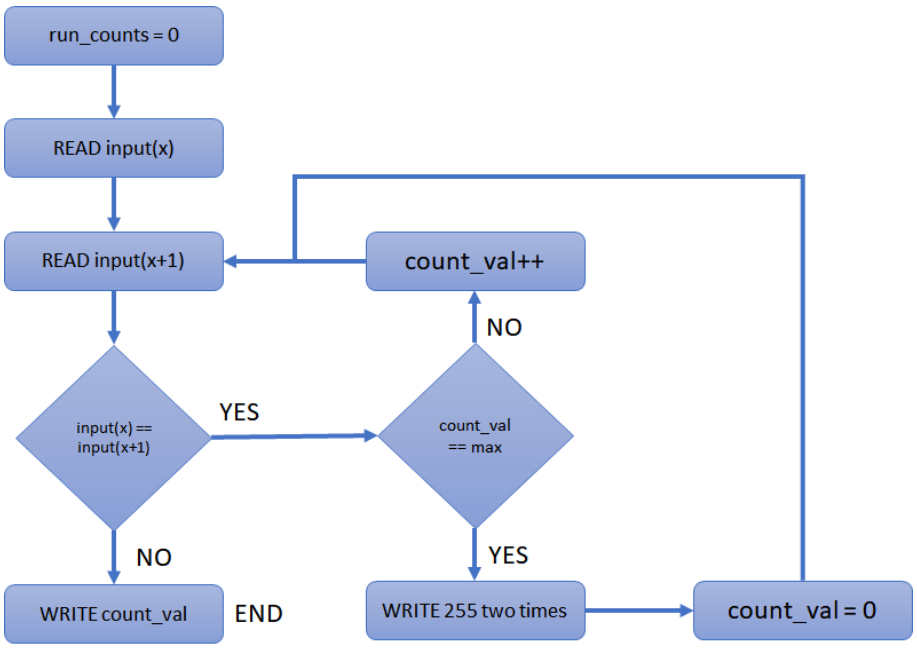

Figure 3.10: Modified RLE flow diagram.

The output of the RLE encoder goes in a huffman encoder for further compression. The huffman codebook is created with statistical data from the output of the RLE encoder. The results of this implementation are shown in Table 3.3.

Table 3.3: SCLA algorithm with X-OR, RLE and huffman encoder applied

	20-bit planes	**17-bit planes**
Original image[a]	2097152 bits	2097152 bits
SCLA	5242880 bits	4456448 bits
XOR-RLE-HUF	≈4407014 bits	≈3409182 bits
Total:	≈+210,14%	≈+162,56%

[a] Gray-scale image of 512 x 512 resolution and 8-bit pixel depth.

From Table 3.3 it is clear that the SCLA algorithm outputs more bits than in the input. It is possible to use SCLA algorithm in a lossy algorithm than in a loss-less. However, the processing of the SCLA output with entropy encoders, there was not enough compression to achieve less bits than the original image.

3.2.4 Lossless compression schemes

For WCE applications, lossless compression schemes are preferred. Compression schemes based on Golomb-Rice coding, DPCM coding, huffman coding and Unary coding are presented below.

Khan et al. [65], presents a lossless compression algorithm based in predictive coding. Color conversion is used, and the error produced from the conversion is encoded by Golomb-rice encoder and Unary coding. This system can compress 2 frames per second with a resolution of 320 $\times$ 240 $\times$ 24 bits per pixel. The maximum operating frequency of the system is 42 MHz and the resources used are 618 cells and 2 k logic gates. Peak signal-to-noise ratio (PSNR) of the reconstructed image is ∞ because it is loss-less.

Table 3.4: Summary of existed lossless and near-lossless methods.

	Color plane	Compression method	Buffer	Lossless	Image size	Clock rate	Compression ratio	PSNR (dB)
Mostafa et al. [69]	YUV	Predictive coding	NO	YES	320 × 240	91MHz	2.4	∞
Mostafa et al. [17]	RGB	DCT	YES	NO	-	150MHz	10	32.95
Li et al. [68]	RGB	JPEG-LS	YES	near-Lossless	640 × 480	40MHz	3.5	45
Khan et al. [65]	RGB	Predictive coding	NO	YES	320 × 240	42MHz	2.2	∞
Mostafa et al. [69]	YUV	Golomb-rice-Unary	NO	YES	QVGA	-	2.7	∞
Mohammed et al. [78]	Bayer	JPEG-LS	10kbit	YES	VGA	-	1.4-2	∞
Tareq et al. [79]	YUN422	DPCM	NO	near-Lossless	QVGA	-	5	43.6
Dung et al. [80]	RGB	H.264	N/A	near-Lossless	512 × 512	-	11	36.2
Chen et al. [81]	RGB	JPEG-LS	17.5kbit	near-Lossless	VGA	-	2	46.4

The average compression ratio (CR) obtained is 2.2:1. Chen et al. [21], have designed a low power compressor based on JPEG-LS. Obviously, the implementation of such a system is complex and hard. The result of this system is a compressor which can process VGA resolution images. The operating frequency of this system is 40MHz. The average CR is 2.5:1 and the PSNR of the reconstructed image is ∞. This implementation needs 110k logic gates, it is apparent that needs too many resources in total. In Table 3.4 an overview of existing lossy and loss-less systems is presented. From the literature review in lossy and loss-less compression algorithms for WCE, the need for a better compression algorithm is obvious and imposed. The main idea is to produce a loss-less compression engine with less computation power which will lead to a lower power consumption of the system.

3.3 Loss-less image compression using smart RGB image layer processing

In previous paragraphs a literature review of existing compression algorithms was presented. Also, an implementation of SCLA algorithm with 5/3 tap filter DWT based on [76]. The results were not satisfying. The output was not loss-less and produces more bits than the original image. A new compression algorithm should be designed and implemented. The design criterion was written in previous homonymous paragraph.

3.3.1 Distribution of color in gastrointestinal images

The first step is to find several endoscopic images. A selection of 200 images from [6, 70, 71] is compiled to create a large database of capsule endoscopy images. These are capsule endoscopy images of various sizes. The resolution of these images varies from 150 $\times$ 150, 250 $\times$ 250, 512 $\times$ 512, up to 1280 $\times$ 1080. In Table 3.5 the total number of images with their corresponding resolution used is shown. Also, the average CR with the standard Deviation for every resolution group can be seen. Those images are from different positions in the GI track and the of them are from healthy people and the other from patients with the most common diseases.

Table 3.5: In this table the total number of image database is used is shown.

Resolution (pixel)	Nr. of images	CR and Standard Deviation
150 $\times$ 150	101	2.12$\pm$0.17
256 $\times$ 256	37	2.15$\pm$0.17
512 $\times$ 512	25	2.25$\pm$0.08
640 $\times$ 480	9	2.31$\pm$0.05
1280 $\times$ 1080	28	2.27$\pm$0.07

Also, the average CR with the standard deviation for every resolution group can be seen. Those images are from different positions in the GI track and the half of them are from healthy people and the other half is from patients with the most common diseases.

(a) Image of patient with Crohn's disease.

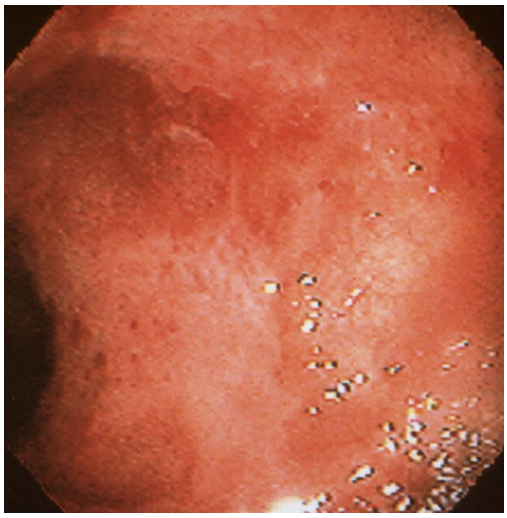

(b) Image of patient with ulcerative colitis.

Figure 3.11: Images of patients with Crohn's disease and ulcerative colitis. [6]

.

In Figure 3.12 there are two images from a healthy person and in Figure 3.11 there are two images, one with colitis and the other one with Crohn's disease. These endoscopic images were not only from capsule endoscopy systems but there are also from traditional endoscopy systems. That is the reason that some images are with a resolution of up to 1280 $\times$ 1080 pixels. These images were used for the evaluation of the compression algorithms. These images was also used in other systems [68, 17, 65] and [69] in their experiments. So, the results will be comparable.

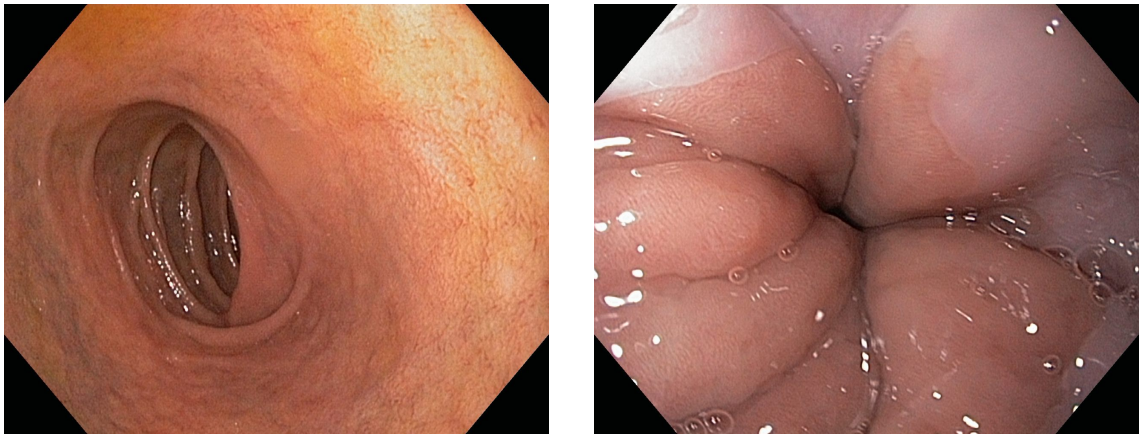

Figure 3.12: Images from healthy patient. [6]

These images were from the beginning of the capsule's travel, mouth, until the end of the colon. 100 of them were from healthy persons and the rest were from patients with the most common diseases found with capsule endoscopic systems, like some types of cancer [48], blooding [50], colitis, Crohn's disease [49], etc.

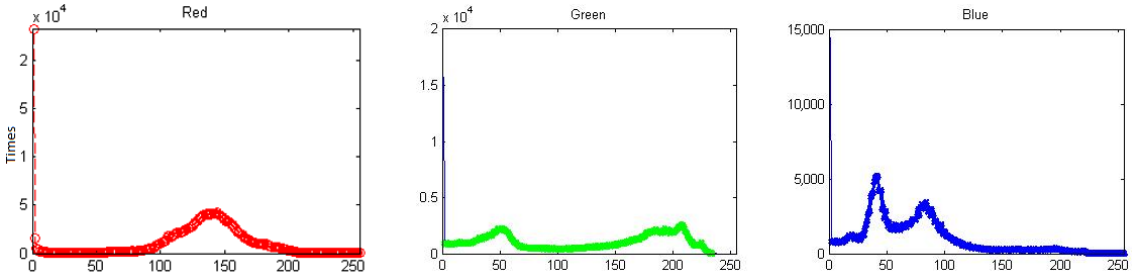

Figure 3.13: Average histogram of RGB pixel value distribution of 200 capsule endoscopy images.

It is quite clear that all images have similarities in color variance. Using Matlab software, a image histogram of pixel values is created. The results are shown in Figure 3.13. All the images used are in RGB format, 24-bit per pixel. Other pixel formats, like YUN444, YUN422 or YUN420 are not preferred. The reason these formats are not preferred, is that they are already sub-sampled and the compression will be lossy. Also, another observation that lead to use DPCM encoding was the difference between consecutive pixels.

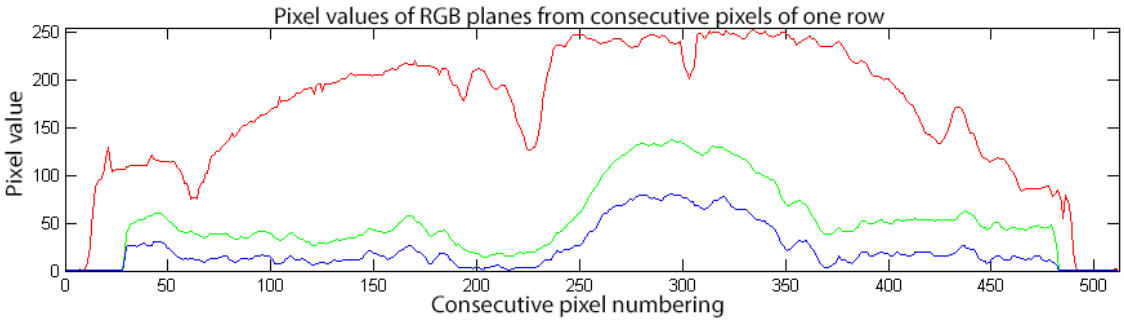

Figure 3.14: Sequence of raw pixel values for each color plane.

In Figure 3.14 the sequence of the pixel values is shown. In other works, they prefer to apply color-space transformation, like Khan et al. [65]. However, color-space transformation might produce some estimation that is not good for lossless image compression. From Figure 3.13 and 3.14, it is clear that the red plane has some characteristics which by the use of huffman encoding will lead to higher compression. Huffman encoding is based in the probabilities of the pixel values. The pixel that appears more, is addressed with less bits in huffman encoder output. Huffman encoder does not care about the neighboring pixels' values. These characteristics are the repeatability of some pixel values and Figure 3.14 shows that that the neighboring pixels do not have similar values. So, huffman coding is more suitable to compress this color plane. The statistics from all the images was used to create a unique huffman codebook that is for the red plane.

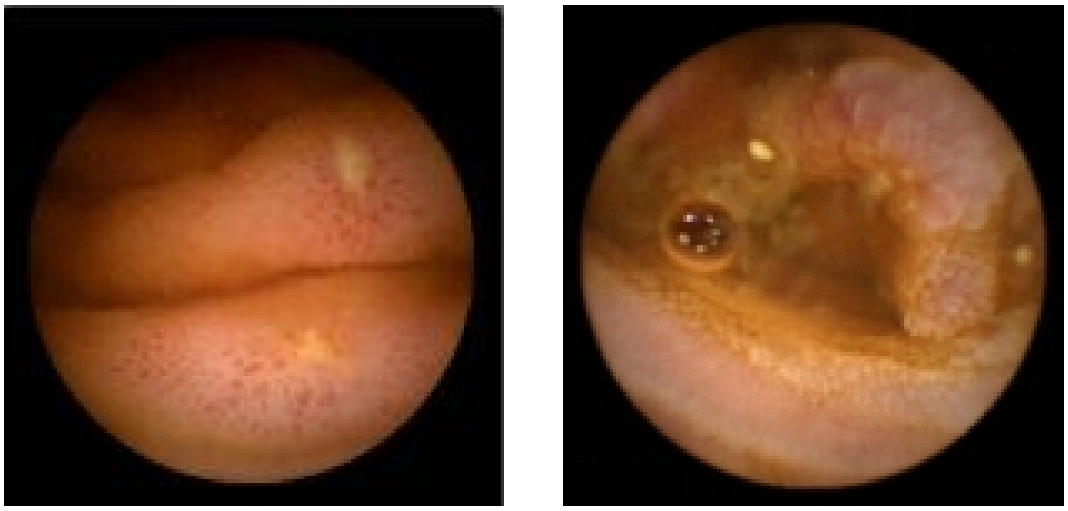

(a) Crohn's Enteritis. (b) Carcinoma of the colon.

Figure 3.15: The left picture is a capsule endoscopic image with Crohn's Enteritis and in the right a picture of Carcinoma of the colon, metastatic to small bowel [6]

.

In order to choose the best compression methods, statistical analysis has been done on every image and for every color plane of every image. The color-space of the original images is RGB. Matlab software was used for the experiments and the design of the compression algorithm.

In Figure 3.13, the average distribution of all RGB images is presented. In other works, researchers prefer to apply color-space transformation, like Khan et al. [65]. However, color-space transformation might produce some estimation that is not good for loss-less image compression. From Figure 3.14, is observed that the red plane has some characteristics that suggest us to compress it with huffman coding. Huffman encoding is based in the probabilities of the pixel values. The pixel that appears more, is addressed with less bits in huffman encoder output. Huffman encoder doesn't care about the neighboring pixels' values

Based on Figure 3.14, it was observed that in green and blue planes, there is correlation between neighboring pixels. There are more repeated values than in the red plane.

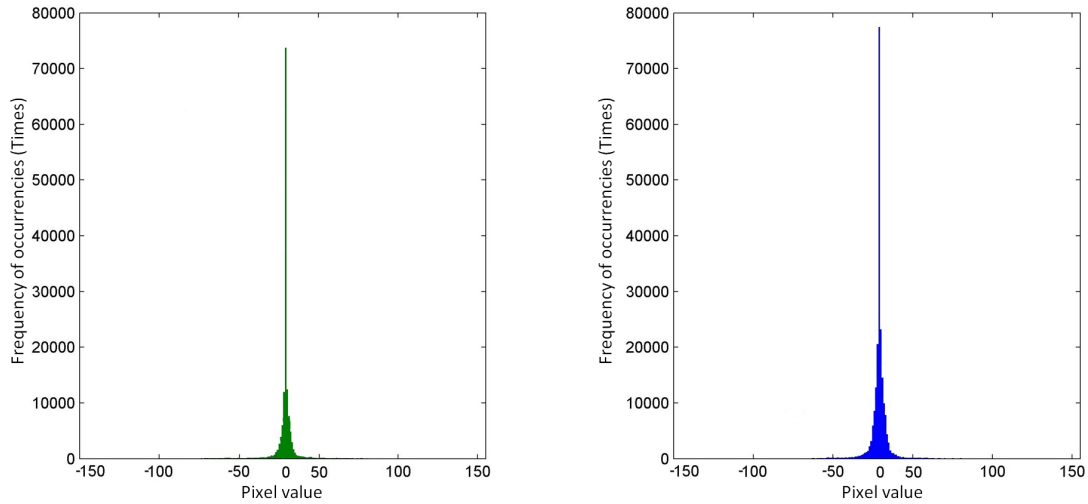

(a) Statistical distribution of color values for green color plane.

(b) Statistical distribution of color values for blue color plane.

Figure 3.16: Green and blue planes statistics after DPCM coding applied.

.

Figure 3.17: Sample of test image. [6]

However, the distribution value is still not good. Due to the repeated values and that the neighboring pixel's values are close, DPCM coding was applied and the distribution for green and blue planes are shown in Figure 3.16. Before DPCM code is applied, in statistical manner, the mostpixel repeated was about the 10% of the total pixels in the image. After DPCM, this value is increased to 50%. After processing green and blue plane, a huffman coding is used.

Table 3.6 is showing the data output of the two DPCM encoders. For both blue and green color planes. The test image is an RGB color space image and its size are 150 $\times$ 150 pixels. The depth of every pixel is 8-bits. Figure 3.16 shows these data plotted. However, from Table 3.6, it is easier to understand the distribution of the DPCM output. It is obvious that both green and blue planes have the most occurrences in the value of "0". This the reason why in Table 3.8, the designed huffman codebook creates an output for input of "0" with the lowest length.

Table 3.6: Table shows a few components of and their time of occurrences of blue and green plane after DPCM code is applied.

Pixel value	Percentages	DPCM output	Blue plane	Percentages	Green plane	Percentages
0	10.7	−42	2	0.009%	1	0.005%
1	14.18	−41	2	0.009%	2	0.009%
2	2.28	−39	2	0.009%	2	0.009%
3	0.59	−38	2	0.009%	1	0.005%
4	0.55	−37	5	0.022%	3	0.013%
5	0.48	−36	1	0.005%	2	0.009%
6	0.23	−35	2	0.009%	1	0.005%
...	...	...	...	...	...	...
120	0.24	−5	429	1.9%	400	1.77%
121	0.2	−4	661	2.94%	623	2.76%
122	0.21	−3	1045	4.64%	988	4.39%
123	0.29	−2	1473	6.55%	1325	5.88%
124	0.25	−1	2322	10.32%	2655	11.8%
125	0.17	0	7386	32.83%	11655	51.8%
126	0.24	1	2451	10.89%	2835	12.6%
127	0.3	2	1737	7.72%	2014	8.95%
128	0.31	3	1126	5%	1057	4.69%
129	0.29	4	836	3.71%	923	4.1%
130	0.29	5	536	2.38%	618	2.74%
...	...	...	...	...	...	...
249	0.13	28	10	0.044%	9	0.04%
250	0.14	29	12	0.053%	12	0.053%
251	0.11	30	8	0.035%	7	0.031%
252	0.08	31	6	0.026%	7	0.031%
253	0.03	32	2	0.009%	3	0.013%
254	0.02	33	5	0.022%	2	0.009%
255	0.01	34	1	0.005%	1	0.005%

However, in green and blue planes was observed that there was a correlation between neighboring pixels. Due to the repetition of the values and the fact that the neighboring pixel's values are close, DPCM coding was applied and the distribution for green and blue planes are shown in Figure 3.16. Before DPCM code is applied, a statistical analysis showed that, the pixel that repeated the most was about 10% of the total pixels in the image. After DPCM, this value is increased by up to 50%. After processing green and blue plane, huffman coding was used.

3.3.2 DPCM encoding

In DPCM encoding the input values of consecutive pixels is subtracted. The result of this mathematical equation is then exported to be processed in the next block which is the huffman encoder. By this way, the original pixel value is decreased because the difference of two successive pixels is small. Equation 3.11 is the mathematical model of DPCM encoder. The result of a DPCM encoder can be decoded, and the result would be lossless, which is something needed for this type of application.

$$S_{out} = I_x - I_{x-1} \tag{3.11}$$

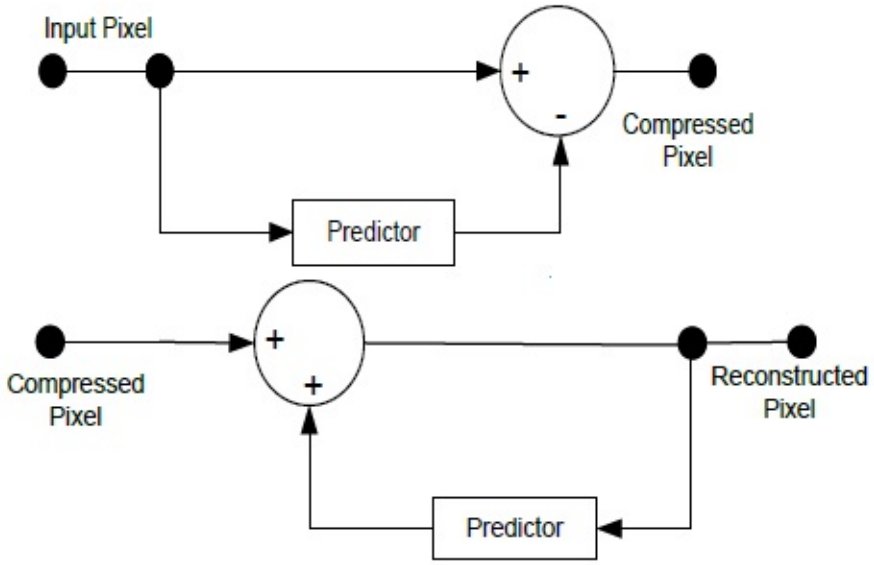

Figure 3.18: DPCM encoder and decoder diagram.

Where S is the processed with DPCM encoder pixel, I_x is the new pixel arrived and I_{x-1} is the previous pixel. The value can be positive or negative.

3.3.3 Huffman coding

As noted in previous paragraph, red color plane was not suitable for DPCM encoding. This color plane is compressed using a modified codebook huffman encoder. Huffman is a variable length encoder. Input pixel values for each color space have 8-bit width per color. By applying huffman coding, the most frequent pixel values will be reduced in the output. In this way a significant bit reduction is achieved. The performance of this method can be calculated using entropy. Entropy measures the amount of information contained in the data or the data randomness. [82] The average bits per pixel, A, needed for huffman coding to represent the original data is given by the Equation 3.12.

$$A = \sum_{k=1,l=1}^{K,L} P_{k \times l} \times N_{k \times l} \tag{3.12}$$

Where P are the probabilities of the pixels value, K and L is the size of the image and N is the number of bits that huffman encoder had generated. Statistical analysis was done using Matlab software and with the probabilities of each color value the huffman codebook for red color produced. For green and blue color planes, at first a DPCM coding scheme was applied. The range of values is not from 0 to 255 but from -127 to 128. The statistical analysis of the DPCM output helps the production of another huffman codebook that is going to be used to compress green and blue color planes. Like DPCM encoding, huffman encoding is a lossless method to compress images. The most important for huffman encoder is that in hardware implementation no multiplications are needed. In the next Table 3.7 a result of compression applied in 10 capsule endoscopy images is shown.

Table 3.7: Compression results applying huffman encoder in red color plane. Huffman is applied after DPCM applied in green and blue planes.

Image[a]	**1**	**2**	**3**	**4**	**5**	**6**	**7**	**8**	**9**	**10**
Black	1.21	1.22	1.22	1.21	1.23	1.21	1.23	1.22	1.22	1.24
Green	2.52	2.63	2.71	2.86	2.83	2.82	2.9	2.57	2.64	2.55
Blue	2.53	2.62	2.7	2.83	2.85	2.8	2.87	2.55	2.65	2.57
Total:(CR)	2.08	2.16	2.21	2.3	2.3	2.29	2.33	2.11	2.17	2.12

[a] RGB image of 512 $\times$ 512 resolution and 8-bit pixel depth.

3.3.4 Proposed algorithm

In the proposed compression algorithm two different huffman trees were used. In Figure 3.19 the block diagram of the proposed compression algorithm is shown. The first huffman tree was used to compress the red plane of the image. To produce this huffman tree, the use of the capsule endoscopy data-set images was used. Probabilities of every red color value was computed and then the huffman tree was produced. The images used were RGB and each color have 8-bit color depth. This means that the minimum value is 0 and the maximum is up to 255.

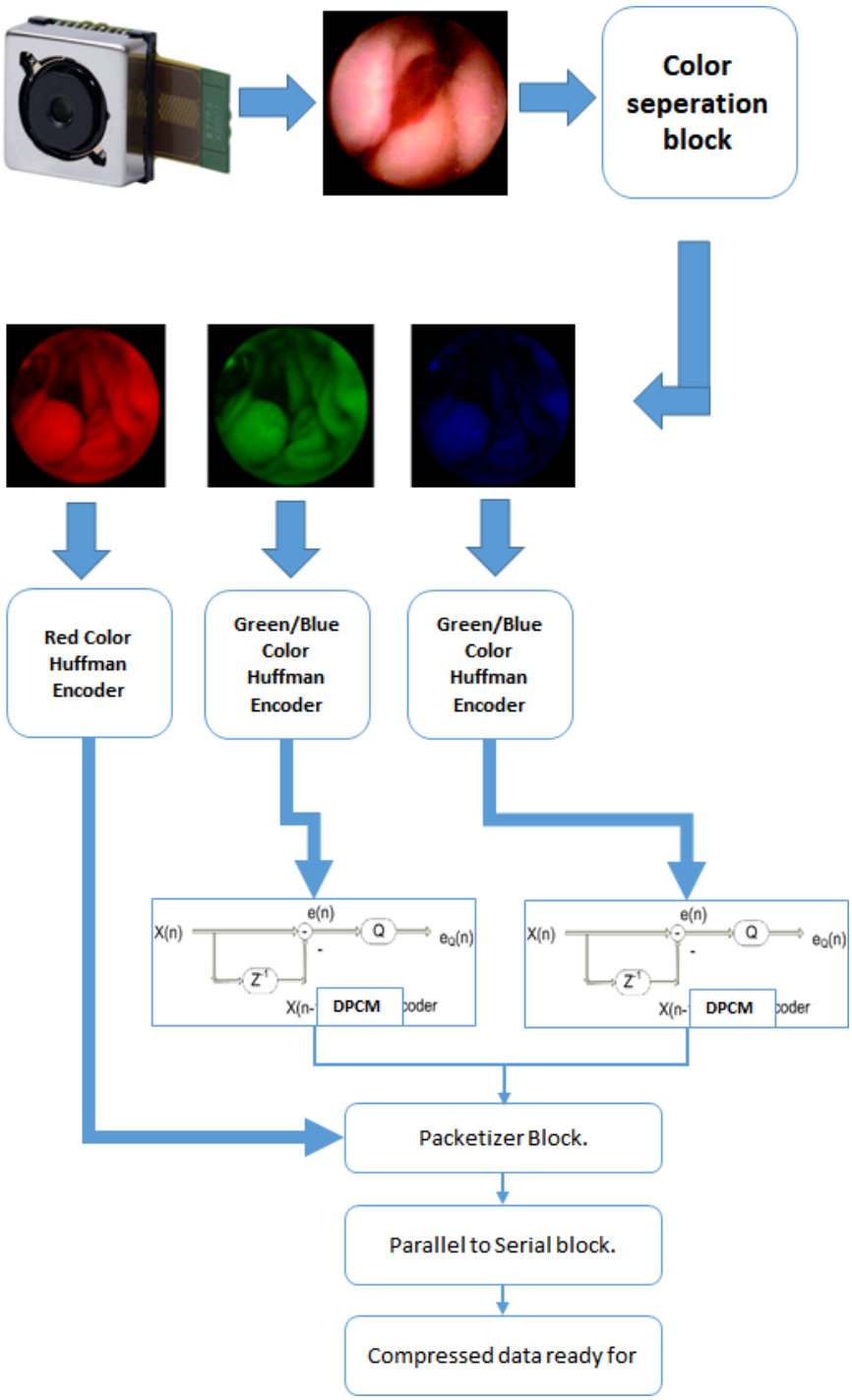

Figure 3.19: Block diagram of proposed compression algorithm.

The results have minimum 2 bits output for the color value appearing the most and 29-bits for the value that is appearing less times. This huffman tree is used to compress the red color plane, for the other two-color planes, green and blue, it is more complicated. The huffman tree used to compress these color planes was produced from the output of a DPCM encoder. In the same way the use of the capsule endoscopy data-set images and for green and blue color planes DPCM was applied. The output of a DPCM encoder was used to generate the probabilities needed to produce the huffman tree. In the beginning two separate huffman trees were produced for each color plane, green and blue. It was observed that the results of the probabilities

were almost the same and finally the same huffman tree was used for both colors. In Table 3.8 a small part of the huffman table and the probabilities for each pixel value, of green and blue planes is shown. These probabilities were used to obtain the final huffman tree for green and blue color planes. The input of this huffman table has negative numbers. The reason is that the input of this huffman table is the output of the DPCM encoder, for both colors. So, the huffman codebook is designed to work with such an input. By this way, an extra huffman tree is not needed. Similarly, to red color plane, in green and blue planes the huffman tree produces 2-bit output for the most found color value and 29 bits for the less found. In Table 3.9 a small part of red color plane huffman codebook is presented. In the end the compressed results of the three color planes are packeted and put into the parallel to serial encoder. The results now are ready to be transmitted wirelessly. The way this system is designed, makes it compatible with the most camera sensors that are used commercially and the output data are in serial form. This makes this system compatible with the most wireless transmitters. Wireless transmitters are using serial data input ports. So, the proposed design can fit to existing wireless transmitter system without any modification.

Table 3.8: Table showing a few components of the huffman tree for green and blue planes.

Input	Output	Probabilities
-127	10001101111000100000111100001	0.00044
-126	10001101111000100000111100011	0.00044
-125	10001101111000100000111101011	0.00044
...		
-1	101	0.1089
0	00	0.32
1	100	0.1032
...		
127	010101101000111110	0.00053
128	01010110100011110	0.00088

Table 3.9: Table showing a few components of the huffman tree for red color plane after the applied DPCM coding.

Input	Output	Probabilities
0	111010010	0.009
1	00100	0.0396
2	11	0.185
3	10011	0.0408
...		
245	01110110100011111111111110	0,0000081
246	0111011010001111111111110	0,0000090
247	011101101000111111111110	0,000032
248	01110110100011111111110	0,000045

In Table 3.10, a small part of the huffman table for green and blue planes and a part of the huffman table for the red color plane is shown. The input for green and blue planes huffman table has negative numbers. The reason is that the input of this huffman table is the output of the DPCM encoder, for both colors. So, the huffman code book is designed to work with such inputs. In this way, an extra huffman tree was not

used. Green and blue planes' huffman tree produces 2-bit output for the most repeated color value and 29-bits for the less found while in Red color plane the most repeated pixel value is reproduced with 3-bits and the less found with 15 bits. Following Equation 3.12, it is found that for the red plane the average bits needed to reproduce the original data is 6.85 bits/pixels. However, in green and blue planes the average bits per pixel are 3.65 bits/pixel.

Table 3.10: Table showing a few components of the huffman tree for green and blue planes.

Input	Huffman Output for green and blue Planes	Input	Huffman Output for red Plane
−127	10001101111000100000111100001	0	101
−126	10001101111000100000111100011	1	010
−125	10001101111000100000111101011	2	11101
...	...	...	...
−1	101	127	11011111
0	00	128	11010111
1	100	129	11110000
...	...	...	...
127	010101101000111110	254	001000111110111
128	01010110100011110	255	001000111110110

Due to the nature of the DPCM and huffman coding schemes, the results are reversible. So, the lossless part of the application is covered. The second part and most important is the CR, which in the proposed scheme 2.2:1 on average.

3.3.5 Complexity analysis of the proposed algorithm

A design criterion was the complexity of the proposed algorithm. The selection of a compression scheme based on DCT, DWT or JPEG-LS would increase the complexity of the compression algorithm. To express and compare the complexity of the proposed algorithm with other algorithms, a Big O notation is used. Big O notation is used in Computer Science to describe the complexity of an algorithm. It is used to describe the worst-case scenario of an algorithm in manner of time and space (memory). [83] In Table 3.11 the type of orders are presented.

Table 3.11: Type of Big O notations [34]

Notation	Name
O(1)	Constant
O(log(n))	Logarithmic
O(log(log(n))	Double logarithmic (iterative logarithmic)
o(n)	Sub linear
O(n)	Linear
O(n log(n))	Log linear, line arrhythmic, quasi linear or supra linear
$O(n^2)$	Quadratic
$O(n^3)$	Cubic
$O(n^c)$	Polynomial (different class for each $c > 1$)
$O(c^n)$	Exponential (different class for each $c > 1$)
O(n!)	Factorial

Table 3.12: Comparison of compression algorithms on Big O manner.

	Color	Compression method	Buffer	Lossless	CR	PSNR (dB)	Complexity	Image size in pixels	Power (mW)
Mostafa et al. [69]	YUV	Predictive coding	NO	YES	2.4	∞	O(n)	256×256	1.78 @ 2 fps
Mostafa et al. [17]	RGB	DCT	YES	NO	10	32.95	O(n log n)	256×256	N/A [1]
Li et al. [68]	RGB	JPEG-LS	YES	near-Lossless	3.5	45	O(n log n)	256×256	N/A
Khan et al. [65]	RGB	Predictive coding	NO	YES	2.2	∞	O(n)	640×480	1.63 @ 2 fps[2]
Mostafa et al. [69]	YUV	Golomb-rice-Unary	NO	YES	2.7	∞	O(n)	256×256	1.8 @ 2 fps
Mohammed et al. [78]	Bayer	JPEG-LS	10kbit	YES	1.4-2	∞	O(n log n)	640×480	0.94 @ 2 fps[3]
Tareq et al. [79]	YUN422	DPCM	NO	near-Lossless	5	43.6	O(n)	256×256	0.042 @ 2 fps[4]
Dung et al. [80]	RGB	H.264	N/A	near-Lossless	11	36.2	O(n log n)	512×512	0.9161 @ 2 fps
Chen et al. [81]	RGB	JPEG-LS	17.5kbit	near-Lossless	2	46.4	O(n log n)	640×480	1.3 @ 2 fps
Proposed	RGB	Huffman+DPCM	NO	YES	2.21	∞	O(n)	512×512	4.5 @ 4 fps[5]

[1] Simulated results.
[2] FPGA simulated results.
[3] Simulated by using SYNOPSYS design compiler.
[4] In this implementation the power consumption is only for the compressor core, without the interface for the camera and the parallel-to-serial converter for the output of the compressor core.
[5] FPGA implementation and simulation results in Cadense Virtuoso tool-set.

Compared with others using Big O notation the proposed algorithm is memory-less, multiplier-less and uses huffman and DPCM encoders which have an O(n) order. Implementations based on DCT have a complexity of O(n log n) and also, they need memory/buffer to process the input image. In Table 3.12 there is a summary of compression algorithms and their complexity compared with the proposed algorithm. Furthermore, in specific research works like [69] and [65] in this table is shown that the results in compression ratio is almost identical with the proposed. However, these designs use less energy than the proposed. The difference that makes the proposed design better, is the performance in frame rate and in maximum resolution. As seen the maximum resolution of the proposed design is 512×512, in contrast with the other designs which are up-to 256×256 and 640×480. Compared also with the frame rate which is in the proposed design 4fps is the double than the others. For these specific reasons the proposed design performs better.

3.4 Experimental results

3.4.1 Software implementation

The proposed algorithm was implemented, as noted, first in software using Matlab. The results were satisfying and the implementation in hardware in an FPGA development board was about to start. In previous paragraphs the experiments and the research in the pixel correlation in capsule endoscopy pixels were described.

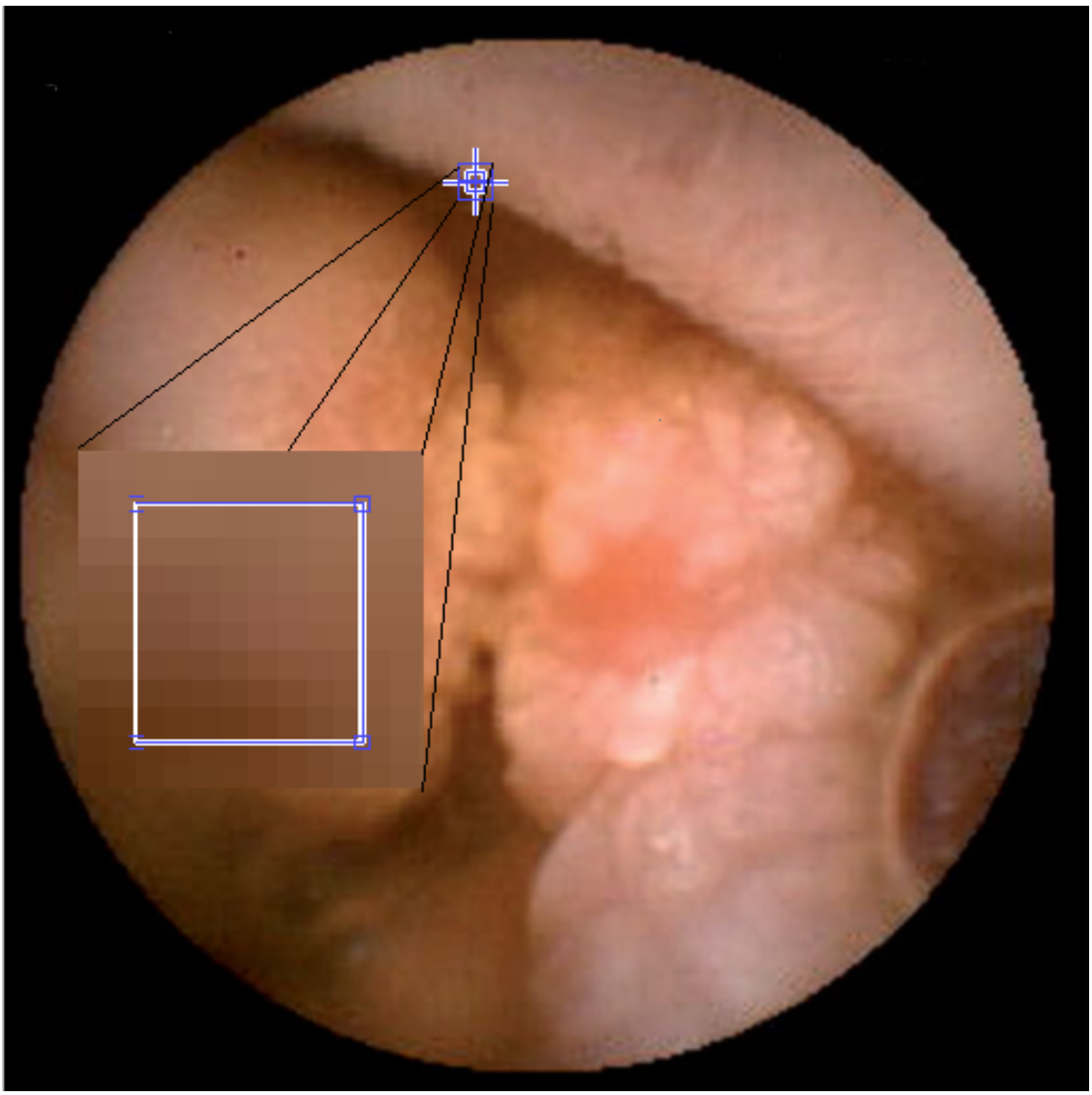

Figure 3.20: Sample of test image.

In difference with the hardware implementation, in Matlab software (FPGA) every process of the proposed algorithm is done one-by-one. The images used are RGB and have an 8-bit color depth. The first step of the proposed algorithm is to separate the color planes of the image in 3 different tables. So, the results are 3 tables for each color. The pixel values of each color have the same position as the original image. Second step is to apply huffman encoding in the red color plane. For this operation there are pre-defined huffman table only for this color plane. The results of this operation are stored in a table. Third step is to apply DPCM encoding in green plane. The results are stored in a temporary table. Then huffman encoding is applied in this table and the results of this operation is the compressed data of the green plane. The fourth step is the same as the third, the only difference is that the operations are applied in the blue plane. The results are stored in a separate table. Finally, there are 3 different tables where are stored the compressed data of red, green and blue color planes.

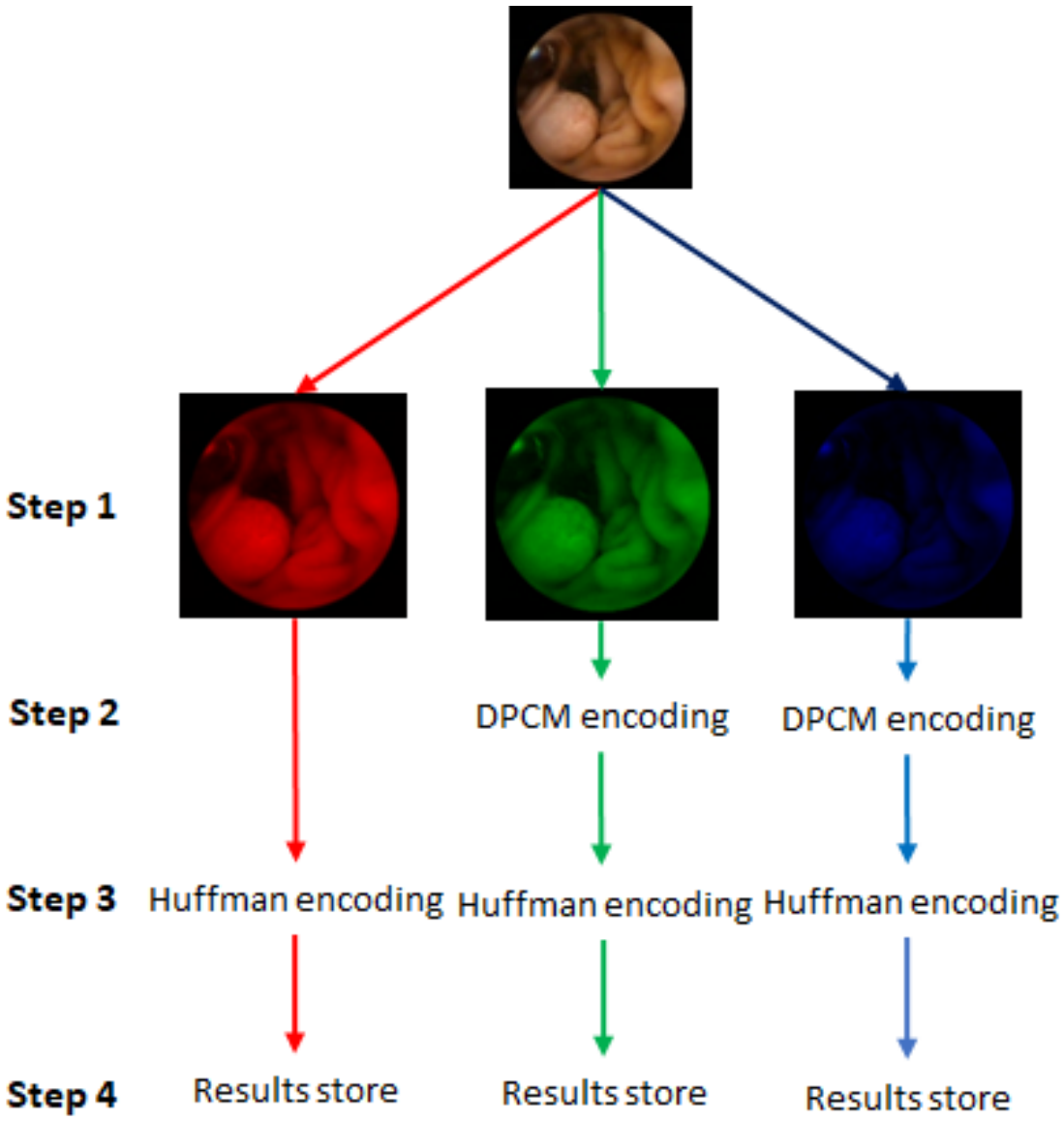

Figure 3.21: Steps of Matlab code operation.

In Figure 3.20 a test image was selected to show that both implementations work correctly. In this image for space reasons, a rectangle of 8x8 RGB pixels was selected to be shown. As mentioned the range values of RGB pixels is 8-bit for each color, so in decimal system is from 0 to 255. The proposed algorithm as statedis lossless. The only mathematical operation used is sub-traction, in DPCM operation for green and blue color planes. This operation is applied for integer numbers, so the result is going to be an integer. This is enough to make the implementation in hardware of the proposed algorithm easier.

R:150 G:104 B: 78	R:151 G:105 B: 79	R:151 G:105 B: 79	R:150 G:104 B: 78	R:151 G:105 B: 79	R:152 G:106 B: 80	R:156 G:109 B: 82	R:157 G:110 B: 83
R:143 G: 97 B: 71	R:144 G: 98 B: 72	R:144 G: 98 B: 72	R:145 G: 99 B: 73	R:147 G:101 B: 75	R:150 G:104 B: 78	R:153 G:106 B: 79	R:154 G:107 B: 79
R:135 G: 88 B: 63	R:136 G: 90 B: 65	R:138 G: 92 B: 67	R:141 G: 95 B: 69	R:145 G: 98 B: 73	R:148 G:101 B: 76	R:150 G:103 B: 75	R:151 G:103 B: 75
R:130 G: 83 B: 59	R:131 G: 83 B: 60	R:135 G: 87 B: 64	R:139 G: 91 B: 68	R:144 G: 94 B: 71	R:146 G: 96 B: 73	R:148 G: 98 B: 72	R:149 G: 98 B: 71
R:126 G: 79 B: 55	R:127 G: 80 B: 55	R:130 G: 83 B: 58	R:135 G: 86 B: 62	R:140 G: 90 B: 66	R:143 G: 93 B: 69	R:144 G: 94 B: 67	R:145 G: 95 B: 68
R:119 G: 72 B: 45	R:120 G: 73 B: 45	R:121 G: 74 B: 47	R:126 G: 78 B: 51	R:132 G: 82 B: 55	R:136 G: 86 B: 59	R:137 G: 87 B: 61	R:139 G: 89 B: 62
R:108 G: 62 B: 32	R:110 G: 63 B: 33	R:112 G: 65 B: 35	R:115 G: 68 B: 38	R:121 G: 72 B: 42	R:126 G: 77 B: 47	R:131 G: 81 B: 53	R:134 G: 84 B: 57
R:101 G: 55 B: 22	R:104 G: 58 B: 25	R:105 G: 59 B: 26	R:108 G: 61 B: 28	R:114 G: 65 B: 33	R:119 G: 70 B: 38	R:124 G: 76 B: 47	R:128 G: 81 B: 53

Figure 3.22: Pixel values of the selected area from Figure 3.20.

In Figure 3.22 the RGB values of the selected area is shown. All the color planes are shown in this figure. Matlab software exports the results of the compressed color planes in matrices. Differently in hardware implementation the output of the compressed image is after the parallel-to-serial converter. The serial data are captured and processed to examine the performance of the hardware implementation and if the data are identical to the algorithm that was implemented in Matlab software. The output result from hardware implementation is in serial-format. Also, the parallel to serial converter implemented in hardware inserts START bits and STOP bits because the design is intended to be used directly in the input of a wireless transmitter that accepts serial data for input. Both START and STOP bits can be configured. In FPGA implementation every compressed pixel is packed for transmission.

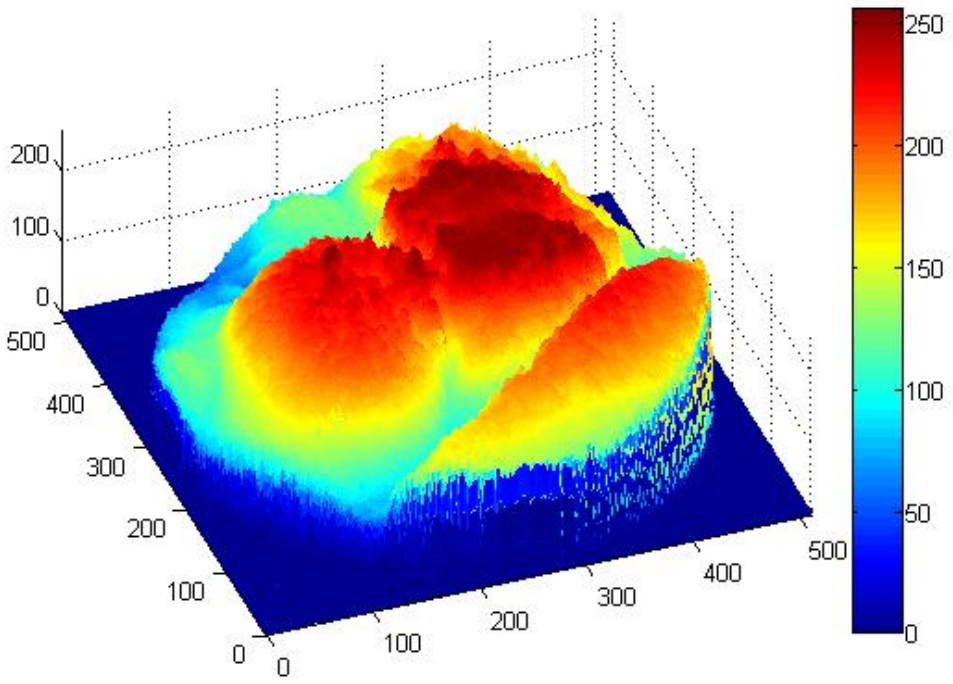

Figure 3.23: 3D plot red color plane.

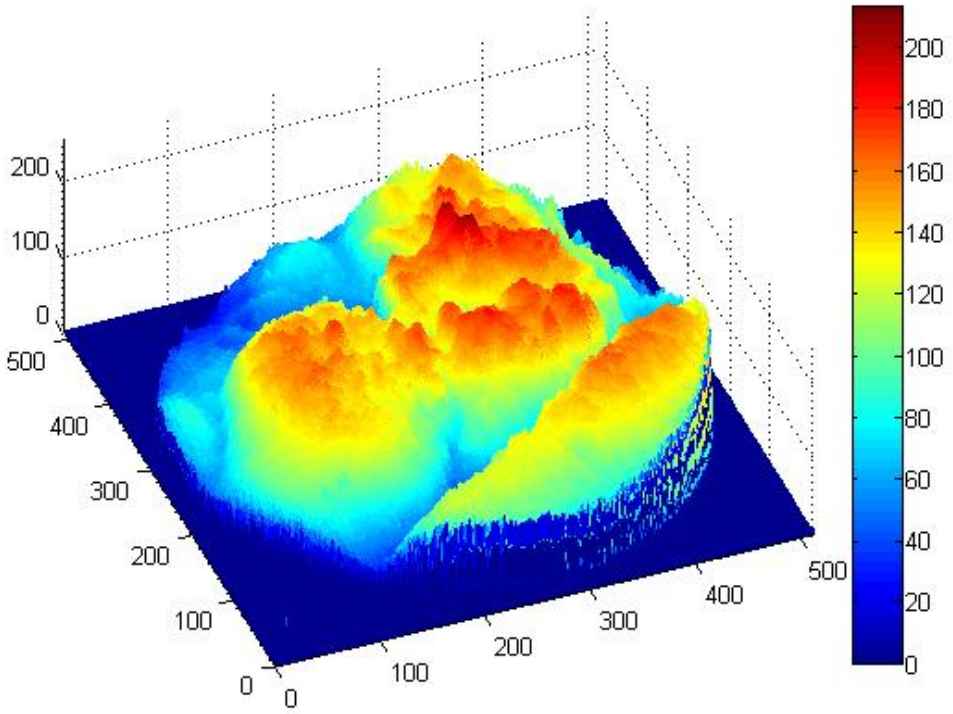

Figure 3.24: 3D plot of green color plane.

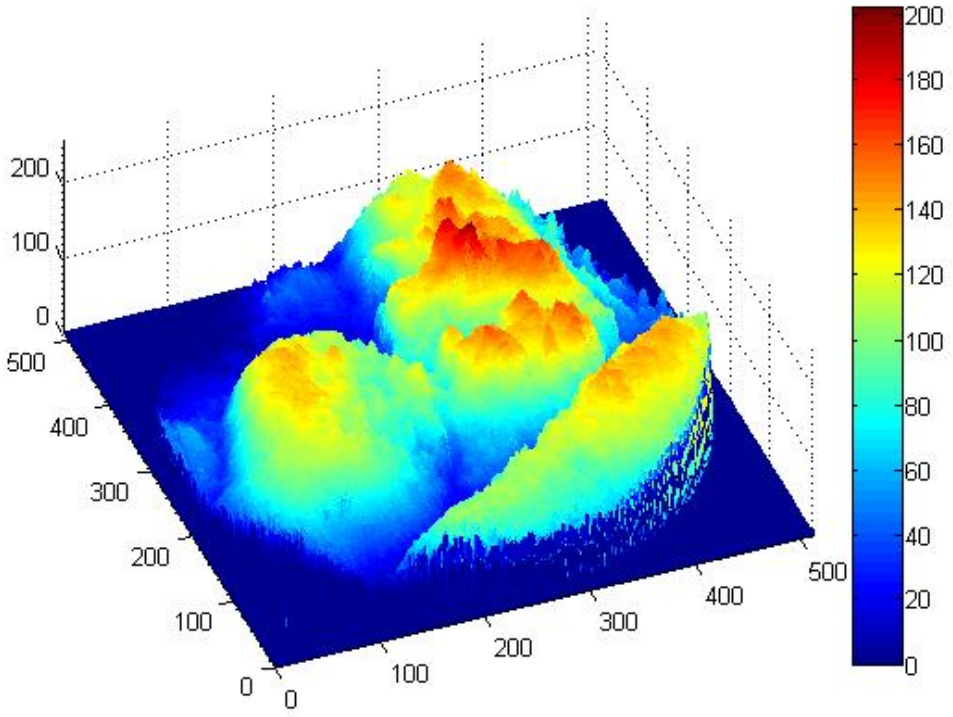

Figure 3.25: 3D plot of blue color plane.

In Figures 3.23, 3.24 and 3.25, 3D plots of the three-color planes is shown. It is obvious how different the of value distribution between red color plane and both green and blue color planes is. It can be seen how the similarities of value distribution of green and blue color planes and how uniformly the pixel values are arranged. These similarities explain the reason of using the same huffman codebook for both green and blue color planes. In Figure 3.27 there is a group of test images used to design, implement and evaluate the proposed algorithm.

Table 3.13: Compression rate of the first image of every row of Figure 3.27

Image	**1**	**2**	**3**	**4**	**5**	**6**
CR	1.85	1.95	2.35	2.15	2.2	2

Table 3.13 shows the compression ratio of the first six images of every row of Figure 3.27. As shown, the first two photos have the worst performance in CR manner. This is because the compression algorithm is based in the statistical analysis of healthy and unhealthy photos. These two photos are from unhealthy patients. However, the rest four images perform better than the other two.

In Figure 3.26 the performance of the proposed algorithm is shown. The average performance of the compression algorithm is 2.21:1 CR. It is obvious that the 2.21:1 compression ratio is not achievable for all the images and some images have a compress ratio of 1.8:1 and some others perform better, about 2.45:1.

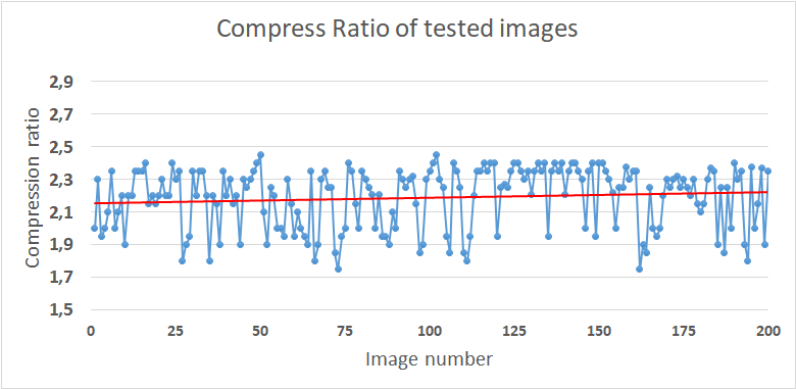

Figure 3.26: Compress ratio performance of 200 test images. The red colored line is the average.

Implementation of other types of compression have been done so it is easier to be compared with the proposed. These techniques were evaluated in software to examine their performance. In Table 3.14, two more approaches of image compression are shown. In the first, Exclusive-Or operation applied to the input data. This operation was made in every bit-plane for all the color planes (RGB). X-OR operation is applied to each bit against the previous. This is the transform coding used to prepare the data for the next stage which is the compression. For compression, run length encoding and huffman encoding was used. The modified data by the transform encoder passed through the RLE encoder and the output imported into huffman encoder. However, the results were not satisfactory. A lossless compression algorithm was produced but with a compress ratio that is too low. The next algorithm designed and evaluated was based in DPCM and huffman coding. It is obvious, this compression algorithm is near-lossless. The reason for this is for reduction of redundancies color-space transformation was used. The input image is in RGB format and it is transformed in YEF. In the Equation 3.13 the mathematical expressions to convert RGB image to YEF, are shown.

$$\begin{aligned} Y &= \frac{R}{4} + \frac{G}{2} + \frac{B}{4} \\ E &= \frac{R}{8} + \frac{G}{8} + \frac{B}{4} + 128 \\ F &= \frac{R}{8} + \frac{G}{8} - \frac{B}{4} + 128 \end{aligned} \tag{3.13}$$

In this table the evaluation of different type of implementations that use predictive coding is presented. A Simple algorithm used to get benefit in complexity, for less power consumption. However, the first evaluated algorithm has low compression ratio performance and the second one has increased compression ration performance than the previous, but the de-compressed results were not identical. The compression was lossy and not lossless.

Table 3.14: Compression performance of different algorithms in software evaluation. XOR-RLE-HUF means applying X-OR logical operation in every bit plane of an 8-bit depth color plane. Then, run length encoding and finally huffman is applied. DCPM-HUF means DPCM encoding is applied in every color plane, and next huffman encoding is applied.

Compression method	color space	Avg. CR	PSNR (dB)
XOR-RLE-HUF	RGB	1.6	∞
DPCM-HUF	YEF	1.9	37.9
This work	RGB	2.2	∞

Divisions are used to perform the color-space transformation. For every division performed, remainders are usually produced. In this compression algorithm, only the integer part of the result is compressed. The remainder is not used. This is the reason why this implementation is lossy. In the inverse operation (de-compression), the result is not equal to the original image because of not compressing the remainder of the divisions.

The proposed algorithm is designed to run inside of an endoscopic capsule that is intended to be used in unhealthy intestines. However, after statistical analysis of multiple images, it is worth performing better in healthy areas that in unhealthy, because the frames that are going to be captured are only few in the entire intestine. So, there is no degradation in the performance of the proposed system. Furthermore, the repeatability of the same values that successive pixels have which are close in value, using a DPCM encoder the entropy is decreased and then huffman encoder compresses the image. This characteristic is seen in the blue and green color plane and it is shown in Figure 3.16.

Figure 3.27: Sample images form human GI used to design and evaluate the proposed compression algorithm.

3.4.2 Hardware implementation

The proposed algorithm was firstly implemented and tested in Matlab software. The compression algorithm then implemented in Very high-speed integrated circuits Hardware Description Language (VHDL). The proposed algorithm was implemented and tested on a development board provided by Avnet with a Xilinx Sparta-6 family chip.

3.4.2.1 Hardware architecture

The design requirements, that were set in previous paragraph, need the compressor to be loss-less, low power, low complexity and to can use commercial CMOS camera sensors. In Figure 3.28 an overview diagram of the proposed design is presented.

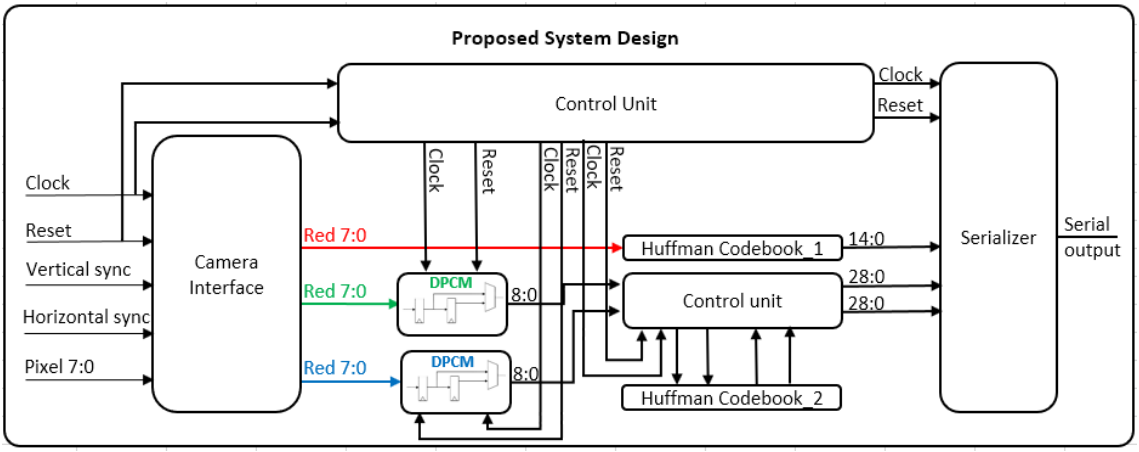

Figure 3.28: Block diagram of the proposed compression algorithm.

The proposed design can be divided into three parts. The first part is the camera interface, the second is the main code of the compressor and the last is the parallel to serial converter unit. The most common camera interface in commercial camera sensors [84], [85] is the Digital Video Port (DVP). It is a parallel interface were the pixels are exported in raster-scan mode. The DVP camera interface consists of the parallel data line, which can be from 8 to 12 bits, the horizontal synchronization, the vertical synchronization and the pixel clock signal. If a 640 $\times$ 480 image need to be transmitted in RGB888 format, the camera sensor will transmit 8-bits per pixel clock. To transmit the three-color values of one pixel, 3-pixel clocks are needed. The horizontal synchronization signal will be triggered after 640 $\times$ 3 = 1920-pixel clock ticks. The vertical synchronization will be triggered after 1920 $\times$ 480 = 921600-pixel clock ticks. The proposed system uses Hsyn, Vsyn, Pclock and Data_input to get the data from the camera sensor. The order of the incoming data is, first the 8-bits of the red color, second are the 8-bits of the green color and last are the blue color pixel value. When the first 8-bits from red color arrive, they are encoded by the dedicated huffman codebook and pushed to parallel to serial module. In the next pixel clock the green pixel value arrive. It is encoded by DPCM module. The first time the initial value of the DPCM encoder is 128, so the first green pixel is subtracted from the value 128. The result is pushed in a huffman encoder which is dedicated for green and Blue color. The output from this huffman encoder is pushed to the parallel to serial module. The

same procedure happens for the blue color pixel. After all these the compression algorithm starts from the beginning.

3.4.2.2 FPGA design

The overall design of the compression algorithm was implemented in a Spartan-6 family FPGA. In Figure 3.29 the development board used is shown. The compression algorithm can be separated in three stages: the camera interface, the compression algorithm and the parallel to serial converter.

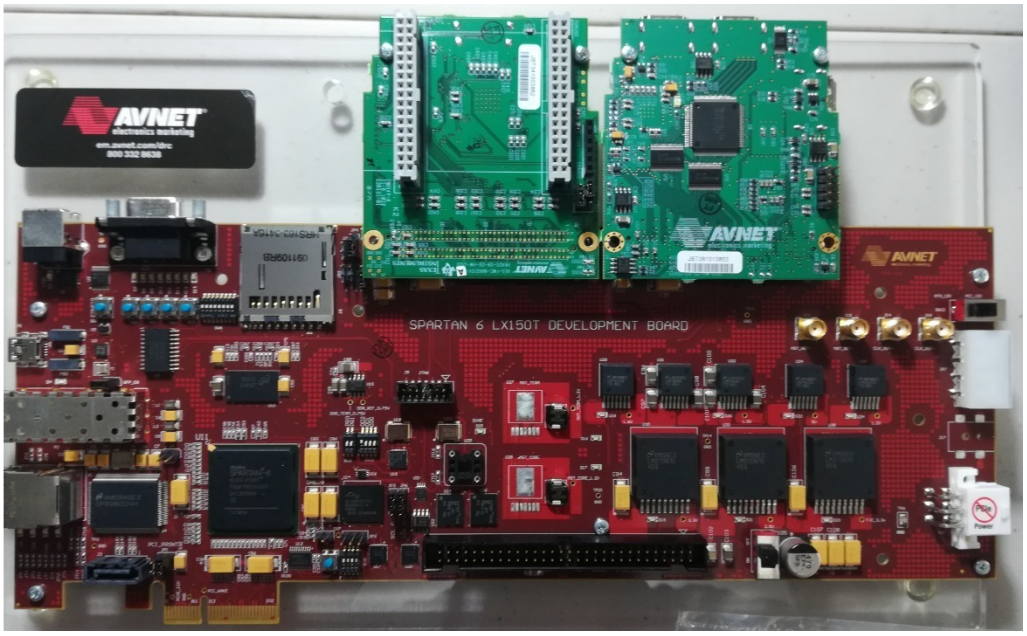

Figure 3.29: Photo of Avnet Spartan-6 industrial video processing kit, used for experiments.

In hardware implementation, the proposed algorithm was designed and tested on a development board with a Xilinx Spartan-6 chip on it. In this implementation, as mentioned, there is a codebook for huffman coding of the red plane and a second huffman codebook for both green and blue color planes. The codebooks selected to be implemented with the use of simple digital logic and not with LUT-tables and SRAM, because both will increase the complexity, the power consumption and the resources for implementation. Truth tables and Karnaugh maps were created and solved to achieve the best performance. In Table 3.19 the comparison results of the proposed algorithm implemented using simple logic is shown. In this design, the implementation of two huffman codebooks used, one for the red plane and the second one for green and blue plane. The huffman codebook for the red plane, directly compress each pixel and send the output to the serializer. However, in the other two-color planes DPCM encoder is applied at first in each color value and in the output of each DPCM encoder the second huffman codebook is applied. Both huffman codebooks were produced using the probabilities extracted by the large capsule endoscopy image data-set. The DPCM output of both color, green and blue, planes produces both positive and negative numbers. After processing of all the capsule endoscopy image, it is found that the range of the output of the DPCM encoder was from -127 and up to 128. In hardware implementation there were negative numbers that are handled like positive. The way this was done is easy and with low complexity. Implementation of huffman encoders are designed

based on memory storage. In this implementation a huffman tree design without the use of memory is proposed, just by using logic gates. Huffman encoding stores the output values in a memory and each input addresses the corresponding output. The proposed algorithm is memory-less and implemented using logic gates. In Figure B.1 is diagram of the huffman encoder, Figure B.2 presents the schematic diagram of the huffman encoder. The proposed huffman encoder was implemented with memory and without memory. The tests took place in the same development board. The results in delay time and power consumption are shown in Table 3.15.

Table 3.15: Comparison of implementing huffman encoder with and without memory.

	Without memory	**With memory**
Max delay time	1.730 ns	3.124 ns
Power consumption	0.88mW	1.28mW

In the proposed implementation, as mentioned in previous paragraph, the output of the huffman encoder is ranging from 2 to 29 bits. A truth table that has 29 output functions is created and simplified. Each of output function was computed separately, then there were combined and produced a huffman encoder without the use of memory and lookup-tables. As said, the output of the huffman codebook is 29-bits wide and its output is a function of a truth table of 8-bit wide input. In Figure 3.31 huffman diagram is shown. In the left side of the figure, input data lines of the incoming pixel are shown. As shown, there are 8-bit wide. Every block from F_0 to F_28 contains a Boolean equation like Equation 3.14. In the right side of the figure is the outputs of the huffman encoder. Every function solved separately from the others and there are 29 functions in the end. In Equation 3.14 the boolean expression of one function out of 29 is shown. The 8-bit wide input is named by letters, A, B, C, D, E, F, G, H. Where A' is the inverse input of A, etc.

$$\begin{aligned}\mathbf{F_0} = {} & A'B'C'E'F'G + C'DE'F'GH' + ABC'D'EH + ABC'EF'G + A'B'C'D'F'G'H' + \\ & A'B'C'D'E'GH + A'B'C'D'F'GH + A'B'C'DE'GH' + A'B'CD'EF'H + A'B'CEF'GH + \\ & BC'DEF'GH + BCD'E'F'GH' + A'BCD'FGH + A'BCE'FGH + A'BCD'EFH' + A'BCEFGH' + \\ & A'BCDF'G'H' + A'BCDE'FH' + AB'C'E'F'G'H' + AC'D'EF'G'H + AB'C'DFG'H' + \\ & AB'C'DE'FH + ACD'E'F'GH' + AB'CD'E'FH + ACD'EF'GH + ABC'D'E'FG + ABC'D'EFG' + \\ & ABC'EFG'H + ABC'DE'F'H + ABC'DEGH' + A'B'C'D'EFGH' + A'B'C'DEF'G'H + \\ & A'B'CDE'F'G'H + A'BC'DE'FG'H + A'BC'DEFG'H' + AB'CD'EF'G'H'\end{aligned} \tag{3.14}$$

In Equation 3.14, the input data is 8-bit wide. The input is represented by letter, from A to H. However, as shown, in this Boolean expression except of simple letters, there are letters with intonation, for example A', this means that in this Boolean expression the invert input of A is used. Huffman table was created using Matlab software as shown in Table 3.16. However, in our implementation memory elements were not used for huffman encoder hardware implementation. So, every output of huffman encoder was solved using Karnaugh map. In Figure 3.30, the Karnaugh map for the 14th output of the huffman encoder for green and blue plane is shown. This is the one of the 29 Karnaugh maps solved to implement the huffman encoder for

green and blue planes.

Also, the use of simple logic gates circuit improves the speed of the huffman encoder. To make the serializer able to detect the size of the output each time there is a 5-bit port for the huffman encoder circuit, which informs the serializer the size of the output each time. In green and blue planes, same huffman code book was used. The reason to do this is are the similarities of the pixel value probabilities of both colors and for less FPGA resource usage. In this way, only two huffman encoders instead of three is used. After applying DPCM encoding in both colors the data need to pass from the huffman encoder.

Table 3.16: Truth table of red plane huffman code book.

Data input	F_0	F_1	F_2	F_3	F_4	...	F_{10}	F_{11}	F_{12}	F_{13}	F_{14}
00000000	1	0	1	x	x	...	x	x	x	x	x
00000001	0	1	0	x	x	...	x	x	x	x	x
00000010	1	1	1	0	1	...	x	x	x	x	x
00000011	1	1	1	0	0	...	x	x	x	x	x
00000100	1	1	1	1	1	...	x	x	x	x	x
00000101	0	0	0	1	1	...	x	x	x	x	x
.											
.											
.											
11111010	1	1	0	1	1	...	x	x	x	x	x
11111011	0	0	1	0	0	...	1	1	x	x	x
11111100	0	0	1	0	0	...	1	0	0	x	x
11111101	1	0	1	x	x	...	1	0	1	0	x
11111110	0	1	0	x	x	...	1	0	1	1	1
11111111	0	0	1	0	0	...	1	0	1	1	0

F_{14}		efgh															
		0000	0001	0011	0010	0110	0111	0101	0100	1100	1101	1111	1110	1010	1011	1001	1000
abcd	0000	x	x	x	x	x	x	x	x	x	x	x	x	x	x	x	x
	0001	x	x	x	x	x	x	x	x	x	x	x	x	x	x	x	x
	0011	x	x	x	x	x	x	x	x	x	x	x	x	x	x	x	x
	0010	x	x	x	x	x	x	x	x	x	x	x	x	x	x	x	x
	0110	x	x	x	x	x	x	x	x	x	x	x	x	x	x	x	x
	0111	x	x	x	x	x	x	x	x	x	x	x	x	x	x	x	x
	0101	x	x	x	x	x	x	x	x	x	x	x	x	x	x	x	x
	0100	x	x	x	x	x	x	x	x	x	x	x	x	x	x	x	x
	1100	x	x	x	x	x	x	x	x	x	x	x	x	x	x	x	x
	1101	x	x	x	x	x	x	x	x	x	x	x	x	x	x	x	x
	1111	x	x	x	x	x	x	x	x	x	x	0	1	x	x	x	x
	1110	x	x	x	x	x	x	x	x	x	x	x	x	x	x	x	x
	1010	x	x	x	x	x	x	x	x	x	x	x	x	x	x	x	x
	1011	x	x	x	x	x	x	x	x	x	x	x	x	x	x	x	x
	1001	x	x	x	x	x	x	x	x	x	x	x	x	x	x	x	x
	1000	x	x	x	x	x	x	x	x	x	x	x	x	x	x	x	x

Figure 3.30: Karnaugh map for the 14th output of the huffman encoder for green and blue plane.

In the DPCM block, the clock used to manage the previous data input. A small FIFO has been created and is used for the DPCM operation. The size of the FIFO is 2 bytes for green color plane and 2 bytes for the blue.

$$\mathbf{F_{10}} = FH' + DF'G + CH \tag{3.15}$$

$$\mathbf{F_{11}} = F'GH \tag{3.16}$$

$$\mathbf{F_{12}} = H + G \tag{3.17}$$

$$\mathbf{F_{13}} = G \tag{3.18}$$

$$\mathbf{F_{14}} = H' \tag{3.19}$$

The last part of this system is the serializer. In this sub-system the conversion of parallel data to serial is implemented. The data input for this system is variable. The reason is the variable output of the huffman encoders, that can be from 2-bits and up to 29-bits for blue and green plane and from 3-bits to 15-bits wide for red color plane. Due to this variation, the parallel to serial converter needs to know the width of the huffman output for every processed pixel. The input in the compression is an 8-bit wide signal. First are coming the value of red color, then the green and last are the blue color pixel value. In red color plane, the system clock is used to latch the output. Huffman coding is implemented with logic gates, so when the input changes, the output is changing directly. Clock latch is the output to make it available for the next unit of the system. Figure 3.28 shows the hardware structure of the proposed system.

As noted previously, the inputs of every huffman encoder are 8-bit wide. While the output of huffman is variable, so there is a need to inform the parallel to serial converter, about the length of the output each time. As seen in Figure 3.31, the huffman block consists of two smaller blocks, the one is the huffman encoder itself and the other is a circuit that exports the length of the huffman encoder.

In Table 3.17, the output of the circuit that outputs the size in bits of every huffman output is shown. For example, if the output of huffman encoder is 10-bits wide, then this circuit outputs the value “0101”. The output range of 4-bit wide. The boolean expression for every bit is solved. So, four functions produced, F_0, F_1, F_2 and F_3. In Equation 3.20. one of the four boolean expressions are shown.

$$\begin{aligned}\mathbf{F_2} = {} & B'CD'E'F'G'H' + B'C'D'E'F'GH + B'C'D'E'FG' + B'C'DE'FG + B'C'DE'FH + BCDEGH \\ & + B'C'DEH' + B'C'DEG' + B'C'DEF' + AEFG + AE'F' + AD' + AC' + AB'\end{aligned} \tag{3.20}$$

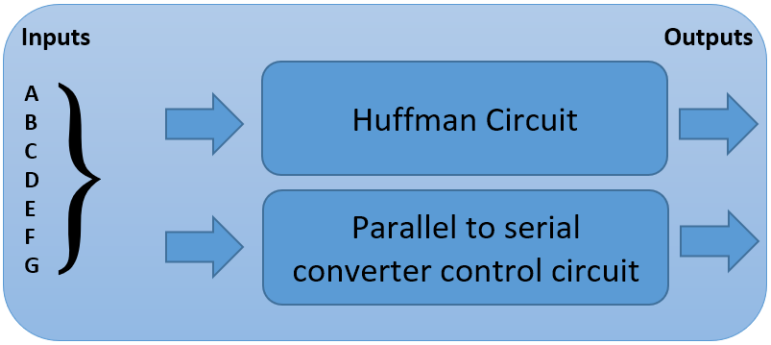

Figure 3.31: Diagram explained in graph, how the proposed huffman encoder works and outputs extra bits to provide information to the parallel to serial converter about the width of every processed output.

Table 3.17: Table of data output in correspondence of huffman output

Size of huffman Output in bits	Data Output
3	0000
5	0001
7	0010
8	0011
9	0100
10	0101
11	0110
12	0111
13	1100
14	1001
15	1010

In Table 3.21, the used FPGA resources are presented. The device is XC6SLX150T, as shown in Table 3.21 requires few resources from the FPGA device used. In Table 3.22, there is a comparison of the proposed design with other implementations. In addition, the simplicity of the algorithms requires the system to use less resources. Furthermore, because of the nature of huffman and DPCM encoders it can be used in variable resolution images in capsule endoscopy applications.

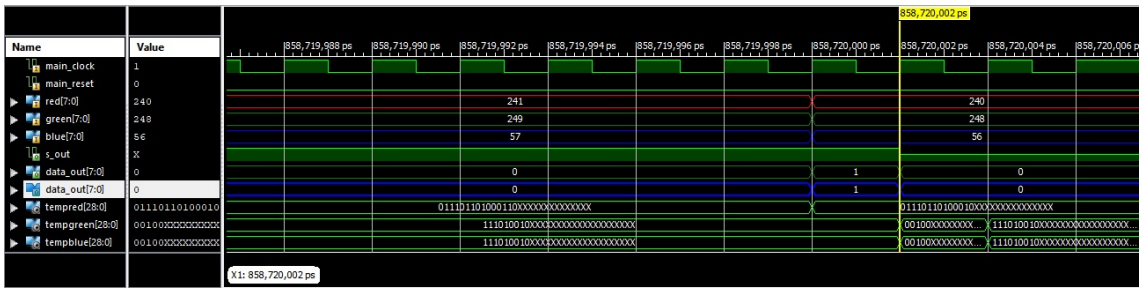

Figure 3.32: Part of FPGA simulation. The DPCM output for both green and blue color planes can be seen.

From Table 3.21, it can be seen that the proposed system can achieve good compression rate for loss-less compression for Table 3.21 larger image size. In addition, with the simplicity of the algorithms and less resource used. It can be used for high resolution capsule endoscopy application.

Also, the output of the huffman encoder for both green and blue planes is shown. These colors use the same huffman codebook and for this reason the result is the same. In this case because the output of the DPCM encoder for both colors is "1" the output of huffman encoder is "100". In the Figure 3.32 the output shown is "00100", this is because the first two binary digits are internally used for processing. So, except these two digits, the result is "100". This part is implemented using VHDL language. The encoder is implemented to be multiplier-less and low complexity. In this module the implementation of both green and blue DPCM encoders is implemented. As previously noted, the colors of each pixel are arriving in this order, first the red color then the green and finally the blue color. In this design due to this characteristic of the camera sensor, the DPCM encoder is implemented and used. In Figure B.3 an overall view of the schematic of the DPCM encoder is shown. At Table 3.18 are shown the power consumption of the proposed algorithm is shown with the maximum frequency this module can achieve.

Table 3.18: Power consumption and max delay time of DPCM encoder block.

	Proposed DPCM
Max delay time	1.240 ns
Power consumption	1.11mW

The last part of the algorithm is the parallel to serial converter. This part should be fast and be able to handle the incoming parallel data. This part should not be counted in the compression algorithm because is not compressing the incoming data. It is just preparing the data from the compressor to be send to the wireless transmission system. The mission of this module is to convert the incoming compressed data from parallel to serial order. Then this serial data is sent to the wireless transmission system to be send outside human body. In Figure B.4 is the schematic diagram of the parallel to serial implementation.

3.4.3 ASIC design and simulation

In this thesis a loss-less, multiplier-less compression algorithm for capsule endoscopy is proposed. The compression at first was designed and tested for its performance in Matlab software. Later the VHDL code of the proposed algorithm was produced to test and verify the performance in hardware. The last part is the implementation and simulation of the compression algorithm in transistor level, ASIC design. The proposed algorithm is tested and works for image size of 512×512 pixel and can work up to HD image resolution. Images used are in RGB format 8-bit color per color plane. For the ASIC design, of the proposed system, the use of 16nm FinFet technology was selected. This technology combined with the multiplier-less algorithm, can perform better in the domain of power. The main characteristic of FinFet technology compared with CMOS is the lower power consumption and the reduced latency in digital circuits. The use of FinFet technology can reduce the power consumption compared to CMOS up to 90%. [83] The proposed system is designed in a way to be able to connect to any commercial image sensor that support digital-video-port (DVP). The proposed compressor module is designed to have one serial output. The parallel data from the compressor is serialized and packeted with start bits and stop bits so it can directly connect to any wireless transmitter which supports serial input. The proposed systems consist of 12 inputs and 2

outputs. For the inputs 8 of them are the color data and the rest 4 are the Clock, reset, vertical and horizontal synchronization. Vertical and horizontal synchronization bits are used to show the finish of a frame and to the finish of a row, respectively. The entire system was simulated and implemented using Cadence Software toolsets. In Figure 3.33 the result of the proposed algorithm implemented in transistor level is shown.

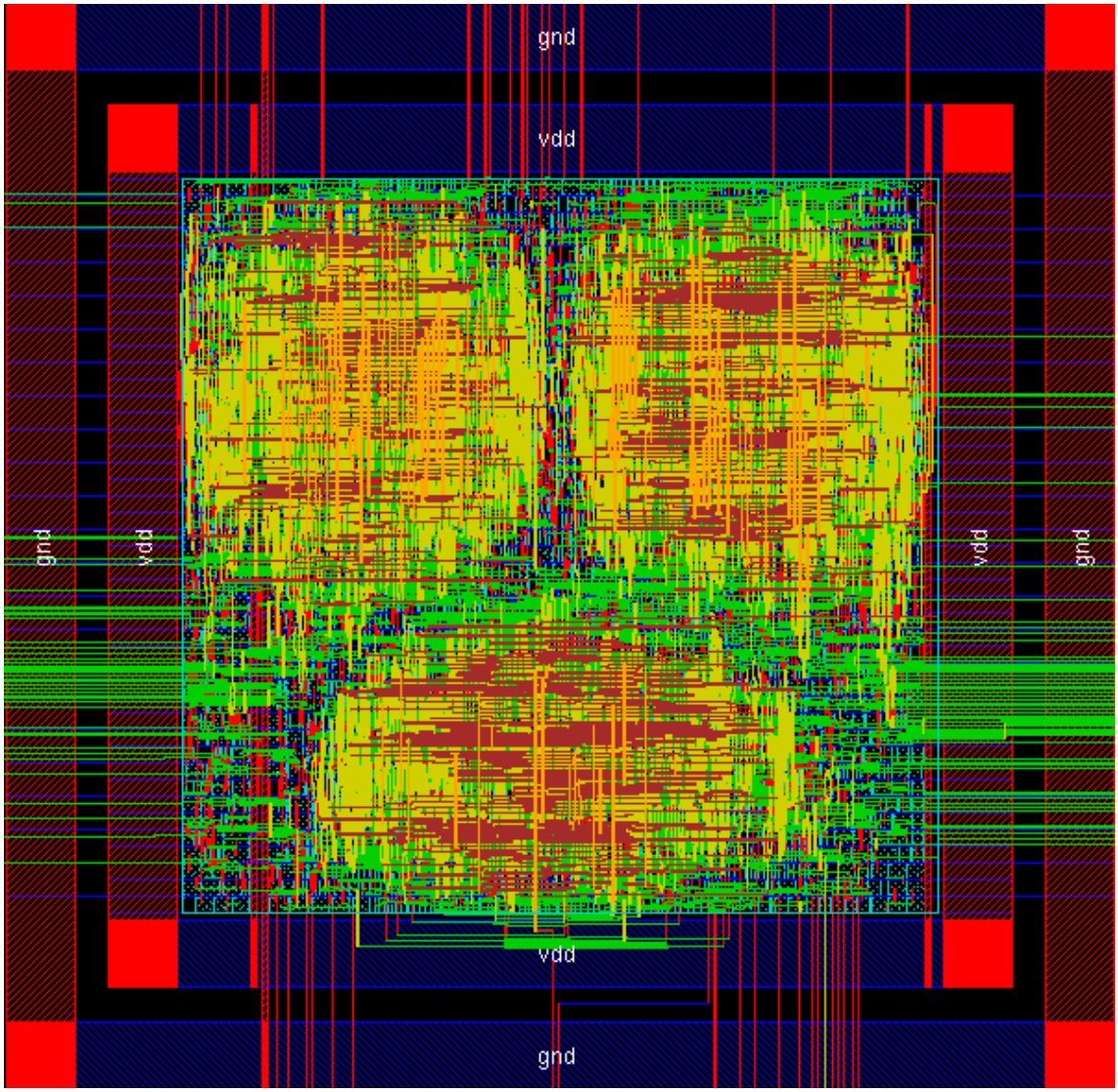

Figure 3.33: ASIC implementation of the compression algorithm using Cadence software tool set.

For the design of the ASIC Cadence RTL compiler and Cadence Encounter were used. In Table 3.19 a comparison of the proposed compressor with existing systems is shown. The proposed design is a loss-less, multiplier-less technique that has a CR of 2.2. The other designs shown in Table 3.19, are based on near-loss-less or lossy techniques that most of them are using buffer to process the input image. Fante et al. [86], Goyal et al. [87], Liu et al. [66] and Lin et al. [67] their designs are based on near-loss-less or lossy techniques with the use of memory buffer and the resolution of the original image is not higher than 256×256 pixels per frame excepts from Lin et al. [67] which is 512×512 pixels per frame.

Table 3.19: Comparison between proposed compression scheme with others in manner of hardware cost.

	Core size (mm^2)	Gate count	Buffer	Power (mW)	Image size	Lossless
Tareq et al. [79]	0.0256	2k	0	18	320 × 240	YES
Liu et al. [66]	23.04	27.8k	100kb	N/A	400 × 400	NO
Lin et al. [67]	0.39	31k	288b	14.92	512 × 512	NO
Goyal et al. [87]	0.019	4.9k	-	14.2	256 × 256	NO
Fante et al. [86]	0.018	2.2k	-	3.5	256 × 256	NO
This work	0.056	16.8k	0	4.5	512 × 512	YES

In Table 3.19 a comparison of other designs and the proposed is shown, emphasizing in the hardware cost. It show that in the two of the designs a buffer memory is used. This hardware is not added in the gate count. Also, the first one, which is lossless has less gate count than the proposed system, but the maximum image size is up-to 320 × 240. Although the proposed system has more gates, it manages to achieve lower consumption and less space due to the use of FinFet technology. A novel design of a lossless, multiplierless and without the use of memory buffer is proposed. The proposed compressor can compress up to HD resolution images. The use of the FinFet technology and the low complexity of the compression algorithm reduces the power consumption to lower levels. In Table 3.20 a summary of the ASIC design of the compression is shown.

Table 3.20: ASIC design performance.

ASIC	Feature
Technology	FinFet 16 nm
Area	0.056 mm^2
Clock frequency	144 Mhz
Voltage	0.85 V
Logic Gate	16.8 K
Memory	0 kb
Power consumption	4.5mW

3.4.4 Results comparison

The Proposed algorithm is a loss-less compressor based on predictive coding (DPCM encoder) and variable length coding (huffman encoder). Due to the loss-less character of the proposed algorithm, the reconstructed image is identical to the original. For this reason, PSNR = ∞. The average compression ratio achieved from the processed test images is 2.21:1. It is important to say that loss-less algorithms are not able to achieve high compression ratios like lossy compression. In Table 3.21 an overview of the FPGA resources used algorithm is shown. Also, in Table 3.22 a comparison of the proposed algorithm with existed systems is shown.

Table 3.21: FPGA resources used.

Resources	Proposed design	With memory	
Slices	288	433	-34%
4-input LUTs	2816	6845	-64%
RAMB16BWERs	0	3	-100%
DSP48A1s	2	2	0%
Max. Frequency	144MHz	144MHz	N/A

Table 3.22: Comparison between proposed method and other existing methods.

Specifications	**[69]**	**[17]**	**[68]**	**[65]**	**Proposed Work**
Color plane	YUV	RGB	RGB	RGB	RGB
Compression method	Predictive coding	DCT	JPEG-LS	Predictive coding	Predictive coding
Buffer	NO	YES	YES	YES[6]	NO
Loss-Less	YES	NO	near-Loss-less	YES	YES
Image size	320 × 240	-	640 × 480	320 × 240	512 × 512
Clock rate	91MHz	150MHz	40MHz	42MHz	144MHz
Compression ratio	2.4	10	3.5	2.2	2.2
PSNR (dB)	∞	32.95	45	∞	∞

In this table the proposed design is compared with existed methods. Is seen that two of the can process image of resolution up-to 320 × 240. The reason for this bottleneck in this design [69] is the implementation architecture which has divisions for the color space transformation, from RGB to YUN format. In [65] also, the maximum resolution is low because this design is not able to increase further the clock rate of the system. In the proposed design the the maximum clock rate is 144MHz, this is due to the use of FinFet technology that has low delay. This increased clock rate, increases the maximum image resolution that it is possible to process.

3.5 Summary

In this chapter, a lossless compression algorithm for capsule endoscopic images has been proposed and evaluated with satisfying performance. It is further designed and implemented on a FPGA chip using only simple arithmetic operations. The ASIC was designed with Cadence toolset using 16nm FinFet technology in 16.8k gates, without the use of any buffer memory and with a power consumption of 0.045mW. Sample RGB endoscopy images are used to create dedicated huffman code books. It is a low energy, low complexity, sufficient compression method which uses simple arithmetic operations. The only arithmetic operation used is subtraction and it was applied only in the DPCM encoders of the green and blue planes. The output of the DPCM encoders is a signed value which are treated as unsigned values due to their statistics by the huffman encoder. So, in this way, the complexity of the design is not increased. The maximum image size that can be processed is up to HD resolution. With the 2.2:1 CR, the same results as other works achieved but with

[6] One row data buffer.

the use of less resources, low energy, higher resolution and simpler technique.

Further improvement can be done by applying a clipping algorithm at [65]. Because the lens of the capsule generates a circular image and the sensor camera is rectangular, the corners of the image have a value of zero. With this cropping algorithm, the compression performance might be improved further.

Chapter 4

Design of FinFet On-Off Keying transmitter for wireless capsule endoscopy

4.1 Overview of telemetry systems

In Chapter 3, the image compression part of a WCE system was introduced. In Figure 4.1 a diagram of a typical WCE is shown. However, to be able to obtain data from camera sensors or typical sensor like temperature, pH, etc., a wireless transmitter need to be used.

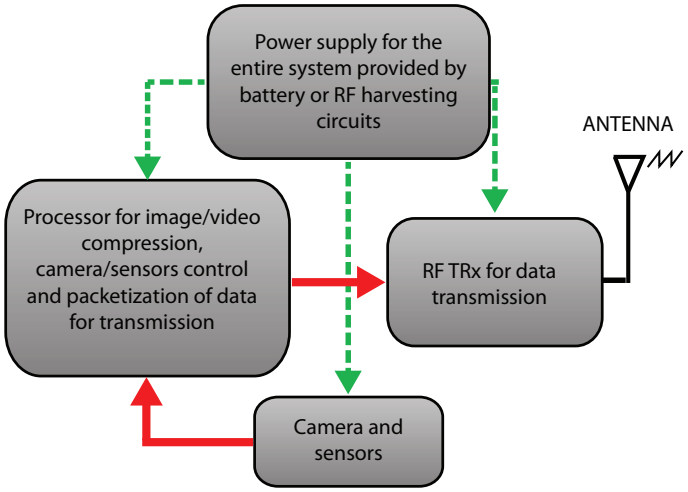

Figure 4.1: Block diagram of the part of an endoscopic capsule, with red color data flow (solid line) is denoted and with green color (dashed line) there is the power supply path.

It is obvious, that without the transmitter it will not be possible to get image data for diagnosis. The use of a high capacity internal memory in the capsule will decrease the time of operation due to increased power consumption. This is one reason why memory is not wanted to be used inside the capsule. This was also discussed in Chapter 3, where an image compression, with the need of buffer memory, was implemented. Unlikely the RF telemetry system is the most used part in medical applications. The image compression is used only in capsules where cameras are used as sensors. Most medical applications use transceivers. These applications are referred to sense vital signs, neuro-prosthetics for stimulation, remote medical diagnoses and capsule endoscopy, the category of application this work focuses. The way of how an endoscopic camera pill is, WCE captures the signals from sensors and takes pictures with the camera. These data are compressed, packed and then transmitted outside of the body in real-time through a Radio Frequency (RF) module inside of the WCE. Outside of the body, there is a receiver that decodes the compressed data and presents it to doctors. With more details, the processor receives the values from the sensors in digital and analog values, converts the analog to digital and then compresses and packs the data to be sent through RF transmission part outside the human body to an external RF receiver. Since the amount of the data from the use of a camera is huge an image compressor with high compression ratio is required. Since the use of a lossy compression algorithm is prohibited in medical applications, the compression of image data must be lossless as required by the doctors for accurate diagnosis. In lossless compression schemes the reconstructed image is identical to the original. The use of lossless compression schemes is the only way, but high compression ratio is not as achievable as in lossy compression schemes. So, the overall performance of the system highly depends on the data communication capability of the RF transmitter. Higher data rates would provide the possibility to use higher camera resolutions which means better results for the physicians.

There are many related works on RF telemetry systems. All of them with their specific approach to resolve the main problems of such systems. The main issues are:

- The area occupied by the system,
- the power consumption and
- the data rate.

It is obvious that by trying to solve these problems, new ones emerged, in the design of the system. Due to the criteria applied, the best approach was designed and implemented.

4.1.1 Related works

Many RF telemetry systems for capsule endoscopy have been developed in recent years [11] [18] [19] [20].The research effort focuses on designs to reduce power consumption and increase the data rate. Thone et al. [11] design a simple, tiny RF transmitter based on FSK modulation. This circuit design works with 1,8V, consuming 2mW of energy. The maximum data rate is 2Mbps. Due to the low data rate, this design is not able to transmit more than 15-17fps of VGA resolution images, which are compressed.

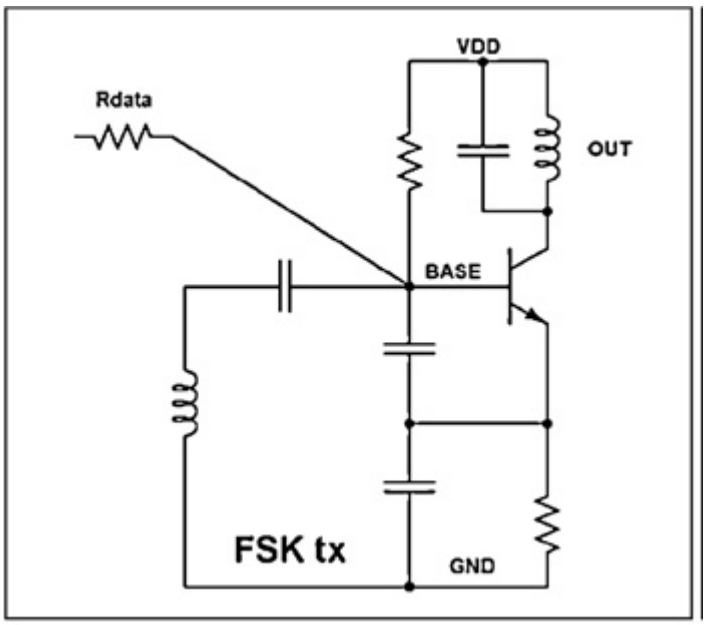

Figure 4.2: Wireless transmitter of 2Mbps data rate and 2mW power consumption. [11]

Liu et al. [18] presents an On-off keying transceiver which works at 1,8V with 3,1mW Tx power and 3,4mW in Rx mode. The carrier frequency of this design is 400MHz and the data rate up to 2Mbps. Using high carrier frequencies causes the signal transmitted to be weakened due to the human tissue absorption [88][89]. The transceiver was implemented with 0,18um and used CMOS process technology.

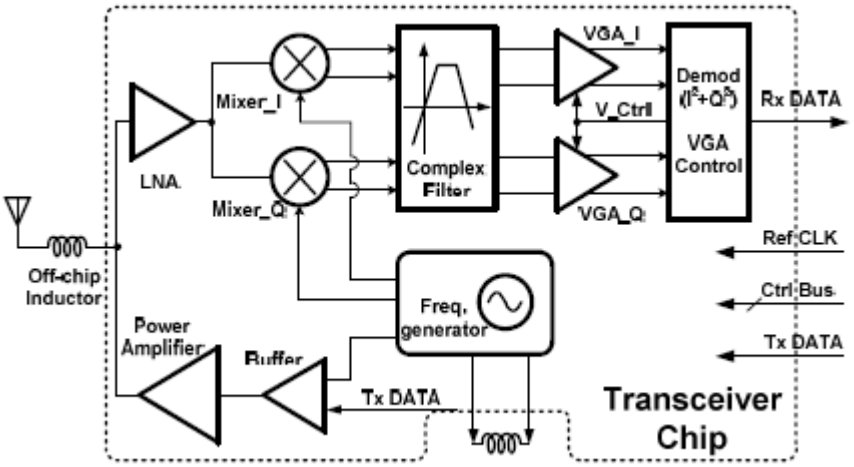

Figure 4.3: Liu's proposed OOK transceiver. [18]

Ryu et al. [19] made a significant contribution to the field of data rate. This design can achieve up to 40Mbps data rate. However, the power source of the design is 3V with 860uA of current, it is a novel design with 2.58mW average power consumption. The carrier frequency of this design is also high in 440MHz and the implementation process is 0,18um and used CMOS technology.

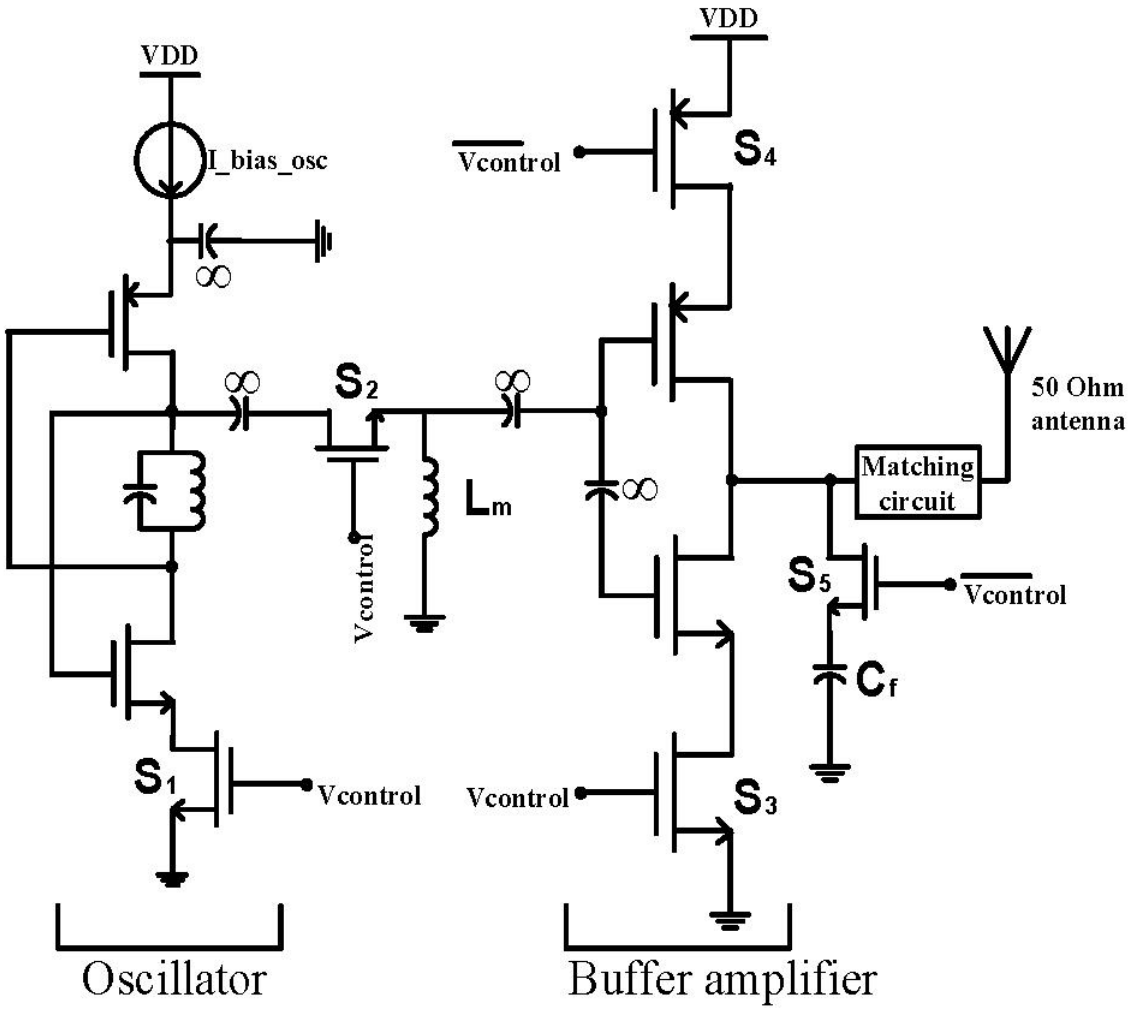

Figure 4.4: Ruy's proposed OOK transmitter with a data rate up to 40Mbps. [19]

A great project mentioned by Raja et. al. [20], implemented an On-Off keying transmitter with adaptable data rate. The data rate of this system is 3-10Mbps with a power supply of 1V at 560ua current consumption. The carrier frequency is 433MHz and the implementation was 0,35um and used CMOS technology.

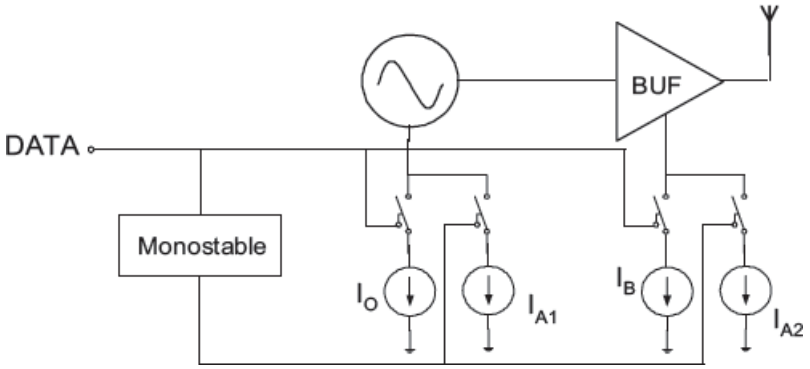

Figure 4.5: Raja's proposed OOK transmitter diagram. [20]

These systems are not able to transmit high resolution images at high rates. Trying to send an HD quality of an uncompressed image a communication link of 22.11Mb/s is needed to transmit one frame per second. An average compression ratio of lossless schemes is almost 2.5. So, in an HD image a transmitter with 8,85Mb/s can send one frame per second. Most of the above systems are not able to send an HD quality compressed image in one second.
Thus, the goal is to provide a novel telemetry system with high data rate and low power consumption.

4.1.2 Design constraints of implanted devices

When designing a system to be used inside human body, one you must overtake some problems. The most important is the energy to be used during the time the implanted device needs to operate. An WCE should be able to work for 8-12 hours, because this is the time that a capsule with passive movement needs to complete its journey inside human GI.
There are also more challenges and constraints that should be considered and analyzed to find the best solution. Especially, the points be focused on this work are:

- The area occupied by the system,
- the power consumption,
- the data rate and
- Frequency selection for data transmission,

In the next paragraphs these problems will be discussed.

4.1.2.1 Ultra-low power

In existing systems there are two ways that the power is delivered in wireless capsules. The first one and most common is using a non-rechargeable battery. The second way is by using a wireless transfer module. In the second way there is a power receiver module consisted by a coil that receives wireless power and use it in the WCE to capture and transmit the images. In Figure 4.6 is shown the main parts of a capsule with power transfer module. More accessories to fit needed to make it work. Also, if the capsule be outside of the power transmission area, the capsule will shut down unexpectedly and will not capture any area of the GI.

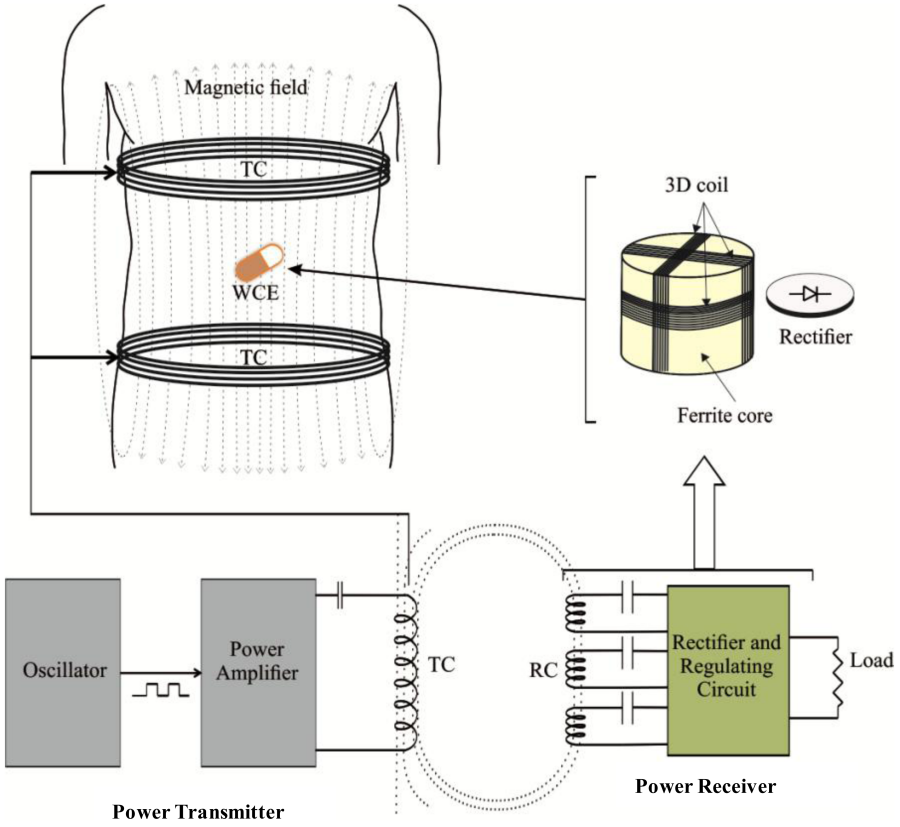

Figure 4.6: Block diagram of the part of an endoscopic capsule which uses wireless power transfer method to work.

These are the two methods used to provide power to the capsule. The use of a hybrid system could provide a satisfactorily amount of energy, but the tiny size of these capsules makes prohibitive the use both the same time.

Implanted devices with battery need to operate for long periods. The circuits used in a wireless capsule endoscopy consists of a mix of analog and digital circuits. The most important factor for both analog and digital circuits about the power consumption is the technology used for implementation. The technique used mainly to consume less power in digital circuits is to power off the circuit when is not operating. In the other side in analog circuits more power can be conserved by making their start-up time as less as possible.

4.1.2.2 Low power implantable wireless transmitter requirements

In wireless capsule endoscopy the main functions taking place at the telemetry system are to modulate the data into the RF carrier frequency, to amplify this signal and to match the PA with the antenna to achieve more efficient transmission.

To obtain a transmitter with low power consumption three points during the design should be considered.

This type of telemetry systems is used for data transmission from inside to outside the human body. It is obvious that the distance takes an important role in the energy needed for the transmission. In case of using less power than the amount needed then the Bit Error Rate (BER) will be increased. By the next formula

the minimum rated power needed for a reliable RF link,is calculated.

$$P = (\frac{4\pi f}{c})^2 \frac{d^n}{G_r G_t} R_{sens} LF \tag{4.1}$$

Where f is the carrier frequency of the transmitter, d is the distance between the transmitter and the receiver, c is the speed of light, Gr and Gt are the antenna gains for the receiver and the transmitter, n is the path loss exponent and the LF is the loss factor due to losses like the losses in matching network.
Another factor in the power efficiency of such system is the efficiency of the Power Amplifier (PA). In these systems switching PA are used due to the efficiency they can achieve. The last part of data transmission is the matching network between the PA and the antenna. Designing a good matching network, more power from the PA could be delivered to the antenna. By this way, more power will be radiated, and there will be better transmission with less power consumed.

4.1.2.3 Human body as medium

The transmission in human body is different than in free air. In capsule endoscopy the human body behaves as an antenna for the capsule endoscopy system. The problem is that this behavior is not constant. While the capsule moves inside human body, the attenuation of the transmitted signal, due to changes of the human body, is changing. In the next table you can see these parameters how they change in various places in the body. In this table ρ parameter is the conductivity of the tissue (S/m).

Frequency (MHz)	403.5		916.5		2450	
Tissue	$\rho\ (S/m)$	dB	$\rho\ (S/m)$	dB	$\rho\ (S/m)$	dB
Skin	0.69	46.71	0.87	41.32	1.46	38.01
Fat	0.041	5.58	0.05	5.46	0.1	5.28
Muscle	0.8	57.1	0.95	54.99	1.74	52.73
SI	1.9	66.05	2.17	59.38	3.17	54.425
Colon	0.86	62.53	1.09	57.86	2.04	53.88
Nerve	0.45	35.37	0.58	32.48	1.09	30.15

Table 4.1: Electrical tissue parameters for selected tissues. [21]

Another problem faced is the absorption of the radiated power by the human body. In the next figure you can see the radiated loss in terms of dB.

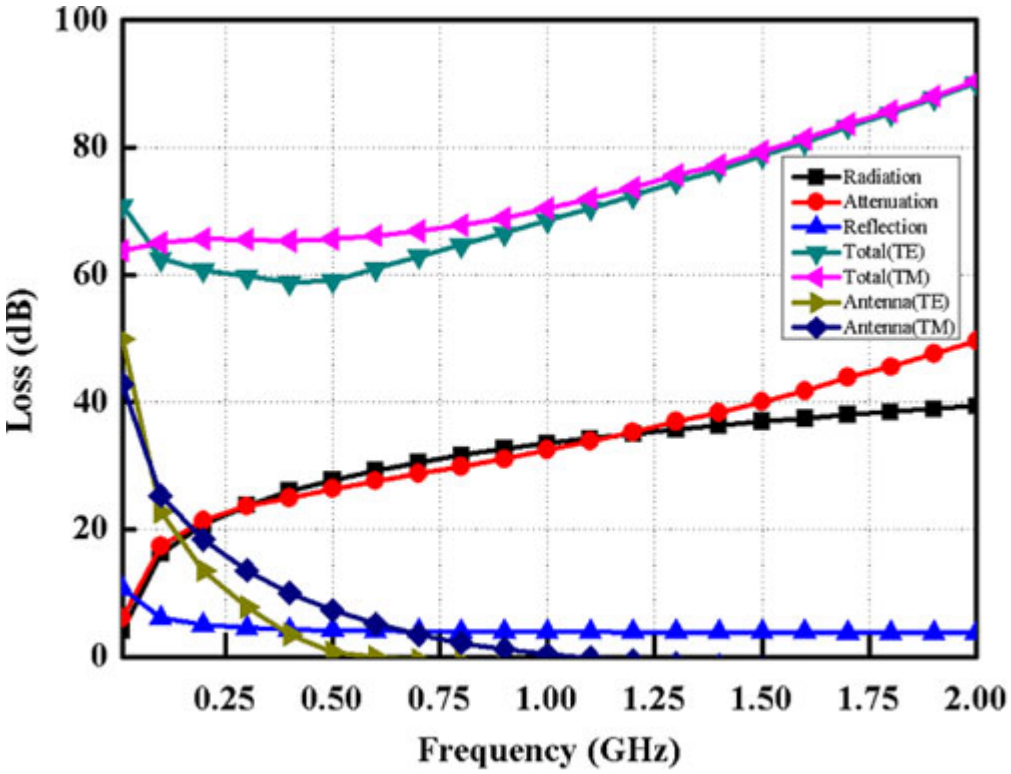

Figure 4.7: Total transmitting loss in the human body model. [21]

4.2 System architecture

As noted in previous paragraph there are some considerations that need to be taken under consideration. In this paragraph these are analyzed, and a solution provided to improve the existing systems.

4.2.1 Data rate

The data rate of the wireless link is required to take into consideration the type of data that is required to be transmitted. For data from simple sensors like pH, temperature, dissolved oxygen, etc., there is no need for high data rate transmitters. WCE uses a camera sensor, for which the amount of data to be transmitted is huge. The most effective way to capture and transmit high resolution image/video, which cannot be compressed with a high compression ratio, is to increase the wireless bandwidth. In existing commercial systems VGA (640 $\times$ 480), HD (1280 $\times$ 720) images are captured and transmitted. Capsules with VGA resolution can achieve 5 to 12 frames per second, but HD capsules can transmit up to 2 frames per second. The proposed system is considered to use a higher resolution image sensor.

Table 4.2: Standard image resolutions and the data size

Resolution	Aspect ratio	X (pixel)	Y (pixel)	Size in Mbit (24 bit/pixel)
QVGA (320 × 240)	4:3	320	240	1,84
VGA or SD (640 × 480)	4:3	640	480	7,37
WVGA (768 × 480)	16:10	768	480	8,85
XGA (1024 × 768)	4:3	1024	768	18,87
SXGA (1280 × 1024)	5:4	1280	1024	31,46
HD (1280 × 720)	16:9	1280	720	22,12
FHD (1920 × 1080)	16:9	1920	1080	49,77
4K UHD (3840 × 2160)	16:9	3840	2160	199
8K UHD (7680 × 4320)	16:9	7680	4320	398

In Table 4.2, is shown that, for the Full High Definition (FHD) (1920 × 1280) resolution images, the bandwidth needed to transmit one frame per second is 22.12Mbps. This is almost 1.5 frames per second of uncompressed 8-bit RGB images with the maximum data rate of the proposed transmitter, which is almost 33Mbps. If a lossless compression is applied then it is feasible to achieve 2-4 frames per second, which is high enough for a capsule endoscopy system. The reason that the proposed system can perform better than the others, is the use of lenses that can capture 360° degrees field of view in one image, as seen in Figure 4.8.

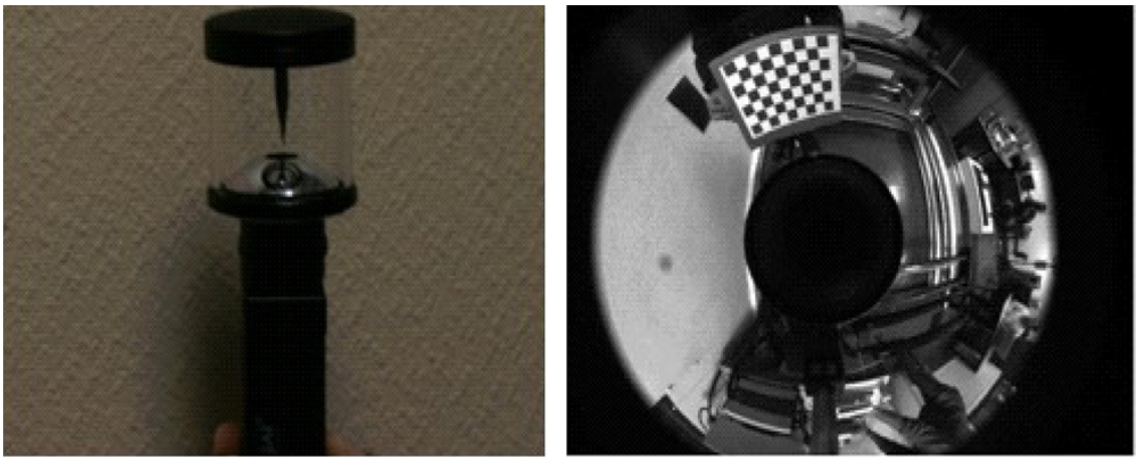

Figure 4.8: Implementation of omni-directional video cameras by using paraboloidal mirrors. [22]

Since the capsule's movement is not self-propelled but its movement is due to peristalsis (passive movement), the capture of 2 to 4 images per second is enough to capture and synthesize a map of the intestine by stitching all of these images like a mosaic. The distance movement of a passive movement WCE is in average about 0.5 centimeters per second. [90] It is obvious that the use of catadioptrical lens with the high data rate transmitter will improve further the performance of the wireless capsule. In other capsules the camera sensor can capture images only in front and behind the capsule, this means that with dual camera sensor, a higher data rate channel is needed to provide the link for the captured images to be transmitted.

4.2.2 Frequency selection

There are several factors that forced the selection of the carrier frequency for the proposed transmitter. The work in [91] suggests using a carrier between 450 MHz and 900 MHz for maximum radiation. However, from experiments reported in [88], [89], [11], [92], it showed that the surrounding tissues do not attenuate the transmitted signal so much for lower frequencies thereby obtaining higher signal-to-noise ratio (SNR). A lower carrier frequency was selected because it required less power to propagate through the body tissue. Also, the frequency of the carrier can be used as the main clock for the digital part of the capsule. So, the use of low carrier frequency resulted in a system with low power consumption with good RF penetration in the human tissue. The disadvantage of this lower carrier frequency is that the maximum data rate cannot be increased further. In this system the data rate achieved was up to 33Mbps which is high enough to transmit 2 - 4 frames per second of FHD images.
From all these, the selection of the carrier frequency is in the 2m amateur band which is between 144MHz to 148MHz.

4.2.3 Modulation scheme

One of the most critical selection in the design of the wireless link of the WCE, is the modulation scheme. The compressed data need to be modulated to be transmitted efficiently. The proper selection of the modulation scheme will increase the overall performance of the transmitter. As noted in the compression algorithm paragraph, a low complexity circuit was designed. Because low complexity circuits use less power than the complicated ones. However, the high performance should be kept. In implanted medical devices, there are few modulation schemes used. These are, QPSK, FSK and OOK. Each of them has disadvantages and advantages. QPSK is more complicated than the other two. So, the selection is between FSK and OOK. Both are phase independent and in the receiver side the detection of the received signal could be done by non-coherent architectures. The transmission of compressed image data needs high- data-rate modulation schemes. Preferred schemes for such applications are QPSK (Quadrature Phase Shift Keying), Frequency Shift Keying (FSK) and ASK (Amplitude Shift Keying). FSK modulation scheme is a popular choice because nonlinear (PA) power amplifiers can be used. However, the need of pulse shaping to perform better spectrum efficiency tends to make the transmitter too complicated. QFSK modulation compared to OOK has double the bandwidth but needs more energy than OOK.

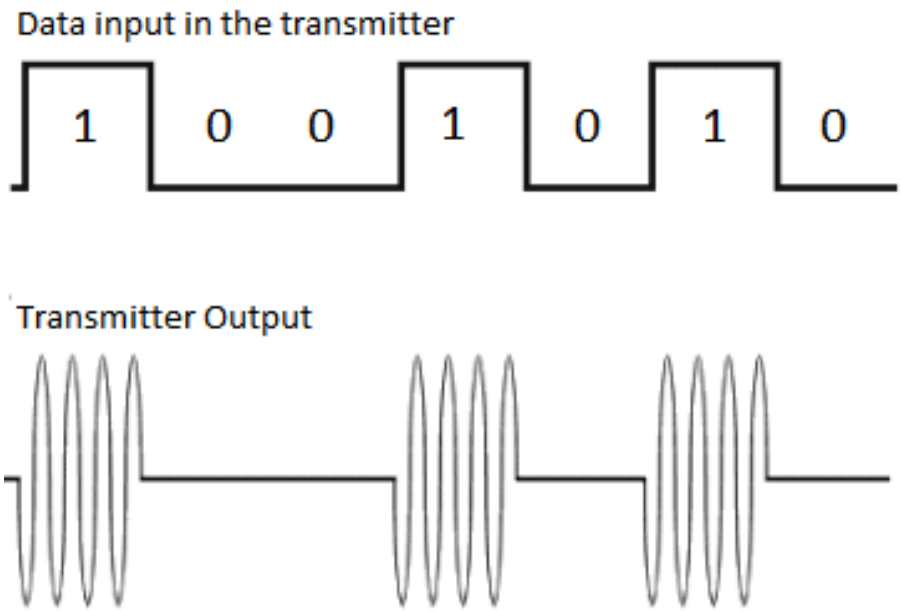

Figure 4.9: Input data in the transmitter and the output of the transmitter.

Transmitters based on OOK modulation scheme is used in [93], [94], [18], [95], [19], and [96] and on FSK modulation in [11]. The main advantage of OOK modulation is the low power consumption, due to the way it works. In OOK the data transmission is made by modulating/mixing the digital data with the carrier frequency. For example, when a digital "1" is going to be transmitted the output of the transmitter will be the carrier frequency and when the digital data are "0" the transmitter output will be zero, or it is not working. By this way when the data are "0" the power consumption of the transmitter is almost zero. Figure 4.9 shows how OOK works. While the input data are "1" then the output is oscillating in the carrier frequency and when the input is "0" the transmitter it does not send anything. Using the OOK modulation scheme is most feasible scheme to consume less energy.

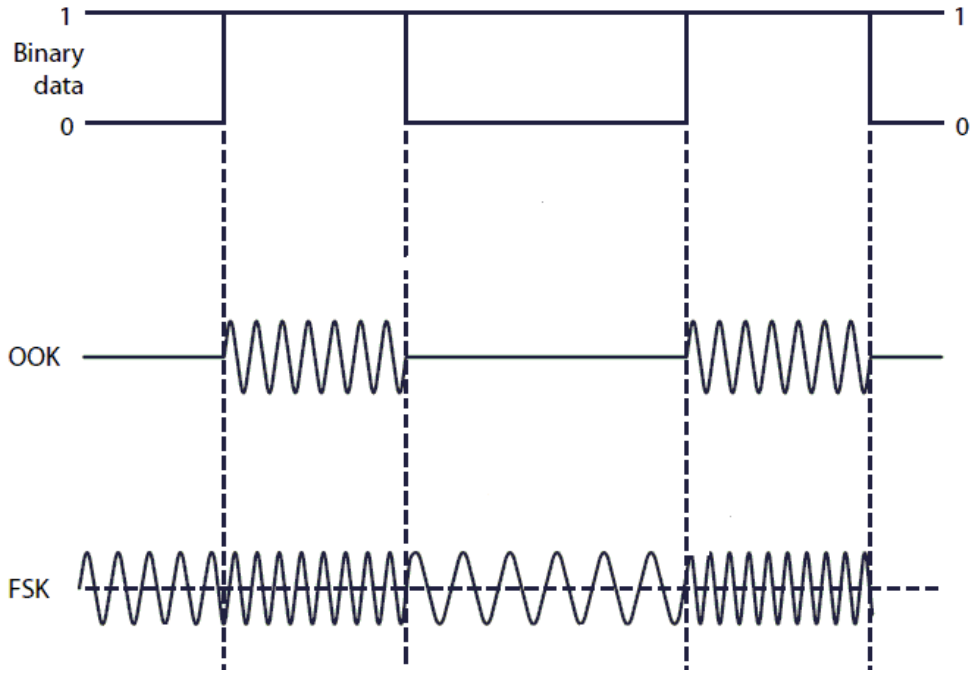

Figure 4.10: Input data in the transmitter and the output of the transmitter for both FSK and OOK modulation.

Unlike OOK, if FSK modulation is used then the transmitter is working all the time and the power consumption is increased more than in OOK. In Figure 4.10 the output signal of an FSK transmitter versus the output signal of an OOK transmitter, with the same binary input is shown. If the half of the data to be transmitted are zeros and the rest are ones; it is clear that up to 50% of less energy could be achieved than FSK modulation.

4.2.4 16nm FinFet technology

Bulk CMOS technology has been used for many years for semiconductor devices. The existing CMOS technology is not able to follow any more the Moore's Law, which says that the number of transistors in a unit chip area of transistors is doubled every two years. While Bulk CMOS technology is pushed to its limits, some unwanted issues have arisen. One of these issues is the power dissipation. While CMOS devices are shrinking, short channel effects have increased, and the performance of the device has decreased [97]. The solution is the use of the FinFet technology [97], a promising technology that can overcome the issues of CMOS technology. While decreasing the size of the transistors in planar architecture (2D structure), you can no longer control your transistors. The solution to this problem is to use FinFet technology, which with its 3D channel, can keep the control of the transistors while decreasing their size. FinFet technology is a relatively new technology which has a 3D structure as compared to CMOS which has a 2D structure. In Figure 4.11 a diagram comparison of 2D planar structure an 3D FinFet structure is shown.

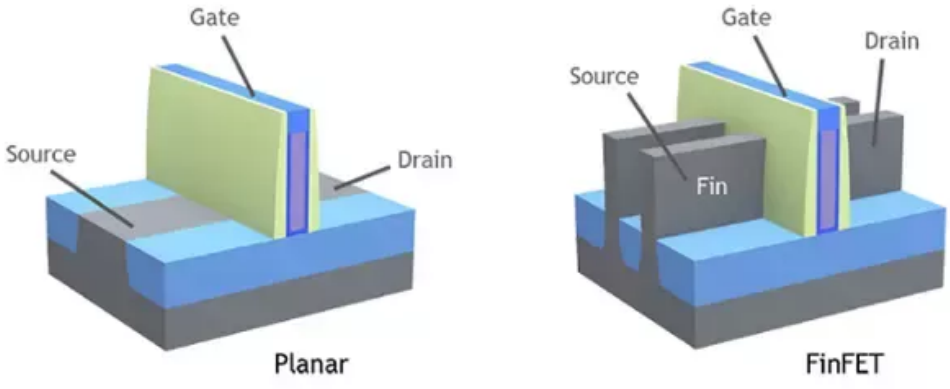

Figure 4.11: Diagram of 2D and 3D architectures.

The performance of this technology is mainly increased due to the low leakage current which leads to lower threshold voltages, allowing FinFet devices to work with lower power supplies [98]. By using lower voltages, the power consumption of the device is decreased [99]. Aggregated , the advantages introduced but the use of FinFet technology are:

- Better performance and reduced power consumption compared to bulk/planar transistors,
- 16nm FinFet can increase the performance over 40% and reduce the power needed by 50% compared to 28nm 2D planar process architecture,
- Higher frequencies can be achieved with the same power used in planar designs, due to their reduced size.
- They can drive more current per unit, compared to 2D planar device, due to the size of Fin. The difference in the size of the Fin can be seen in Figure 4.11 and
- reduced power usage due to low voltages needed to operate and less amount of leakage.

In Figure 4.12 a chart with the comparison of FinFets and 2D planar devices is shown.

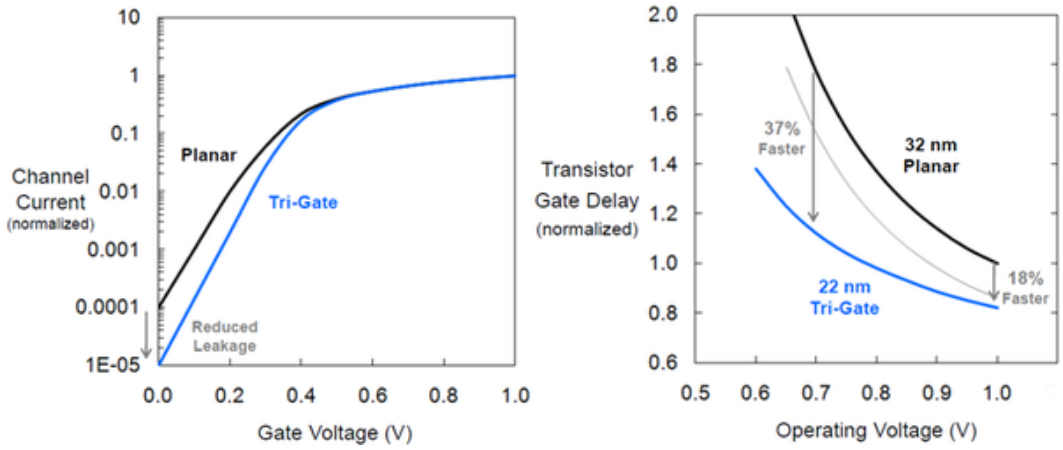

Figure 4.12: Chart shown the performance between FinFet and planar devices.

These are the main benefits gained using of FinFet technology. However, there are some disadvantages that should be considered.

- FinFet technology is harder to manufacture. Need complex challenges to overcome in the design to make the circuit reliable.
- FinFets have increased manufacturing cost.

The use of FinFet technology, because is a device technology that is growing up now, an open-source library is not found to be used in Cadence Virtuoso software suite. For this reason, An open-source simulation models found and used for the design, implementation and simulation. Predictive Technology Model (PTM) used which is provided from the Arizona State University [100].

4.2.5 System architecture

In general, a typical WCE system consists of four main components:

i) Sensors/Camera

ii) Image Compressor/Signal processing unit

iii) RF transmitter/receiver and

iv) the power sources

In Figure 4.13 a simple block diagram of the main components of a WCE is shown.

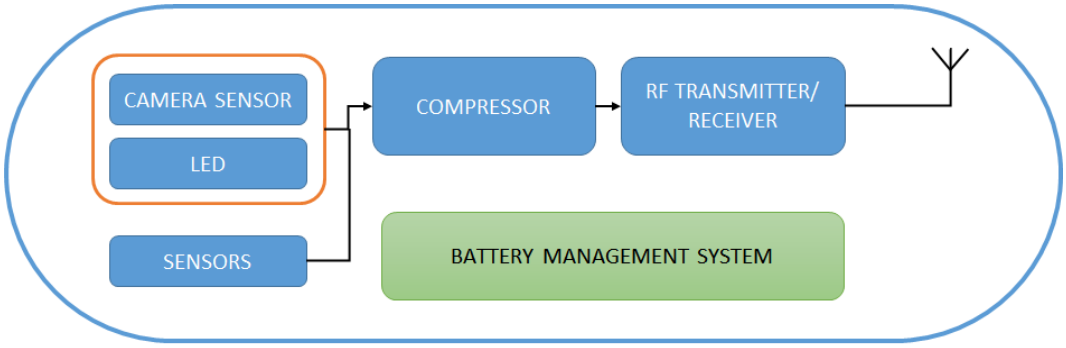

Figure 4.13: A simple block diagram of a typical WCE system is shown.

Obviously , this chapter is focused in the RF telemetry system. Most of the related works, referred previously, use bi-directional architecture in their telemetry system. They use this approach to send some control signals to the capsule from outside human body and mainly to correct a damaged image packet. An RF telemetry link with uni-directional system is proposed. This means that the capsule is able only to send data outside human body. In the next chapter a robust RF multi-receiver system that can solve the problem of lost packets or noise or interference from various sources, is described. In Figure 4.14 the proposed design is shown.

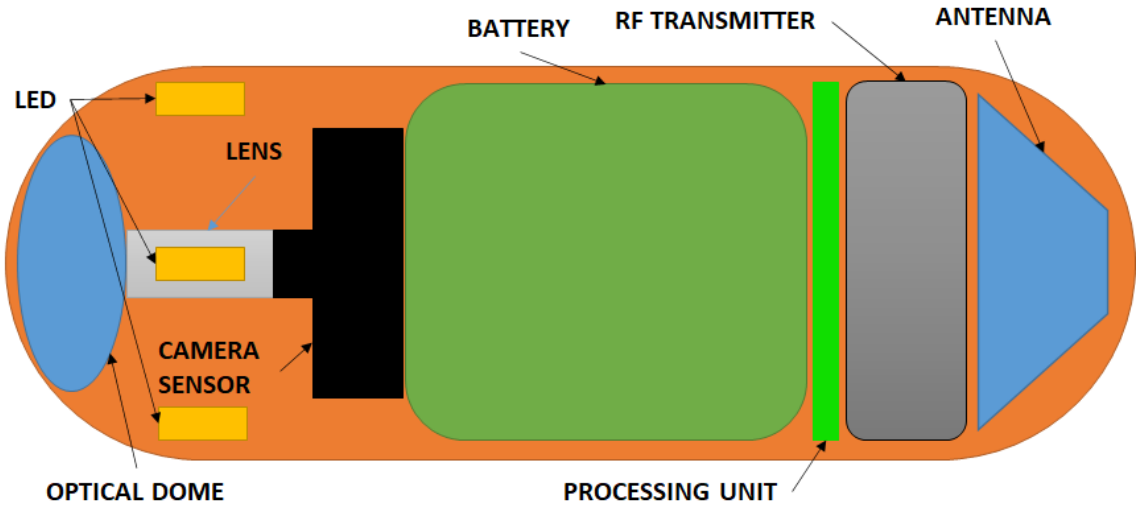

Figure 4.14: Block diagram of the proposed wireless camera capsule with its' components exposed.

4.3 System design

This chapter describes the design of the proposed system. As noted said in previous paragraph, is found the best carrier frequency for this application is as low enough to retain the high data rate of the transmitter. This frequency selected to be at 144MHz. Also, the modulation selected, which is OOK.

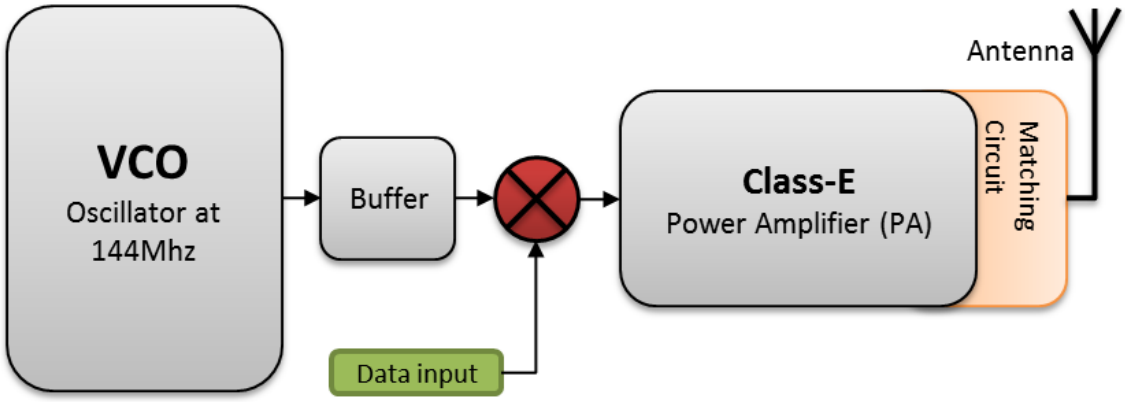

Figure 4.15: Block diagram of the transmitter.

The proposed design of the transmitter is shown in Figure 4.15. Where the main components are shown:

- The LC oscillator,
- the buffer stage,
- the modulator in red color,
- the class-E power amplifier and
- the matching network with the antenna.

It includes the oscillator, the buffer stage, the modulator and the class-E power amplifier with the matching circuit. For the proposed transmitter, the most important part is the oscillator which oscillates at the carrier frequency which is selected to be at 144MHz. The transmitter is used for medical applications, so power consumption and bit-error-rate (BER) are under consideration. The proposed transmitter is expected to work with a battery for up to 8 hours. For a transmitter, the phase noise is highly independent of the BER. So, taking care of this, the design of a ring oscillator is not selected because differential cross couple LC oscillator has better performance in phase noise.

4.3.1 Low power LC oscillator

The main part of this transmitter is the differential LC- oscillator, which uses a cross-coupled transistor, as shown in Figure 4.21, which produces the 144 MHz carrier frequency. The oscillator is designed with two nMos transistors. Inductors L1 and L2 with the capacitor C compose the LC circuit that is oscillating at the carrier frequency. The values of the L1, L2 and C are computed by the Equation 4.2.

$$f_0 = \frac{1}{2\pi\sqrt[2]{LC}} \tag{4.2}$$

In this work a better phase noise tried to be achieved. In LC oscillators the quality factor of the resonator can improve the phase noise. So, the need to design an LC-circuit with a good Q-factor, which is mainly dependent on the inductors Q is required. The design of the inductor is made using of Sonnet software and the results are also simulated in Cadence. Tail current source has been added to control and minimize the power consumption and the stability of the oscillator. By adding a current source, noise in the oscillator was added. So, an inductor and a capacitor are added to decrease the noise and improve the noise performance of the oscillator. The length and the width of the transistors are computed in a way that the current flows inside them is high enough to induce oscillation and as low enough to keep the power consumption at low levels.

4.3.2 Modulator and power amplifier

In the proposed design the implementation of the modulator is integrated in the power amplifier (PA). In RF transmitters there are some Classes of amplifiers that can be used based on their performance and characteristics. The basic classes of PA are Class-A, AB, B, C, D, E and F. RF PA are used in a variety of applications. The selection will be between pre-defined classes. There are some parameters that should be considered; these are the linearity, the stability, the gain, the output stage and the efficiency. The selection of the most suitable power amplifier, the performance of the entire system can be increased. The main goal of the power amplifier is to achieve low power consumption. Defining as n PA's efficiency in the next equation is the computation of it:

$$n = \frac{Power\ delivered\ to\ load}{Power\ applied\ to\ the\ circuit} \tag{4.3}$$

Power that is not converted to useful signal decrease's the efficiency of the system. Also, the lost power is converted to heat. So, an PA design with high efficiency is needed. In the next paragraph a discussion about all the PA classes and their performance is made.

As mentioned previously there are seven power amplifiers classes that can be used, Class-A, AB, B, C, D, E and F. All of them have some characteristics, based on them the selection of the most suitable is made. A simple Class-A amplifier consists of a transistor, a parallel L-C resonance circuit, a ballast coil L_f (RLC) and a capacitor C_c. The output goes to the load, R. In this class the transistor works in the active region of the transistor.

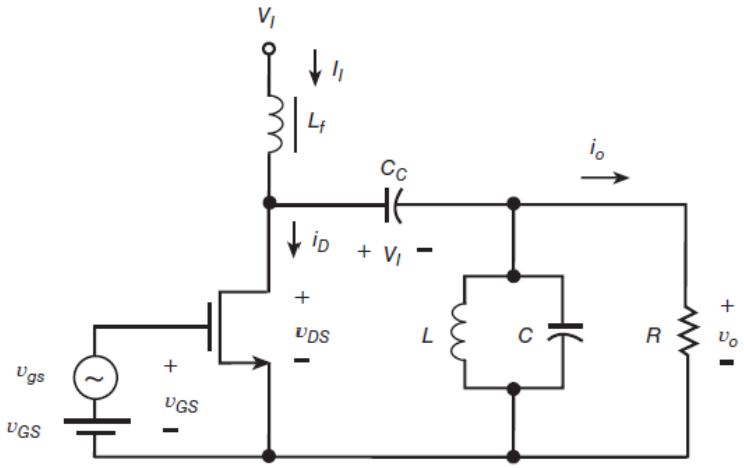

Figure 4.16: Circuit diagram of Class-A power amplifier.

The DC voltage at the V_GS gateway is higher than the threshold voltage of the transistor V_t. The transistor acts as a dependent source current-controlled voltage. The waveform of id is in phase with voltage $_gs$. The two waveforms have the same shape for as long as the transistor works in the cut-off area, On the resonant circuit in frequency f_o a phase shift of 180 degrees is generated between the id stream and the idle stream voltage trend. The point of operation is selected so that the discharge angle of the effluent stream 2 is 360° degrees. Class A amplifier is considered a linear amplifier because the u_{GS}-u_o characteristic is almost linear, generates small harmonic deformations (HD) and inter-modulation distortions (IMD). It is suitable for AM signals. In summary, Class-A power amplifier is not selected. The reason is that in practice, a power amplifier of Class-A is not able to achieve a power performance of more than 40%.

In class A the transistor always drives the quiescent current. This leads to reduced performance for the class A amplifier. Better performance can be achieved if the PA is not working continuously. This leads to more efficient but less linear power amplifiers. Stopping the transistor operation can easily be done by lowering the polarization voltage of the transistor at the gate. Since the transistor is closed, the voltage and current waveforms cannot be determined by the transistor. An important role in these waveforms now plays the passive circuit. It will also play an important role in the performance of the amplifier. Also, non-operation of the transistor leads to higher harmonics. How these harmonics will be eliminated plays an important role in the voltage / current shape and power amplifier performance. [101]

In Figure 4.17 a simple circuit diagram of a Class-B power amplifier is shown. The same circuit is used for

AB, B and C power amplifiers. The only difference is the operating point. There is different conduction angle of the drain angle.

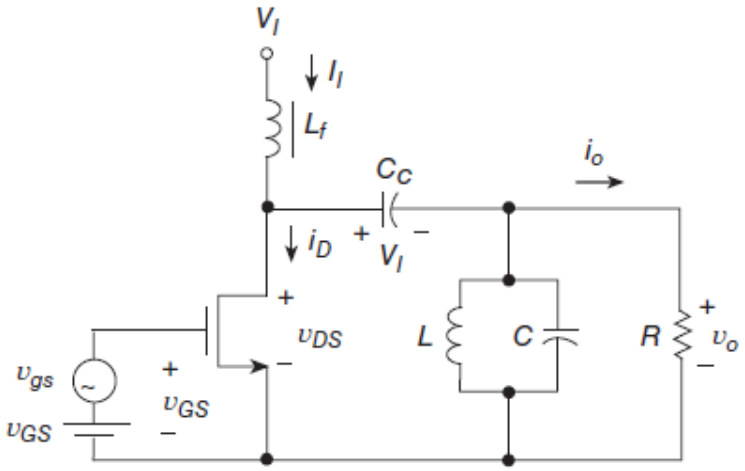

Figure 4.17: Circuit diagram of Class-B power amplifier.

In summary, Class-B power amplifier is not selected. The reason is that in practice, a power amplifier of Class-B is not able to achieve a power performance of more than 78.5%.

As mentioned previously Class-B, AB and C power amplifiers have the same circuit diagram. The main difference is the conduction angle of the transistor. In Figure 4.18 the different angles of the power amplifiers are shown. It is obvious that power amplifiers after Class-C are working with the maximum performance, theoretically, which is 100%.

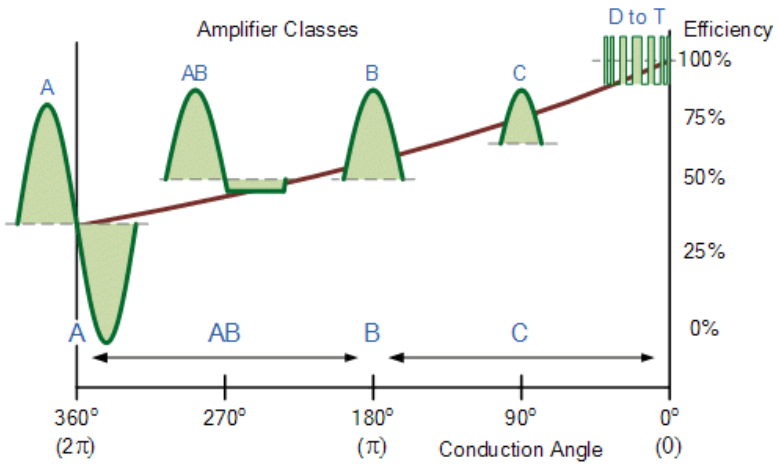

Figure 4.18: Conduction angles of different power amplifier classes in comparison with the efficiency.

Class C power amplifier is like A, B by changing only the transistor conduction point. This reduces losses. Theoretical maximum power performance of the C-class amplifier is 100% when the transistor does not work at all, so there is no meaning in, its usefulness. Otherwise its performance is like class B but suffers from larger non-linearities as the conduction angle decreases from 180 degrees. Theoretically maximum performance of Class-A amplifier is up-to 50%, for Class-B up-to 78.5%, for Class-C up-to 100% and for Class-AB can be up-to $50 - 78.5\%$.

The Class-E power amplifier belongs to another amplifier category. In this category, the transistor acts as a switch. There are two classes of Class-E amplifiers, Zero-current switching power amplifiers (ZCS), and Zero-voltage switching power amplifiers (ZVS). ZVS are the most efficient power amplifiers. Due to the transistor's interruption, theoretically there should be no losses. Practically the losses on the transistor are small. In particular, the switching is done when the voltage is zero if the passive elements of the resonant circuit are correctly selected. Since waveforms of current and current do not coincide now of switching, this in theory leads to a very high efficiency.

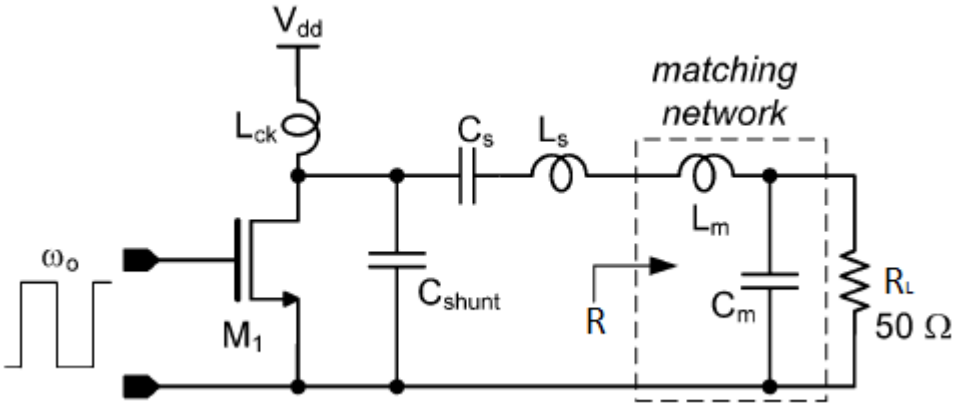

Figure 4.19: Fundamental circuit diagram of Class-E power amplifier.

In the proposed transmitter the PA is selected to be a Class-E PA. The reason for this selection is the maximum efficiency that can be achieved, which is ideally at 100%. In the next table a simple comparison of the amplifier classes is presented. In class-E amplifier the main transistor M1, as shown in Figure 4.19, acts as a switch. Therefore, ideally the maximum efficiency can be 100%. An ideal switch has either zero voltage across it or zero current passes through it, and the power dissipation is zero. Since the ON-resistance of the transistor reduces the efficiency of the class-E amplifier from the ideal efficiency of 100%, a power efficiency of more than 85% is not feasible. The reason of selection is not based only in the efficiency of this class. It is based on the modulation selected, which is On-Off Keying modulation, since with Class-E amplifier a better performance could be obtained, with less components for the design of the transmitter. A nonlinear switching mode PA whose operation is based on a switch typically uses a transistor. When the transistor/switch is closed the current flows through the switch and when the switch is open the current flows through the output load, which causes a voltage drop. Ideally the output is a square wave without overlap, so there is no power dissipation over the switch/transistor. A significant amount of power is lost as a result of the harmonic frequencies because they are not transmitted. The solution to this problem is a resonator placed at the output of the PA. The resonator consists of a capacitor in series with an inductor, resonating in the fundamental (carrier) frequency which is 144MHz. Using the resonator, a new problem occurres. When the switch/transistor is closed the current flows from the resonator through the switch, but when the switch/transistor is open the resonator tries to retrieve some current to create a sine wave. Since the switch is open this is not possible. For this reason, a shunt capacitor is placed before the resonator and this problem is solved. The RF circuit used allows only DC current to pass and ideally has no resistance.

Also, the high Q of the resonator plays a major role in the performance of the PA, since it can provide high impedance conditions for the harmonics. The current that flows through the load has a sinusoidal form and can be computed from the equation:

$$i_R(\omega t) = I_R sin(\omega t + \varphi) \tag{4.4}$$

To design the entire system there are a few component values that need to be computed. Those are the L-C resonator, the shunt capacitor and the load resistance. From the next equations can be used to compute these

$$R = 0.5768 \frac{V_{cc}^2}{P_{out}} \tag{4.5}$$

$$C = 0.1836 \frac{1}{\omega R} \tag{4.6}$$

And for the resonator the equations are,

$$C_0 = \frac{1}{\omega^2 L_0} \tag{4.7}$$

$$L_0 = 1.026 \frac{R}{\omega} \tag{4.8}$$

The equation to find the Q_L of the resonator is the below.

$$Q_L = \frac{\omega_0 L_S}{R} = \frac{\omega_0 (L_a + L_b)}{R} = \frac{1}{\omega_0 C_s R} + \frac{\omega L_b}{R} \tag{4.9}$$

These equations are used if a theoretically perfect inductor is used. In practice to reduce the ripple of the input current it should be $\omega L_f \gg$ R. To have a ripple less than 10% the value of the inductor must be:

$$L_{f_{min}} = \frac{7R}{f_o} \tag{4.10}$$

The design selection of the transistor characteristics is selected by the working current. The W and L of the transistor can be computed by the next equation.

$$\frac{W}{L} = \frac{2I_{D_{sat}}}{K_n (V_{D_{sat}})^2} \tag{4.11}$$

Another factor that should consider in the design, is the parasitic capacitance. In Figure 4.20 the parasitic capacitance C_p in the gate of the transistor is shown.
Transistor M_1 can be considered to have an ON resistor r_{on} when conducting, and parasitic capacitance C_P to the ground. Considering as elementary capacitance c_{p-o} and as elementary resistance of the transistor r_{on-o}, then can be computed by the following equations.

$$C_p = c_{p-o} W \tag{4.12}$$

$$r_{on} = \frac{r_{on-o}}{W} \tag{4.13}$$

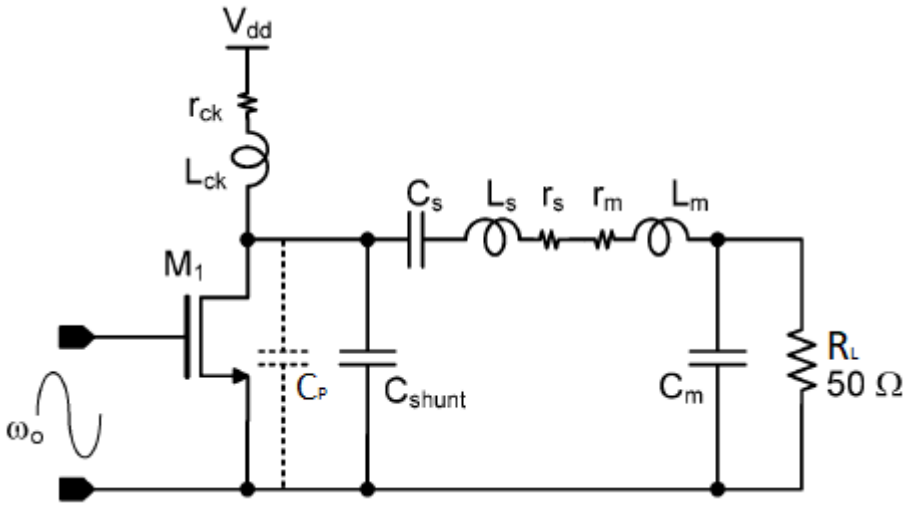

Figure 4.20: Fundamental circuit diagram of Class-E power amplifier with parasitic capacitance.

4.3.3 Matching network

The output of the amplifier is connected to the matching network before the load. The Matching circuit is applied for the maximum transfer of power from stage to stage. In the proposed design the matching circuit is the same with the resonator as described in the previous paragraph and is shown in Figure 4.21.

4.4 Implementation

All the components of the system are designed with schematic editor of Cadence Virtuoso and simulated with Spectre software.

4.4.1 Oscillator

In Figure 4.21, the circuit of the oscillator is designed in Cadence Virtuoso Schematic Editor. The proposed transmitter is composed from an LC complementary oscillator, which is designed with FinFets.

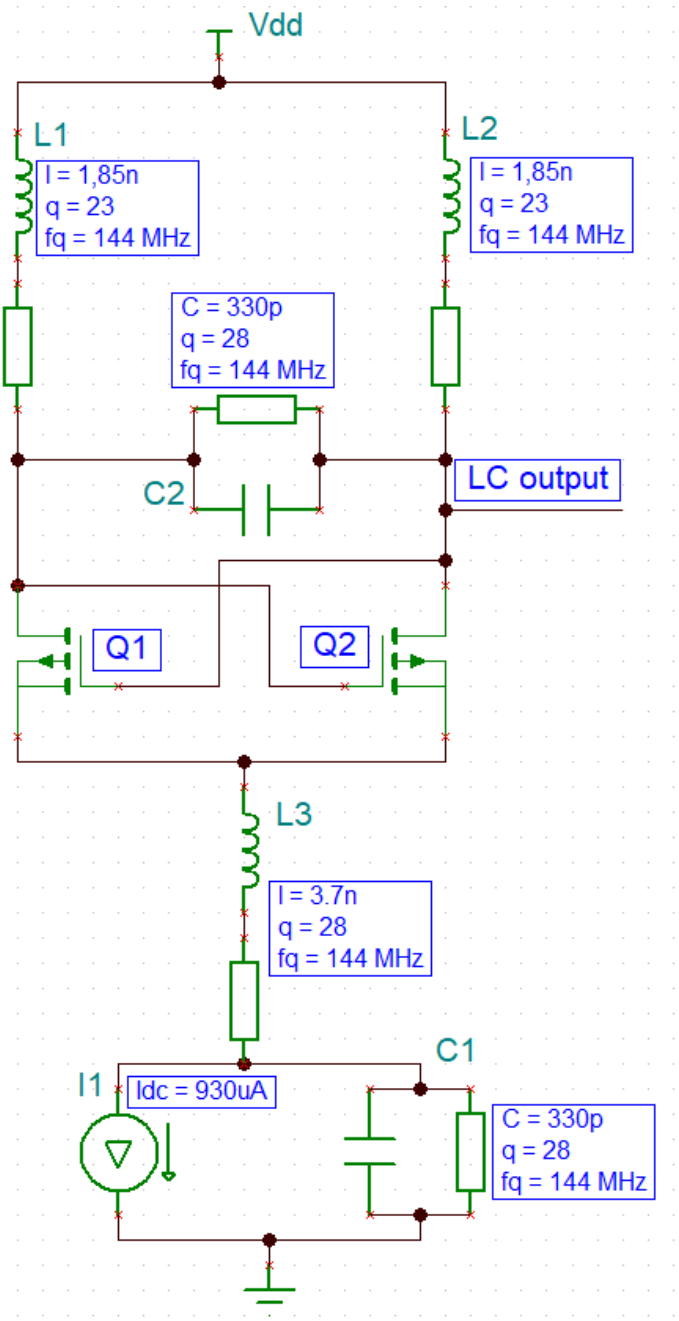

Figure 4.21: LC oscillator designed in Cadence Virtuoso Schematic editor.

The oscillator is simulated with different tail currents. From the results the proposed system has better performance in oscillation and phase noise with a small increase of the current. The current used by the oscillator to work is 0.66mA.

$$V_{amp} = \frac{4}{\pi} R_p I_{bias} \tag{4.14}$$

As seen from Equation 4.14 the voltage amplitude of the oscillator is based on the equivalent resistance of the oscillator circuit and the bias current which is 0.66mA. As seen in Figure 4.21 the oscillator is working all the time, while the power amplifier only while transmitting “1”.

4.4.2 Modulator

In this section a Class-E Power Amplifier with the modulator is designed. A Class-E power amplifier with a center/carrier frequency of 144MHz designed. FinFet 16nm technology is used. The library used to design and simulate the overall design was PTM (Predictive Technology Model).

The first stage designed was the power amplifier and then the matching network. In this implementation, a Class-E power amplifier is selected without the use of cascade mode. The use of FinFet 16nm implementation technology let power source voltage drop as low as 0.85V.

The next equation is used to compute the value of the capacitor C_3, as can be seen in Figure 4.22. This capacitor is used in parallel with the existing parasitic capacitance of the Mosfet transistor.

$$C = \frac{P_o}{\pi \omega V_{DD}^2} \tag{4.15}$$

At Figure 4.22 , the final circuit of the PA-modulator is presented. The circuit is designed with the schematic editor of Cadence Virtuoso and the simulator used is Spectre. As seen the amplifier, uses two switches/transistors because the one is used for the carrier frequency and the other is the data input. The first one is used to modulate the data with the carrier, transistors are used in common gate mode. Transistor named switch 1 is used to modulate the carrier frequency with the data for transmission. Then the modulated signal is applied in the gate of the mosfet named switch 2 and amplifies the modulated signal for transmission.

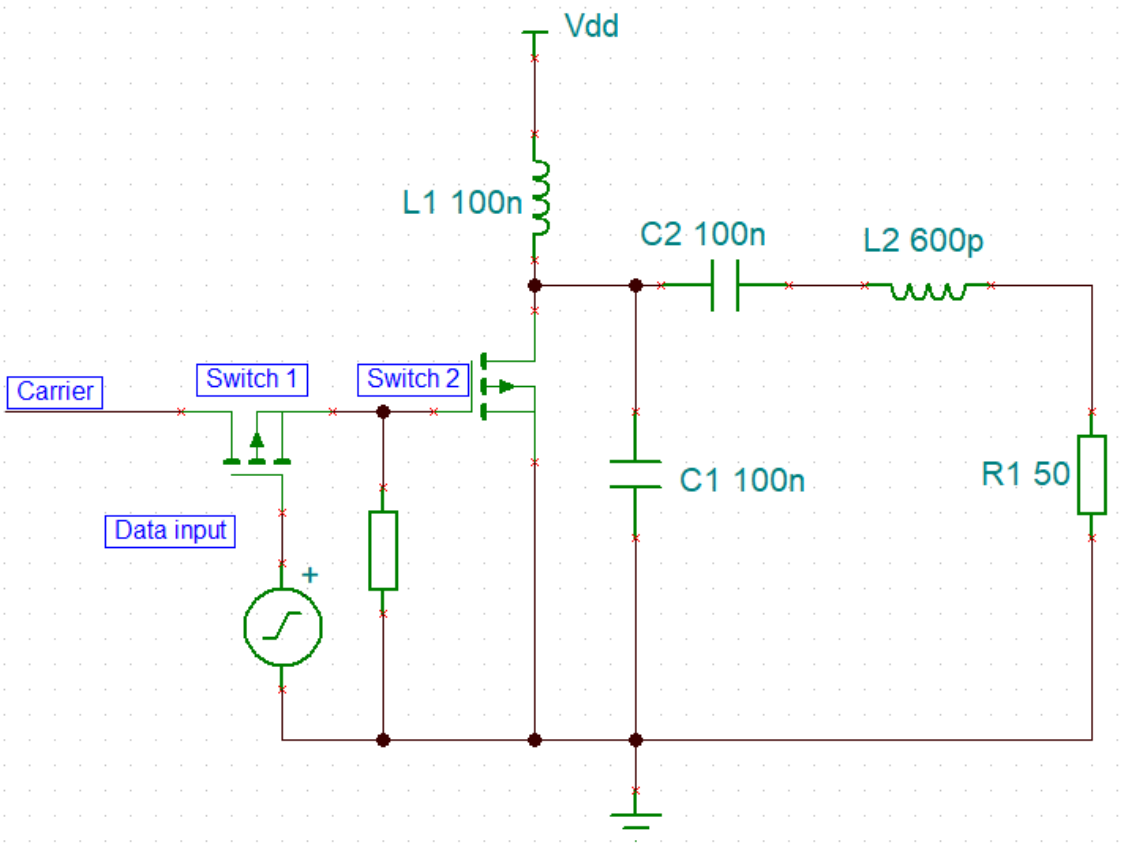

Figure 4.22: Class-E amplifier and modulator designed in Cadence Virtuoso Schematic editor, it includes the oscillator, the class-E power amplifier and the final stage before the antenna.

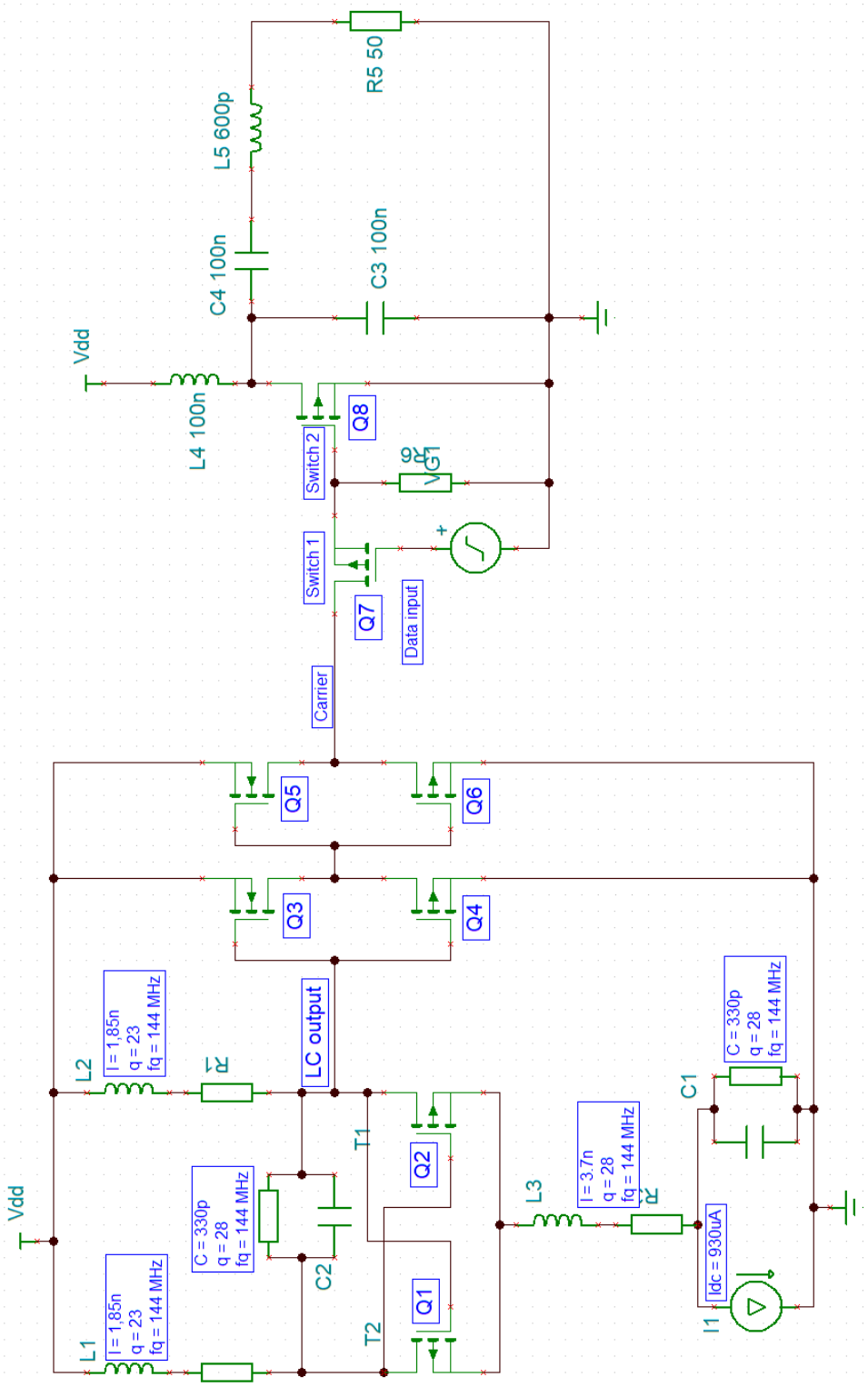

Figure 4.23: Circuit diagram of the proposed transmitter. It includes from the LC oscillator, the class-E PA and the matching circuit.

4.4.3 Transmitter

The proposed low power OOK transmitter has been designed with 16nm FinFet technology and the design was simulated with Cadence tools. The carrier frequency of the oscillator, for minimum energy loss and minimum tissue absorption, is at 144MHz.

In Figure 4.23, the final circuit diagram of the transmitter is shown.

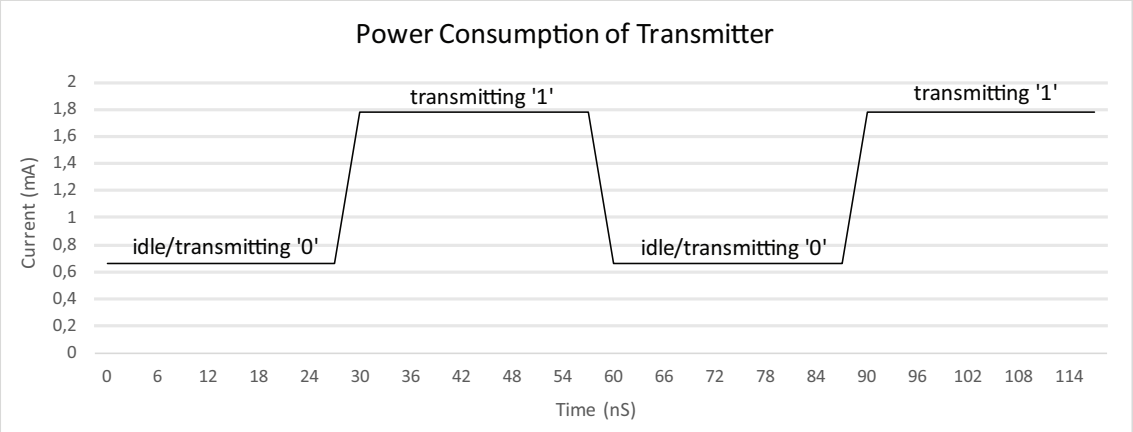

Figure 4.24: Power consumption while transmitting “0101” at 33Mbps.

Our design can achieve a data rate up to 33Mbps.The average current flow is 1.223mA at 0.85Vdc. As seen in Figure 4.24 the current flow while the transmitter is in idle/ transmitting “0” mode is almost 0.66mA. While the transmitter is transmitting “1”, the overall current of the circuit is 1.786mA. If the 50 percent of the data are “0” and the rest are “1”, then the average current is 1.223mA.

4.4.4 PVT analysis

PVT (Process, Voltage, Temperature) analysis was done in order to examine the stability of the oscillation frequency of the proposed system. It is based on the variance of the Process, Voltage and Temperature. Process corners means the performance of devices due to variations in the die that have occurred in minor changes of humidity or temperature of the clean room when wafers are transported, or due to the position of the die relative to the center of the wafer. The combinations used for Process variation are SS, SF, FS, TT and FF where the first letter corresponds to the NMOS component and the second one stands for the PMOS component. State S stands for slow performance, F stands for fast performance and T stands for typical performance. In the PVT analysis SS, TT and FF was used. For voltage variations, the simulation was done with a $\pm 10\%$ variation of the nominal power supply which is 0.85 V. For temperature variation, three different temperatures were used, 30°C, 37°C and 44°C. The device will be used in a capsule endoscopy inside human body where the temperature is stable at approximately 37°C, except from cases like fever where temperature is higher than 37°C. The results of voltage and temperature variations are shown in Figure 4.25.

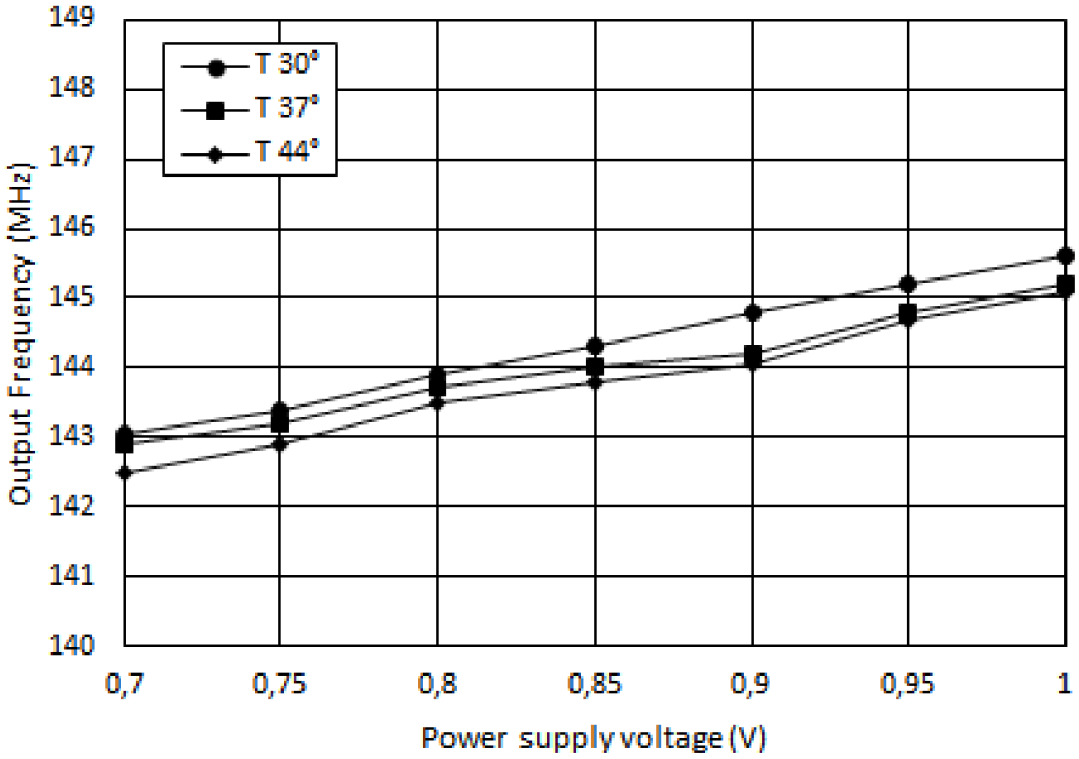

Figure 4.25: Frequency drift due to temperature and voltage variations.

The overall results of PVT simulation are shown in Table 4.3. The frequency variation achieved is around 2.1%. These results have shown a stable oscillator with predicted frequency drifts. For PVT simulation, Cadence ADE (Analog Design Environment) XL was used.

Voltage (V)	Temperature (°C)	SS	TT	FF
0.7	30	141.60	142.50	142.60
	37	141.90	142.90	142.80
	44	142.50	143.05	143.40
0.85	30	143.20	143.80	144.10
	37	143.90	144.00	144.30
	44	144.15	144.30	144.70
1	30	144.85	145.10	145.60
	37	145.00	145.20	146.20
	44	145.10	145.60	146.90

Table 4.3: Oscillator frequencies based on PVT variations.

4.4.5 Performance comparison and simulation results

In Table 4.4, there is a summary of the designed transmitter.

The transmitter can send up to 4 HD 1920×1080 images per second, using of a compression scheme of an average compression rate of 2.5. Also, at Table 4.5 there is a comparison table of the proposed transmitter with other existing systems.

From Table 4.5, the proposed transmitter has a relatively high data rate of 33Mbps and lower average power

Table 4.4: Summary of transmitter's characteristics

Vdd	0.85
Carrier frequency	144MHz
Data rate	33 MB/s
Avg DC current	1.223 mA
Avg DC power consumption	1.04mW
Phase noise of oscillator	0.144
Output power	-4dBm

Table 4.5: Performance comparison of similar works.

	J. Liu [18]	J. Thone [11]	J. Ryu [19]	Raja [20]	This work
Process (μ m)/Voltage (V)	0.18/1.8	-/1.8	0.18/3	0.35/1	16nm/0.85
Carrier frequency	400MHz	144MHz	440MHz	433MHz	144MHz
Data rate	2M	2M	40M	10M	33M
Image resolution	-	VGA	-	-	FHD
Frame rate	-	15-17	-	-	6
Modulation	OOK	FSK	OOK	OOK	OOK
TX Max. output (dBm)	-2.17	18	-0.22	-12.7	-4
Power (mW) (TX)	3.1	2	2.58	0.518	1.04

consumption of 1.04 mW. Compared to Raja et al. [20], the power consumption is slightly increased, but the data rate is increased by more than 3 times. In comparison with others, the power consumption is much lower. In this design, 33 MB per second data rate achieved and can be transferred up to 2 FHD high resolution images per second without compression. With a compression rate of 2.5, it can transfer up to 4 images, which is good enough for WCE applications.

It should be mentioned here that there are designs implemented in hardware such as Ryu et al. [19] who made a significant improvement to the data rate. This design can achieve up to 40Mbps data rate. The carrier frequency is 440MHz and the implementation process is 0.18um CMOS technology. The power source of the design is 3V with 860uA of current, it is a novel design with 2.58mW average power consumption. Raja et al. [20] implemented an OOK transmitter with adaptable data rate. The carrier frequency is 433MHz and the implementation is 0.35um CMOS technology. The data rate is 3-10Mbps with a power supply of 1V at 560uA current consumption.

4.5 Summary

In this Chapter, an energy efficient, high data rate wireless transmitter has been presented. Methodology used to create the proposed transmitter, was by creating the performance profile of the wireless transmitter needed.

There were some requirements taken under consideration. The main requirements were that the system should work inside human body, the second was the low power consumption and the third was the high data rate wireless link that is needed for transmission of high resolution-images.

Because the pill is working inside the human body, the carrier frequency is selected to be 144MHz. So, there is less absorption of the RF signal from human body. The use of 16nm FinFet technology that was selected

for the implementation improves the power performance of the transmitter and decreases the operating power supply at the level of 0.85V. Apart from these, FinFet technology enables the integration of the matching network with the power amplifier of the transmitter.

Finally, an OOK wireless transmitter designed and simulated using of Cadense Virtuoso software suite. The performance of the proposed design is up to 33Mbps of data rate and an average power consumption as low as 1.04mW.

Chapter 5

Robust wireless multi-receiver system

5.1 Introduction

Previous paragraphs focused on the internal sub-systems of a wireless capsule endoscopy system. In this paragraph the research effort is focused in the design of a wireless multi-receiver system to obtain better performance in the reception of the transmitted signal from the capsule. The systems that have been discussed until now are located inside the capsule/pill. Except from the internal located parts that a capsule endoscopy has, sensors, telemetry system, processing unit and the power source, there is the external part that is located in the jacket that is been used by the patient. In this jacket, the receiver is located with the data logger. Existing systems use bi-directional RF communication systems. The reasons for bi-directional RF link are two. The first one is for error correction. In type of camera capsules, the use of bi-directional RF links improves the performance of the wireless link in the error correction. While a packet is transmitted with error due to noise errors or low RF reception the part outside the human body communicates with the capsule to re-transmit the lost packet. The second reason, is in robotic capsules, where need to be controlled from outside the human body. In this work, the research work is focused in endoscopic capsules that transmit images/video outside human body. Until now, there is no research effort in the part outside the human body. Investigation performed in this area is to export critical information and design a new more effective robust multi-receiver system. In the next paragraph state-of-art RF communication links are presented and their bottlenecks.

5.2 State-of-art wireless systems

There are several telemetry systems designed for WCEs. The research effort is focused on designs that reduce power consumption and increase data rate of the wireless link. The research community is mainly focused on the improvement of the part inside the capsule. For example, a wireless system like Thotahewa et al. [23], which proposes a two-way communication link. This system uses both a transmitter and a

receiver. In Figure 5.1 a block diagram of this system is shown. This transmitter can achieve up to 10 Mbps of data rate and has a receiver inside the capsule which is using to retrieve any lost packets and configure the pill's camera parameters outside human body. The power consumption of the transmitter is 4mW and for the receiver is 5mW. The total power consumption of this system is 57mW. If that this system did not contain a receiver, then the power consumption will be decreased about 7%.

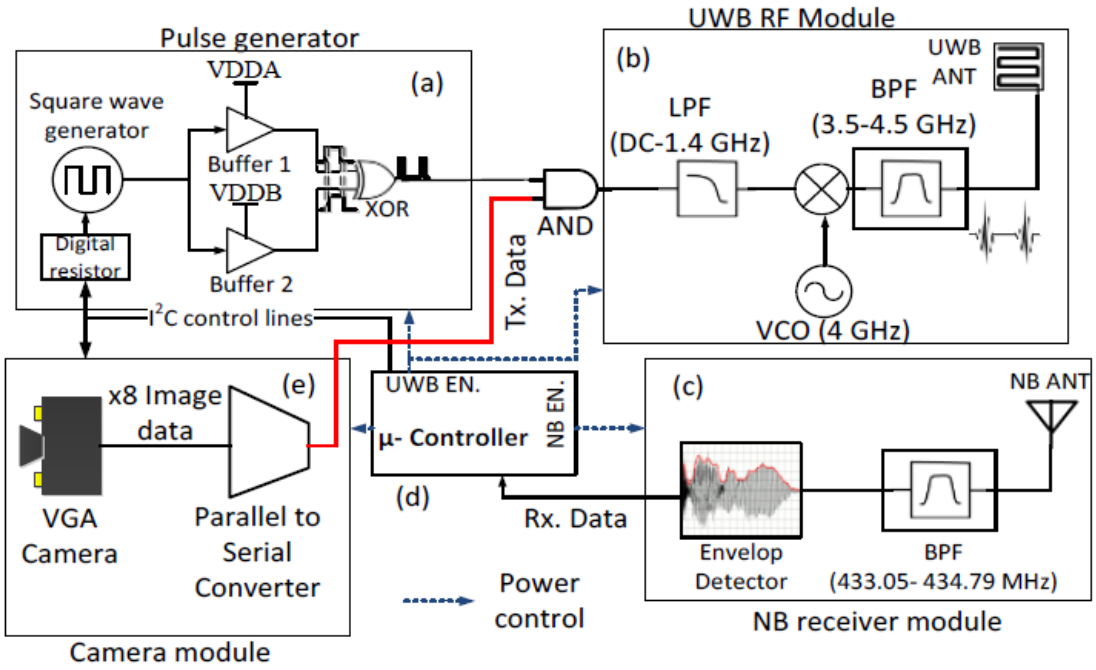

Figure 5.1: Key components of the WCE system proposed by Thotahewa et al. [23]

Gao et al. [24] proposes another wireless system which is composed by a transmitter with a data rate of 3Mbps and a receiver with a 500Kbps of data rate. Transmitter is using QPSK modulation and receiver uses non-coherent OOK modulation. In Figure 5.2 is shown the complexity of the system due to the addition of the receiver.

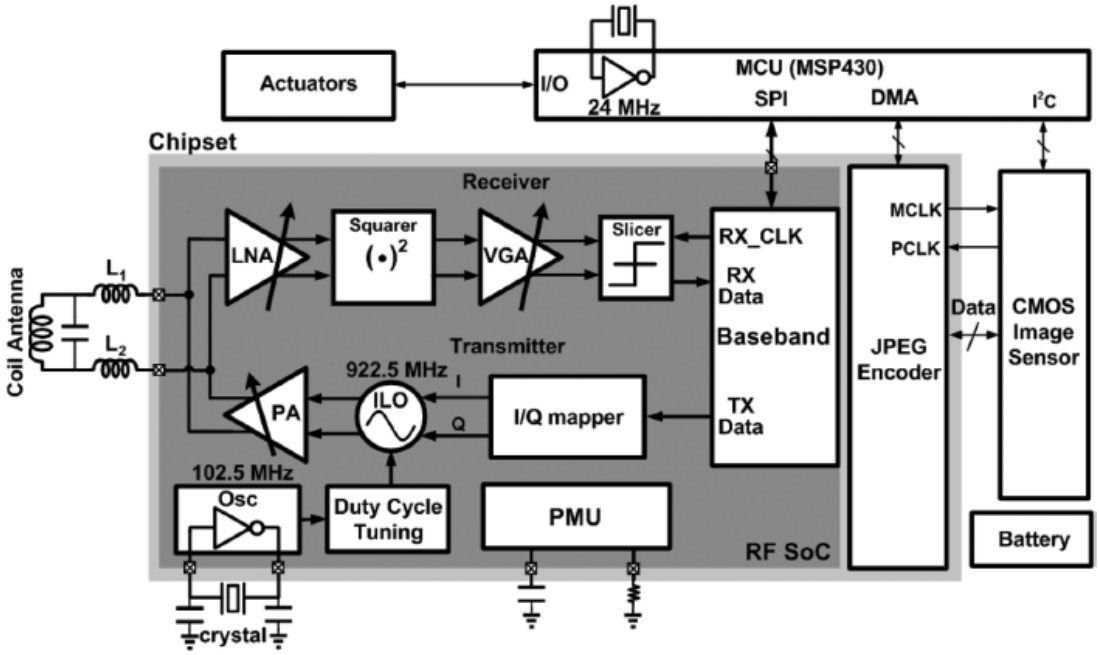

Figure 5.2: Key components of the WCE system proposed by Gao et al. [24]

The power consumption is 5mW for the transmitter and 4.5mW for the receiver. The total power consumption for the telemetry part is about 9.5mW. About the 43% of the power needed for the telemetry system is consumed by the receiver. If this system uses only transmitter, the power cost will be reduced dramatically. Cho et al. [25] proposes a transceiver RF telemetry system for WCE that works at the medical frequency of 402-405MHz. This system consumes 10.8mW at RX mode and 4.9mW in TX mode.

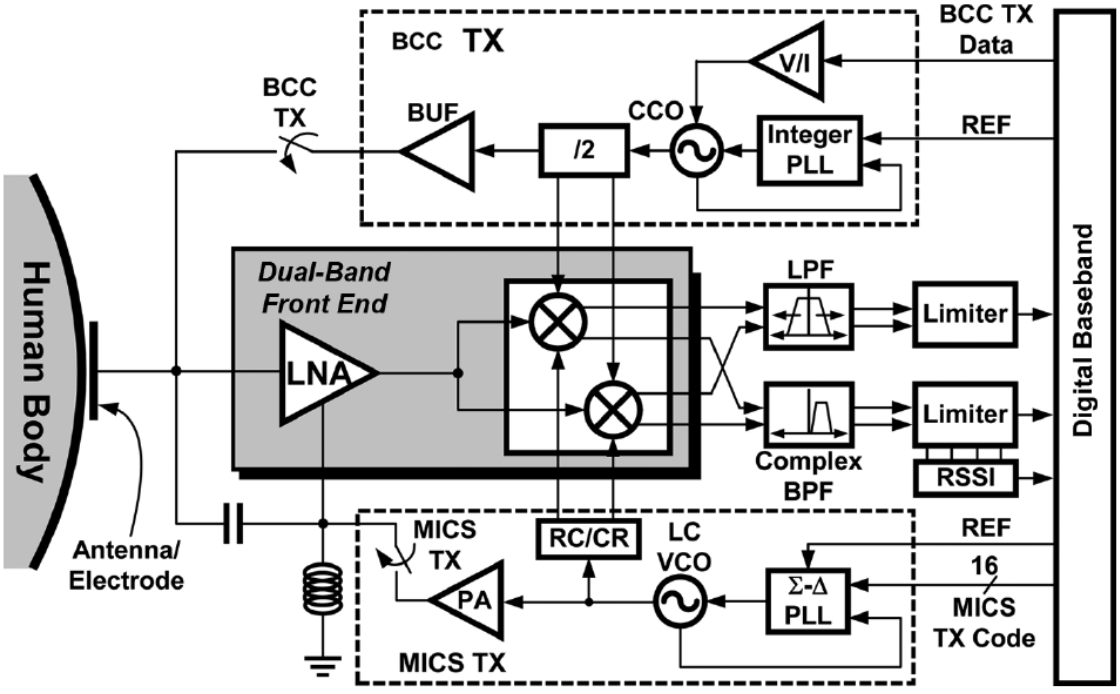

Figure 5.3: Key components of the WCE system proposed by Cho et al. [25]

This system has a transceiver that is not working at the same time with the receiver. As seen in the Figure 5.3, there are two switches that change the operation from Tx to Rx mode. So, it is difficult to compute the power performance of this system without the use of the receiver part.

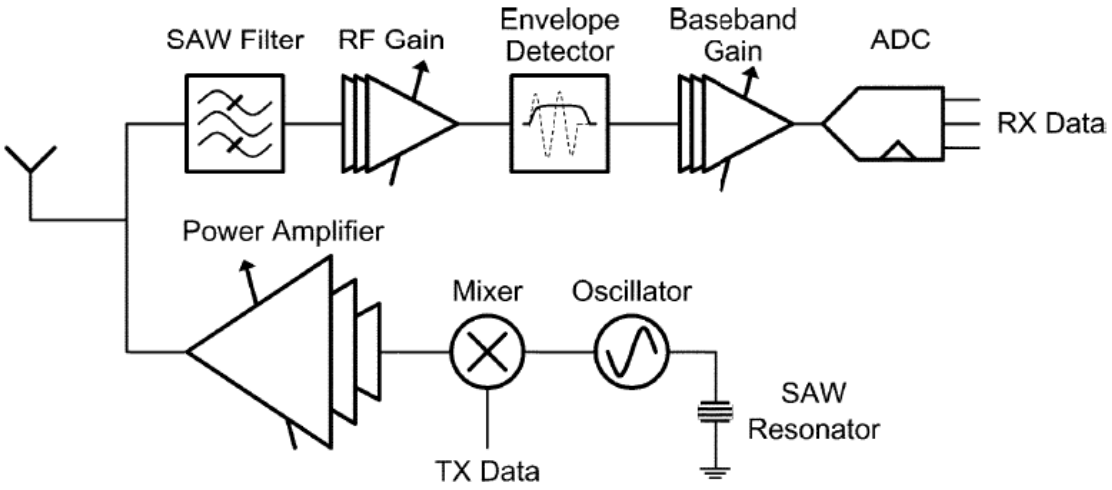

Figure 5.4: Key components of the WCE system proposed by Daly et al. [26]

Daly et al. [26] have designed and implemented a telemetry system that works at the frequency of 916.5MHz. The modulation scheme for both transmitter and receiver are OOK. This system has a data-rate of 1Mbps. The big advantage of this system in difference with the others is that it can control the power consumption in both transmitter and the receiver. Power consumption of the transmitter can vary from 3.8 to 9.1mW and for the receiver is from 0.5 to 2.6mW. Is is clear that without the use of the receiver huge amount of energy could be saved for other operations of the capsule.

All these implementations were based on telemetry system with transceivers. The use of bi-directional RF link increases the power needs of the capsule to operate. The receiver module of each system is almost consuming the half power of the entire wireless system. However, there are RF telemetry systems based on a single transmitter.

Diao et al. [27] have designed and implemented a wireless transmitter that operates at the frequency of 902-928MHz and performing 15 Mbps of data rate with a power consumption of 7.2mW. The modulation technique used was ASK.

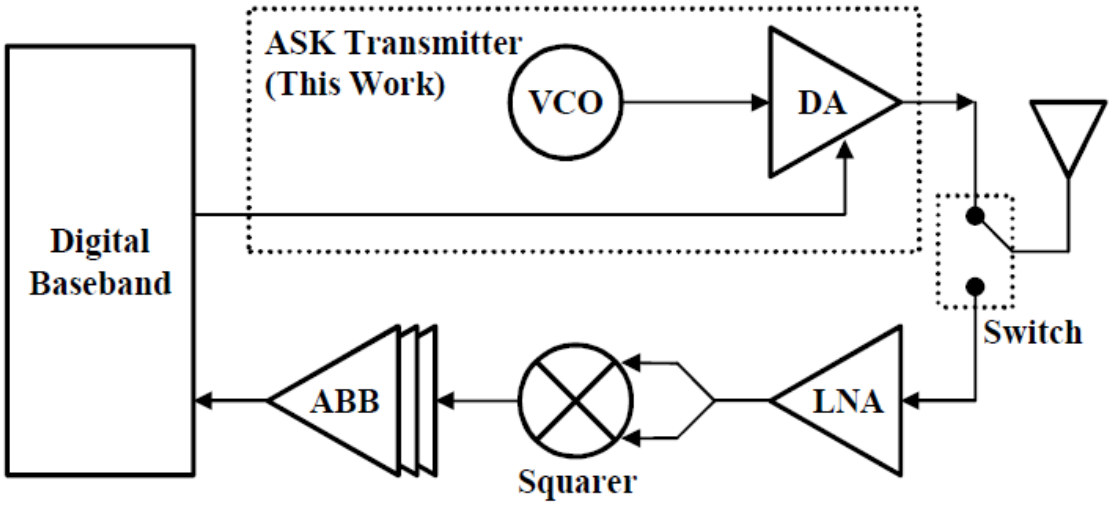

Figure 5.5: Key components of the WCE system proposed by Diao et al. [27]

The design of Diao et al. [27] consists only of a VCO and the stages of the RF PA. The data rate achieved is high and the power consumption is low.

Another telemetry design based in one-way communication proposed by Huang et al. [28]. This system consists of an ASK/OOK transmitter with digital pulse shaping. It can achieve up to 10Mbps of data rate and the power consumption is as low as 2.3mW. This design has extremely low power consumption. The carrier frequency of the transmitter is 2.4GHz.

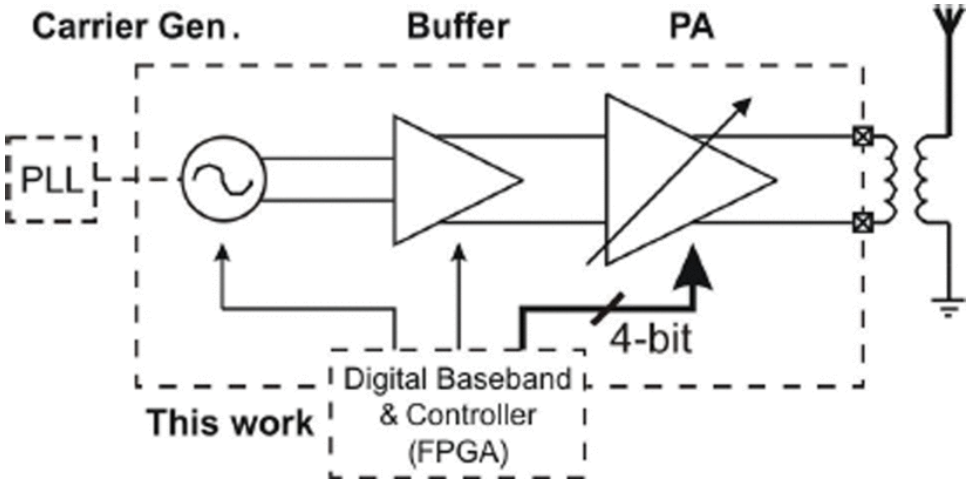

Figure 5.6: Key components of the WCE system proposed by Huang et al. [28]

In Figure 5.6 the block diagram of this design is shown.

In this chapter a novel telemetry system is introduced. Two main categories of telemetry systems is discussed. The two-way communication systems and one-way communication systems. Both have advantages and disadvantages. The two-way communication systems have the advantage that they can re-transmit the lost packets, however they use transmitter and receiver and they increase the amount of energy they need to work. In the other hand there is the one-way communication systems, where the use only of the transmitter

increases the performance in the power domain. Less energy to operate is used. The main disadvantages of such systems are that there are not able to re-transmit the lost packet, because the transmitter is not able to know if the data packet has arrived correctly. The only thing that such systems can do is FEC (Forward Error Correction), however this is not enough to correct data packets that are damaged.
All of these need improvements so that an increase in the performance to the entire system of a wireless capsule endoscopy is possible.

5.3 System requirements

Wireless Capsule Endoscopy is a state-of-art technology. The part that consists the entire system is not only the hardware part inside human body. Besides the pill, the overall system consists of the RF receiver jacket and the computer station, where data is deployed for doctors to perform diagnosis. This chapter is focused on the RF part of the WCE which is outside human body. However, there are still some system requirements to consider.

- Power Consumption

  The proposed system is placed outside human body. So, the energy for this equipment will be a rechargeable battery. There is plenty of energy to work, in difference with the pill. This concept increases the overall performance of the WCE design. Also, decreases the power needed for the in-body system to correctly transmit the valuable data.

- Bit-Error-Rate

  In RF reception systems, bit-error-rate is a factor of a well-designed system. The way that this system is structured provides a good performance in BER factor.

- Size and Placing

  Since this system is used outside the human body, the main consideration is where to “house” this system and how to place the output receivers’ antennas to achieve the maximum performance. Normally the placement is in the center of the jacket that the patient wears. In this implementation, due to the use of multiple receivers, there are located in both sides of the jacket.

5.4 System design and implementation

The proposed system provides a one-way wireless data link, where the low power, high data rate transmitter is inside the capsule and outside human body there are many receivers to receive the transmitted data. An example of an wireless transmitter that can be used is proposed by Intzes et al. [102] where an On-Off keying (OOK) is designed with a power consumption of 1.04mW at 0.85V and with a maximum data rate of 33Mbps. At Figure 5.7 a simulation of human body with 32 receivers placed outside human body is shown. In this Figure the receivers are placed outside the human body to perform capsule localization.

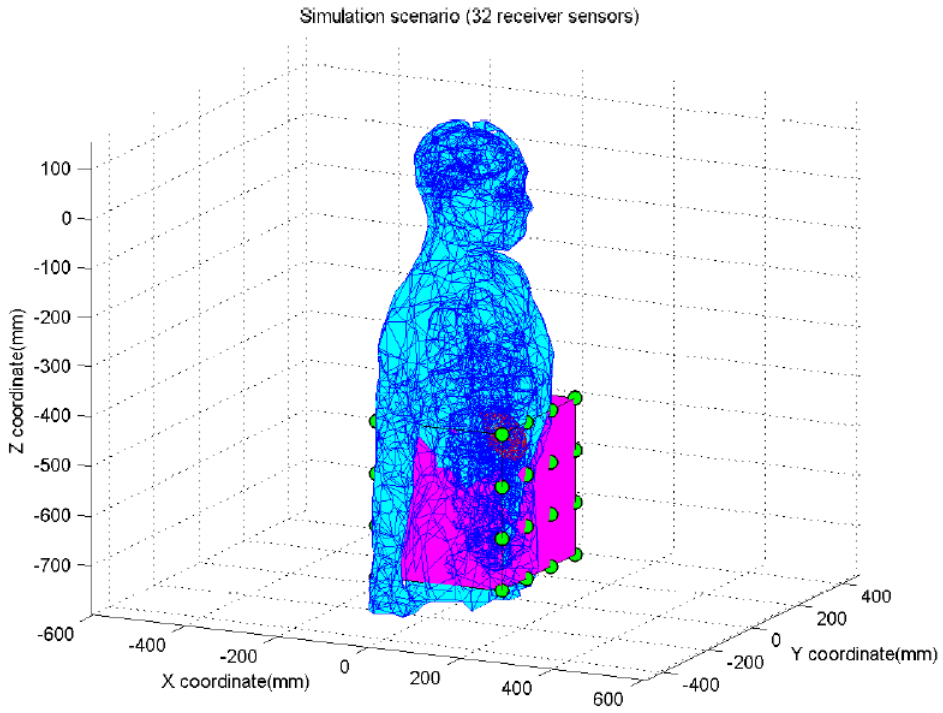

Figure 5.7: Example use of 32 receivers outside human body. [14]

Capsule localization is happening by the triangulation of the RSS (Received Signal Strength). These receivers are not used to capture data transmitted from the capsule. The power consumption of the receivers that are placed outside human body are not considered because there is a lot of room to place bigger power sources (battery).

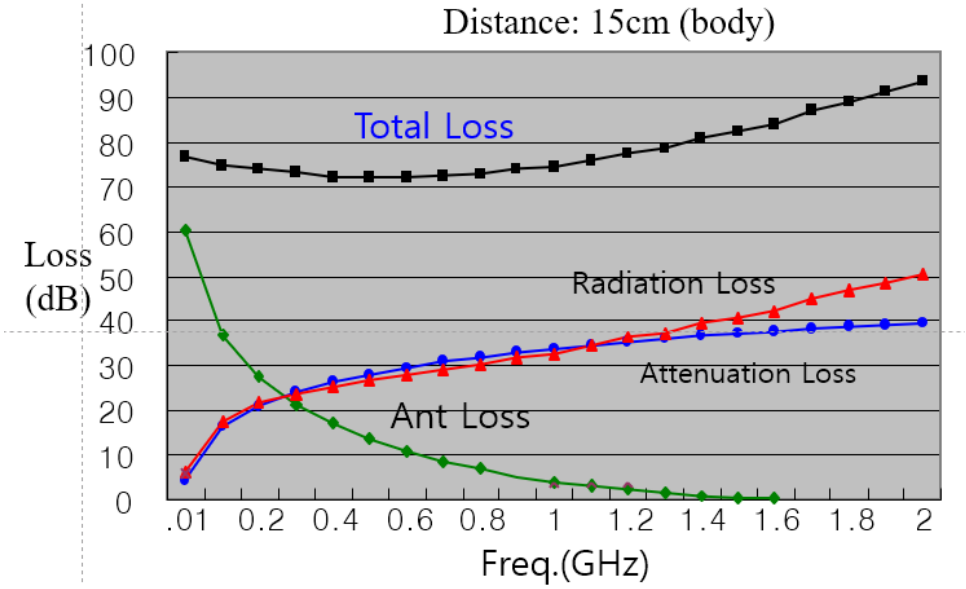

Figure 5.8: Path loss due to radiation losses, antenna losses and human body absorption. [19]

In a wireless telemetry system, the composed parts are the transmitter the medium of transmission and the receiver. For this system, the transmission medium is the human body. There are path losses of the signal, due to absorption from human body. It is possible to use only one receiver to retrieve wrong data packet

due to signal loss or noise. In Figure 5.8 the various reasons that attenuate the received signal is shown. As seen in the figure at a distance of 15cm (15cm of human body path) there are radiation losses, attenuation losses and antenna losses. These three types of losses produce the total signal losses of the system. As seen, there are various reason for the signal to be weak in the receiver side. Another reason the transmitted signal to be lost, is the distance of the transmitter to the receiver. In Figure 5.8 the total losses are shown only for about 15cm. In Figure 5.9 the attenuation of the signal due to the distance is shown.

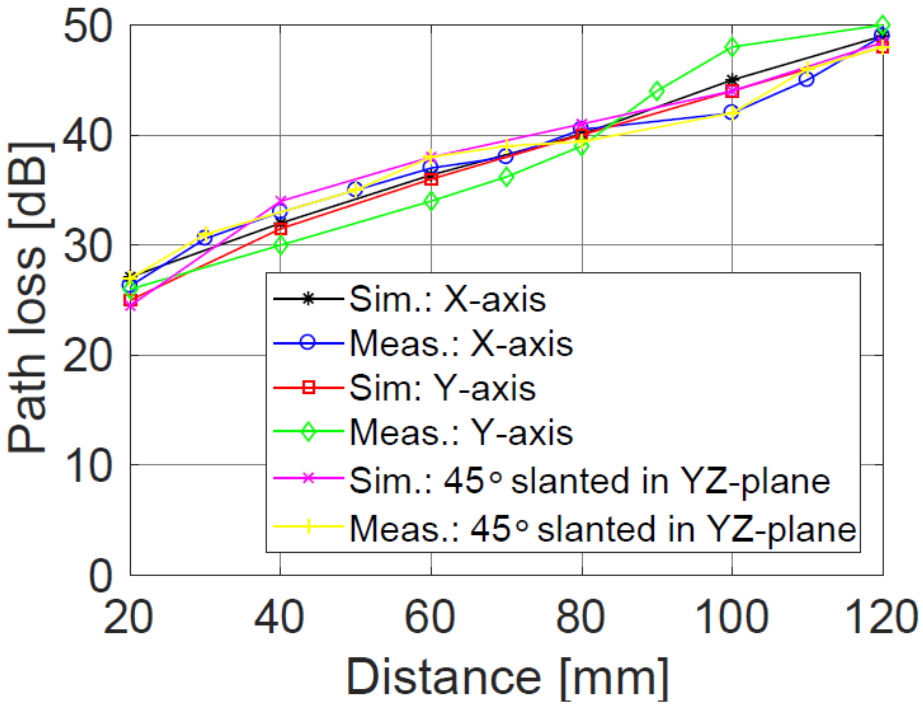

Figure 5.9: Path loss due to human body absorption in various distances. [29]

The design of a wireless link with multi-receivers, it is more likely to receive the correct data in some of them. Below there is the algorithm used to obtain the correct data transmitted.

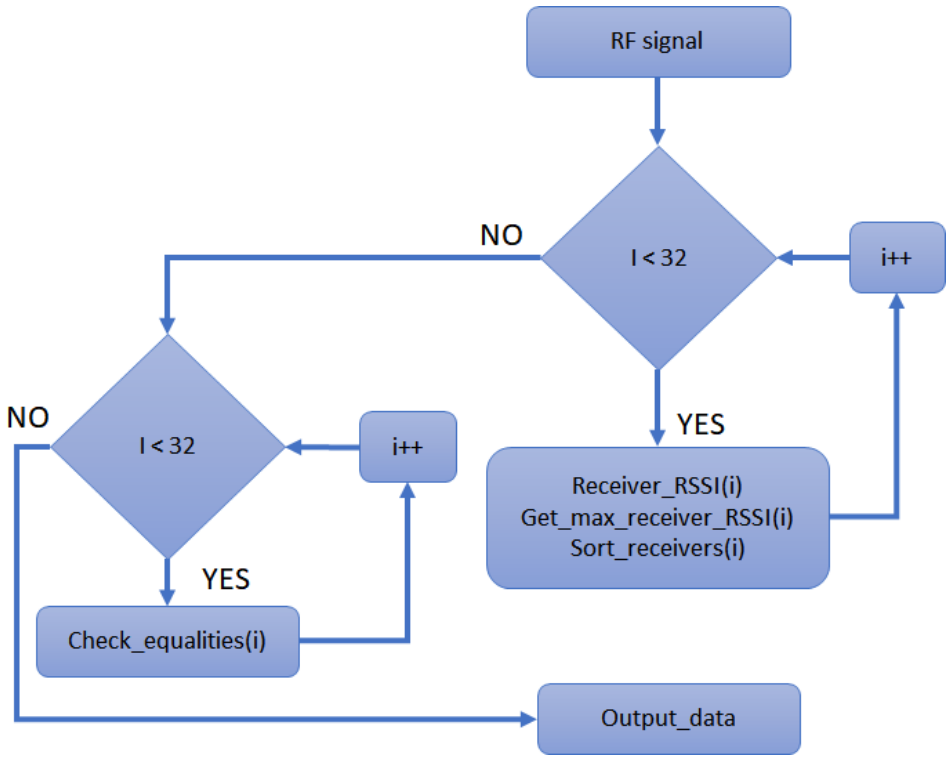

Figure 5.10: Flow diagram of the proposed algorithm.

At first, the algorithm stores the value of the signal level together with the value it receives. This is done for all the receivers. Then a sorting algorithm is implemented to sort from higher received signal level to lower. The next step is to compare the received data one by one and the result is going to be averaged. If the average is greater than 0.5 then the output value is "1" else, it is "0". The entire algorithm was implemented and simulated with the use of Matlab Simulink. To obtain more accurate results human model designed to obtain the correct path loss and propagation. So, the results could be nearer to the reality. Path loss data and signal propagation were obtain from other works like Hany et al. [103] and Vermeeren et al. [104].

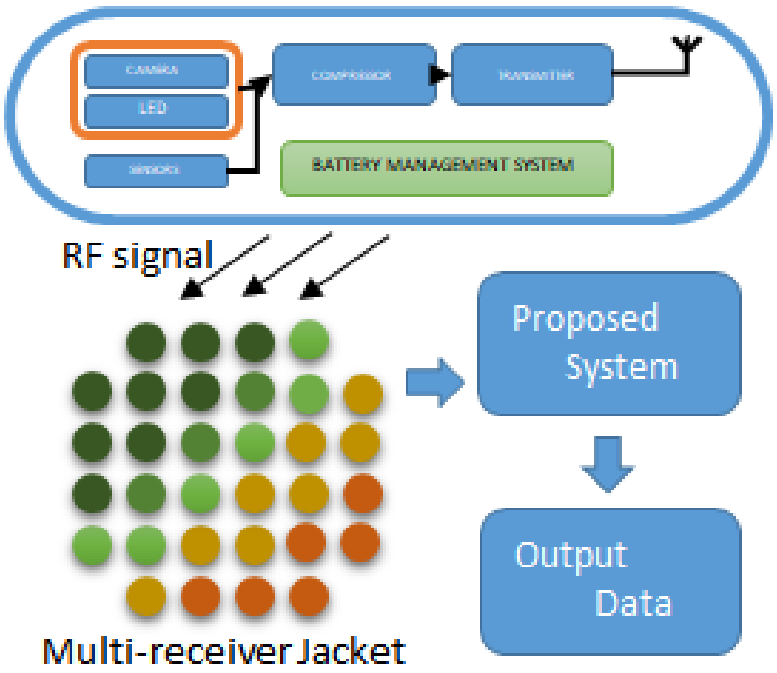

Figure 5.11: Block diagram of 32 receivers outside human body.

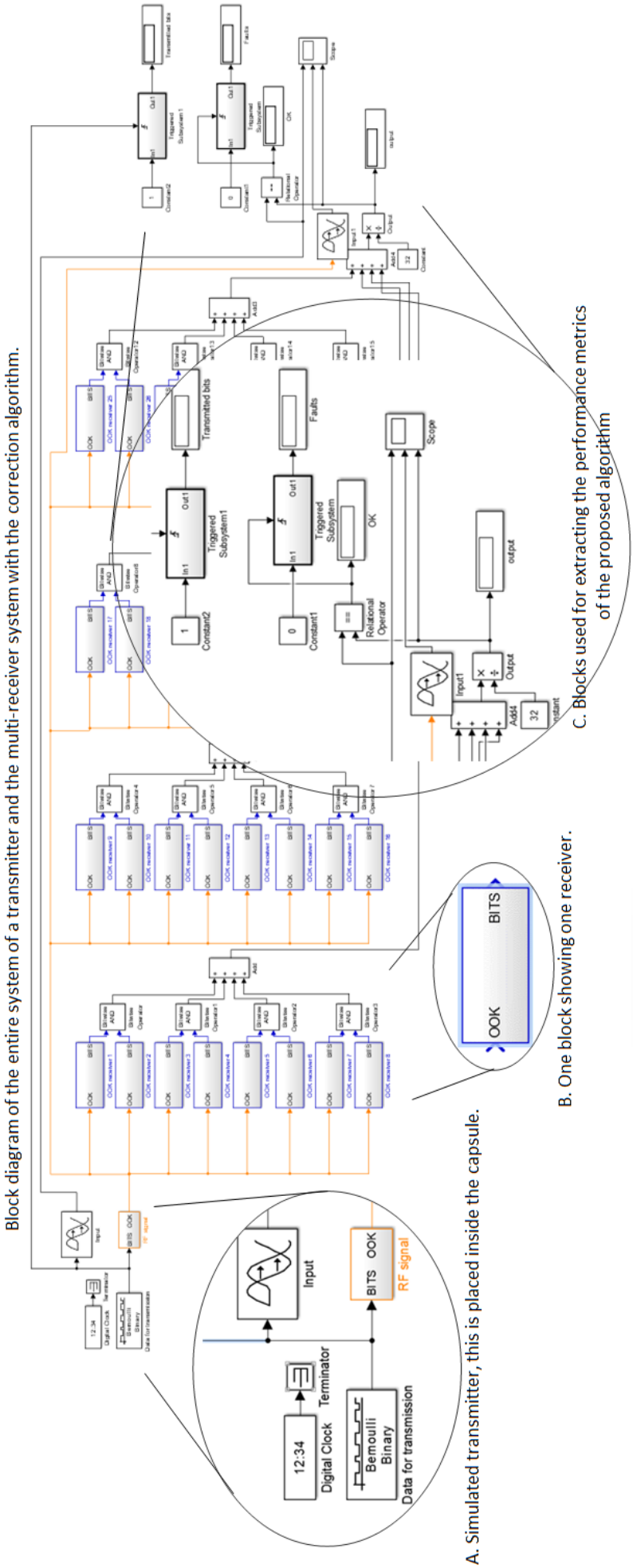

Figure 5.12: Block diagram of the proposed system simulated in Simulink software.

In Figure 5.12 the entire system is shown. The transmitter, which is in the capsule side, is in the left side of the figure. In the middle of the figure are the receivers used with the part of the proposed algorithm and in the right side of the figure is a part of the algorithm with the metrics used to measure the performance of the proposed algorithm.

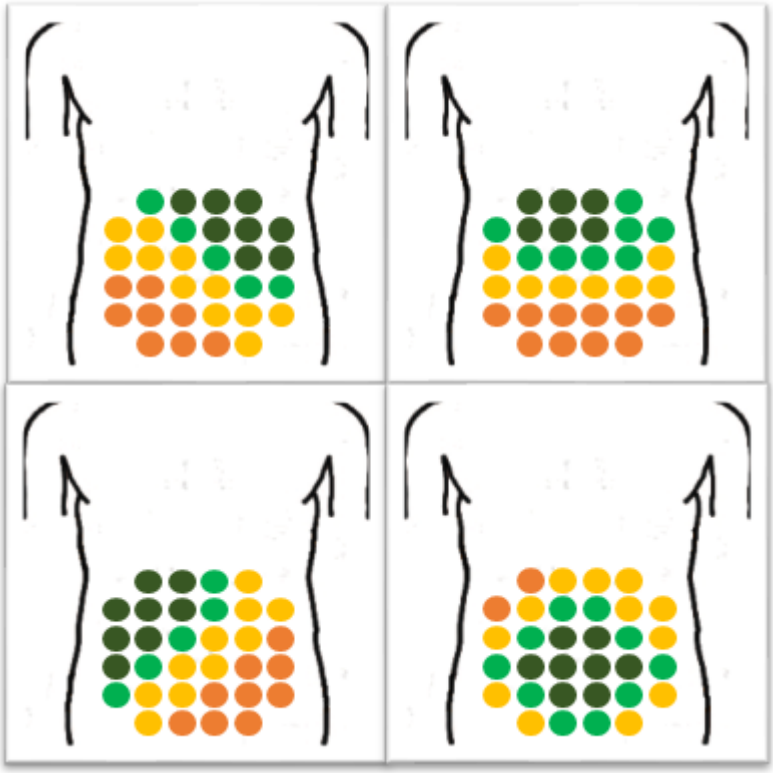

Figure 5.13: Variable scenarios for evaluation. Its image shows the reception of each receiver due to the path loss of the transmitted signal.

However, various scenarios should be considered for the simulation. In Figure 5.13 the different scenarios, where the capsule is in different position inside human body is visualized. The circles are the receivers in the jacket and the color represents the reception of each of them. With green color are the receivers with the higher reception signal and in red color are the receivers with the worst reception.

5.5 Results

The design of an robust algorithm to retrieve from a multiple receiver system data was designed and simulated. The proposed system can be modified to work with more or less receivers, depending on the desired accuracy needed. It was achieved by removing the excess power consumption from the capsule and in the time to retrieve any data packets that are lost. The power performance of wireless link of the capsule has been increased and the energy needed is almost the half. Furthermore, this system will promote the use of higher resolution in camera sensor due to excess available power. The proposed system was designed, implemented and simulated in Matlab Simulink. An OOK transmitter was designed to evaluate the transmission performance. The human body characteristics used to model and design using Simulink software

to perform simulations and to observe the different receptions in different positions in human body. At Figure 5.15 are shown in the top axe the digital input data, in the middle the modulated signal and finally the digital output. The signal is received from the team of receivers and processed by the proposed algorithm. The results show that there is a good recovery without any bit loss. The proposed system consists of an OOK transmitter inside the capsule and the multi-receivers are in the jacket outside human body. To perform the simulations an OOK transmitter was designed in Simulink. The input of the OOK transmitter is digital data. That are shown in the top axes of Figure 5.15. In the middle axes is the modulated output of the OOK transmitter and final the bottom axes are the corrected demodulated output by the multi-receiver system.

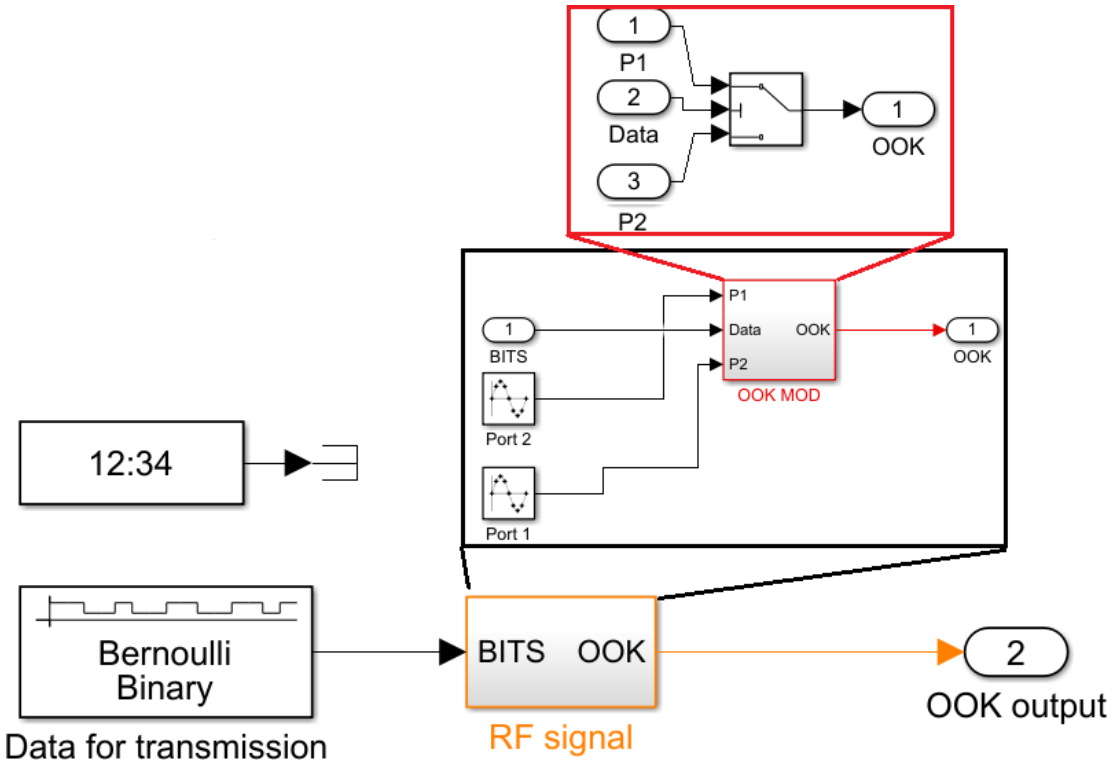

Figure 5.14: OOK transmitter designed in Simulink.

In Figure 5.14 the OOK designed transmitter in Simulink is shown. A Bernoulli binary module is used to produce random binary values. These values are fed into the OOK module. This module consists of a virtual switch that modulates the carrier with the data. These data are fed to the multi-receiver system that is shown in the Figure 5.12. Figure 5.15 shows the digital input data in the top row, the modulated signal in the middle row and finally the digital output. The signal is received from the team of receivers and processed by the proposed algorithm. The simulation results have shown that there is a good recovery without any bit loss. The simulated system consists of an OOK transmitter inside the capsule and the multi-receivers in the jacket outside human body. To perform simulations, an OOK transmitter was designed in Simulink. The input of the OOK transmitter is digital data that can be seen in the top row of Figure 5.15. The middle row is the modulated output of the OOK transmitter and finally the bottom row is the corrected demodulated output by the multi-receiver system.

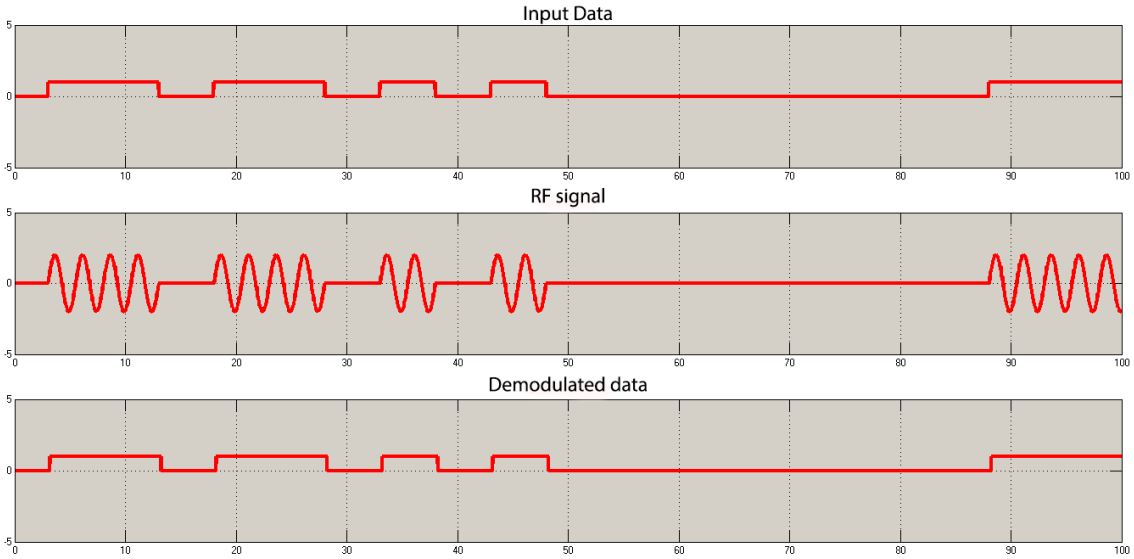

Figure 5.15: Input and Output data of the proposed system.

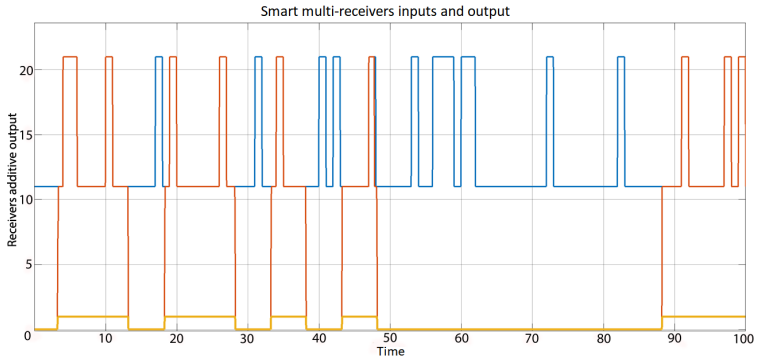

(a) First scenario from WCE

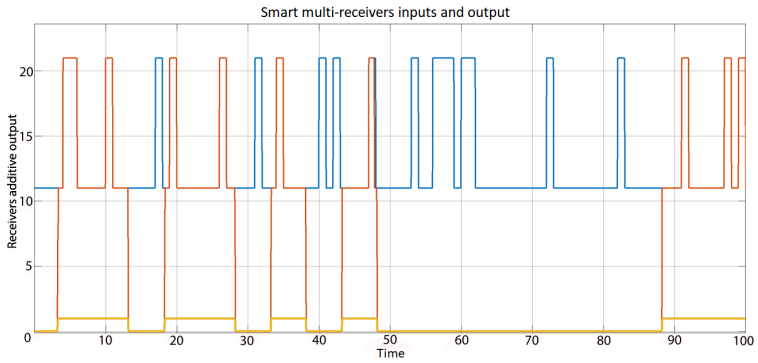

(b) Next scenario from WCE movement.

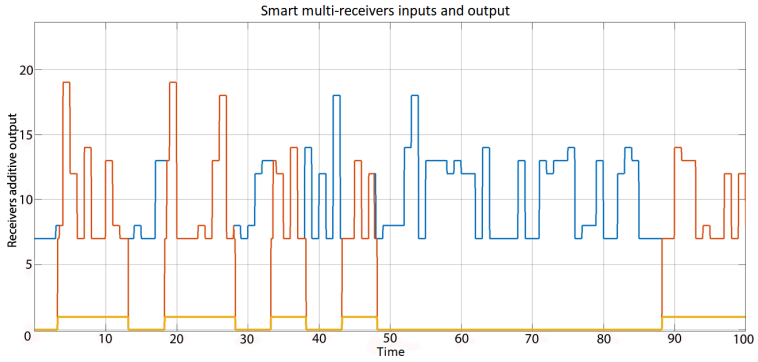

(c) Reception view while in the middle of small intestine.

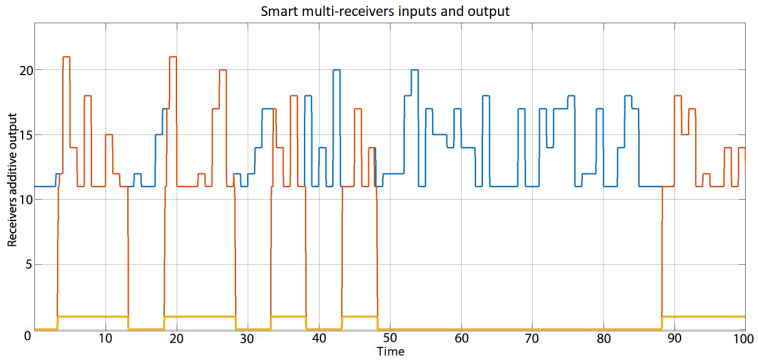

(d) WCE reception before the end of the journey.

Figure 5.16: Various scenarios with the wireless capsule in different position in the small intestine and the colon.

.

In Figure 5.16 the four different scenarios from Figure 5.17 are shown. In Figure 5.16 is shown the different reception that the proposed system gets. In blue color is the addition of the input data of all the transmitters, while in red color is the number of receivers that have an RSSI value that is acceptable. The algorithm then computes and extracts the output decoding values that are presented in yellow color. The performance in all these four different simulations extract the correct data. A comparison of the output with the input data is shown in Figure 5.15. Figure 5.17 shows, how the small intestine and colon inside human body are arranged. It is obvious that the small intestine has more length than the colon. Also, colon can be diagnosed by traditional methods. However, small intestine has not the ability to be diagnosed by traditional methods. The only way is the use of a smart pill. Capsule endoscopy is preferred to be used for diagnoses of small intestine because there is no other painless method to perform. To ensure that the system performs as designed, a lot of tests performed with different variables.

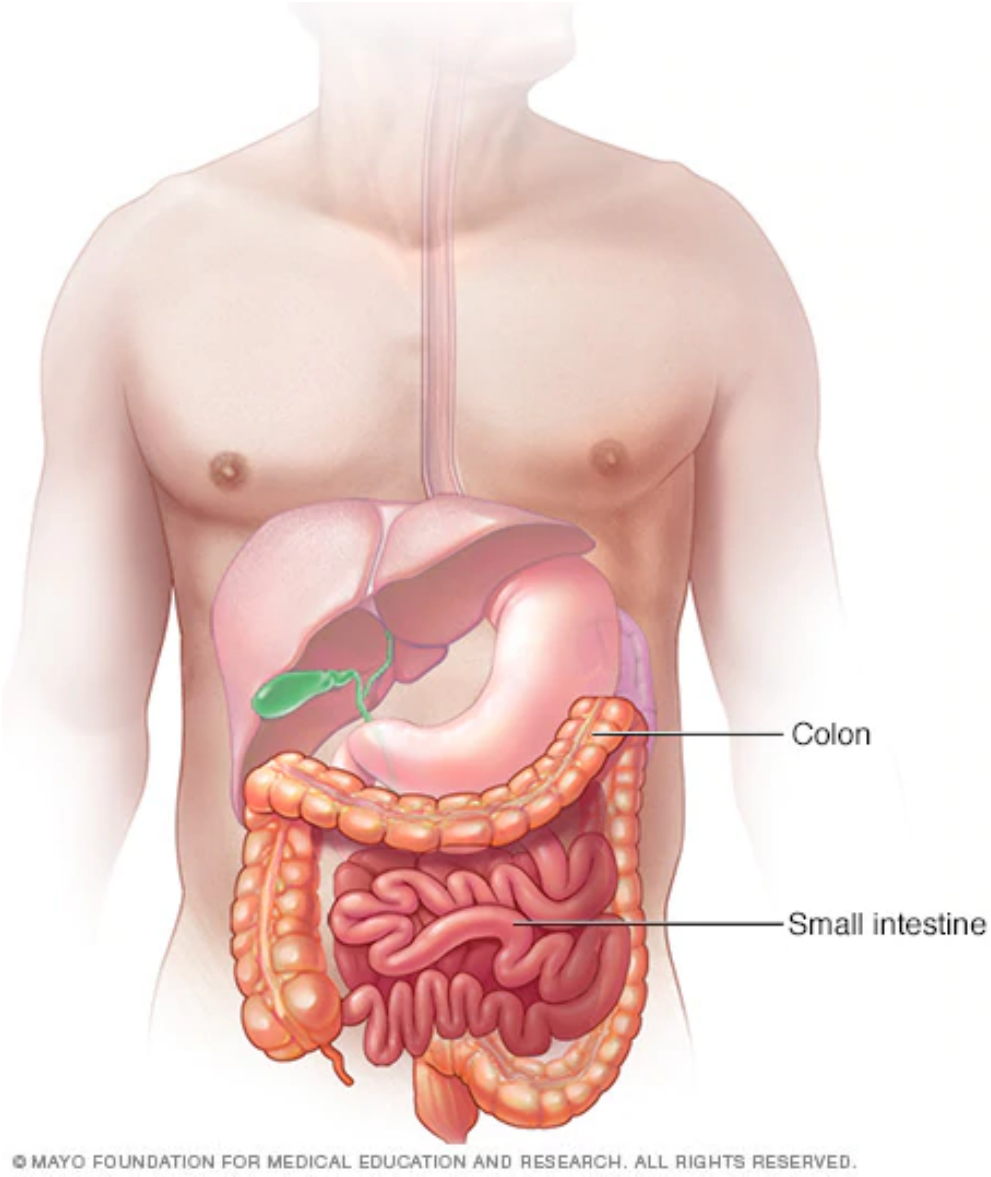

Figure 5.17: Sketch of human's small intestine and colon as it is placed inside human body. [30]

Knowing that the power transmitted from the capsule is always the same. A lot of tests with different

parameters in the reception of the transmitted signalare performed. To make the simulation of the proposed system,a number of parameters need to be added in the simulation. Additive White Gaussian Noise (AWGN) was added to all the receivers. By this way, the noise was simulated and the results in the demodulated data. The main parameter that increases the errors of reception was the human absorption of the RF signal. To simulate this there were four different levels of signal attenuation that were added in the proposed system. By this way, it is test like in real operation. The highest reception signal has a value varying from 0.9 to 1.0 of the transmitted power. That is from the 90% of the transmitted power up-to 100%. The second level of received signal was varying from 0.8 to 1.0. The third from 0.6 to 0.8 and the fourth from 0.3 to 0.6 of the transmitted signals. In the tests performed, different scenarios investigated. Like the four are seen in Figure 5.18. While the test run is applied, the values of attenuation for the four different group of receivers is changed randomly. For example, in the simulation performed, the third group of attenuation has values from 0.6 to 0.8. The attenuation in this group of receivers is varying during the simulation in the gap of 0.6 to 0.8.

If the capsule is always transmitting the same power, the only variables that change are the position of the pill in the human body and the transmitted power that is absorbed by the human body.

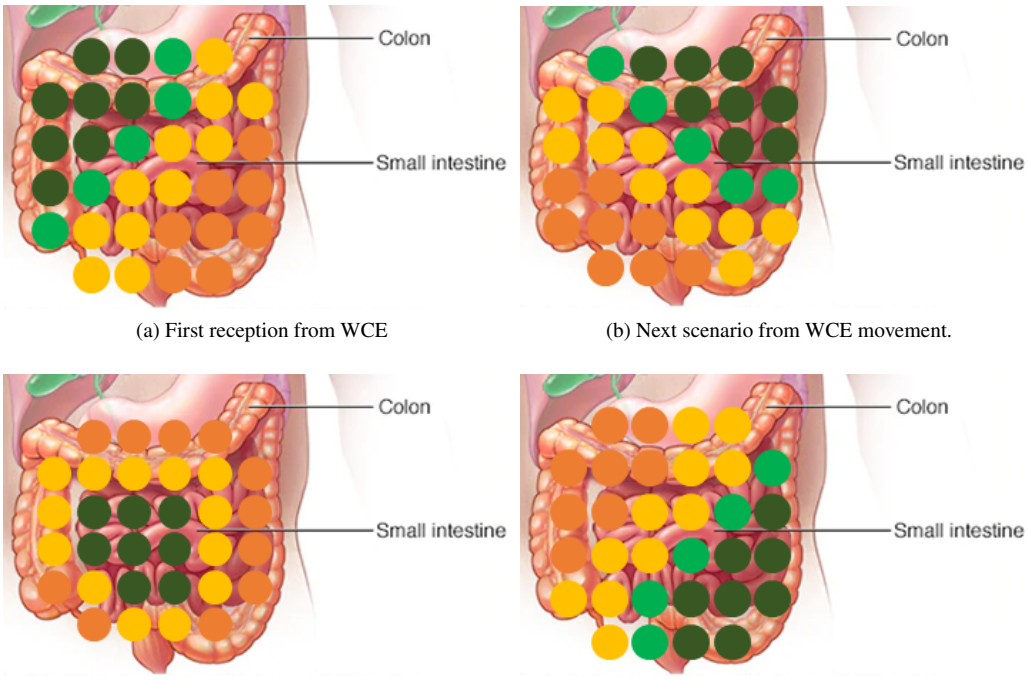

(a) First reception from WCE

(b) Next scenario from WCE movement.

(c) Reception view while in the middle of small intestine.

(d) WCE reception before the end of the journey.

Figure 5.18: Various scenarios with the wireless capsule in different position in the small intestine and the colon. In this figure every receiver is shown in different color. The color means the reception level. In Green color is the good reception while the yellow and red colors show that receiver has bad reception.

In Figure 5.18, there are four separated figures that shows the different position of the capsule during its journey through the small intestine and the colon of the patient. In Figure 5.18a is shown the reception performance of the receivers while the capsule is in the entry of the small intestine. As seen, the upper left receivers have the best reception than the others. The same situation can be observed in Figure 5.18b where the capsule has been moved in the upper right section of the small intestine. It is obvious that the

capsule is always in movement and different RF receivers are receiving better. In Figure 5.18c is shown the most common view of RF reception. It shows that better reception have the middle receivers. This is because the small intestine is huge, in comparison with colon, and the most time of the travel, the capsule is in the middle of the belly, where is the main part of the small intestine. The last Figure 5.18d shows the RF reception while the capsule is in the end of the colon which is the end of its entire journey. Good reception have only the lower right receivers. These are a few scenarios used in the performance analysis of the multi-receiver system. To examine the performance and conclude a random bit generator as an input of the simulated transmitter is used and in the receiver output, a comparison of the received results with the random input is happen. In Figure 5.18 there are only four different scenarios. More than four scenarios are performed to examine the performance of the proposed system. The results can be seen in Figure 5.19.

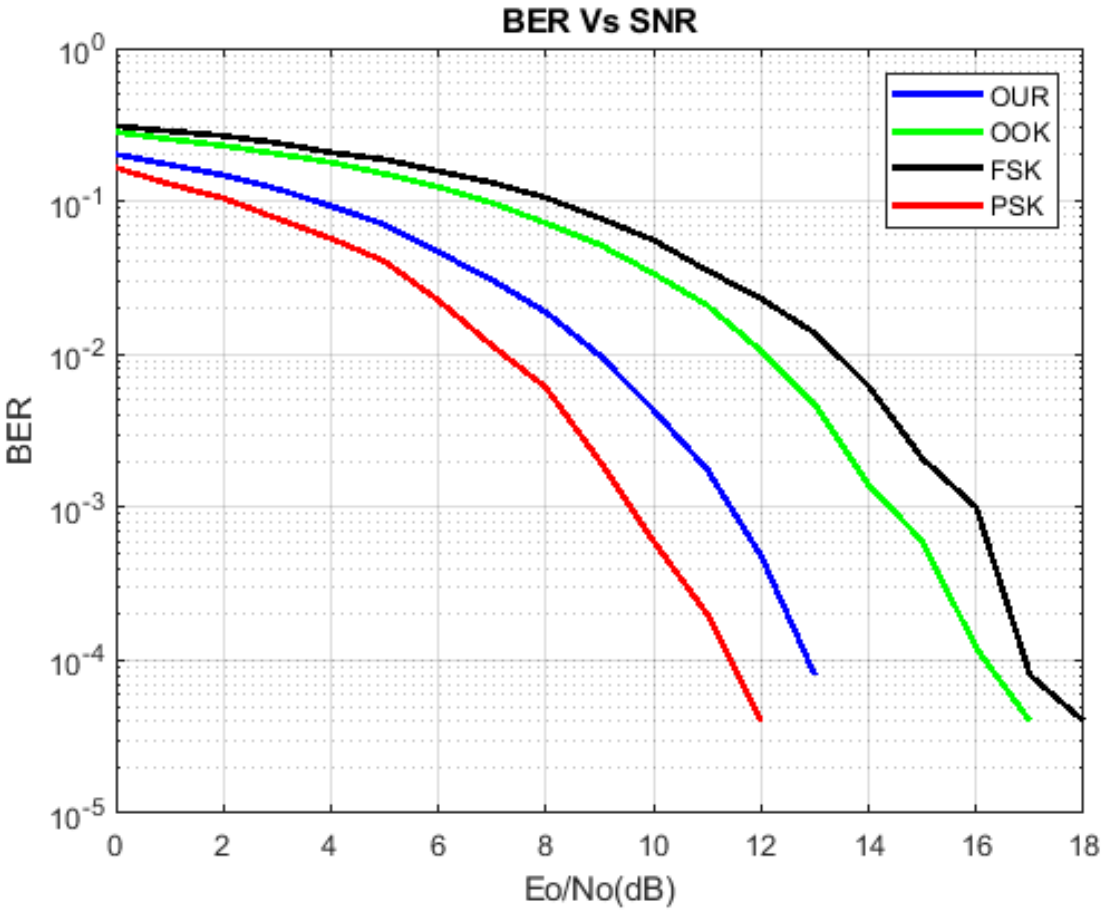

Figure 5.19: Comparison performance of the proposed system with typical systems.

In Figure 5.19 the output performance in Bit-Error-Rate (BER) is shown. Different modulation techniques and their BER performance, tested. PSK (Phase Shift Keying), FSK (Frequency Shift Keying) and OOK (On Off Keying) modulations with the performance of the proposed system checked and compared. For all of them, BER was tested using a simple transmitter and receiver system. The proposed system consists of one transmitter and 32 receivers. The modulation used was OOK. In Figure 5.19 is shown that PSK modulation and the modified OOK system can achieve better BER performance in comparison with the simple OOK system and the FSK modulation system. More clearly, in this plot shows that both PSK and

the proposed OOK system can keep the BER performance while the SNR is increasing. Also, it is obvious that the proposed OOK system has less Bit-error-rate than the simple OOK system in lower SNR. This means that the proposed system can keep the BER in low in less SNR in comparison with the simple OOK system. However, the proposed system is designed mainly for use with OOK modulation scheme. The reason is because in OOK modulation the transmitter is switch-off while the incoming data are logical "0". In difference in PSK modulation, the transmitter is switch-on all the time. So, in the proposed system, the advantages of the characteristics of the OOK transmitter obtained and the same time the proposed system can optimize further BER performance.

5.6 Summary

The design of a multi-receiver system for capsule endoscopy increases the BER performance of these systems. Also, there is no need for a bi-directional wireless communication. So, there is an overall increase in performance in the power consumption domain. Furthermore, there can be more improvements in the BER performance.

The system proposed is designed and simulated. The algorithm is applied in the digital output of each receiver. A more intelligent system could apply the algorithm in the base-band signal of each transmitter. The proposed system applied the algorithm in the output of each receiver. So, the decision for each receiver for the output is already made. Every analogue receiver has a threshold value for the output result. This is constant so the performance of the system is only relied in the performance of the proposed algorithm. For future work it is proposed the design of a system without the use of hardware design RF receivers. The new system will consist of multiple A/D (Analog-to-Digital) converts that can work for RF signals frequencies and then the new algorithm could be applied in this data. In Figure 5.20 is shown the proposed system in the left and the enhanced future work in the right.

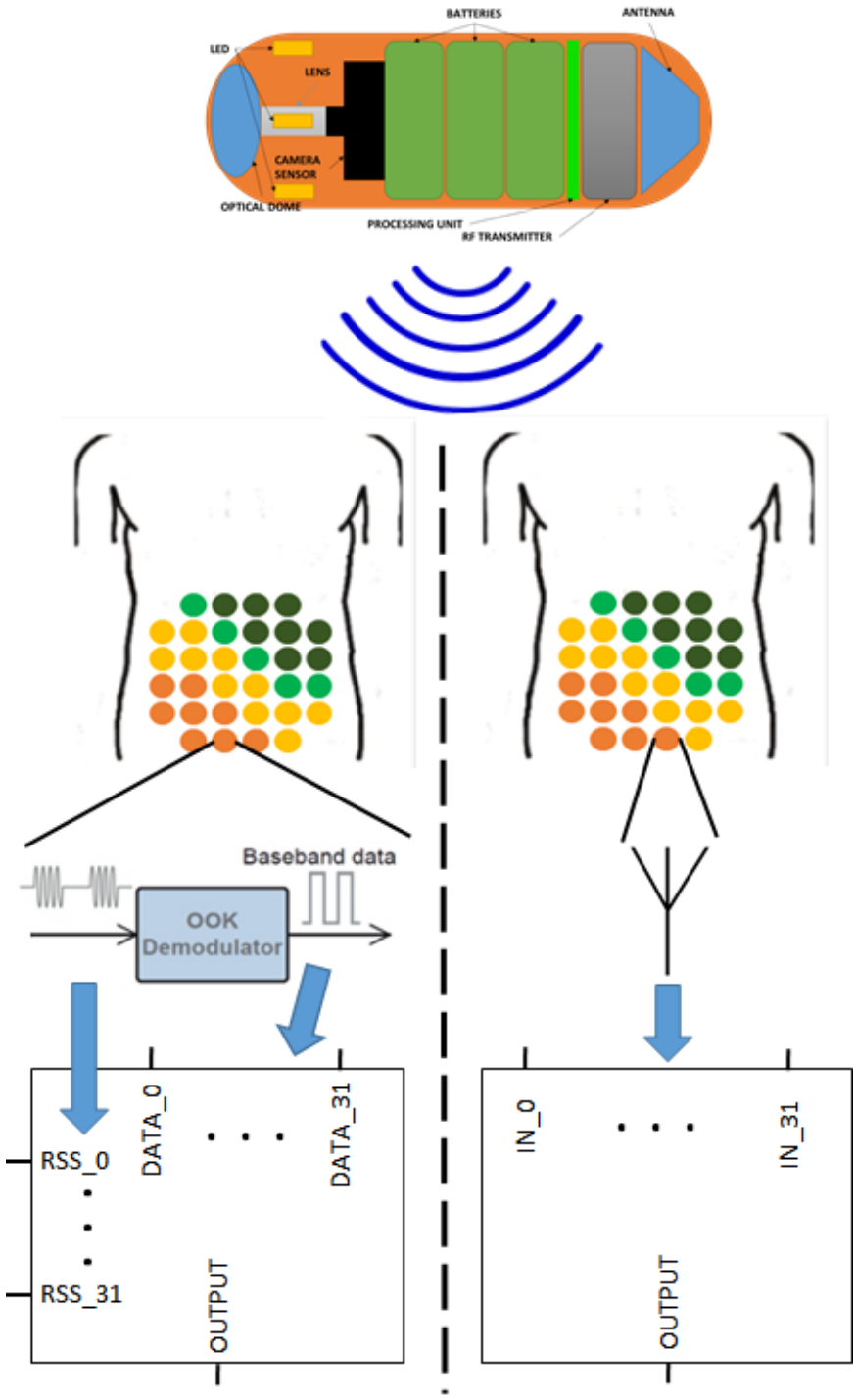

Figure 5.20: Comparison of the proposed system with the new version featured.

Chapter 6

Omnidirectional lens for use in wireless capsule endoscopy systems

6.1 Introduction

In this chapter an overview of WCE lens' used is provided. A walk-through the investigation of the most suitable type of lens for capsule endoscopy is provided. A discussion about different type of lens that have been used and the advantages and disadvantages of them, will be held.

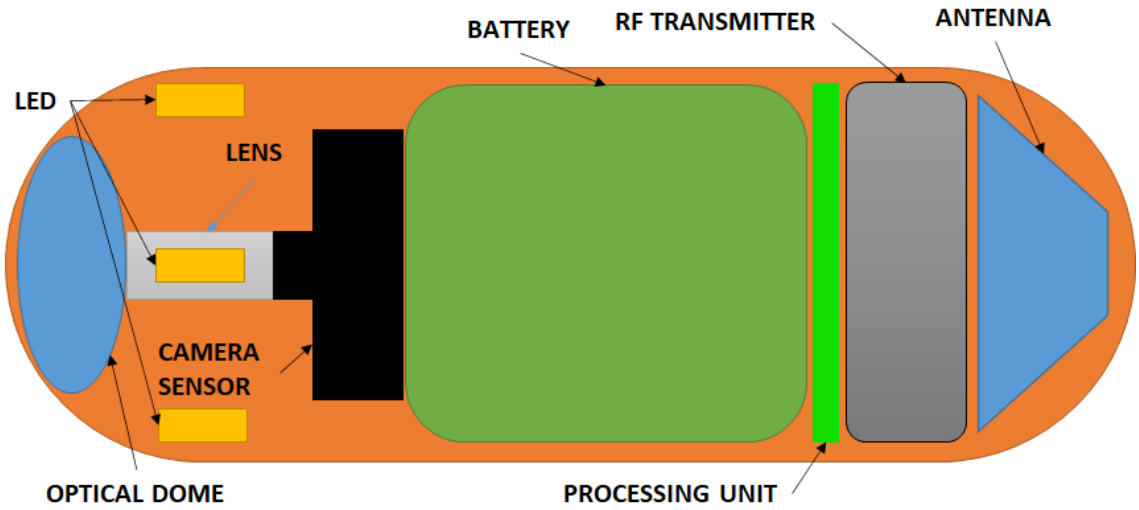

Figure 6.1: A diagram of the components an endoscopic capsule consists of.

As noted in the previous three chapters, in recent years there is a lot of research effort in different WCE components. In previous chapters investigation and improvements in three different WCE components is made. In Chapter 3 a better solution in image compression algorithm for WCE is proposed. In Chapter 4

a low complexity, high data-rate OOK RF transmitter is designed and simulated and in Chapter 5 an ingenious multi-receiver system for better reception performance is proposed. However, there are a few more components that are used in an endoscopic capsule to work. In Figure 6.1 is shown a typical endoscopic capsule with the components it consists of. In this figure the components of a WCE are shown. In green color are the batteries used to operate the entire system of the WCE. As seen, most of the available area is mainly captured by the batteries. In black color is the camera sensor and in the same side with light blue the lens used. In the same side there are in yellow colors the LEDs used to illuminate while the camera sensor captures image/video. In the left side of this figure in light blue color is the antenna used to transmit outside human body the captured information and near the antenna is the RF transmitter. RF receiver is not used as mentioned in Chapter 5. A WCE is a state-of-art electronic device that is mainly consist of:

- One or two camera sensors,
- camera lens,
- power unit, that could be a battery pack or a wireless power receiver module,
- a main controller board that is responsible for processing of captured data and to prepare them for RF transmission,
- an antenna for RF transmission,
- an RF transmitter for RF transmission and
- various sensors like temperature and pH, that could provide more info to doctors/physicians and they could perform better diagnosis.

As seen, there are a lot of components in an endoscopic capsule that can be investigated and improved. In this Chapter the use of special type of lens that could improve the performance of the entire system in the domains of power and diagnosis performance is investigated.

6.2 Camera lens

In general, in wireless capsule endoscopy the main sensor is a camera. The purpose is to let the doctors investigate areas of the intestine that without a surgeon operation is not possible. In the area of colon usually doctors use the classical colonoscopy method which is painful for the patients and sometimes causes injuries. But, in the area of the small intestine, if a doctor wants to do a diagnosis the most easy and painless method is the wireless capsule endoscopy procedure. In most smart-pills the placement of the camera sensor is horizontal in the pill, like in Figure 6.2 where is shown a commercial WCE pill that uses only one camera sensor.

Figure 6.2: Commercial used wireless endoscopic capsules with one and two camera sensors. [3]

In the same layout, there is a commercially used WCE that uses two camera sensors. They capture in opposite directions. [3] This implementation is shown in Figure 6.2 and in Figure 6.4. The reason for using two camera sensors is to provide more info to the doctor for better diagnosis. The use of only one camera in the capsule leads to about 20% - 30% miss rate. [38] It is obvious, the miss rate is big enough to lead to a wrong diagnosis from the doctor. This practice leads to increase of power consumption and the need of the double data rate for the RF transmitter. Nevertheless, there are other implementations that try to fill the gap between the one camera perspective and 360° degrees of view perspective. Li et al. [31], proposes an endoscopic capsule with multiple cameras. The idea of this implementation is to use as many cameras is possible to capture as many areas of the intestine. The maximum area coverage they achieved is up-to 98% of the processed area. The results are magnificent, if one thinks that with only one camera it is possible to lose about 20% to 30% of the processed area. However, there are a few drawbacks in this implementation. They mention that it is a multi-camera system.

Figure 6.3: Micro-ball prototype with six camera sensors. [31]

As a camera sensor they use an OV7660 from Omnivision. This camera sensor has a power consumption of up-to 40mW. In this implementation the use of multi-camera (six cameras) increases further the power consumption of the entire system. Also, to handle the amount of data from camera sensors they use a

flash memory IC which has a power consumption when it is working of 30mW. In their implementation they provide a lossy JPEG compression algorithm that has a -40.7 dB PSNR and it can compress the data up-to 86%. Moreover, they design the system to capture image frames only when the capsule is moving. This works with to sensor, a magnetometer and an accelerometer. By this way they increase the power management performance. However, the entire system is too complicated, and it is not feasible to be powered by a battery. They power it with wireless energy transmission system. An intelligent multi-camera system was proposed, but it has many drawbacks, the most significant are the complexity, the power consumption and the lossy compression algorithm that is not accepted in this type of application.
Another interesting investigation can be seen by Sheu et al. [32]. Unlike previous attempt, they tried to have a wider optical range without using more than one camera sensor. Their idea is clearly based on the mechanical parts of making a lens that will allow the widest range of vision. They have proposed the manufacture of a lens that has the capability of recording both from the front of the capsule and from the back. A corresponding attempt has been made by GivenImagine [3]. However, this commercial capsule utilizes two camera sensors, one at the front of the capsule and one at the back.

Figure 6.4: Commercial products that uses two camera sensors [3]

The idea of Sheu et al. [32] is to use special lens to provide better field of view in the doctors, while maintaining the use of only one camera sensor. Their designed lens can capture the forward of the capsule view with a FOV of 90 degrees and for the back view a FOV of 260 to 290 degrees. In Figure 6.5 the total capture view of the capsule is shown. It can capture with one camera sensor both the front side of the capsule and the back side of the capsule.

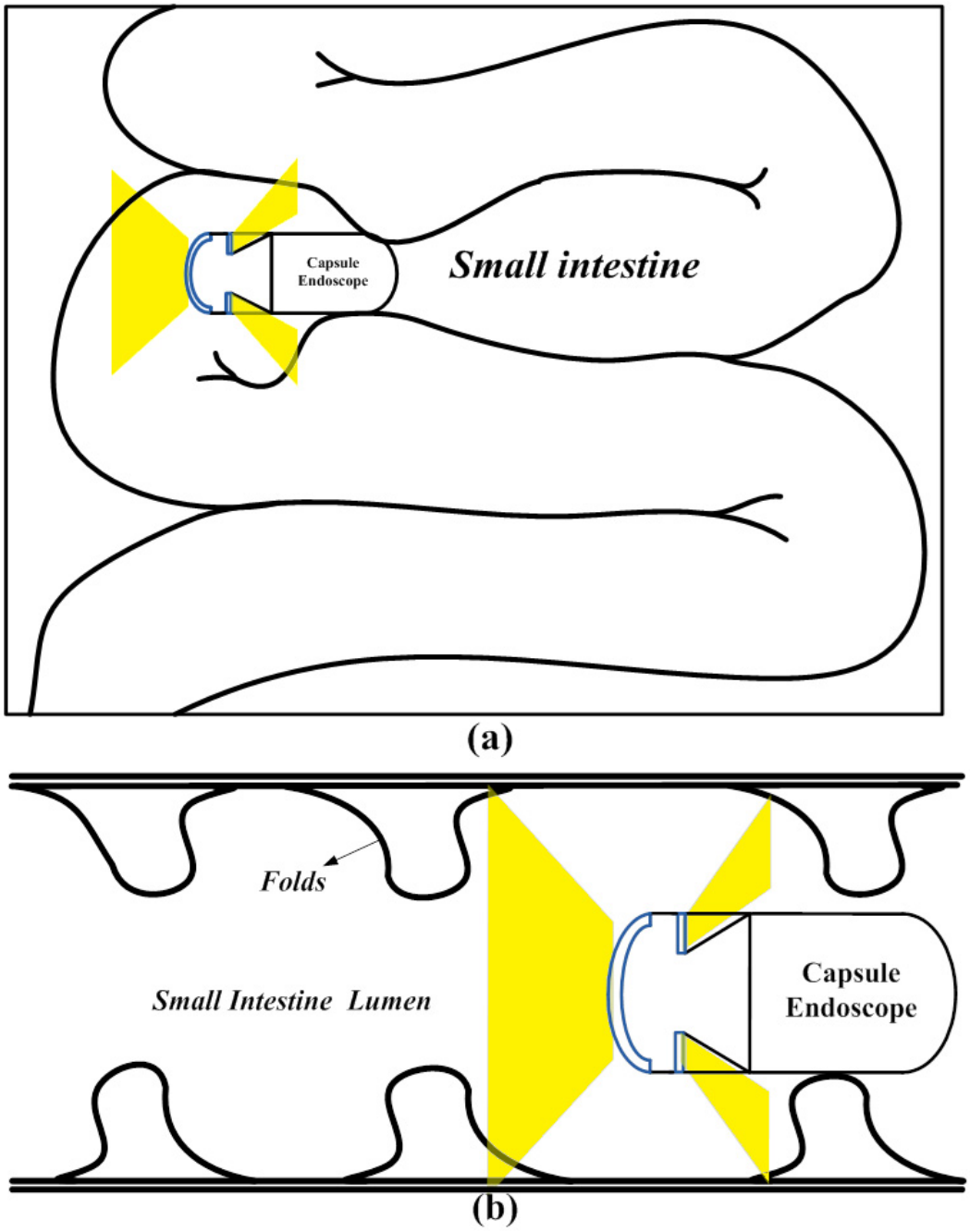

Figure 6.5: Dual field of view with the use of special lens and one camera sensor. [32]

Walking through our research on the design of WCE lens, another work was observed. This work is proposed by Ou-Yang et al. [105]. This work is focused on the design of a WCE lens with wide field of view that is up-to 86 degrees. In this paper they propose a miniature lens that is capable to have a wide-angle view. However, the previous work presenred is capable to capture 90 degrees of the front view of the capsule plus, the 260 to 290 degrees of the back view. It is obvious that the previous system performs better. The last finding in the research area of WCE lens was proposed by Ou-Yang et al. [33]. The idea was to design a system that is capable to capture 360° degrees around from the capsule. Typical capsules use front

imaging capsule endoscope (FICE) and this type of capsule have some drawbacks. It is not able to capture some useful details like some hidden regions that are not captured, also the system m does not has the ability to understand the movement of the capsule. That is only a few reasons that motivate them to design a radial imaging capsule endoscope (RICE).

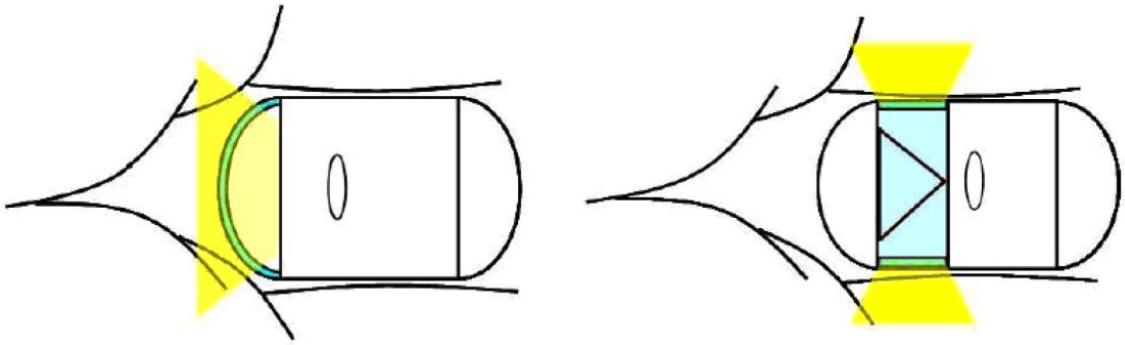

Figure 6.6: FICE and RICE capsule design compared view. [33]

In Figure 6.6 a FICE and the proposed RICE system is shown, definitely the RICE system is capable to capture more of the intestine that the FICE system. All these introduced systems help to understand the needs of doctors and the area that need to give more attention and increase the performance of the capsule lens.

6.3 Requirements

As noted in Chapter 3, in this type of application the need of clear images is a must. The compression algorithm of these systems should be a lossless one and not a lossy that could lose information that is useful to doctors and maybe make the doctors perform a bad diagnosis. Considering the application that is going to be used these lenses there are some requirements that should be considered.

- Low distortion,
- high definition imaging,
- wide view of the intestine,
- multiple angles of views,
- small enough to fit inside the capsule and
- to be able to work with one camera sensor,

To be more specific there is a need of a camera lens design that is small enough to fit inside a WCE. Furthermore, this lens should be able to capture the entire intestine with different angles of view, because this can lead doctors to better diagnosis. The lens should not distort the captured image because the image the doctor will see must be as clear as possible. The last and important is that the system should work

with only one camera sensor, because this will help the design of a low complexity electronic circuit that will capture, process, compress and transmit the image outside the human body. The use of multi-camera system has a lot of drawbacks, like the size needed to make it work and the most important is the energy resources needed to make the sensor and the electronic circuit to operate. A system with multiple cameras increases the complexity of the electronic circuit that that it needs to operate. The proposed system could operate with the proposed image compression algorithm, presented in Chapter 3. The existing systems the raw image produced is like the one in Figure 6.7.

The proposed system will produce a raw image that it will look like a “donut”. This means that there will be more black areas in the raw data. For this reason the statistics used to produce the Huffman tables should change and produce new ones. The new image looks like in Figure 6.17. As it is seen there are more black areas in the raw data of the captured image. While new statistics applied to the new data, the new Huffman table can be produced. By this way it is possible to combine both the compression algorithm system with the omnidirectional lenses.

6.4 System design and implementation

Based on the research effort, a design of a lens for capsule endoscopy is proposed. Considering the shape of the camera sensor and the shape of the commercially used lens, there is a lot of areas of the camera sensor that is unused. This phenomenon is due to the shape of the lens, that is round and the shape of the camera sensor that is rectangular.

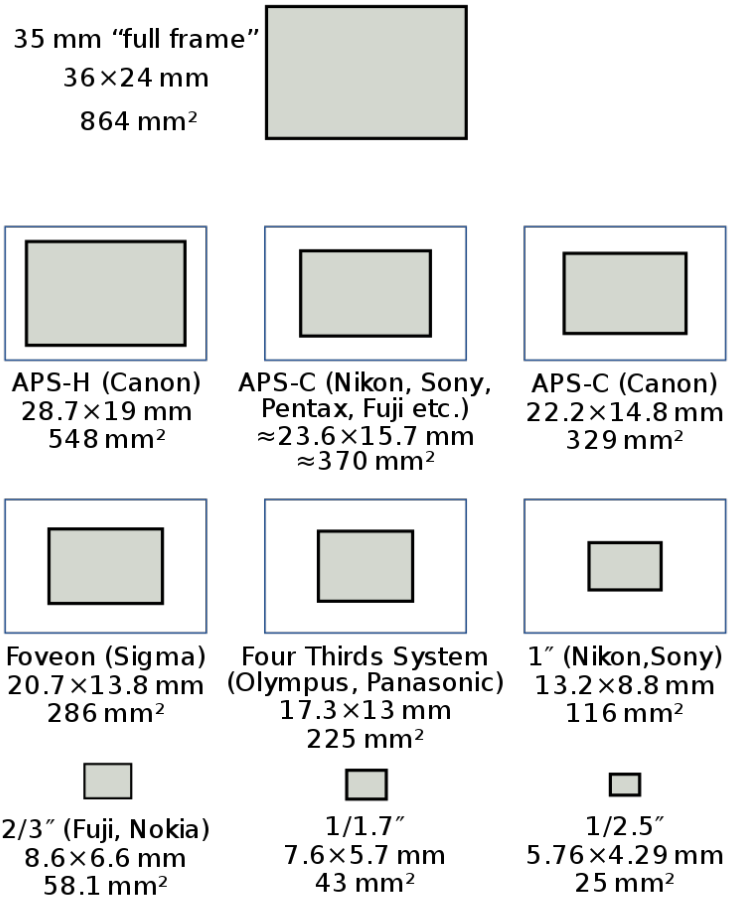

Figure 6.7: Typical size and shape of commercial camera sensors.

In Figure 6.7 commercial camera sensors' shape is shown. Compared with the image retrieved by the camera sensor of a capsule endoscopy system, it is obvious, there are a lot of black areas, where there is not information. These areas do not contain any info, but the camera sensor is working and consuming energy.

Figure 6.8: Typical capsule endoscopy image, where the unused black areas is shown. [6]

In Figure 6.8 a typical capsule endoscopy image is shown with the black areas. The energy consumption from these areas are from three fields. The first is the consumption of energy from the same pixels of the camera sensor. There are working without providing any usable information, just black areas. The second field is the compression of the image. The compression system consumes energy to compress a black area without information inside. The last field is the wireless transmission, where the capsule transmits outside human body unusable information and consuming energy.

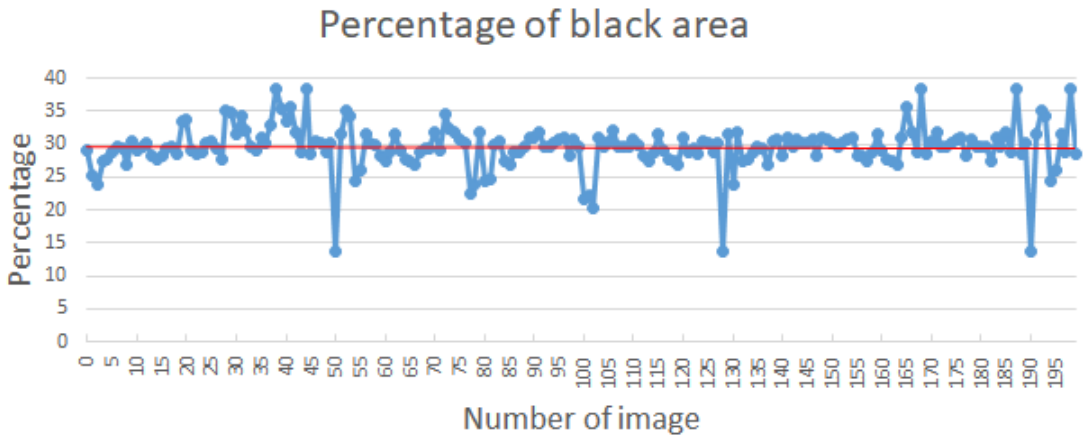

Figure 6.9: 200 images of capsule endoscopy and the percentage of unused black areas, produced due to the shape of the round lens in the rectangular shape of the camera sensor.

As it is obvious by the results in the Figure 6.9, there is in average a 30% of black areas without any carrying

information that are still captured, compressed and transmitted. Those results are from capsule endoscopy images from existing systems like the one in Figure 6.8. Those images are from wireless capsules that have the camera positioned in the front of the capsule. Same view have also capsules that have the camera positioned in the back of the capsule. A new type of lens that can capture 360° degrees of view, images is proposed. This type of lens is a catadioptric type and looks like the one in Figure 6.10 As seen at Figure 6.9 there is a lot of black area in the existing capsule endoscopy images. In these images the compression algorithm presented at Chapter 3 can achieve up-to 2.21 compression ratio. With the proposed lens it is possible to reduce further the black areas, that contain unused information. The use of this type of lens means that modifications in the compression algorithm are needed. Due to the fact that the compression algorithm presented is based in statistical analysis of existing capsule endoscopy images, a new statistical analysis should be performed and produce the new data for the Huffman tables. The combination of the proposed compression algorithm with the catadioptric lens can lead to capture more areas of the human intestine, which is now around 70%.

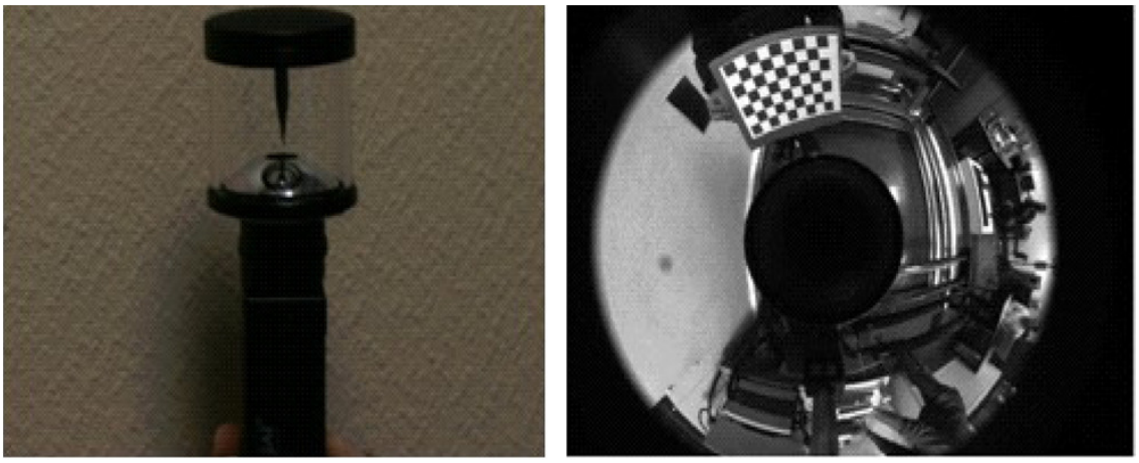

Figure 6.10: Catadioptric lens in the left side of the figure and the output result in the right side of the figure.

However, this type of lens produces more black areas than a typical capsule endoscopy lens. This is because catadioptric lens exports an image like a “donut”, as it can be seen in Figure 6.10. To understand what is shown, unwrap process to the image should be performed and the created image will look like a panorama image. After performing the unwrap task then the doctor should be able to understand what is shown and perform diagnosis.

Figure 6.11: Image captured with catadioptric lens used commercially in mobile phones.

Figure 6.11 shown an image captured with a mobile phone that uses commercially available catadioptric lens. In the red box, zoom is applied, to the person that is captured. In this image it is not so clear the black areas around the "donut" due to the fitting of the lens in the mobile camera. There is a lot of light coming in from these areas. However, it is obvious that around the "donut" there is a lot of unused areas and in the middle of the "donut". Using such type of lens, the utilization of the camera sensor is increased, with useful information that could be captured. In Figure 6.11 the unused areas that are still captured from the camera sensor is shown. So, energy is consumed without useful data captured. In camera sensor there are two metrics for the pixel area. These metrics can be used to extract the utilization of the camera sensor. These metrics are the effective and the actual pixel rating. Actual pixel rating is the total pixels that a camera sensor consists of and the effective pixel rating is the number of pixels that are carrying information. Normally the effective pixel rating is smaller than the actual pixel rating. If a camera sensor with the lens are ideally designed, then the actual and the effective pixel ratings should be the same. These two numbers can be used to understand the utilization of the camera sensor. The percentage utilization of the camera sensor can be

computed by the following equation.

$$Utilization = \frac{Effective\ pixels}{Actual\ pixels} \times 100\% \tag{6.1}$$

This indicator can be used to extract useful information about the combination of the lens and camera sensor combination. The higher this indicator is, the better performance in power consumption the camera sensor and lens have. Applying Equation 6.1 to normal capsule endoscopy images the result will be around 70%. This means that only the 70% of the camera sensor is effectively used . The smaller this indicator is, the less effective is the system. This is because less pixels are used from the total number of pixels that the camera sensor has. By applying this equation in a catadioptric image it is obvious that less pixels are used than in a normal capsule endoscopy system and this indicator is smaller than 70% of a typical capsule endoscopy system. The main idea is to use catadioptric lens that can capture 360° degrees of view and from the center of the lens to capture the front view of the capsule. So, the main idea is a lens that can combine both RICE and FICE views. Until now there is not a research or implementation of such type of lens. Normally, RICE and FICE implementations are used separated. In Figure 6.12 a drawing of this implementation and the field of view is shown.

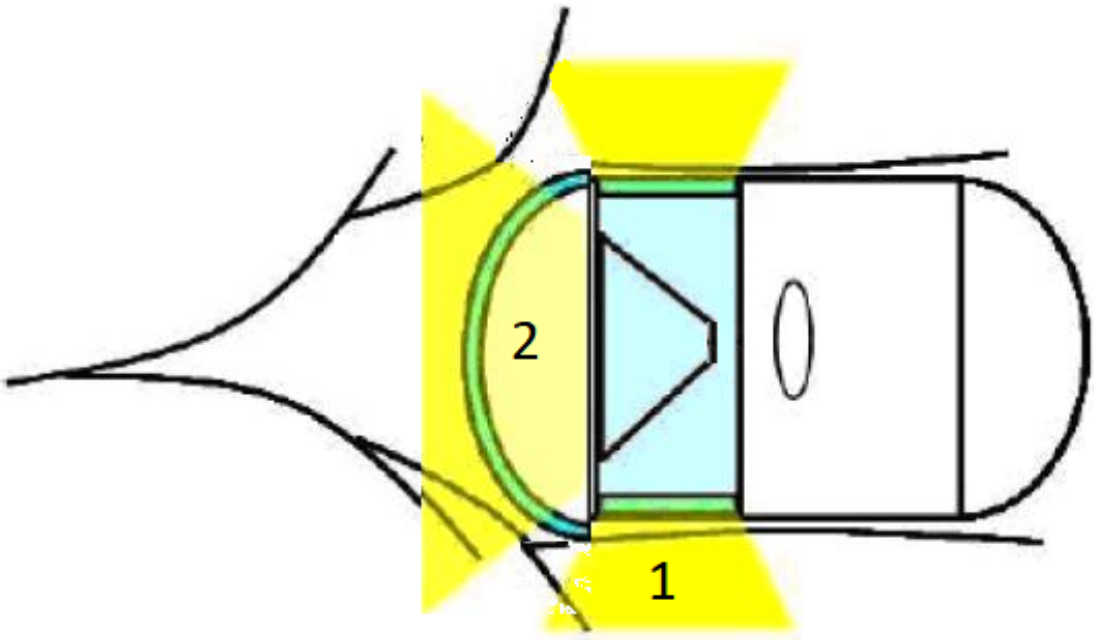

Figure 6.12: In yellow color is the field of view of the proposed capsule lens.

In yellow color the field of view of the proposed lens is shown. The yellow area named “1” is the field of view that is capable to capture around the capsule 360° degrees. The yellow field of view name “2” is the field of view that can capture the front area of the capsule. Using this lens, the pixel utilization of the camera sensor is increased in the levels of typical capsule endoscopy image. However, a typical capsule lens can capture only the front or back of the capsule. So, it is obvious that with the same utilization of the camera sensor more areas of the human intestine could be captured.

The result of this system of lens and camera are presented in the next paragraph. A commercial used catadioptric lens used in performed experiments. A commercial used lens designed for mobile phones was modified and attached in a commercial USB camera. To attach the lens to the camera a connector was designed and printed in a 3D printer.

Figure 6.13: USB camera connected with commercially available catadioptric lens.

It is obvious that this system is not able to fit inside an endoscopic capsule. However, it can show what results can be obtained by its use. In Figure 6.13 this system is shown. The size of the used equipment is not in the same size like a camera used in endoscopic capsules. The camera used is a tiny, simple commercial USB camera, the height is 22mm, the upper diameter 25mm and the diameter of the bottom is 35mm. The USB camera used is not a High Definition one. The reason is that it was the only one that has a manual focus screw. It is used to adjust the focal length and clear the captured image from the catadioptric lens. The maximum captured resolution for this camera was only VGA or 640×480 pixels. The proposed experiment is to capture a few images and unwrap them. Later, stitching process will be performed and the results will be presented like a tube that the doctor can navigate inside and perform diagnosis. Since that in-vivo tests were difficult to be performed, a human intestine was printed in a paper of A3 size and wrapped like a tube. Plastic elements designed and printed in a 3D printer, were used to keep the A3 page in tube shape. Later, a scissor lift was designed, and 3D printed. This part was used to move the camera with

the lens inside the paper tube. As mentioned previously the paper tube has inside of it a human intestine printed. The scissor lift moves the camera with the lens and the intestine was captured.

Figure 6.14: Materials used to perform experiments.

The USB camera is connected in a Raspberry PI 3B. Python algorithm was used to capture and unwrap the image. In Figure 6.14 the overall system, that was previously described, is shown. The tube used to simulate human intestine is seen in the left side of Figure 6.14 and in the right side there is the scissor lift with the camera attached. In the base of the scissor lift a big plastic screw is used to increase or decrease the height of the scissor lift.

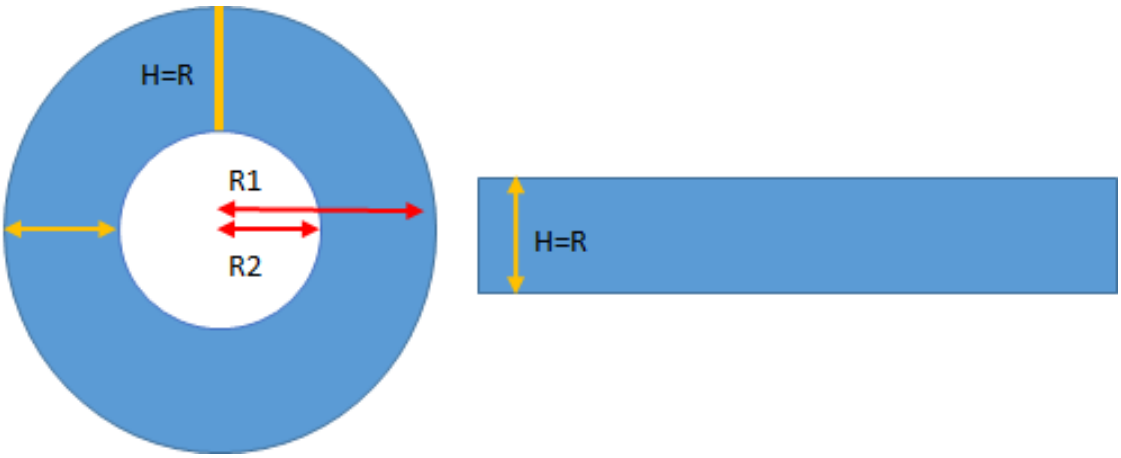

Figure 6.15: How image is unwrapped.

In Figure 6.15 tothe left of the figure the captured image shape and to the right the desired output shape. The yellow arrows in both sketches, is the maximum width of the effective pixels. However, it is not possible to use the maximum width due to the distortion produced by this type of lens. For this reason, only the middle area of the captured width is better to be used. The algorithm produced in python code, captures this shape of image and re-arrange the pixel values in a way to produce a rectangular image.
Behind the python code there are some mathematics that used to provide the desired result. The first equation used is to find the area from "donut" image where there is the intestine view. The area as seen in Figure 6.15 is the blue "donut" shape, the height of this image is computed by subtract the big red line minus the small red line.

$$H = R = R_1 - R_2 \tag{6.2}$$

The height of the image has been found, next step is to compute the width, which is the perimeter of the outer line of the blue "donut". It can be computed by the next equation.

$$W = 2 \times \pi \times r = 2 \times \pi R_1 \tag{6.3}$$

Next step is to locate every pixel in the source image and relocate it to the rectangular image. The distance from the center and the degrees to locate the pixel in the "donu" image can be done by the next equations.

$$k = (\frac{y}{H_d} \times (R_1 - R_2)) + R_L \tag{6.4}$$

and,

$$z = \frac{x}{W_d} \times 2 \times \pi \tag{6.5}$$

Where x and y are the pixel location in the source image and k and z is the distance from the center of the "donut" and the degrees of the pixel in the "donut", respectively. Also, H_d and W_d are the height and width values for the destination image and R_L is the maximum length of the image. Next step is the use of these

values to re-map the pixel values for the result. This can be made by the next equations.

$$X_{result} = x_0 \times k \times \sin z \tag{6.6}$$

and,

$$Y_{result} = y_0 \times k \times \cos z \tag{6.7}$$

Where x_0 and y_0 is the center of the "donut". These are the equations used in python code to transfer the values of the pixels of a "donut" image to a rectangular.

```
Data: Captured image
Result: Rectangular image
initialization;
while True do
    capture current_image;
    if Captured then
        donut_image = current_image;
        rectangular_image = re-arrange (donut_image);
        save rectangular_image;
        print "Image processed";
    else
        print "Error in image capturing";
    end
end
```

Algorithm 1: Simple algorithm to show the way python code processes captured images from catadioptric lens.

In Figure 6.16 real images captured using of catadioptric lens. As said the images were captured using of a USB camera and a Raspberry PI 3b.

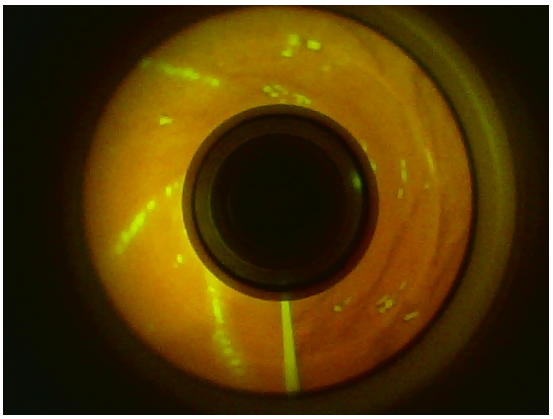

(a) First captured image.

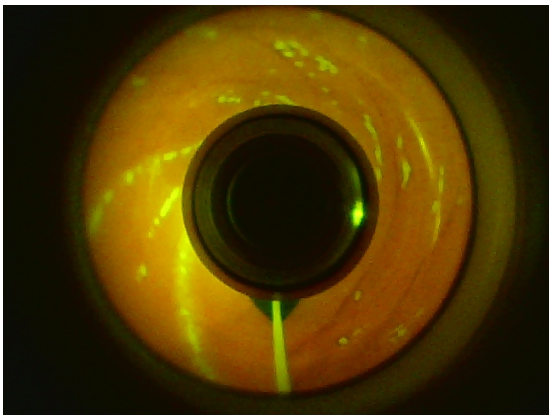

(b) Second captured image.

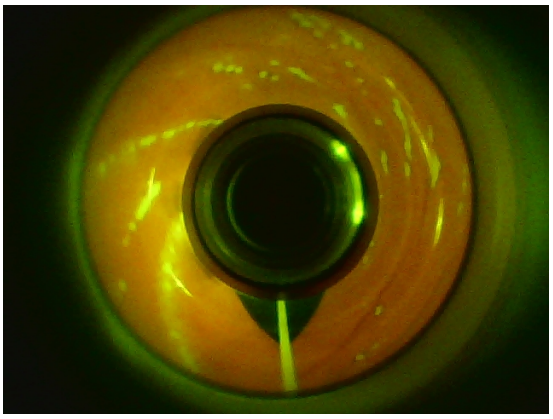

(c) Third captured image.

(d) Fourth captured image.

Figure 6.16: Four successive images.

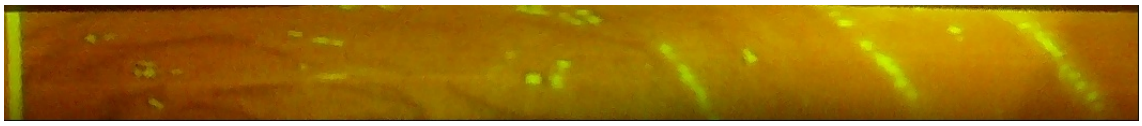

(a) First captured image after un-wrapped.

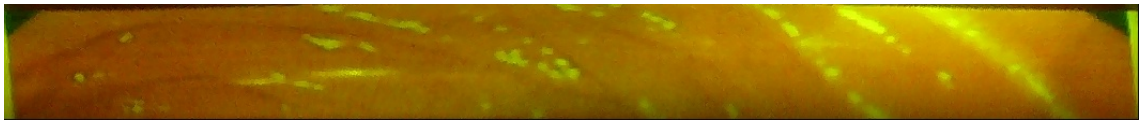

(b) Second captured image after un-wrapped.

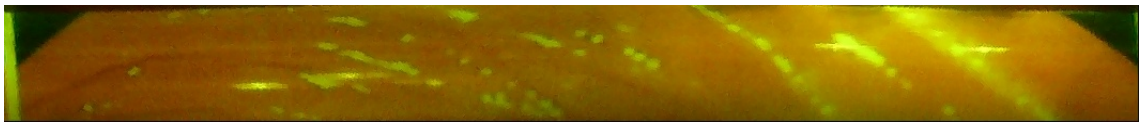

(c) Third captured image after un-wrapped.

(d) Fourth captured image after un-wrapped.

Figure 6.17: Four successive images.

In Figure 6.17 four successive images are seen. From a to d the movement of the camera with the lens is shown. These images have a resolution of 640 $\times$ 480 pixels. In the last image the colors are not the same with the other three, because the camera with the lens almost came out from the system, that was used to emulate the human intestine, as a result the camera was exposed in more light. These images were processed. The result is shown in the next figure.

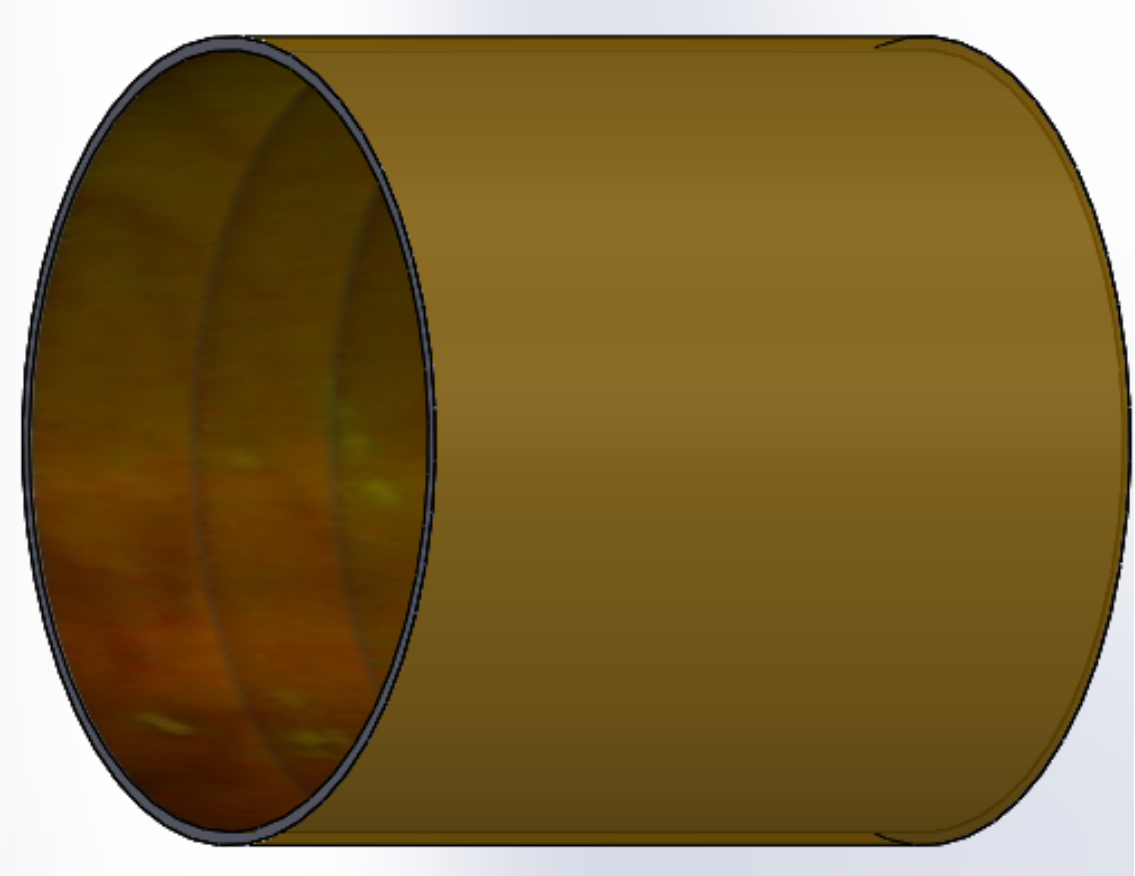

Figure 6.18: Final reconstructed image.

In Figure 6.18 the reconstruction of the received images is shown. This result was implemented using CAD software. At first, MATLAB was used to stitch the images and then with CAD software the image was wrapped inside a tube. Now the doctor can have a "walk" inside human intestine and perform diagnosis.

6.5 Summary

The design of a small catadioptric lens to fit inside a endoscopic capsule could increase the overall performance of the WCE. The combination of this type of lens with tiny sensors like temperature, pH, orientation sensor, etc. could improve the diagnosis made by the doctors. More data will be provided. Also, the use of this type of lens needs high resolution type of camera sensors. However, because of that, the result of the captured image is not rectangular but "donut" shaped. It is possible the capsule to compress only the necessary data. This could improve the power consumption of the entire system and finally the overall performance of the smart pill.

Chapter 7

Conclusion and future works

This is the last chapter of this thesis. A review of the research objectives and the results produced by this thesis was made . Also, there will be a paragraph for the future works. Considering that the goals of this thesis has been achieved and promote further improvements that could be applied and improve further the performance of a WCE.

7.1 Conclusion

The need to provide better images with high quality to doctors/physicians and perform better diagnosis to the small intestine and the colon of the patients, inspire us to set the objectives of this thesis.
In the passed decades the use of classical endoscopy for diagnosis was increased. However, classical tools for endoscopy could not capture more than the area of the colon, esophagus and stomach. It is not possible to perform diagnosis in the small intestine with the classical endoscopy. For this reason, doctors start to use the alternative of the classical tool, which is the WCE. This is a small swallow-able pill which consists of a camera, an RF transmitter, a CPU controller and the power source, that is usually a battery. The use of a WCE help doctors to perform diagnosis to areas that previously was not feasible without surgical operation. The use of WCE led doctors to improve diagnosis. However, there are a few drawbacks in the use of WCE. With the size of the WCE, producing most of them. Due to the size, that should be small enough to become swallow-able, there is not enough space for all the components. For this reason, small batteries are used, and the provided power is not, most of the times, enough. Research effort is focused on how to decrease the power consumption of the components that consist a WCE and at the same time to increase the performance of WCE. There are four main contributions in this thesis about WCEs:

- The compression algorithm,
- the RF transmitter,
- the intelligent multi-receiver system and

- the smart one frame 360° degrees lens.

About the compression algorithm part, there was a lot of research effort in these areas. Especially in image compression, there were a lot of work that was looking promising. Our objective was to implement a better compression algorithm that will be able to process multi-dimensional image input, and be able to support/connect commercial camera sensors without special circuitry and the most important to consume less energy. Finally, an algorithm, based on statistical analysis of capsule endoscopy images, was designed in Matlab. The compression algorithm transformed to hardware in VHDL language and the results were compared with the software evaluation results. Finally, the ASIC of the compression algorithm was designed. Cadence Virtuoso software suite used for the design and Spectre software for the simulation. For ASIC design 16nm FinFet technology used and achieved as low as 4.5mW of power consumption. The design of the ASIC includes the control circuit of the input data, that makes the compressor able to connect to commercial camera sensors, and the parallel-to-serial converter that provides the serial to the RF transmitter.

The second contribution is the design and simulation of an RF transmitter for high speed and low power consumption use. It is a research area with a lot of research effort. However, there were some bottlenecks that observed, and used to achieve our objective. We need to design an RF transmitter that should use as less components as it is possible. Also, we need to select a modulation technique that is not complicated. For these reasons we conclude in an RF transmitter that uses OOK modulation scheme. Furthermore, the selection of the carrier frequency was based in the RF signal absorption of the human body. A frequency that is less absorbed by human tissue was selected. So, less energy needed to transmit the same amount of data. The selection of OOK modulation was not based only in its low complexity. Another benefit that this modulation scheme has is that that transmitter is working only when it is transmitting digital “1”, while in “0” it shuts down. While thinking the last reason it is obvious that considering the half of the data are “0”, then transmitter is working only in the half time. This is a 50% reduction of power consumption in comparison with other modulation techniques. The last thing that is added to the proposed RF transmitter design and improve a lot the performance was the use a better IC process implementation. This improves the power consumption by the reduction of the supply voltage. This improves the overall performance of the RF transmitter.

The third contribution is an intelligent multi-receiver system. The idea behind of this was the need of only a transmitter inside the pill without the use of a receiver. However, if there are some missing transmitted packets then it will be a problem for the entire system. For this reason, an intelligent multi-receiver system designed and simulated using MATLAB-Simulink, a system that consists of a lot of receivers. The received signal from the receivers is demodulated and the digital data are going into a processor that decides if the received bit is digital “1” or digital “0”. As an example, think a crowd that listens to a speaker. If someone is not listening correctly then asks to other members of the crowd to help him understand. In the proposed system every receiver provides the demodulated data to the processor and the reception level of the RF signal. The processor by knowing the position of its receiver can decide when the signal is received correctly or not. This system is not only improving the performance at the receiver side in Bit Error Rate performance, it also helps to use unidirectional communication in the capsule system. By this way power

is saved by not using a receiver in the pill side.

The fourth and last contribution is the smart 360° degree of view lens. All the WCE system that are used by doctors and in the research area of WCE are using one or two cameras and they are positioned in horizontal placement in the pill. By using one camera sensor you can see in-front of the pill and using two sensors you can see from both sides, in-front and back of the pill. However, a lot of areas of the intestine are not captured. For this reason, a company using a tiny electrical motor, tried to rotate a camera that was placed vertically to the pill. By this way they try to capture the entire intestine. All these works and research ideas inspire us to provide a more energy feasible idea and with the use of the same space in the pill. The use of a catadioptric lens helps to capture 360° degrees image. Then this image is unwrapped. The idea behind this system is to capture less frames per second, the frame to be high in resolution and to capture most of the areas of the intestine. Knowing that the common peristalsis speed is about 1-2cm per minute then is easily understandable that using this type of lens less frames can be sent and capture the entire intestine or at least the most of it. The captured image then is transmitted outside human body and unwrapped in a personal computer with dedicated software. The unwrapped images are stitched together, and the result is a 3D view if the human's intestine that the doctor can "walk-through" and make the diagnosis. In conclusion, the use of this lens improves the entire system in power performance, due to the capture of less images that need to be transmitted.

The four contributions, as it shown in the results of this thesis, are successful and improve the performance of the WCE. The combination of the extra low complexity and power consumption image compression algorithm with the 360° degrees view camera lens, promote a system that can map almost the entire intestine without the use of extra camera sensors and additive power consumption. The package of camera lens with the compression algorithm fit perfectly with the low energy, ultra-fast, one-way RF transmitter. This transmitter can transmit high resolution images outside human body. In addition, the intelligent multi-receiver system improves the bottleneck of the OOK modulation, which is used by the proposed transmitter.

7.2 Future works

The work in this thesis, proves that the methodology and research used, improves the performance of the entire WCE system. However, will always be some points that can be improved.

1. In the first contribution, which is the compression algorithm. The proposed future work is based in the use of the 360° degree lens. This type of lens let the captured image in camera sensor in the shape of a "donut". This means that in an image frame there are a lot of black areas. Our suggestion is to exclude these black areas and achieve better compression ratio. These black areas should not be sent outside human body because there are not holding any information. This is possible to work in the compression system. Due to the known camera sensor resolution and the focal length of the lens, the compressor can be designed in a way that it can exclude these black areas from the compression process.

2. In the second contribution, which is the RF transmitter, a future work that should be done, is the

fabrication of the IC in ASIC and make some measurements and compare the simulated data with the real measurements. We have applied already PVT analysis in our system, but there will be some modifications that will be needed after the fabrication of the IC in order to improve further the performance. Another optimization in the RF part will be the research in the area of the antenna design to achieve better performance in the RF transmission. The last future work that we suggest in this part of the WCE, is to examine the introduction of the wireless power transmission to the capsule from transmitters outside human body. This will improve further the available energy for the WCE. It should be examined while the transmitting frequency if the capsule transmitter is the one, we selected. By this way we will check if we can combine them together without any interference from the circuit of wireless energy transfer to the transmitted signal coming out from the pill.

3. In our third contribution, which is the intelligent multi-receiver system, there is some work we can do. In our system we apply an algorithm that corrects the received signal. However, a system designed where the RF input signal is received by separate antennas and receivers and the demodulated output from the receiver is the input to our controller, where the algorithm is applied. So, the controller is applying the correction algorithm to the digital data that we get from the receivers' output. Due to lack of time we were not able to design a system that can apply this algorithm to the RF signal. So, we suggest designing again the system to work with input the RF signal from a multi-antenna system. This work with the use of machine learning can improve the performance of the receiver system. It will be more dynamic and as more input data it has it will increase the performance of correction. In our proposed system we do not have this ability, but the objective to increase BER performance is achieved. We should have in mind that this system is working outside human body. This means that we have more space and power to use.

4. In our fourth and last contribution we have the 360° degree of view lens. For further development we propose a camera lens that could be able to capture not only the 360° degrees, but also to be able to capture both 360° degrees of view and the view in-front of the capsule. We mean that the existing lens provides this field of view by a catadioptric mirror. However, in the middle of the captured frame, there is a black circle with nothing to show. This lens can be modified in a way so it can capture 360° degrees of view and the view that is vertical to camera sensor. The last image view will take the place of the black circle of the existed frame. By this we take advantage of the unused place in the captured frame.

Bibliography

[1] Mount Nittany Health. Anatomy of the digestive system, 2020. URL: https://www.mountnittany.org/articles/healthsheets/316.

[2] Olympus 2019. Olympus enderoscope, 2019. URL: https://www.olympus-europa.com/medical/en/Products-and-Solutions/Medical-Specialities/Gastroenterology/.

[3] MEDTRONIC. Pillcam horizontal camera placement, 2019. URL: http://www.pillcamcrohnscapsule.eu.

[4] Ltd. RF Co. Sayaka vertical camera placement, March 2020. URL: http://rfsystemlab.com/en/sayaka/index.html.

[5] F. A. M.Herbella, I. Nipominick and M. G. Patti. From sponges to capsules. the history of esophageal ph monitoring. *Diseases of the esophagus : official journal of the International Society for Diseases of the Esophagus*, 22 2:99 – 103, 2009.

[6] Images from capsule endoscopy @ONLINE, March 2020. URL: https://www.endoatlas.net/ea/AtW01/106.aspx.

[7] J. Guillaumin, D. Sadowski, K. Kaler, and M. Mintchev. Ingestible capsule for impedance and pH monitoring in the esophagus. *IEEE Trans. Biomed. Eng.*, pages 2231 – 2236, 2007.

[8] J. McKenzie and D. Osgood. Validation of a new telemetric core temperature monitor. *J. Therm. Biol.*, pages 605 – 611, 2004.

[9] C. Cavallotti, P. Merlino, M. Vatteroni, P. Valdastri, A. Abramo, A. Menciassi and P. Dario. An FPGA-based versatile development system for endoscopic capsule design optimization. *Sensors and Actuators A 172*, pages 301 – 907, 2011.

[10] A.L. Fred, H. A. Kumar, S. N. Kumar and w. Abisha. Bat optimization based vector quantization algorithm for medical image compression. *Intelligent Systems Reference Library*, pages 29 – 54, January 2019. doi:10.1007/978-3-319-96002-9_2.

[11] J. Thone, S. Radiom, D. Turgis, R. Carta, G. Gielen and R. Puers. Design of a 2 mbps fsk near-field transmitter for wireless capsule endoscopy. *Sensors and Actuators A 156*, pages 43 – 48, 2009.

[12] Y. Gao, Y. Zheng, S. Diao, W-D. Toh, C-W. Ang, M. Je, C-H. Heng. Low-power ultrawideband wireless telemetry transceiver for medical sensor applications. *IEEE transactions on bio-medical engineering*, 58:768–72, 03 2011. doi:10.1109/TBME.2010.2097262.

[13] B. Lenaerts and R. Puers. An inductive power link for a wireless endoscope. *Biosensors and Bioelectronics*, pages 1390 – 1395, 2007.

[14] Y. Ye, U. Khan, N. Alsindi, R. Fu and K. Pahlavan. On the accuracy of RF positioning in multi-capsule endoscopy. *IEEE 22nd International Symposium on Personal, Indoor and Mobile Radio Communications*, pages 2173 – 2177, 2011. doi:10.1109/PIMRC.2011.6139900.

[15] M. E. Karagozler, E. Cheung, J. Kwon, and M. Sitti. Miniature Endoscopic Capsule Robot using Biomimetic MicroPatterned Adhesives. *Biomedical Robotics and Biomechatronics*, pages 105 – 111, 2006.

[16] Olympus Europa. Olympus ec1 capsule, March 2020. URL: https://www.olympus-europa.com/medical/en/Products-and-Solutions/Products/Product/ENDOCAPSULE-10-System.html.

[17] A. Mostafa, T. Khan, K. Wahid. An improved YEF-DCT based compression algorithm for video capsule endoscopy. *Conference Proceedings IEEE Engineering in Medicine and Biology Society*, 2014.

[18] J. Liu, C. Li, L. Chen, Y. Xiao, J. Wang , H. Liao and R. Huang. An ultra-low power 400MHz OOK transceiver for medical implanted applications. In *ESSCIRC*, pages 175 - 178, 2011. doi:10.1109/ESSCIRC.2011.6044893.

[19] J. Ryu, M. Kim, J. Lee, B. Kim and S. Nam. Low power OOK transmitter for wireless capsule endoscope. In *Microwave Symposium*, pages 855 - 858. IEEE, June 2007.

[20] M.K. Raja and Y. P. Xu. A 52 pj/bit OOK transmitter with adaptable data rate. *in Proc Solid-State Circuits Conference*, pages 341 - 344, November 2008. doi:10.1109/ASSCC.2008.4708797.

[21] X. Chen, X. Zhang, L. Zhang, X. Li, N. Qi, H. Jiang and Z. Wang. A wireless capsule endoscope system with low-power controlling and processing ASIC. *IEEE Transactions on Biomedical Circuits and Systems*, 3:11 – 22, 2009.

[22] S. K. Nayar. Catadioptric omnidirectional camera. *IEEE*, pages 482 – 488, 2007.

[23] K. M.S. Thotahewa, J-M. Redouté and M. R. Yuce. A UWB wireless capsule endoscopy device. *2014 36th Annual International Conference of the IEEE Engineering in Medicine and Biology Society*, pages 6977–6980, 2014.

[24] Y. Gao, S. Cheng, W. Toh, Y. Kwok, K. B. Tan, X. Chen, W. Mok, H. Win, B. Zhao, S. Diao, C. Alper, Y. Zheng, S. M. Je, and C. Heng. An Asymmetrical QPSK/OOK Transceiver SoC and 15:1 JPEG Encoder IC for Multifunction Wireless Capsule Endoscopy. *IEEE Journal of Solid-state Circuits*, 2013.

[25] N. Cho, J. Bae and H. Yoo. A 10.8 mW body channel communication/MICS Dual-Band transceiver for a unified body sensor network controller. *IEEE Journal of Solid-State Circuits*, 44:3459 – 3468, 2009.

[26] D. C. Daly and A. P. Chandrakasan. An energy-efficient OOK transceiver for wireless sensor networks. *IEEE Journal of Solid-State Circuits*, 42:1003 – 1011, 2007.

[27] S. Diao, Y. Zheng, Y. Gao, C. Heng and M. Je. A 7.2mW 15Mbps ASK CMOS transmitter for ingestible capsule endoscopy. *IEEE Journal of Solid-State Circuits IEEE Asia Pacific Conference on Circuits and Systems*, pages 512 – 515, 2011.

[28] X. Huang, P. Harpe, X. Wang, G. Dolmans and H. de Groot. A 0dBm 10Mbps 2.4GHz ultra-low power ASK/OOK transmitter with digital pulse-shaping. *IEEE Radio Frequency Integrated Circuits Symposium*, pages 512 – 515, 2010.

[29] S. Miah, A. N. khan, C. Icheln, K. Haneda and K. Takizawa. Antenna Systems for Wireless Capsule Endoscope: Design, Analysis and Experimental Validation. *IEEE Transactions on Antennas and Propagation*, 2018.

[30] Mayo Foundation for Medical Education and Research (MFMER). Colon and small intestine, 2019. URL: https://www.mayoclinic.org/colon-and-small-intestine/img-20008226.

[31] Y. Gu, X. Xie, G. Li, T. Sun, D. Wang, Z. Yin, P. Zhang and Z. Wang. Design of Endoscopic Capsule With Multiple Cameras. *IEEE Transactions on Biomedical Circuits and Systems*, pages 590–602, August 2015. doi:10.1109/TBCAS.2014.2359012.

[32] M. Sheu, C. Chiang, W. Sun, J. Wang, and J. Pan. Dual view capsule endoscopic lens design. *Optics Express*, March 2015. doi:10.1364/OE.23.008565.

[33] M. Ou-Yang and W. Jeng. Design and analysis of radial imaging capsule endoscope (rice) system. *Optics Express*, February 2011. doi:10.1117/12.645731.

[34] F. Cucker and P. Bürgisser. Condition: The geometry of numerical algorithms. pages 467 - 468, 2013.

[35] J. A. DiSario, B. T. Petersen and W. M. Tierney. Enteroscopes. *Gastrointestinal Endoscopy*, 44:872 – 880, 2007.

[36] C. Piet and D. Groen. History of the endoscope. *Proceedings of the IEEE*, 105:1987 – 1995, 2017.

[37] E. Rondonotti, J. M. Herrerias, M. Pennazio, A. Caunedo, M.Mascarenhas-Saraiva, and R. De Franchis. Complications, limitations, and failures of capsule endoscopy: a review of 733 cases. *Gastrointestinal Endoscopy*, 62:712 – 716, 2005.

[38] T. Nakamura and A. Terano. Capsule endoscopy: Past, present, future. *Journal Gastroenterology*, pages 93–99, 2008.

[39] P. Swain. Wireless capsule endoscopy and Crohn's disease. *Gut*, 54:323 – 326, 2005.

[40] C. A. Burke, J. Santisi, J. Church, and G. Levinthal. The utility of capsule endoscopy small bowel surveillance in patients with polyposis. *American Journal of Gastroenterology*, 100:1498 – 1502, 2005.

[41] A. Culliford, J. Daly, B. Diamond, M. Rubin, and P. H. R. Green. The value of wireless capsule endoscopy in patients with complicated celiac disease. *Gastrointestinal Endoscopy*, 62:55 – 61, 2005.

[42] L. A. Ries, P. A. Wingo, D. S. Miller, H. L. Howe, H. K. Weir, H. M. Rosenberg, S. W. Vernon, K. Cronin, and B. K. Edwards. The annual report to the nation on the status of cancer, 1973–1997, with a special section on colorectal cancer. *Cancer*, 88:2398 – 2424, 2000.

[43] A. Glukhovsky . Wireless capsule endoscopy. *Sensor Review*, 23(2):128 - 133, 2003. doi:http://dx.doi.org/10.1108/02602280310468233.

[44] A. Moglia, A. Menciassi,P. Dario, A. Cuschieri. Capsule endoscopy: progress update and challenges ahead. *Nature Review Gastroenterology Hepatology*, 6:353 - 362, June 2009. doi:10.1038/nrgastro.2009.69.

[45] C. M. Caffrey, O. Chevalerias, C. O'Mathuna and K. Twomey. Swallowable capsule technology. *IEEE CS*, pages 23 - 29, 2008.

[46] H. Cao, S. Rao, SJ. Tang, HF. Tibbals, S. Spechler and JC. Chiao. Batteryless implantable dual-sensor capsule for esophageal reflux monitoring. *Elsevier*, 77(4):649 - 653, April 2013. doi:http://dx.doi.org/10.1016/j.gie.2012.10.029.

[47] 2020 Medtronic. 2020 medtronic, March 2020. URL: https://www.medtronic.com/covidien/en-us/clinical-solutions/gastrointestinal-health/products.html#expandName0.

[48] G. M. Cobrin, R. H. Pittman and B. S. Lewis. Increased diagnostic yield of small bowel tumors with capsule endoscopy. *Cancer*, July 2006. doi:10.1002/cncr.21975.

[49] M. A. Ciorba and C. Prakash. Wireless capsule endoscopy in the diagnosis of small bowel Crohn's disease. *Inflamm Bowel Dis*, 2003.

[50] E.J. Carey and D.E. Fleischer. Investigation of the small bowel in gastrointestinal bleeding–enteroscopy and capsule endoscopy. *Gastroenterol Clin North Am*, 34:719 - 734, 2005.

[51] E. A. Johannessen, L. Wang, L. Cui, T. B. Tang, M. Ahmadian, A. Astaras, S. W. J. Reid, P. S. Yam, A. F. Murray, B. W.Flynn, S. P. Beaumont, D. R. S. Cumming and J. M. Cooper. Implementation of multichannel sensors for remote biomedical measurements in a microsystems format. *IEEE Trans. Biomed. Eng.*, pages 525 – 535, 2004.

[52] S. W. Seo, S. Han, J. H. Seo, W. B. Choi and M. Y. Sung. Liquid Lens Module with Wide Field of View and Variable Focal Length. *Electronic Materials Letters*, pages 141 – 144, 2010.

[53] X. Xie, G. Li, X. Chen, X. Li, and Z. Wang. A Low Power Digital IC Design Inside the Wireless Endoscopic Capsule. *IEEE Journal Of Solid-State Circuits*, 2006.

[54] M. J. Park, T. Kang, I. G. Lim, K. Oh, S. Kim, J. Lee and H. Park. Low-Power, High Data-Rate Digital Capsule Endoscopy Using Human Body Communication. *Applied Science*, pages 1 – 17, 2018.

[55] C. E. Shannon. A Mathematical Theory of Communication. pages 379 – 423, 623 – 656, 1948.

[56] K. Sayood. *Introduction to Data Compression*. Morgan Kaufmann, 2012.

[57] J. Gat and N. Vidya. *Complete Arithmetic Coding: Basic Concepts, Theory, Practical Implementation*. LAP LAMBERT Academic Publishing, 2010.

[58] D. Salomon. *Data Compression The Complete Reference*. Springer-Verlag New York, 2004.

[59] A. Moglia, A. Menciassi, P. Dario and A. Cuschieri. Capsule endoscopy: progress update and challenges ahead. *Nat. Rev. Gastroenterol. Hepatol.*

[60] M. Quirini, R. J. Webster, A. Menciassi and P. Dario. Design of a Pill-Sized 12-legged Endoscopic Capsule Robot. *2007 IEEE International Conference on Robotics and Automation Roma, Italy*, 2007.

[61] M. Nazmul Huda, Hongnian Yu, and Shuang Cang. Robots for minimally invasive diagnosis and intervention. *Robotics and Computer-Integrated Manufacturing*, 41:127–144, 10 2016. doi:10.1016/j.rcim.2016.03.003.

[62] Medtronic. Pillcam™ ugi system, March 2020. URL: https://www.medtronic.com/covidien/en-us/products/capsule-endoscopy/pillcam-ugi-system.html.

[63] O. Ergeneman, G. Dogangil, M. P. Kummer, J. J. Abbott, M. K. Nazeeruddin and B. J. Nelson. A magnetically controlled wireless optical oxygen sensor for intraocular measurements. *IEEE Sen. J. Am. Chem. Soc.*, pages 29 – 37, 2008.

[64] C. Van de Bruaene, D. De Looze and P. Hindryckx. Small bowel capsule endoscopy: Where are we after almost 15 years of use? *World Journal of Gastrointestinal Endoscopy.*, pages 13 - 36, 2015.

[65] T. H. Khan and K. A. Wahid. Lossless and Low-Power Image Compressor for Wireless Capsule Endoscopy. *Hindawi, VLSI Design*, 2011, 2011.

[66] G. Liu, G. Yan, B. Zhu and L. Lu. Design of a video capsule endoscopy system with low-power asic for monitoring gastrointestinal tract. *Medical Biological Engineering Computing*, 54, 03 2016. doi:10.1007/s11517-016-1472-2.

[67] M. Lin, L. Dung and P. Weng. An ultra-low-power image compressor for capsule endoscope. *BioMedical Engineering OnLine*, 2006.

[68] X. Li, X. Xie, G. Li, L. Zhang and Z. Wang. Low-complexity near-lossless image compression method and its application-specific integrated circuit design for a wireless endoscopy capsule system. *Journal of Electronic Imaging 16*, 2007.

[69] A. Mostafa, T. Khan and K. Wahid. Design of a Lossless Image Compression System for Video Capsule Endoscopy and Its Performance in In-Vivo Trials. *Sensors (Basel, Switzerland)*, 2014.

[70] Hepatology North American Society for Pediatric Gastroenterology and Nutrition. North american society for pediatric gastroenterology, hepatology and nutrition, June 2016. URL: https://www.naspghan.org/content/102/en/jejunum-and-ileum.

[71] GASTROLAB the Gastrointestinal Site. Gastrolab - the gastrointestinal site, March 2020. URL: http://www.gastrolab.net/ni.htm.

[72] F. Liu, M. Hernandez-Cabronero, V. Sanchez, M. Marcellin, and A. Bilgin. The current role of image compression standards in medical imaging. *Information*, page 131, 2017.

[73] P. Turcza and J. Mlynarczyk. Design of Wide Band OOK Transmitter for Biomedical Application. *20th International Conference "Mixed Design of Integrated Circuits and Systems"*, pages 540 - 544, 2013.

[74] L. Jiankun, J. Li and C. Kuo. Layered DCT still image compression. *Circuits and Systems for Video Technology, IEEE Transactions*, pages 440 – 443, 1997.

[75] C. Hu, Q. Max, H. Meng, L. Liu, Y. Pan and Z. Liu. Image Representation and Compression for Capsule Endoscope Robot. *International Conference on Information and Automation, Proceedings of the 2009 IEEE*, pages 506 – 511, 2009.

[76] H Meng and Z. Wang. Fast spatial combinative lifting algorithm of wavelet transform using the 9/7 filter for image block compression. *IEEE Electronics Letters*, pages 1766 – 1767, 2000.

[77] S. G. Mallat. A theory for multiresolution signal decomposition: the wavelet representation. *IEEE Transactions on Pattern Analysis and Machine Intelligence*, 11(7):674 - 693, July 1989. doi:10.1109/34.192463.

[78] S. K. Mohammed, K. M. M. Rahman and K. A. Wahid. Lossless Compression in Bayer Color Filter Array for Capsule Endoscopy. *IEEE Access*, 5:13823 – 13834, 2017. doi:10.1155/2008/912536.

[79] H. K. Tareq and K. A. Wahid. Low Power and Low Complexity Compressor for Video Capsule Endoscopy. *IEEE Transactions on Circuits and Systems for Video Technology*, 21:1534 – 1546, 2011. doi:10.1109/TCSVT.2011.2163985.

[80] L. Dung, Y. Wu, H. C. Lai, and P. Weng. A modified H.264 intra-frame video encoder for capsule endoscope.

[81] X. Chen, X. Zhang, L. Zhang, X. Li, N. Qi, H. Jiang, and Z. Wang. A wireless capsule endoscope system with low power controlling and processing ASIC. *IEEE Trans. Biomed. Circuits Syst.*, 3:11 – 22, 2009.

[82] K. Gupta, R.L. Verma and S. Alam. Lossless Medical Image Compression Using Predictive Coding and Integer Wavelet Transform based on Minimum Entropy Criteria. *International Journal of Application or Innovation in Engineering & Management (IJAIEM)*, page 2, 2013.

[83] W. A. J. Kosmala. A Friendly Introduction to Analysis. *New Jersey: Pearson Prentice Hall*, 2004.

[84] Inc. 2020 OmniVision Technologies. Omnivision technologies, inc., March 2020. URL: http://www.ovt.com/sensors/OV9715.

[85] ON Semiconductor. On semiconductor, March 2018. URL: http://www.onsemi.com/pub/Collateral/MT9D115-D.PDF.

[86] K. A. Fante, B. Bhaumik and S. Chatterjee. Design and implementation of computationally efficient image compressor for wireless capsule endoscopy. *Circuits Systems and Signal Processing*, pages 1677 - 1703, 2016.

[87] K. Goyal, A. Lal and B. Bhaumik. DWT based Low Power Image Compressor for Wireless Capsule Endoscopy. *In Proceedings of the 10th International Joint Conference on Biomedical Engineering Systems and Technologies*, pages 17 - 24, 2017.

[88] M. Basar, F. Malek, K. Juni, M. Saleh,M. Idris, L. Mohamed, N. Saudin, N.Mohd Affendi and A. Ali. The use of a human body model to determine the variation of path losses in the human body channel in wireless capsule endoscopy. *Progress In Electromagnetics Research*, 133:495 - 513, 2013. doi:10.2528/PIER12091203.

[89] P. Theilmann, M. A. Tassoudji, E. H. Teague, D. F. Kimball, and P. M. Asbeck. Computationally efficient model for UWB signal attenuation due to propagation in tissue for biomedical implants. *Progress In Electromagnetics Research B*, 38:1 – 22, 2012. doi:10.2528/PIERB11112111.

[90] X. Wang and MQ. Meng. An experimental study of resistant properties of the small intestine for an active capsule endoscope. *Proc Inst Mech Eng H*, pages 107 – 118, 2010. doi:10.1243/09544119JEIM540.

[91] L. Wang, T. D. Drysdale and D. R. S.Cumming. In Situ Characterization of Two Wireless Transmission Schemes for Ingestible Capsules. *IEEE Transactions on Biomedical Engineering*, 54(11):2020 - 2027, November 2007. doi:10.1109/TBME.2007.895105.

[92] L. C. Chirwa, P. A. Hammond, S. Roy and D. R. S. Cumming. Electromagnetic radiation from ingested sources in the human intestine between 150MHz and 1.2GHz. *IEEE Trans Biomed Eng.*, 50(4):484 - 482, April 2003. doi:10.1109/TBME.2003.809474.

[93] J. L. Bohorquez, J. L. Dawson and A. P. Chandrakasan. A 350mW CMOS MSK transmitter and 400mW OOK Super-Regenerative Receiver for Medical Implant Communications. *2008 IEEE Symposium on VLSI Circuits*, pages 32 - 33, 2008. doi:10.1109/VLSIC.2008.4585940.

[94] M.R. Nezhad-Ahmadi, G. Weale, A. El-Agha, D. Griesdorf, G. Tumbush, A.Hollinger, M.Matthey, H.Meiners, S. Asgaran. A 2mW 400MHz RF Transceiver SoC in 0.18um CMOS Technology for Wireless Medical Applications. In *Radio Frequency Integrated Circuits Symposium*, pages 285 - 288, 2008. doi:10.1109/RFIC.2008.4561437.

[95] M. Yousefi, Z. D. Koozekanani, J. Sobhi and N. N. Azizkandi. A 430 MHz fully integrated high efficiency OOK transmitter for wireless biomedical application. *International Journal of Electrical & Computer Sciences IJECS-IJENS*, 4(3):1 - 5, June 2014.

[96] M. Vidojkovic. A 2.4 GHz ULP OOK Single-Chip Transceiver for Healthcare Applications. *IEEE Trans. Biomedical Circuits and Systems*, 5(6):458 - 460, December 2011. doi:10.1109/ISSCC.2011.5746396.

[97] H. Farkhani, A. Peiravi, J. K. Madsen and F. Moradi. Comparative study of FinFETs versus 22nm bulk CMOS technologies: SRAM design perspective. *System-on-Chip Conference (SOCC),27th IEEE International*, pages 449 – 454, 2014. doi:10.1109/SOCC.2014.6948971.

[98] D. A. Lourts, D. Likhitha and P. R. P. Cyril. Performance comparison of CMOS and FinFET based SRAM for 22nm technology. *International Journal of Conceptions on Electronics and Communication Engineering*, 1:6 – 10, December 2013.

[99] M. Sathe and N. Sarwade. Performance comparison of CMOS and FinFET based circuits at 45nm technology using spice. *Mugdha Sathe Int. Journal of Engineering Research and Applications*, 4:39 – 43, 2014.

[100] PTM. Predictive Technology Model, March 2020. URL: http://ptm.asu.edu/.

[101] P. Reynaert and M. Steyaert. *RF Power Amplifiers for Mobile Communications*.

[102] K. Gono, T. Obi, M. Yamaguchi and N. Oyama. Appearance of enhanced tissue features in narrow-band endoscopic imaging. *Journal of Biomedical Optics*, 9:568 – 577, 2004.

[103] U. Hany and L. Akter. Local parametric approach of wireless capsule endoscope localization using randomly scattered path loss based wcl. *Wireless Communications and Mobile Computing*, 2017.

[104] G. Vermeeren, E. Tanghe, A. Thielens, L. Martens and W. Joseph. In-to-out body path loss for wireless radio frequency capsule endoscopy in a human body. *2016 38th Annual International Conference of the IEEE Engineering in Medicine and Biology Society (EMBC)*, pages 3048–3051, 2016.

[105] M. Ou-Yang, Y. Chen, H. Lee, S. LU and H. Wu. Wide-angle lens for miniature capsule endoscope. *Advanced Biomedical and Clinical Diagnostic Systems IV*, 2006. doi:10.1117/12.645731.

Appendices

Appendix A

Working algorithm of the proposed multi-receiver system.

```
Initialization;
while i=0; i< 32; i++ do
    receiver(i) = measure_receiver_RSS(i);
    if max_RSS < measure_receiver_RSS(i) then
        max_RSS = measure_receiver_RSS(i);
    end
    max_RSS = measure_receiver_RSS(i);
end
min = receiver(i);
while i=0; i< 32; i++ do
    for j=i+1; j< 32; j++ do
        if (receiver[j] < min) then
            min = receiver(j);
        end
    end
    temp = receiver(i);
    receiver(i) = min;
    min = temp;
end
while k=0; k=< 32; k+2 do
    result(k) = receiver(k) ⩔ receiver(k+1);
end
while i=0; i =< 16; i++ do
    sum = sum + result(i);
end
Average = sum/16;
if Average < 0.5 then
    output data=0;
else
    output data=1;
end
```

Algorithm 2: Working algorithm to correct received data

Appendix B

Hardware implementation of image compression algorithm in FPGA development board.

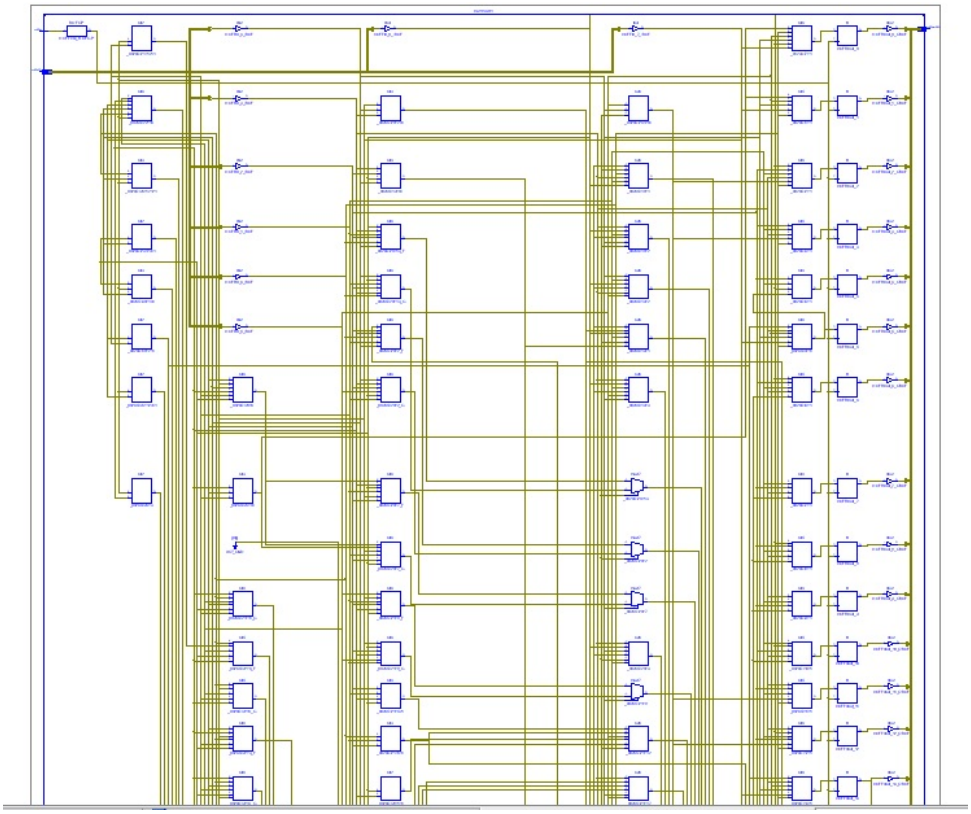

Figure B.1: Block diagram of the proposed memory-less huffman implementation.

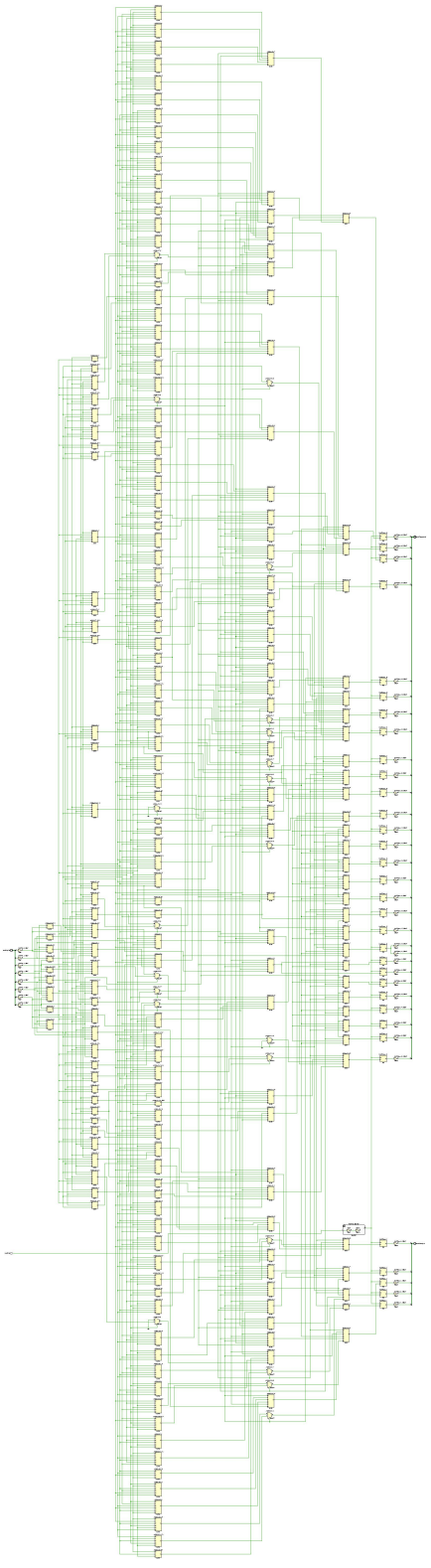

Figure B.2: Schematic of the huffman implementation.

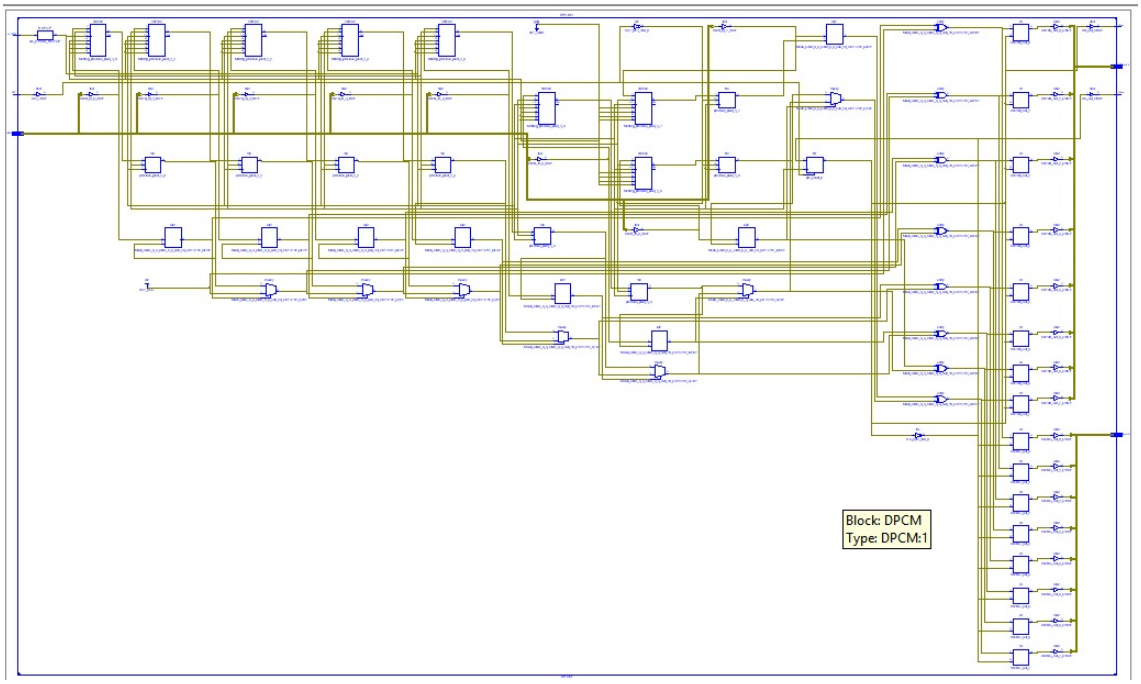

Figure B.3: Schematic of the DPCM encoder implementation.

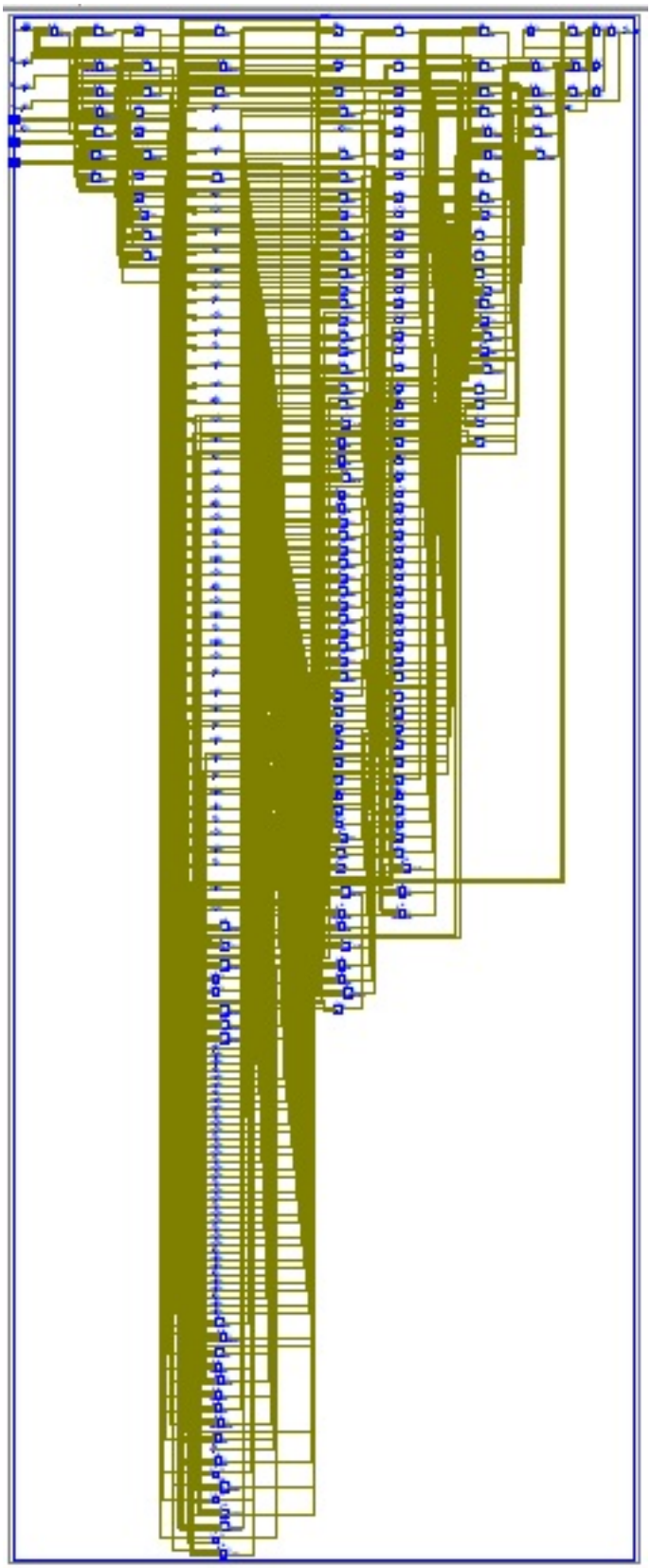

Figure B.4: Schematic of the parallel-to-serial converter.